University of Milano-Bicocca
Department of Materials Science

The growth of *in situ* sol-gel silica in Natural Rubber. Synthesis, morphological and mechanical characterization of the composites.

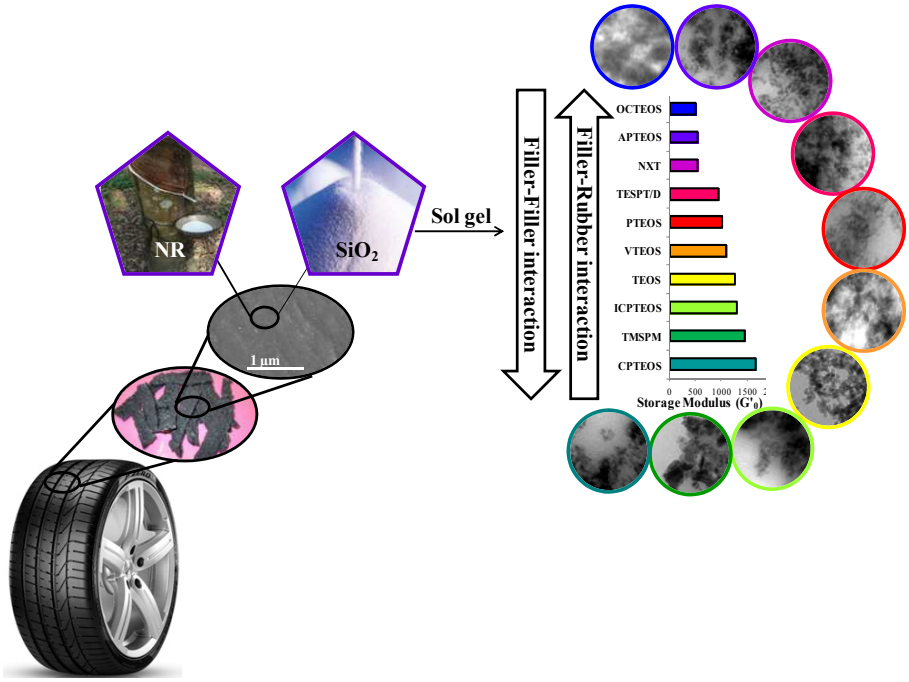

Wahba Laura
(matr. 734538)

Supervisor: Prof. Franca Morazzoni
Tutor: Dott. Raffaella Donetti
Dean of the Doctorate: Prof. Gian Paolo Brivio

PhD School in Materials Science – XXV cycle
Thesis presented for the degree of Doctor Europaeus

January 2013

Dedicated to my Mum:
Kamilia

Table of contents

Chapter 1

Motivation, objectives and organization

1.1. Objectives and aims of study

Great interest was recently devoted to the use of inorganic particles as a reinforcing filler [1,2,3] in tires for the automotive industry[4,5]. In fact, the reinforcing of elastomers by the addition of these fillers affects the stiffness, strength, elongation at break, fracture toughness[6], energy dissipation (rolling resistance)[7], friction to ice or wet grip[8,9], wear (abrasion resistance)[10], and on the material processability[11,12].

Therefore, the technology improvement of tires currently has to satisfy the requirements of sustainable development in order to reduce fuel consumption, environmental pollution and acoustic noise[3].

Carbon black has been the only additive used for this purpose for a long time[13, 14], but silica is now becoming the alternative reinforcing filler; as it offers a lot of advantages, such as better rolling resistance and reduction of the heat buildup[15,16,17]; moreover, it can be suitably employed in all cases where the black color is not required.

Natural rubber-silica (NR-SiO_2) composites are usually prepared by mechanical mixing[18]. Unfortunately, silica particles have a strong tendency to interact with each other within the elastomeric matrix, favoring the inhomogeneous dispersion due to particle tendency to agglomerate and in principle to reduce the filler-rubber interaction.

Significant contributions to overcome the disadvantages derived from filler-filler interaction of the silica particles; they are obtainable by enhancing the filler-rubber interaction, which causes additional cross-linking in the rubber structure. The enhancement of filler-rubber interaction is obtained by the use of coupling agents which interact with both the polymer (hydrophobic) and the silica (hydrophilic) surface groups, due to the presence of different functionalities at the ends of the molecules[19,20,21].

An alternative approach and object of the present Ph.D thesis, is to prepare composites by *in situ* formation of the silica filler particles by sol-gel[22] hydrolysis and condensation of tetraethoxysilane (TEOS)[23]. Therefore, the aim of this work is to prepare silica-natural rubber (NR-SiO_2) composites, with the intention of improving the properties which normally the compound, prepared by mechanical blending possesses.

Several factors like nature of the solvent, nature of the catalyst, medium pH, molar ratio between alkoxysilane and water or solvent, gelling and drying temperatures are fundamental sol-gel parameters[24] which can modify the process of the nanocomposite preparation in order to optimize the better homogeneity of the filler distribution inside the rubber matrix.

Therefore, considering the filler particle growth *in situ* in the polymeric matrix, it is possible to distinguish two possible preparation techniques which differ in some of the factors affecting the sol-gel process: aqueous and non-aqueous *in situ* sol-gel methods.

In addition to these factors that influence the preparation of the composite, the amount of the filler present in the silica-rubber composite affects the final performance.

In fact, the enhancement in mechanical properties can be achieved when the composite contains the optimal amount of the filler required to form a continuous filler network within the rubber matrix; filler amounts less of this percolation threshold show mostly constant and poor mechanical properties.

The presence of a continuous filler network and its homogeneity depends on the filler characteristics, such as size and shape of the particles and on the *in situ* composite preparation method used.

The formation of a convenient filler network is in turn relatable to the physical and chemical interactions among the particles and among their aggregates (filler-filler interaction) and to the chemical and physical interactions between the particles and the matrix (filler-rubber interaction). The presence of functional groups on the particle surface can significantly influence the interface between the filler particles and the rubber matrix; consequently, modifying the filler-filler and filler-rubber interaction leads to the variation of the reinforcement level of the composites.

With the intention to investigate and to rationalize the effects induced by surface functionalization of the filler on the properties of rubber composites, during the aqueous sol-gel synthesis of the silica the surface was functionalized by using trialkoxysilane having different functional groups.

These functionalities were selected among those which are suitable for promoting the formation of differently shaped silica particles or for modulating the filler-filler and the filler-rubber interactions.

Silica particles were modified by molecules containing alkylthiol, thiocarboxylate, alkyldisulfide, alkyltetrasulfide (silica functionalized with containing S groups)[23]; vinyl, propyl, octyl chains, alkylamine, alkylcyanate and alkylisocyanate groups (silica functionalized with containing N groups).

For this purpose a mixture of TEOS and TMSPM ((3-mercaptopropy)trimethoxysilane) or TESPD (bis(3-triethoxysilylpropyl)disulfide) or TESPT (bis(3-triethoxysilylpropyl)

tetrasulfide) or NXT (3-octanoylthio-1propyltriethoxy) or VTEOS (vinyltriethoxysilane) or PTEOS (triethoxy(propyl)silane) or OCTEOS (triethoxy(octyl)silane) or APTEOS ((3-aminopropyl)triethoxysilane) or CPTEOS (3-cyanopropyltriethoxysilane) or ICPTEOS (3-(triethoxysilyl)propylisocyanate)[25] were introduced in NR latex (containing 60 % dry rubber, 39.3 % of water and 0.7% of NH_3) during the aqueous sol-gel process.

The functionalized molecules were selected with the aim of promoting the formation of different shapes on silica particles (anisotropic or spherical), moreover of modifying the filler-filler and filler-rubber interaction through the chemical functionalities of substituents.

In the aqueous *in situ* sol-gel method, the presence of large amounts of water helps the silica precursors to react quickly in the early stage of the synthesis in rubber matrix, allowing thus to increase the hydroxyl group numbers on particle surfaces, making them less compatible with the rubber and in this way favoring particle aggregation.

Through the non aqueous *in situ* sol gel method, the oxygen present in silica nanoparticles is provided by a suitable reaction and not, as in the aqueous *in situ* sol gel method, by the water solvent.

During this method, the addition of two simple solvents on the metal oxide precursor can generate water[26] *in situ* that can start sol-gel hydrolysis and condensation reactions.

In order to work in an environment without the presence of the water as initial reactant, the silica-rubber composite by the non-aqueous *in situ* sol-gel method was prepared starting from a solution of dry NR with toluene (inert solvent) and TEOS, which was added to formic acid and alcohol (ethanol of benzylalcohol).

Therefore, well defined amounts of water were formed through the esterification reaction produced by formic acid and alcohol, which control the formation of metal oxide growth within the rubber matrix.

Moreover, in order to understand better the morphology of the silica particle growth in NR through the *in situ* sol-gel method, bare silica and functionalized silica powders were prepared by using the same method without the rubber.

These powders were morphologically characterized with the intention of more easily evaluating the shape, the size, the surface area, the effect of the metal oxide precursor and the modification of the silica surface.

Regarding the composites, the amount of silica was determined by thermogravimetric analysis (TGA) in air.

The stability and the reactivity of the functional groups and the hydrolysis rate of the alkoxy groups of the trialkoxysilanes in the early stage of the sol-gel reaction were evaluated by Attenuated Total Reflection-Fourier Transform Infrared Spectroscopy (ATR-FTIR).
The homogeneity of the particle dispersion, the dimension and shape of silica aggregates were investigated by Scanning Electron Microscopy (SEM) and Transmission Electron Microscopy (TEM), to draw appropriate relations between the filler morphology and the reinforcement of the elastomeric network.
The efficacy of the filler network in reinforcing the rubber matrix was assessed by swelling measurements. The Electron Spin Resonance (ESR) behavior of nitroxide radical, introduced as spin probe in order to check the rigidity of the rubber chains, was also investigated.
The static and dynamic-mechanical properties of the nanocomposites, both uncured and vulcanized, were investigated and discussed referring to the network morphology, allowing to suggest a connection between the silica precursors used and the functional properties and the amount of the filler.
The vulcanization kinetics was also studied, as well as the homogeneity of the dispersion of the filler and the rubber networks.
Hardness, abrasion resistance, tensile analysis and compression set results of vulcanized composites were discussed taking into account the structural, morphological and mechanical characteristics determined before.

1.1. Thesis organization

To better understand what composites are applied in the automotive sector, in the 2nd chapter an overview is described of the major constituents (filler and rubber) and characteristics, general properties and synthetic procedures.
A last paragraph of this chapter is dedicated to explain the tire structure, the preparation by the vulcanization process and its major properties in order to appreciate the effect of adding filler to rubber matrix.

Chapter 3 reports characterization techniques and the method used for analyzing fillers, composites and compounding/curing processes.

Chapter 4 is centered on the aqueous *in situ* sol-gel silica and functionalized silica rubber composites. Silica, composite and compound preparation procedures are described in detail.

Chapter 5 focuses on discussion of the various morphologic and mechanical characteristics of the aqueous *in situ* sol-gel silica-rubber composites with the properties presented after the vulcanization process. Different amounts and kinds of functional groups are chosen in order to modify the filler surface and the structure of the interface between filler and rubber, with the intention to change the filler-filler and filler-rubber interactions. All of these composite characteristics are also discussed considering the final properties.

Chapter 6 describes the non-aqueous *in situ* sol-gel preparation method used for preparing silica-rubber composites with different filler concentrations, in order to study the effect of the efficacious filler network on the final properties of the composite. In detail, materials and the preparation procedure for preparing composites and compounds are reported.

Chapter 7 reports the discussion and correlation of the characteristics shown from non-aqueous *in situ* sol-gel silica-rubber composites, from the morphological and mechanical point of view, with the aim to understand how the distribution of the filler network influences the final properties of the composite.

Chapter 8 concluded the thesis and points out the results obtained from a deep characterization of aqueous and non-aqueous *in situ* sol-gel silica-rubber composites in relation to the morphology of the filler particles and the amount of filler in rubber and mechanical properties. Also perspectives are indicated.

---

[1] M. Maiti, M. Bhattacharya and A. K. Bhowmick, *Rubber Chemistry and Technology*; 2008, **81** (3), 384-469.

[2] G. Heinrich, M. Klupper and T. A. Vilgis, *Current Opinion in Solid State and Materials Science*; 2002, **6**, 195-203.

[3] A. K. Bhowmick, *Current topics in elastomers research*; CRC Press Taylor & Francis Group: Broken Sound Parkway NW, 2008.

[4] T. Sabu and S. Ranimol, *In Rubber Nanocomposites: Preparation, Properties and Application, 1st ed.*; Wiley-Interscience: New York, 2010.

[5] L. Bokobza and O. Rapoport, *Journal of Applied Polymer Science*; 2002, **85**, 2301-2316.

[6] G. Wypych, *Handbook of fillers 2nd edition;* Published by ChemTec Publishing, Canada, 2000.

[7] D. E. Hall and J. C. Moreland, *Rubber Chemistry and Technology*; 2001, **74** (3), 525-539.

[8] A. Lechtenboehmer, H. G. Moneypenny and F. Mersch, *British Polymer Journal*; 1990, **22**, 265-301.

[9] M. Barquins, *Wear*, 1992, **158**, 87-117.

[10] A. N. Gent and C. T. R. Pulford, *Journal of Applied Polymer Science*; 1983, **28**, 943-960.

[11] A. I. Isayev, *Encyclopedia of Polymer Blends, Vol.2: Processing*; Wiley-Interscience: New York, 2011.

[12] S. Thomas, K. Joseph, S. K. Malhotra, K. Goda and M. S. Sreekala, *Polymer Composites, Vol.1: Macro-and Microcomposites*; Wiley-Interscience: New York, 2012.

[13] F.R. Eirich, *Science and Technology of Rubber,* Academic Press, Orlando, 1978.

[14] G. Kraus, *Reinforcement of Elastomers*; Wiley-Interscience: New York, 1965.

[15] S. Kohjiya and Y. Ikeda, *Rubber Chemistry and Technology,* 2000, **73**, 534-550.

[16] S. Wolff, *Rubber Chemistry and Technology*, 1996, **69**, 325-346.

[17] B. Schwaiger and A. Blume, *Rubber World*, 2000, **222**, 32-38.

[18] R. F. Grossman, *The Mixing of Rubber*; Published by Chapman & Hall, London 1997.

[19] A. A. Ward, A.I. Khalf and C. Dokki, *KGK Kautschuk Gummi Kunststoffe*; 2009, **62**, 650-656.

[20] O. Klockmann, A. Hasse, and H. D. Luginsland, *KGK Kautschuk Gummi Kunststoffe;* 2003, **56**, 471-477.

[21] J. W. Ten Brinke, S.C. Debnath, L. A. E. M. Reuvekamp and J. W. M. Noordermeer, *Composites Science and Technology*; 2003, **63**, 1165-1174.

[22] J. W. ten Brinke, V. M. Litvinov, J. E. G. J. Wijnhoven and J. W. M. Noordermeer; *Macromolecules*; 2002, **35**, 10026-10037.

[23] R. Scotti, L. Wahba, M. Crippa, M. D'Arienzo, R. Donetti, N. Santo and F. Morazzoni, *Soft Matter*; 2012, **8**, 2131-2143.

[24] C. J. Brinker and G.W. Scherer, *Sol-Gel Science: The Physics and Chemistry of Sol-Gel Processing*; Academic Press Elsevier, 1990.

[25] L. Wahba, M. D'Arienzo, R. Donetti, T. Hanel, F. Morazzoni, R. Scotti and L. Tadiello; *In situ sol-gel obtained silica-rubber nanocomposites: influence of the filler precursors on the improvement of the mechanical properties,* Accepted *RSC Advantaces.*

[26] M. Niederberger and N. Pinna; *Metal Oxide Nanoparticles in Organic Solvents: Synthesis, Formation, Assembly and Applications*; Springer 2009.

Chapter 2

Filler-polymer nanocomposites

This chapter is written with the intention to describe general information and characteristics of composites materials. After looking at different kinds of composite applications, the attention is focused on nanocomposites applied in the automotive sector. Following is a description of the two main important components and a summary of advantages and disadvantages of three different preparation approaches.
In the last part of this chapter the tire application is described in depth, explaining the structure, the preparation by the vulcanization process and its major properties.

2.1. Basic concepts: nanocomposites are a new class of materials

Inorganic/organic composite[1] materials have received great attention in recent years, even if they have been studied for a long time, since they have been employed in a variety of applications. Inside the huge class of these materials, where the inorganic component is dispersed in the organic one, great interest is focused on the nanocomposites.
The reason for all this attention on the study of these materials regards the "dimension" of the components that should have at least one of their three dimensions at the nanoscale (in the range of approx. 1-100 nm)[2,3]. In fact, the small size of the inorganic component, intimately mixed and better dispersed at the nanoscale, provides close contact with the organic part, giving extraordinary properties to the nanocomposite. Today, the view of science and technology is pinpointed on working with increasingly small sizes because small objects in our world are going to have ever more importance, along with a larger number of functionalities.
Obviously, nanocomposite material properties of the end product are not only the sum of the individual contributions, but depend on the important role played by the interface between these two simple materials.
Consequently, the change of the physical and chemical properties[4,5,6] of the materials produced, is due to a good interface, which combines the advantages of the filler as the inorganic material (e.g., rigidity, thermal stability) with the advantages of an organic polymer (e.g., flexibility, dielectric, ductility and processability)[7].
In the past, fillers were probably added to the polymer to decrease the price of the composite, but in recent years many other advantages have been found with their addition to the pure polymer. Whereupon, the properties of the composite materials are affected by the inorganic and organic component characteristics.

Regarding the inorganic part, its contribution to the composite is related to the kinds and characteristics of the filler: average particle size (ranging from a few nanometers to tens millimeters), specific surface area, particle shape (spherical, cubical, irregular, block, plate and flake), reactive groups, wettability and surface energy. The knowledge of these characteristics can help to predict dispersion within an organic polymer, which is sometimes related to the orientation and strong aggregation tendency of the particles. An insufficient homogeneity and rigidity of the composites, which can generate a loss in performance, may be caused by a faulty distribution of the network particles.

The role of the organic polymer (chosen between thermoplastics and thermosets) is connected to its thermal and mechanical behavior, processability and good chemical resistance at low specify gravity. Therefore the choice of the organic part is made considering the operating temperature limit, which determine the appropriate application, but by trying to achieve improvement in strength, modulus properties, enough balance between hydrophobic and hydrophilic characters, bio-compability, optical and/or electronic properties and chemical functionalities (solvation, wettability, templating effect etc)[1].

Good knowledge of all these factors contributes to the achievement of a good overview of interfacial interaction between the polymer and the inorganic part, which can be useful for understanding and predicting the final properties of the composites. Therefore, the role and the nature of the interface are fundamental to modulate the physical and chemical properties of the composite by tailoring and tuning[8].

Two distinct classes of nanocomposites can be distinguished due to the nature of the hybrid interface[1,9]. In *Class I* materials organic and inorganic components additively exchange weak bonds (hydrogen, Van der Waals or ionic bonds). In *Class II* materials, the two phases are totally or partly linked through strong chemical bonds characterized by a strong orbital overlap (covalent or iono-covalent bonds).

For class I hybrids, homogeneity of interface can be adjusted by controlling their extension and by optimizing hydrogen bonding between both organic and hydrophilic inorganic components. For class II hybrids, the extended but weak class I interface can be reinforced through strong chemical bonding. The hydrolytic stability of the resulting chemical bond depends on the nature of the metallic center[9].

During the last fifty years, with the help of new analysis techniques and spectroscopic methods, the structure/properties relation of interface and organic and inorganic components

has become clearer and their general properties, tendencies and performances have been well defined. Before illustrating some nanocomposite applications, several key points and market trends that laboratories and companies follow will be reported, along with the innovations regarding nanocomposites.

For example, in the area of energy storage, the innovation related to the use of new materials regards the improvement of current batteries with nanostructured electrodes, electrolytes and capacitance prepared with composites. Within the development of new materials for the automotive sector, modernization is concentrated on weight, CO_2 and NO_X emission reductions on fuel consumption, decline on operating costs and the use of solar energy. Another promising field is in solid-state lighting, where more robust organic parts with better light and thermal stability are needed, through the use of new compositions and functional innovative materials[10].

Observing all of these market trends, there are different applications of nanocomposite materials, some examples are reported in Figure 1.

Figure 1: Examples of some nanocomposites.

The development of new nanocomposite are widely used in construction industry. Among the various applications, the use of TiO_2 mixed with different polymers, as a white pigment for self-cleaning, is currently of great interest.

For instance TiO_2 nanoparticles incorporated into paving stones in noxer blocks or paints, can substantially reduce concentrations of airborne pollutants such as a volatile organic compounds and nitrogen oxide.

Another application of nanocomposites reported in Sanchez et al. review[1] is the incorporation of clay as a filler in polyamide 6 or in ethylene vinyl alcohol for food packaging. The main role of the addition of clay in the rubber matrix is used to create a sort of labyrinth within the structure which physically delays the passage of molecules of gas and vapor that can deteriorate food inside the container[11].

One of the major challenges of nanocomposites is in medicine, where small nanostructures encapsulate drugs at high concentrations materials and efficiently cross the cell membrane[12]. Livage[8] reported a bio-sensing nanocomposite, made from natural and synthetic polymers (polysaccharides, polyacryloamides etc.), which immobilize enzymes or catalytic antibodies as bioactive molecules that can react in a specific part of the body.

Cosmetics and hair represent a new approach to the use of formulation with hybrid nanocomposites. Research is focused on finding a new hydrolyzed water soluble amino functionalized organosilane, which can easily penetrate hair cuticles, restoring the fiber without damage anything. Other applications of composites are available, but now we will focus on nanocomposites for the automotive sector, and in particular for tires[13].

These special materials are made by elastomers as organic parts (NR Natural Rubber, IR Isoprene rubber, BR Butadiene Rubber, SBR Styrene Butadiene Rubber) and inorganic fillers[14] (chiefly SiO_2, Carbon Black). Choosing fillers and their appropriate concentration can vary the degree of reinforcement[15], stiffness, hardness, abrasion, elongation at break and mechanical properties. The particle network thus formed in rubber and the strength of the interface can change the tire properties.

2.2. Fundamental materials and their interaction: elastomer matrix and typical fillers

Many different polymers and their blends have already been used to synthesize elastomer nanocomposites. This particular thermosetting polymer class is malleable before curing, has a very low glass transition temperature and high viscosity.

Within this class there are NR, IR, SBR, BR, NBR and CR which are briefly described here below.

In the absence of stress the macromolecular chains of these elastomers show random coil conformation due to the presence of high elasticity. In this conformation, the action of a tensile force on the polymer induces a rearrangement of the macromolecular chains, through the modification of the bond angles between the carbon atoms.

This variation is always combined with a decrease in entropy, which is a stress function and is identifiable with the decrease in spatial arrangements. The elastic restoring force comes from the natural tendency of the system to increase its entropy. Natural rubber is the most widely used naturally occurring polymer. The literature shows that many research groups have prepared nanocomposites based on this rubber[13,16,17,18,19,20,21].

Natural rubber (NR) is the only natural product in the rubber family and is composed of more *cis* 1,4 polyisoprene, and than *trans* configuration (see Figure 2).

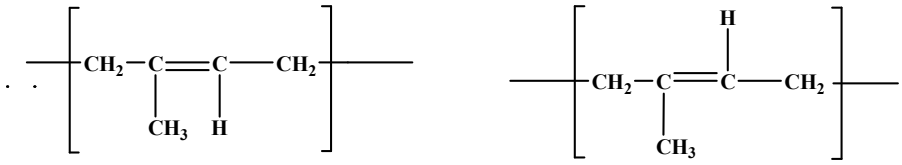

Caoutchouc / *cis*-polyisoprene Gutta Percha / *trans*-polyisoprene

Figure 2: Two possible configurations of Natural Rubber.

In fact, it is a renewable resource which is available as a source of high quality rubber.

It has been identified in about 2000 plant species. However, only the *Hevea Brasiliensis* species[22] has commercial significance. The best quality NR comes from Brasil, Indonesia, Malaysia, India, and the Philippines.

The important commercial development of NR was associated with the discovery of Charles Goodyear[23] and later Thomas Hancock[24], who after elevated temperature treatment of NR in presence of sulfur created an unsticky product.

This vulcanization process[25] allowed entrepreneurs to manufacture and successfully market a wide range of products. Rubber is collected from the tree in a latex solution by tapping. Rubber is separated from the latex[26] by coagulation, usually by acidification. The latex is subsequently coagulated and then the precipitated material is collected. The resultant polymer is then processed into different marketable forms of NR such as sheet rubber, technically specified rubber and crepe rubber. Most of the natural rubber based products are made from these forms. Certain products are also made by concentrated latex.

The molecular weight of polymers is approximately in the range of 1.300.000[27] or more with a relatively broad molecular weight distribution[28]. Isoprene, or 2-methyl-1,3-butadiene is a bifunctional monomer that can form four different types of structural units: 1,4-cis, 1,4-trans and the structures 1,2 and 3,4 (see Figure 3).

Rubber separated from latex contains not only polymers, but also small amounts of resins, proteins, sugars and ammonia (0.2-0.7 % wt) are present.

Even if natural rubber is very strong even without reinforcement by filler, with the exception of a few latex products, most elastomers require filler reinforcement.

The natural 1-4 *cis* polyisoprene is characterized by a high isomeric purity (more than 99 % of 1,4-cis isomer), high molecular mass (M_W between 0.8×10^6 and 2.7×10^6), less ability of polymer chains to move and a high tendency to crystallize (increasing the rigidity).

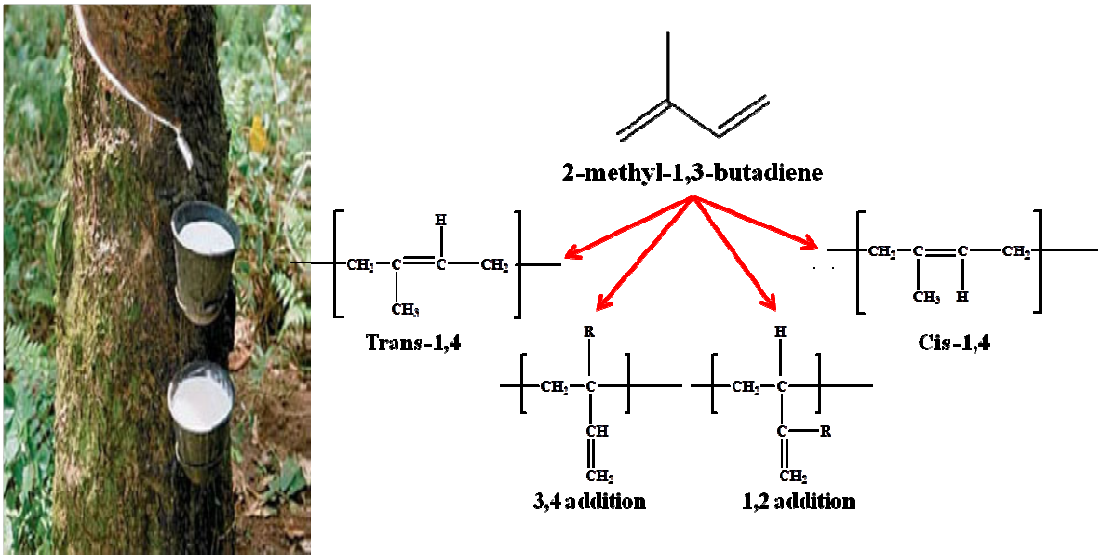

Figure 3: Polymerization process from isoprene produces four different structural units.

All these properties offer the composite material better dynamic-mechanical properties, abrasion resistance, breaking load and elastic modulus compared to *synthetic polyisoprene* (IR). Synthetic polyisoprene is characterized by lower isomeric purity and molecular mass (M_W between 7×10^5 and 8×10^5), leading to less tendency to crystallize.

Low molecular weight of the synthetic polymer means an increase in the flexibility of polymer chains and a decrease in the strength force which may reduce the properties of the composite after curing.

There are two processes to produce synthetic polymer (IR) with high isomeric purity (1,4-cis exceeding at least 90%): the anionic and metal coordinated polymerization.

Developed by Shell Oil, anionic polymerization performed in hydrocarbon solvents uses alkyl-lithium as polymeric initiators, which provides a material classified as “low-cis” where the amount of 1,4-cis units is present as 92-93% and the remaining percentage is made up of the 3,4 unit structure.

In metal-coordinated polymerization, developed by Goodyear Tire & Rubber, $TiCl_4$ and aluminum trialkyls in hexane are used as catalysts, producing polyisoprene, which is "high cis" because this unit is present in 96-97% of the product.

Polyisoprene is not the only elastomer used in tire production. In fact, depending on the use properties and required characteristics, this polymer can be mixed or completely replaced by other synthetic polymers such as: styrene-butadiene rubber (copolymer of styrene and butadiene, SBR), polybutadiene (BR), chloroprene rubber (CR), nitrile rubber (copolymer of butadiene and acrylonitrile, NBR) see Figure 4.

Summarizing, elastomeric materials show three main properties: i) glass transition temperature below room temperature deriving from macromolecular chain flexibility; ii) absence of strong intermolecular interactions due to the presence at room temperature of low degree of crystallinity; iii) high molecular mass. Thereby, cross-linked elastomers are capable of supporting a significant deformation, when they are under stress and quickly recover to their original shape and size when the stress is removed.

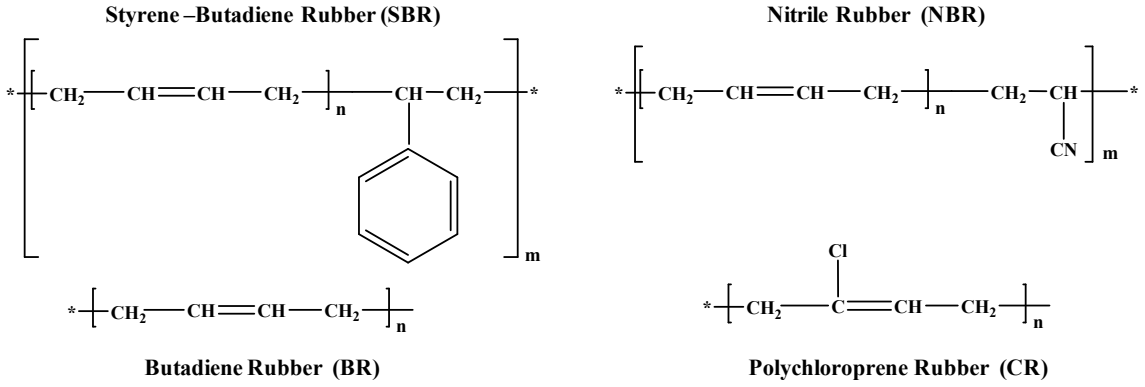

Figure 4: Elastomers used in tire production.

NR has all these characteristics: its glass transition temperature is below room temperature (Tg = - 71 °C), the degree of crystallinity is about 25-30% and the molecular mass is in the order of 10^6. Its high polymerization degree and the absence of sterically blocked side chains confer to the material great mobility of the individual macromolecules, which allow important deformations also after application of modest force.

Styrene butadiene rubber (SBR) is non-polar synthetic rubber and is a copolymer of styrene and butadiene, is the most commonly used in combination with NR.

The ratio between these two copolymers influences the behavior of the polymers: the higher the amount of styrene used, the harder they are.

Some of the properties of SBR are worse than those of NR, such as strength, heat buildup and stickiness. SBR has lower viscosity than NR which allows to use it in industry without pre-mastication and shows abrasion resistance and resistance to the degradation under heat better than NR.

Butadiene rubber (BR) is also a synthetic rubber, produced by addition chain mechanism and is less used in tire application in comparison to NR and SBR. BR based materials show better resistance to ozone, and to abrasion at high temperatures; flexibility at low temperatures is higher than those of NR and SBR. Furthermore, with BR compounding, it is possible to incorporate high amounts of oil and fillers without significant deterioration of the end properties of the materials. Unfortunately, adhesiveness to the other components of the tire, tear resistance and some of the mechanical properties are worse than NR and SBR.

Chloroprene rubber (CR, Neoprene) is considered one of the specialty rubbers, used in specific applications which require further solvents, fire and thermal resistance. Neoprene, in contrast to synthetic polymers (previously discussed), does not require sulphur curing. Its general physical properties are enhanced after the compounding with vulcanization ingredients such as ZnO or MgO. This rubber is heat and flex resistant and can be used for specific applications.

Acrylonitrile Butadiene rubber (NBR, nitrile rubber) is a copolymer of acrilonitrile and butadiene rubber with polar characteristics. NBR has good resistance to a wide variety of oils and solvents and a high viscosity which can be reduced by mastication.

Through the vulcanization process[25], it is possible to promote stable bonds between the rubber chains, (*cross-links*) creating a rubber network which can also withstand significant material deformation prolonged in time.

During the curing process, the free rubber chains crosslink together to form a three-dimensional elastic network by reacting with sulphur (see Figure 5).

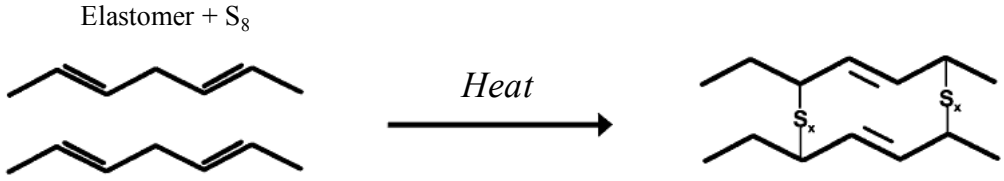

Figure 5: Cross-linking by using sulphur.

The formation of the elastomer network structure[29] is an essential condition for generating the elastomeric properties of rubber; thereby transforming the material from a viscous liquid to a tough elastic solid.

The role of the sulphur in vulcanization process will be discussed in section 2.4.2 while the characterization kinetic in 3.3.1 paragraph.

Filler is the second main part of the composite. In the rubber network, particles of filler are distributed in order to form a filler network. The presence of the filler network is crucial for appreciating the reinforcement of the rubber.

The distribution of the filler network in rubber matrix is mainly influenced by particle structure assembly; the higher the dispersion degree is, the better the reinforcing effect is. Good knowledge of the size and shape of the particle and aggregate can contribute to predicting the characteristics of the filler network in rubber composites. In fact, during the filler synthesis the elementary particles thus generated assembly to form aggregates[30]. Within an aggregate, particles are fused and cannot be separated during the thermo-mechanical mixing with the elastomer. A weaker attraction (predominantly Van der Walls forces) also exists between the aggregates. It leads to the formation of a reversible secondary structure, made of agglomerates, as shown in Figure 6.

Agglomerates can be destroyed by thermo-mechanical mixing in the presence of elastomers or during mechanical loading conditions (stretching, shearing) during their use.

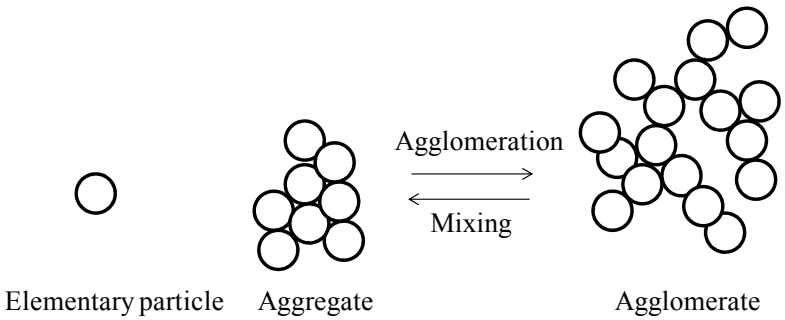

Figure 6: Schematic representation of particle structure.

In order to achieve the best performance it is necessary to limit the filler-filler interaction because they could provoke an aggregation phenomena, which would decrease the composite performance. An improvement in composite materials can be obtained minimizing interaction between the filler. Common nano-sized fillers aiming to improve mechanical properties of elastomers include carbon black (C_{black}), silicon dioxide (SiO_2), calcium carbonate ($CaCO_3$), barium sulfate ($BaSO_4$), magnesium hydroxide ($Mg(OH)_2$), clays ($Al_2O_3\ 2SiO_2\ 2H_2O$), etc.

Due to their major importance, a detailed description of only the first two fillers is reported below.

Carbon black was one of the most commonly used reinforcing fillers, which has been partially replaced by silica due to a more friendly environmental impact. It consists of

spherical particles with diameters from 10-600 nm, fused into aggregates. Depending on the process and the formation conditions, it can contain many individual particles or, on the contrary, aggregates of very different shapes. Carbon blacks are prepared by incomplete combustion of hydrocarbons or by thermal cracking and are classified into furnace blacks, channel blacks, thermal blacks, lamp black and acetylene black, depending on their method of manufacture. The major types of rubber reinforcing carbon blacks are manufactured by the furnace process. Moreover, due to its color, it is an excellent absorber of light. In fact, it absorbs most of the ultraviolet components of sunlight, which can otherwise initiate oxidative degradation of the rubber. The incorporation of carbon black into rubber, is easily achieved due to their similar affinity; in the final composite properties it enhances the modulus, resistance to fatigue and abrasion, in addition to better overall technological characteristics.

Silica is a user name for silicon dioxide (SiO_2), assigned to different minerals belonging to the silicate class. In its pure form, silica is white, insoluble in water, and slightly soluble in alkali and in a dilute hydrofluoric acid.

In the silica structure, silicon atoms are at the center of a tetrahedron of four oxygen atoms, bridging two silicon atoms. Two different forms of silica are commercially available for various industrial applications, namely crystalline (natural) silica and amorphous (synthetic) silica. The last one is commonly used for polymer composites.

Depending on the method of preparation, the amorphous silica is mainly classified into three forms: precipitated silica, fumed silica or pyrogenic silica, and silica gel.

Precipitated silica is produced from sodium silicate, obtained from sand and sodium carbonate, in aqueous[31,32,33] solution through its reaction with sulfuric acid.

$$3\ SiO_2 + Na_2CO_3 \rightarrow 3\ SiO_2 \bullet Na_2O + CO_2$$

$$(SiO_2 \bullet Na_2O)_{aq} + H_2SO_4 \rightarrow SiO_2 + Na_2SO_4 + H_2O$$

The sulfuric acid hydrolysis of the sodium silicate (see Figure 7), leads to the formation of silicic acid $Si(OH)_4$ which, by polymerization, creates silica nuclei.

From these reactions it is quite evident that the concentration of the remaining Na_2SO_4 is one of the quality factors. Therefore, hot water washing is required in the final step in order to purify the silica obtained at the end of the process.

Concentration of reactants, rates of addition, fraction of theoretical silicate in the reaction, and temperature are the process variables which determine the properties of the final

product, such as specific surface area, porosity, primary particle and agglomerate size and shape, brightness, density and hardness. Rhodia and Degussa are the main producers of precipitated silica, and their materials are often used as a reference for new silica preparation processes.

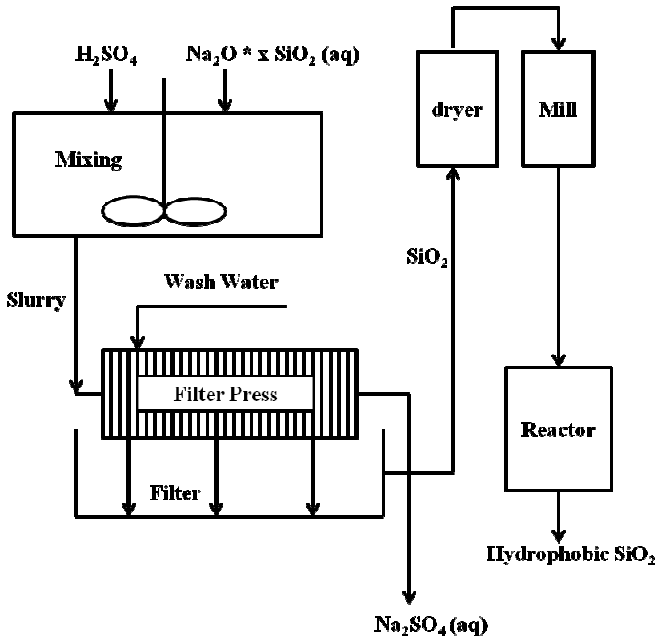

Figure 7: Chart of the industrial process for the preparation of precipitated silica.

Fumed silica (see Figure 8) is produced from the reaction of metallic silicon and gaseous dry HCl to form silica tetrachloride $SiCl_4$, which is mixed with hydrogen and oxygen and fed into the burner tube of the reactor at a temperature higher than 1800°C.

$$SiCl_4 + 2\ H_2O \rightarrow SiO_2 + 4\ HCl$$

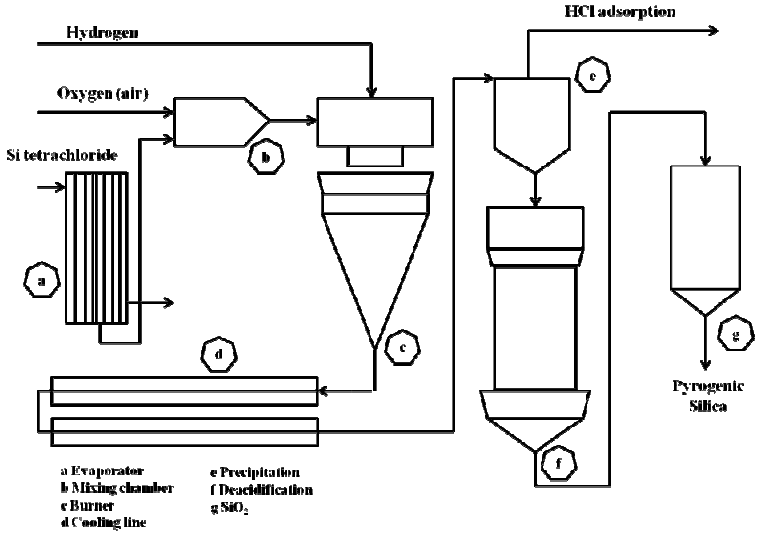

Figure 8: Chart of the industrial process for preparing fumed silica.

The HCl formed in the process is recycled. When the primary particles of silica leave the burner, they are in a molten state; therefore, during their collision they are able to increase their dimension.

When particles proceed through the reactor, they cool down; at around 1710°C, and recombine producing aggregate and agglomerate.

Agglomeration, also occurs in the collection process due to the exposition to the air. The last type of amorphous silica is silica gel, which is produced according to the following reaction:

$$Na_2O\ (SiO_2)_x + H_2SO_4 \rightarrow x\ SiO_2 + Na_2SO_4 + H_2O$$

The product of reaction contains about 75% H_2O and is subjected to a drying process. Drying takes place in a rotary kiln followed by milling of the material that has been previously washed with hot alkaline water (which reinforces the matrix, decreases shrinkage, and produces larger pores).

Super-critical drying or replacing water by methanol before drying, decreases the crushing force and produces aerogels which have up to 94% air space.

The average particle size is in a range from 2 to 15 mm. The specific surface area is very high due to the high porosity (40-850 m^2/g).

Silica lattice, which consists of silicon and tetrahedrally bound oxygen in a imperfect three-dimensional structure, has a strong polar surface group, mostly constituted by hydroxyl groups bound to the silicon center, known as silanol (-Si-O-H).

The imperfections in its lattice structure provide free silanol groups on the surface.

The number of silanols [34,35,36] and their distribution depends on the method of preparation. The type and concentration of these surface silanol groups significantly influence the processing and final properties of the composites.

Three different types of silanol groups are formed -isolated (-OH groups on the separated silicon atom), geminal (two -OH groups on the same silicon atom), and vicinal (-OH group on the adjacent silicon atoms).

These functional groups are arbitrarily located on the filler surface. Isolated hydroxyls exists predominantly on dehydrated silica, fumed silica, and to a lesser extent on precipitated silica (see Figure 9).

Vicinal hydroxyls have stronger adsorption sites and hence, have a stronger reinforcement effect than isolated hydroxyls.

The different types of synthetic silica differ on particle size and specific surface area.

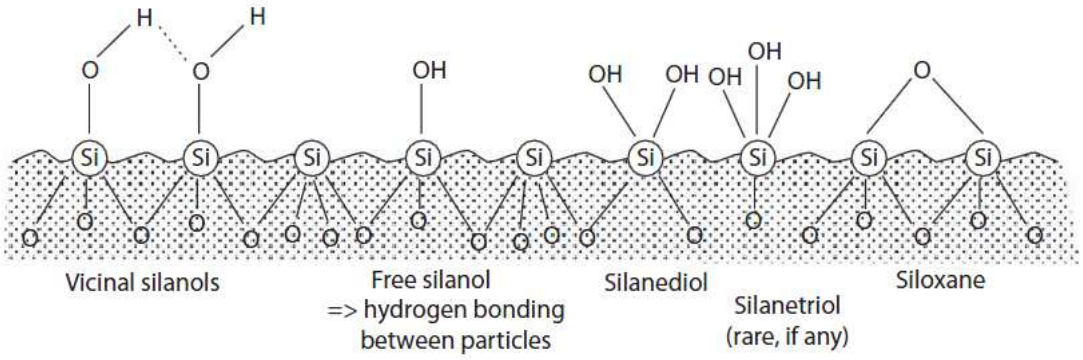

Figure 9: Surface chemistry of the silica.

Due to the presence of highly populated surface silanol groups, there is a tendency of primary particles to aggregate and further associate through strong hydrogen bonds to form agglomerates.

Usually the high shear forces generated during the compounding process, can break the relatively stable agglomerates but may not disrupt the aggregates formed by the primary filler particles.

Compared to carbon black, silica generally offers less affinity to elastomers due to the silanol groups present on the silica surface which behave as acids. In order to increase the compatibility of silica with the polymer, the filler surface has to be modified by physical and chemical methods.

Therefore, research on new syntheses to change the silica surface, in order to make the filler a more reactive ingredient for rubber reinforcement, opens up new perspectives for the generation of innovative composite materials; this might great benefit to industry.

Physical modification results after weak interaction between the adsorbed surface modifier and the polymer matrix and the filler surface through polar interaction, hydrogen bonding and acid/base interactions. An example of physical modification is reported by Wen[37], who modifies physically the silica nanoparticles surface by absorption of poly(ethylene oxide) in presence of selective solvent[38].

Consequently, the filler network can be dispersed better in a rubber matrix and the finished materials show less viscosity and hardness than composite where filler has not physical modification.

Regarding the chemical modification of the filler surface, two methods are available:

a) Chemical graft on a filler surface can change filler characteristics (this takes place when the surface modifier and the filler surface have a strong interaction, and the adsorbed surface

modifier and polymer have a weak interaction). In this case the functionalization of silica surface with various organic moieties can be made by reaction of the silanol group on the silica surface (previously prepared) with alkoxysilane functionalized with wanted group. Many different silanes with a large variety of organic moieties are commercially available for that purpose. Unfortunately, the distribution of functional molecules is limited by the number of OH group available on silica surface.

Another common method is the co-condensation method by using only one direct step graft for synthesizing functionalized silica surface.

In detail, during the synthesis of the silica, with the precursor of metal oxide some molecules of precursor of functionalizing species are added together. With this synthetic approach, it is possible to control the distribution of the functionalization molecules and ensure that all the precursor of functionalizing molecules are present on the inorganic particles surface.

b) Graft chemical groups can react contemporaneously with the filler as well as with the polymer.

It is the case of special functionalizing molecules, which in the same instant, can react both with inorganic particles surface and with the polymer. This method can occur during the inorganic particles synthesis or on particles previously formed.

In depth, these coupling agents can form a stable bond between organic and inorganic materials. The interface thus formed, in such materials, has became a dynamic area of chemistry in which surfaces of filler and polymer have been modified in order to generate the required properties.

2.3. Preparation method

Preparation of composites is one of the fundamental and important steps which influences the interaction between organic and inorganic parts.

Elastomer composites may be prepared according two different preparative methods: blending and *in situ* synthesis.

Commonly, blending method is used to prepare composite applied in tire application.

The last one may regard the synthesis *in situ* of the inorganic part (*in situ* sol gel method) or the synthesis *in situ* of the organic part (*in situ* polymerization).

Moreover, the sol gel method can be differently classified depending on the system in which the synthesis is carried out: aqueous or non aqueous.

2.3.1. Blending

Solid rubber and other materials such as fillers and various additives have to mixed together to obtain compounds. This can be realized with either of two machines: internal mixer and two-roll mill.

From the industrial point of view, the most economical mixing and environmental friendly technique used for preparing elastomer composites is melt compounding[39]. This technique, also called blending, is the easiest, simplest, fastest and traditional preparation and uses a top down approach.

Materials in the solid state (SiO_2 powder, dry polymer etc.) are thermo-mechanically mixed by a closed mixer. The mixing of rubber with compounding ingredients, such us a fillers, is a rather complicated process since components differing in structure, viscosity and rheological behavior have to be homogenized.

During the mixing, several physical processes take place: the adsorption on the polymer or other additives onto the filler surface and the incorporation of polymer into voids of the filler structure. In addition to these characteristics, the internal mixer (the equipment) does not modify the chamber volume during their use; therefore, sometimes it can take a long time to adjust the mixing conditions.

In order to guarantee a homogeneous blend of polymer matrix, fillers and compound ingredients, there are three physical mixing process steps: *i)* Laminar mixing: the first mechanism of the mixing process is deformation of the rubber matrix; *ii)* distributive mixing (the randomness distribution of principal components within a matrix (masterbatch)); *iii)* intensive or dispersive mixing (breakdown of filler agglomerates into smaller aggregates).

The most challenging part of rubber mixing is the dispersion of the filler; it is important to create a homogeneous network in the rubber matrix in order to optimize particle size distribution.

During the thesis, BraBender and Haake Rheomix are common internal mixers used in lab scale; while Banbury (see Figure 10) is internal mixer used in pilot scale. Therefore the volume of the chamber which is the difference among them varies from less than a few hundred cubic centimeters to more than 1200 liters.

The mixers differ also for the type of mixing rotors, their variable design, the numbers of wings and the blade angle relative to rotation. Small batch mixers, such as a Brabender or a Haake Rheomix are used for product and process development work.

Figure 10: Internal mixers for compounding.

During the mixing process several parameters must be tailored: the energy input for the rotation of the rolls, rotor speed, the mixing time, the heating and cooling profiles.

To summarize briefly, fillers and rubber are placed into the device and pushed by a piston in the chamber in order to mix, where the two rotors mix and compact the materials, thus giving rise to the compound.

All of these processes are done in a temperature controlled environment. Therefore, the mixing takes place at high temperatures (melt blending between 90-150°C), which significantly improves the workability of the rubber.

The advantage of this method is that it can be useful for industrial composite preparation because it requires less time and cost production.

Another great advantage consists in the possibility of incorporating different polymers at the same time.

Unfortunately, the blending limits regard the limited ability to disperse large aggregates, which sometimes cause an inhomogeneous dispersion of fillers in rubber matrix, especially in the case of hydrophilic and polar filler as silica and not matching the hydrophobic and non-polar nature of polymer.

In the case of silica as a filler, in order to overcome the incompability between the two components, it is necessary to add a compatibilizing agent during the mixing step [40, 41, 42] it interacts with both polymer and the hydrophilic filler surface[43]; the most used *compatibilizers* are those of the silane coupling agent family.

Surface modification of silica with silanes may generate the following performance benefits: improve stability of the filler and rubber networks, change surface characteristics (water

repellency or hydrophobicity), improve filler dispersion (reduce filler agglomerates by reducing the amount of OH groups) and improve mechanical and rheological properties.

The most common silane coupling agents, in commercial use for tire application, are TESPT (bifuctional silane linked by a tetrasulphur chain) and TESPD (bifuctional silane linked by a disulphur chain).

The role of these special molecules with their functionalities is to interact both with polymer and silica[44,45,46].

The action of TESPT can be subdivided into two separate reactions. First, ethoxy groups react with silanol on the silica surface during the mixing. In addition, polymer-filler bonds are formed by the reaction of the tetrasulphide group with polymer under curing conditions. Therefore, this coupling agent contains a hydrophilic silane and hydrophobic chain able to interact with rubber.

Obviously, the amount of these molecules strongly influences the vulcanized properties and both the filler-filler and filler–rubber interactions.

The two-roll mill (open mill) is another instrument for rubber compounding, which can be used to add a small amount of ingredients to the composites or to prepare a sheet.

This open mixing reactor consists of two adjacent, hardened-steel rolls which are set horizontally. The rolls rotate at the set up speed in an opposite direction, in order to produce a friction or grinding action between the rolls. The mixing process involves a breakdown and mastication of the composite.

At lab scale in this thesis, the two roll mill is used to add small amount of ingredients. When the composite becomes soft, the ingredients can be added. The two-roll mill is a mixing method that is entirely dependent on control by the operator. During the processing, the powders drop into the mill tray, to be collected by the operators and added back to the compound. Moreover, in order to improve the dispersion of the ingredients, folding and cutting are continuously done.

Rubber compound behavior on two roll mill mixing depends on its flow characteristics and on the method adopted. An optimal compounding behavior consists in banding around the working (front) roll during the loading, and rolling bank, with little or no stagnation of the bands which have not remained in full contact with the roll mill[47].

Sometimes after mixing, the compounded rubber has to be formed into a shape for vulcanization process; for this reason open two-roll mills can be used.

2.3.2. *In situ* sol-gel method

An alternative approach to thermo-mechanical mixing is the *in situ* generation of metal oxide particles in rubber matrix by sol-gel process which allows the formation of organic-inorganic hybrid[3].

The sol–gel process can be defined as the conversion of a precursor solution into an inorganic solid. The precursor is either an inorganic metal salt or a metal organic species like a metal alkoxide or acetylacetonate. The oxygen for nanoparticle formation is provided by the solvent (water, ethers, alcohols, ketones or aldehydes) or by the organic constituent of the precursor (alkoxide or acetylacetonate).

The sol-gel method[48], applied to metal oxide growth, consists of a few basic steps: hydrolysis and polycondensation of metal oxide precursor, gelation, aging and drying[49] (see Figure 11).

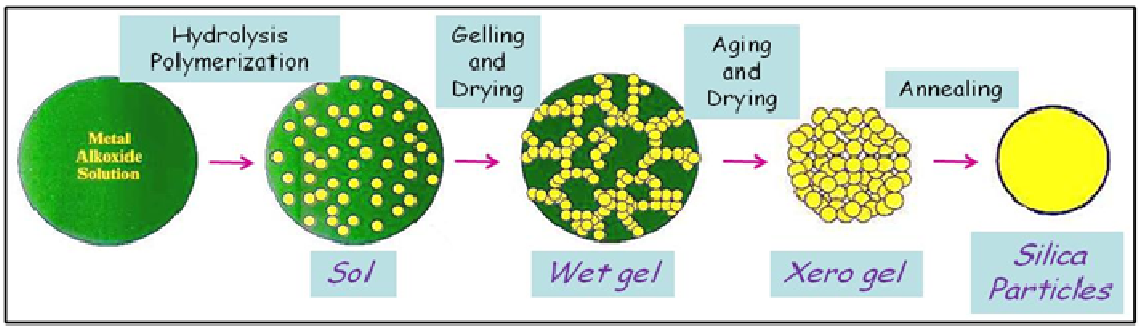

Figure 11: Scheme of the sol-gel process applied to the formation of metal oxide powders.

The first step of the sol-gel method is *sol* formation (dispersions of colloidal particles in a liquid). It results from the hydrolysis reaction of metal alkoxide and appears as a stable colloidal dispersion of particles.

Colloids, thus formed, are solid particles with diameters of 1-100 nm; while gel is an interconnected and rigid network, with pores of sub-micrometer dimensions, and particles chains whose average length is greater than a micrometer.

Theoretically, through the hydrolysis reaction the sol formed is reversible. In order to decide which direction the reaction takes, it is necessary to choose between acid or basic catalysts. Therefore, the correct catalyst choice influences the kinetics of both the hydrolysis and condensation reaction, determining the end shape of the particles. If sol-gel reactions were carried out by using acid catalysts (see Figure 12), hydrolysis is faster than condensation

reaction, and particles tend to assume an elongated shape since they only grow in one direction.

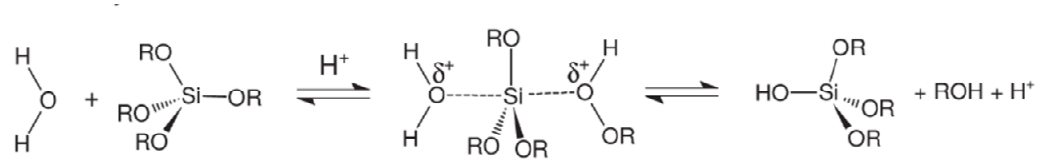

Figure 12: Acid catalysis mechanism for TEOS.

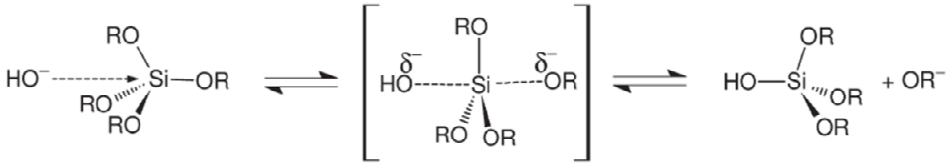

Figure 13: Basic catalysis mechanism for TEOS.

Instead, if the reactions were carried out in a basic environment (see Figure 13), the condensation reaction will be more rapid, and the particles will tend to have a spherical shape.

Due to these factors, pH control is fundamental in order to obtain the desired particle shapes (see Figure 14).

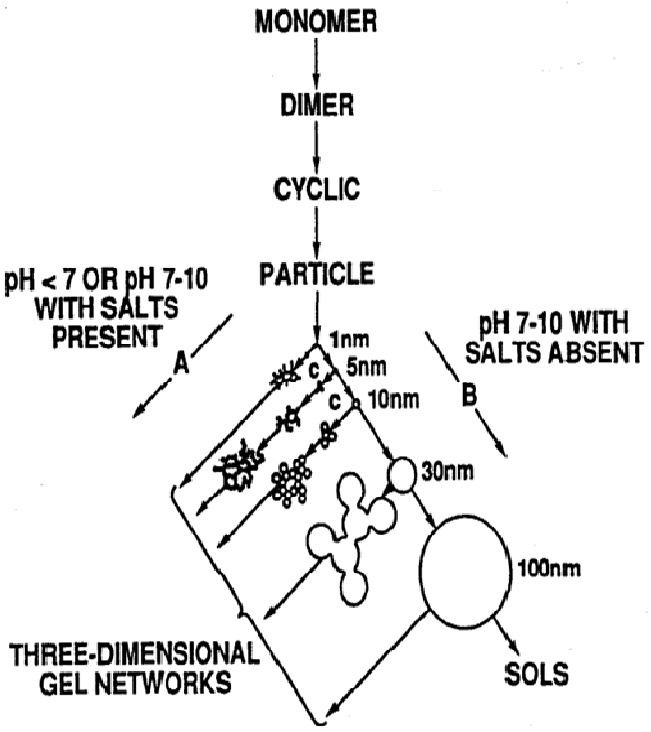

Figure 14: Influence of pH synthesis on particles shape[42] .

In the sol, the increase of viscosity is due to the gradual condensation of the particles trapped inside the water during the network formation. Therefore, during this phase, called gelation, the process continues to form wet gel.

Thereafter, the solvent has to be removed from wet gel during the drying and aging step of the process; shrinkage of the pores occurs. Throughout this part the network that has been created can be modified by structural rearrangement in its conformation.

In depth, the gel consists of a porous, three-dimensionally continuous solid network surrounded by a continuous liquid phase.

During the thermal treatment that occurs between 100-180°C, physically adsorbed water is completely evacuated from the gel. During the aging step, heat treatment of gel, at elevated temperatures, substantially reduces the number of pores and their connectivity due to viscous-phase sintering [50, 51].

Moreover, the synthesis can be done at lab scale in three different kinds of apparatus: in a flask immersed in an oil bath, in a Teflon autoclave or in a glass tube immersed in a microwave field. Each of these synthesis methods allows different parameters set up of pressure, heating and stirring.

The huge interest in this technology reflects its potential for making materials or composites at low-temperatures.

One of the most exciting opportunities offered by sol–gel processing is the possibility to create hybrid materials with organic and inorganic components mixed at the molecular level, where small diameter particles of metal oxide are uniform. In general, the goal of sol-gel processing applied to nanocomposite preparation is to control the surfaces and interfaces of materials during the earliest stages of production.

Metal oxide nanoparticles used can damage the body's natural defenses and causes allergies. Workers in nanotech industries are at risk due to exposure to high concentrations of nanoparticles. Therefore, the growth of nanoparticles inside the rubber could be a solution for reducing these potential health problems (such as respiratory problem, calcinogenic). The sol-gel process used for inorganic material synthesis can be considered a new way of decreasing exposure to dangerous nanoparticles in factory environments.

Within the rubber, by means of a silica precursor and the sol gel method, it is possible to produce nanocomposites with better dispersion of silica particles. Therefore, this can be considered the main advantage of the technique.

By adding a suitable amount of functionalizing precursors to the silica precursor at the beginning of the filler particle growth, a new way to create functionalized particles in the rubber is created in one step. In addition, the presence of the functionalized molecules between particles may reduce their aggregation effect.

2.3.2.1. Aqueous sol-gel method

Metal alkoxides are the most widely used precursors for sol-gel processes in aqueous systems; their chemical transformation into oxide network is provided through the oxygen supplied by water molecules[52].

According to the literature, one of the major uses of the sol gel process is for the preparation of silica, which is useful for different applications, starting from the most common silica alkoxides precursor: tetraethoxysilane (TEOS) (see Figure 15).

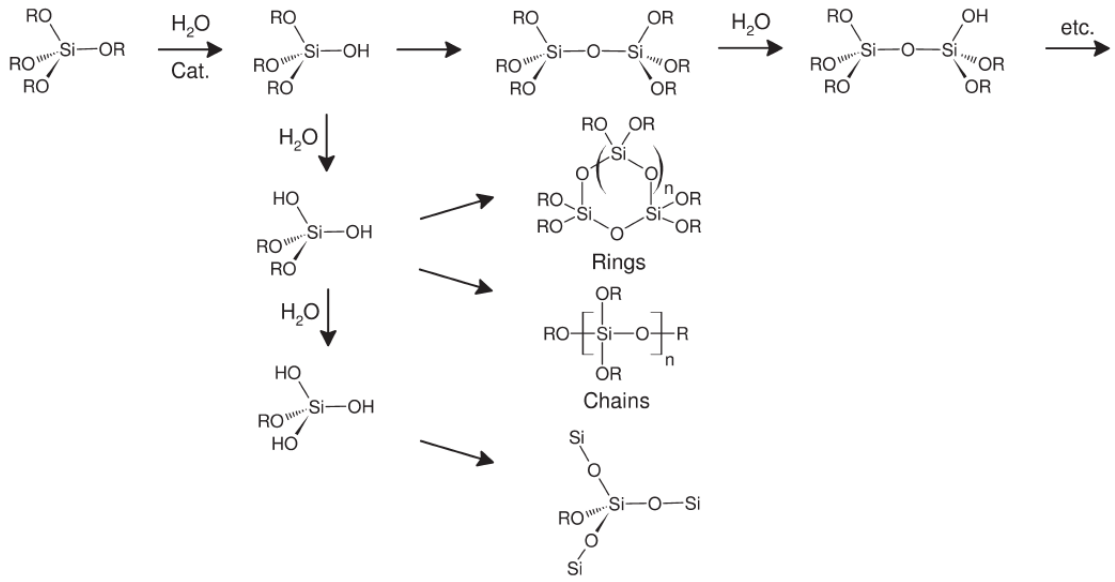

Figure 15: Fundamental reaction steps in the sol-gel process based on tetriaalkoxysilanes [53].

In 1968, Werner Stöber[54] et al. published a work about the generation of monodispersed particles (diameters between 50 and 2000 nanometers) of silica starting from TEOS which is added to an excess of water containing a low amount of ammonia and a small amount of alcohol (EtOH).

Following the Stöber method, many contemporary research works have described the process modification of nanosilica particles previously synthesized. In particular, in 2003 Seong Huh[55] et al. published a paper for silica production by using a different molar ratio

between solvent, silica precursor, ammonia catalysis and varying the synthesis time and temperature.

They were both able to control particle morphology by changing the size and shape (from spheres, rods and hexagonal tubes) through the addition of a suitable amount of various organoalkoxysilanes to TEOS, chosen with a different degree of hydrophilicity/ hydrophobicity character, which functionalize the silica surface.

Regarding the preparation of elastomeric nanocomposites by the sol gel method, in the literature many works describe different synthetic approaches, starting from different rubber phases: solid or liquid (latex solution).

In the last ten years, Yoko Ikeda [21, 56, 57, 58, 59, 60, 61, 62, 63, 64, 65] et al. have described the silica sol-gel formation in natural rubber composites by using solid rubber.

In detail, the synthesis starts with the swelling of thin NR sheet in TEOS for several hours at room temperature, followed by immersion in a catalyst solution (n-butyammine) in 40°C for 72 hours and concludes with air and under vacuum drying .

Messori et al.[66,67] show a similar approach: they start with the swelling of rubber sheets in toluene, followed by the addition of TEOS, DL (dibutyltin dilaurate, as a sol-gel catalyst) and DCP (dicumyl peroxide) and complete with an exposition to the environmental humidity of the samples to activate the hydrolytic reaction of TEOS.

A similar approach is given by Poompradub [68,69], who prepares the composites by using THF for swelling and n-hexylammine as a catalyst, which can generate a major amount of silica *in situ*.

Analogously, Bandyopadhyay[70,71] dissolves rubber in THF/$CHCl_3$/CCl_4, with HCl as the acid catalyst that hydrolyzes TEOS for the preparation of a NR composite.

An alternative approach is given by Siramanont[20] and Tangpasuthadol[72], who prepare composites from rubber latex adding together different silica precursors, followed by the aging of the material for lengthy period in an oven.

This work, is the only one which uses different kinds of silica precursors (TEOS, VTEOS, ETEOS, BTEOS) having one of the four chains that are suitable moieties to modify the degree of the silica particle dispersion during the synthesis.

In detail, tetraethoxysilane, viniltrietoxysilane, ethyltriethoxysilane, isobutyltriethoxysilane are used in order to improve the dispersion of the silica in the polymer due to the functionalizing previously produced. In fact, using different sizes of structures of

hydrocarbon moieties present in silica precursor can increase the compatibility of this rubber without reacting together.

Another advantage, presented in these works regarding the preparation of nanocomposite thought sol gel method, is the use of rubber, in particular NR latex, that contain a small amount of ammonia, which in sol gel transition can be as a catalyst without the need of further catalysts addition.

Very recently, another option given by Watcharakul[73] et al. report the sol-gel formation of silica particles within the rubber modified by copolymers which is suitable to chemically interact with the silica surface (PMMA).

Their synthesis was performed both in solid state and by using silica precursor in latex. Regarding composite preparation starting from polymer latex, inhomogeneity dispersion of the filler network among the rubber matrix is shown. Furthermore, the authors with their synthesis are not able to introduce more than 10% in mass silica filler.

However, in the literature there are no works available on the functionalized silica synthesis *in situ* into rubber with moieties, which are strongly linked on the silica surface and can change the huge compatibility difference during the composite preparation. In fact, small amounts of functionalizing molecules added during the synthesis of filler may influence the morphology of the particles (in terms of shape, surface area, porosity, size), the homogeneity of the network and the interaction with the rubber. Within the different chemical groups present, no works are reported to explain the composite mechanical behavior obtained with the charge, surface area, shape and functionalizing molecules located on filler surfaces, and the degree of their interaction with polymers.

Moreover, there are also no in depth studies on the relationship between the morphology of the particles, which have functionalizing molecules on the surface, and the mechanical properties, in order to explain the filler-filler and filler-rubber interactions shown.

In addition, a profound explanation of the mechanical behavior of composites, obtained from different kinds of fillers respect to SiO_2 or mixed fillers, the distribution degree of the obtained filler and the interaction among the rubbers are completely absent.

In comparison, with the blending technique preparation, the generation of filler in rubber by aqueous sol-gel method offers a new way to produce composites with more homogeneous dispersion of the filler in rubber matrix made with a smaller size of the particle aggregate. Furthermore, it is possible to generate functionalized or mixed fillers at the same time

during the synthesis of the composites, which requires less strong conditions in terms of temperature.

Unfortunately, working in water can, in the case of the silica as a filler, increase the number of hydroxyl groups on particle surfaces, making them less compatible with the rubber and favoring the aggregation of the particles. Another disadvantage is that sometimes the preparation synthesis requires the use of filler precursors or functionalizing molecule precursors, which react rapidly in water by decomposing.

2.3.2.2. Non-aqueous sol-gel method

Through the mechanism of the non-aqueous sol-gel method, as opposed to aqueous, the oxygen for nanoparticle formation is provided by the solvent (ethers, alcohols, carboxylic acid, ketones or aldehyde) or by the organic constituent of the precursors (alkoxides, acetyacetonates). This process can also be called non-hydrolytic method if during the hydrolysis reaction of halide metal oxide precursors, hydroxyl groups are formed[52].

The advantage of this method is the absence of water in mass, which improves the kinetic reaction rate during the sol-gel transition.

In fact, the presence of large amounts of water helps the metal oxide precursors to react quickly. In addition, the rapid reaction with water of the metal oxide precursor, does not allow a full study of the growth mechanism of the particles in the early stage of the synthesis.

Therefore, the non aqueous route can provide an attractive alternative way to hydrolytic synthesis for the preparation of nanocomposites with control of the homogeneity of metal oxide growth at the molecular level homogeneity.

The main advantage, in comparison with the aqueous sol gel route, is that the non-hydrolytic method used with metal oxide precursors which react quickly with water, to control better their hydrolysis and condensation rate reaction.

Moreover, this method can improve the addition of another metal oxide or the doping during the synthesis.

Regarding the silica production *in situ* within composites, the low presence of water can reduce their aggregation in the rubber matrix, improving the distribution of particles due to small amounts of OH groups on the surface.

In agreement with the literature and regarding silica preparation, the majority of synthesis starts from silicon alkoxide or halide.

A group form Montpellier, A. Vioux [74,75,76,77] et al. reviewed and found that a simple method to produce silica is to thermally decompose metal alkoxide (carboxylate) precursors (in the temperature range 200-300°C), where hydroxyl groups are produced via a cyclic elimination mechanism that removes alkene molecules (see Figure 16).

Another non-hydrolytic synthesis combined with the hydroxylation method is provided by the reaction of alcohols with halides.

The reaction of primary and secondary alcohols with tetrachlorosilane usually allows the preparation of tetraalkoxysilanes[78], instead with ternary alcohols (Benzyl alcohols, BzOH) the reaction for silica preparation gives some sub products, corresponding to alkyl halide and RCl[79] respectively.

Both reaction modes, at the beginning of the reaction, involve the coordination of an electron pair of alcoholic oxygen atoms linked to the silicon center; the atoms contribute to the successive cleavage of the hydroxyl or the alkoxyl group (see Figure 16).

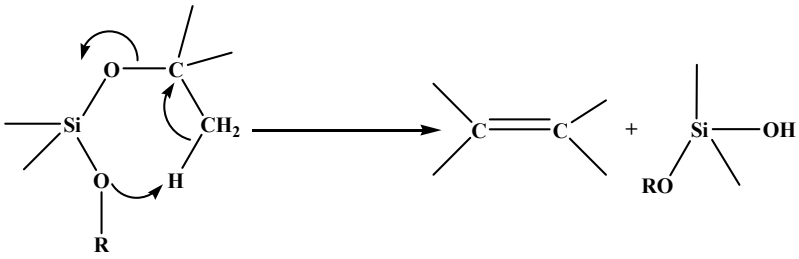

Figure 16: Thermal decomposition of metal alkoxide/carboxilate.

Another interesting method of non-hydrolytic hydroxylation is the reaction of carbonyl compounds (such as ketones) with basic metal alkoxides, which are able to induce ketolization.

An attractive point of the formation of an oxobridge during the non-hydrolytic method is related mostly to the condensation reaction between two different functional groups bonded to two different metal centers, which during their reaction eliminate small organic molecules (see Figure 17).

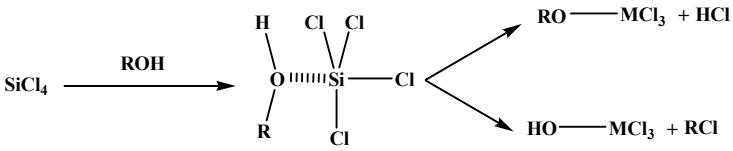

Figure 17: Alcohol and halide reaction [80].

Therefore, the formation of the metal-oxygen-metal bond as the basic structural unit can be summarized in only five different pathways[81]: alkyl halide elimination, ether elimination, condensation of carboxylate groups (ester and ammine eliminations), C-C coupling of benzylic alcohols and alkoxide molecules and aldol-ketimine condensation. (see Figure 18).

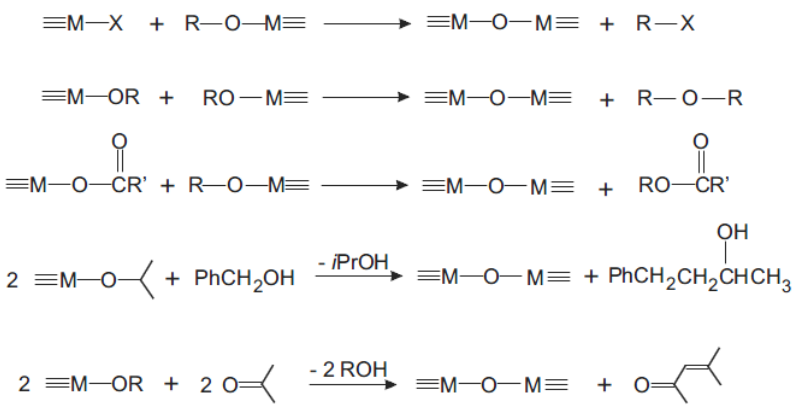

Figure 18: Main condensation steps in non-aqueous sol-gel process resulting in the formation of metal-oxygen-metal bond [52].

It is evident that it is possible to choose different solvents and oxide precursors which reacting together may produce different filler morphologies. Moreover, this synthesis can easily be varied, by adding the precursors together at the beginning of the synthesis, to produce a mix of two or more metal oxides, with a good ratio control [82,83].

This method is less applicable for the preparation *in situ* of metal oxide particles in elastomer composites; sometimes due to the formation of the sub products it is difficult for them to be removed and to use the metal oxide precursor (such us halide) which can react with the rubber by degrading it, before obtaining the desired metal oxide.

Another approach, not non-hydrolytic, but non-aqueous sol-gel method, is to add two simple components, which can generate water *in situ* during the reaction, to metal oxide precursors. It is evident that a parallel reaction has to produce water in small amounts, which must not be present as an initial reactant.

This route involves the condensation of an alcohol with a carboxylic acid to form an ester and a water molecule, or by the condensation of two alcohols forming an ether and water, or by the elimination of water from tertiary alcohols.

Non-aqueous sol-gel approaches to obtain silica filler for elastomer composites have been rarely used in the literature.

J. N. Hay et al.[84] first reported the formation of polystyrene/silica hybrid by using these approaches. In particular, the polymerization of styrene monomer using AIBN and the formation of silica gel by non aqueous processes simultaneous is shown.

Another example, was done by Sharp[85] et al group, which studied the effect of carboxylic acid and alcohol on the gelation steps of silica prepared from TMOS (tetramethoxysilane) and TEOS (tetraethoxysilane).

2.3.3. *In situ* polymerization

Generally, this method involves the dispersion of fillers, previously synthesized, in monomer(s) or in dissolved polymer. The formation of the nanocomposites occurs during the polymerization reaction of the monomers and follows the removal of polymerizing solvents.

Often for the production of *in situ* polymerization composites nanofillers are modified by functional groups or with monomers or with initiators which can start the polymerization reaction. Therefore, the main requirement is to physiadsorb or graft molecules on the filler surface. In this way, it is possible to grow the polymer around the filler particles, improving the dispersion of the filler in rubber[7, 86].

For this reason two different approaches are possible to be used to graft polymer chains or a polymer initiator on the filler surface: “grafting-to” and “grafting-from” techniques.

In the grafting-to approach, functionalized polymer chains react with a special site allocated on the filler surface.

The relatively easy formation of the composites is influenced by the degree of attachment of polymer chains with spatial hindrance to filler surface. Therefore, the composites shows a low grafting densities.

In the grafting-from approaches, the polymer chain is directly grown from the inorganic particle and depends on the degree of functionalizing molecules which are able to start the polymerization.

Through this method, it is possible to control the amount of polymer which surrounds the filler particles to change the interaction between these two main parts. It is clear that these approaches create nanocomposites characterized by a high grafting density.

Therefore, silica-rubber composites can also be synthesized via a surface-initiated living radical polymerization with a reversible addition fragmentation chain transfer reaction (RAFT).

2.4. Tire application

2.4.1. Tire structure

Since the invention of the pneumatic tire, fillers have played an important role in tire performance, together with that of the polymer. A deep understanding of the role of the rubber and filler within the elastomer composites can be exploited to tune the final properties of the tire. Before an explanation of the basic functions of the tire, a full description of tire construction will follow.

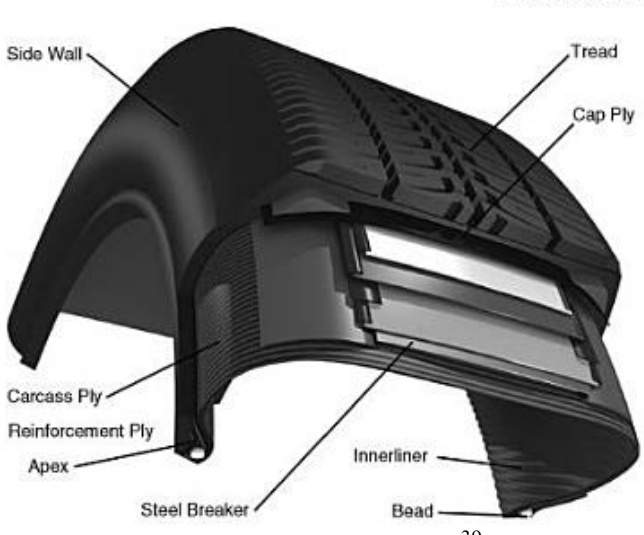

Figure 19: Tire construction[39].

The pneumatic tire consist of two basic areas: the tread, which is responsible for the ground contact, and the casing whose function is to support load and transmit power to the tread area (see Figure 19). These components can be broken down further to distinguish properties and functions in relation to performance. Varying these properties and functions permits the tweaking of the performance to meet specific rendition targets.

The rubber compounds used in these basic components have three main roles: i) contact area between the vehicle and the road surface; ii) cohesive material that holds the tyre together allowing it to act as an integral unit; iii) protection for the strength-bearing components.

The *tread* is the part of the tire in contact with the road at a given moment in time, and is composed of two subcomponents that allow to tune performance: outer and under tread.

The outer is characterized by the geometric shape (voids, grooves, lugs and sipes) that enable maximum contact with the road under all circumstances.

Contrarily, the under tread functions as a transition component and reduces tire rolling resistance. As a result, treads are designed and compounded for low rolling resistance, traction, abrasion and high protection of the casing.

The *sidewall* is the segment of the tire adjoining the beads and tread. The sidewall formulation is designed to protect the ply and must have resistance to weathering, ozone, abrasion, and tearing yet providing flex fatigue resistance. On the other hand, the *bead* is a combination of different strands of high-tensile, copper or zinc steel wires coated with rubber and formed into inextensible rings. These provide anchorage to the carcass plies and retain the inflated tire on the rim of the wheel.

In the steel belted radial automotive tire the ply is usually a flexible textile of polyester or nylon. On the other hand, on trucks the steel belted radial tire usually uses a steel cord ply.

The *innerliner*, or liner is a thin layer of rubber located on the inside of the tire with the purpose of retaining tire inner pressure.

The elastomers used in tire compounds, and particularly tread parts, are important to the structural design parameters of the tire. A properly designed tread compound guaranties best tire performance targets. Tread compounding materials fall into one of five general categories: polymers, fillers, protectives, vulcanization system and various special purpose additives.

2.4.2. Tire compounding and vulcanization: ingredients and their role

Associated with each tire component is a rubber compound formulated specifically to achieve the optimum balance of properties required for that particular part of tire.

The preparation of the tire goes through several stages: raw material handling, mixing, forming and vulcanization.

A typical rubber formulation[87] consists of four basic components: the polymer, filler or particulate reinforcement, protectives and vulcanization system. In addition, a series of secondary materials such as a compatibilizers, resins, processing oils, and short fiber reinforcement may be included in the formula. The first two ingredients have been discussed in chapter 2.2.

The protective system[88] has to be added in order to control aging and the degradation of the rubber composite accelerated by a number of factor including heat, heavy metal

contamination, light, moisture, dynamic fatigue, oxygen and ozone. These ingredients are called *antidegradants.*

In addition, most of the natural and synthetic rubbers containing unsaturated backbones that are susceptible to degradation, have to be protected.

Moreover, particular attention needs to be paid to the choice of the antidegradant system, polymer type and cure system, which have to adapt to the compound formulation to optimize the degradation resistance.

Generally, antidegradant agents can be divided into three categories: antioxidants, antiozonants and waxes.

Antioxidants react with oxygen to prevent oxidation of vulcanized rubber and react with free radicals that degrade vulcanized rubber. They are the most commercially used antidegradants, because they are able to protect rubber at temperatures below 120°C.

Oxidative degradation of the polymers is considered a free radical process and consists of three steps: initiation, propagation, and termination. Free radicals are formed during initiation reactions. Energy from heat, mechanical shearing or high energy radiation can dissociate the chemical bonds in the polymers (RH) resulting in the formation of free radicals ($R^{\bullet}$). In auto-oxidation mechanisms of polymers, the molecular reaction is promoted by thermal energy. In this reaction the first free radicals form in the polymer and initiate a reaction of oxygen with the polymers.

During the auto-oxidation advance reaction, the concentration of hydroperoxide which decompose producing alkylperoxyl ($ROO^{\bullet}$) radical (see Figure 20). The alkyl and alkylperoxyl radicals are the chain-propagating species.

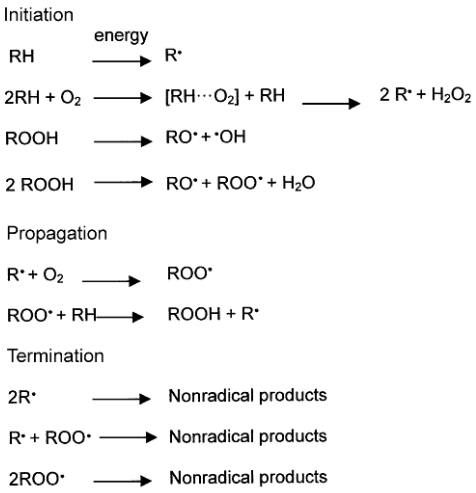

Figure 20: Mechanisms of polymer degradation by oxidation under thermal energy.

Termination occurs when two free radicals, alkyl and/or alkylperoxyl radicals, react together to form the stable non-radical products.

Antioxidants are used during processing, storage and service, inhibiting the rate of the auto-oxidation reaction. The protection factors depend on the temperature. In fact, the protection increases with decreasing temperatures and increasing concentrations of the antioxidant[89].

Commercially available antioxidants can be divided into three categories: phenolic antioxidants, aromatic amine antioxidants and hydroperoxide decomposing antioxidants.

Phenolics act as a chain terminator and in general are non staining and non discoloring.

Aromatic amine is better than phenolics, but is staining and discoloring.

For tire compounding, secondary aromatic amine is the most used. The chain termination mechanism are represented in Figure 21[41].

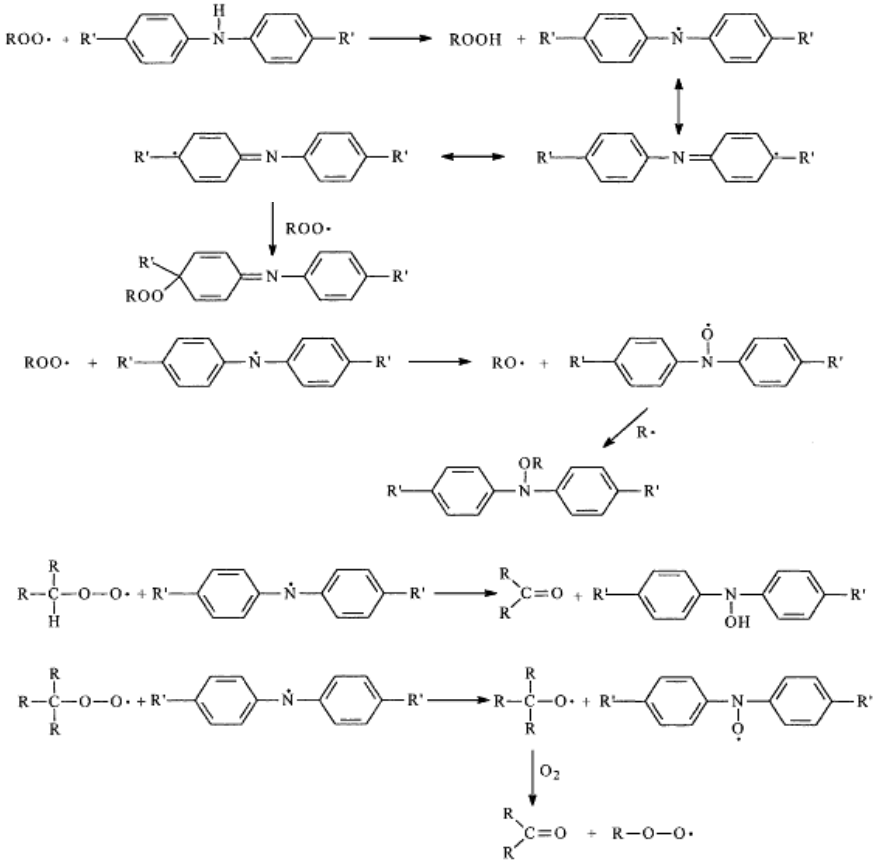

Figure 21: The chain termination mechanism by N, N'-dialkyldiphenylamines (6PPD).

The first is the scavenger theory, while the second consists of the ozonized antiozonant, Regarding the hydroperoxide-decomposing antioxidant, it decreases the rate of chain initiation. In detail these antioxidant are phosphate esters and sulphides, which during the reaction with hydroperoxide form an alcohol, phosphates and sulfoxides, correspondingly.

Unfortunately, these systems are more efficient at high temperatures and not at room temperature. Another important class of antidegradant is antiozonant.

The *antiozonants* are added to the unsaturated rubbers to avoid the fracture of the surface of the rubber caused by the attack of ozone to the double bond. Usually, they are used to protect external parts which are exposed to atmospheric environments, thus obtaining a long term service of the materials without any cracks. Industrially existing aniozonants are dialkylparaphenylenediamine, alkylarylparaphenylenediamine, and diarylparaphenylene-diamine. Therefore, aromatic amine act as an antioxidant and antiozonant. There are three principal theories on the mechanisms of antiozonant protection.

The first one is the scavenger theory, while the second consists of the ozonized antioxidant, which forms a protective film on the surface of the vulcanized rubber preventing further attack. The last mechanism involves the antiozonants reacting with elastomer ozonide fragments, re-linking them and restoring the polymer chain. Therefore, aromatic amine acts as an antioxidant and antiozonant.

The last categories of antidegradants are *waxes*. Two major types of waxes are available: paraffin and microcrystalline. Waxes are hydrocarbon compounding ingredients which physically protect the rubber surface against oxygen and ozone attacks under static conditions. Usually waxes, less soluble in rubber, are able to migrate to the surface of the rubber article at different rates, offering a wide range of protection.

Vulcanization system

First of all, vulcanization is the process of treating an elastomer with chemicals to decrease its plasticity, tackiness and sensitivity to heat/cold and providing elasticity, strength and stability. During these chemical processes, the conversion of thermoplastic elastomers into three dimensional elastic networks takes place (see Figure 22).

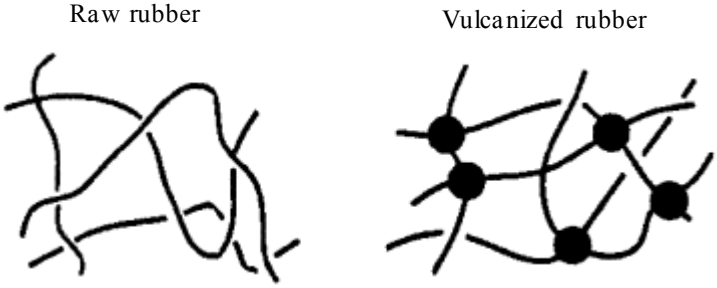

Figure 22: In vulcanization the randomly oriented chains of raw rubber become cross-linked.

There are four basic ingredients which compose the vulcanization system: sulphur, accelerator, activator and retarder agents.

Sulphur is the oldest and most widely used vulcanizing or cross-linking agent.
In nature, sulfur is available for the compounding in two forms: amorphous and rhombic.
The amorphous form, also known as insoluble sulfur, is a metastable high polymer that is insoluble in rubber and most of the solvents.
Rhombic sulphur, normally used for vulcanization, because it is soluble in rubber, is constituted by a crystalline lattice of rings of eight sulfur atoms. About 1 to 4 phr (parts per 100 parts of rubber elastomer) of sulfur are used for most rubber products. Sulfur vulcanization alone is a slow and inefficient process.
Therefore, an accelerator has to be used to reduce the time of the vulcanization process by improving the reaction rate between elastomer and sulfur.
In this way it is possible to control the onset, speed and extent of reaction between sulfur and elastomer.
The majority of cure systems, in use today, involve the generation of sulfur containing cross-links, by combining elemental sulfur with an organic accelerator.
Sulfur vulcanization occurs by the formation of sulfur linkages or cross-links between rubber molecule.
Thus, the so-called efficient vulcanization systems are produced when higher cross-link densities are observed for the same loading of sulfur and the network produced is predominantly composed of monosulfide and disulfide cross-links.
Accelerators are classified as primary or secondary: the primary ones provide considerable scorch delay, medium fast cure, and good modulus development; the secondary ones are usually scorchy and provide very fast cure.
There are a wide variety of accelerators (more than 100), hence they are classified as their generic chemical structure: class 1 sulfenamide (CBS, TTBS, DCBS, MBS), class 2 thiazoles (MBT, MBTS), class 3 guanidines (DPG, DOTG), class 4 thiurams (TMTD), class 5 dithiocarbamates (ZDMC) and class 6 dithiophosphates (ZDBP) (see Figure 23[28]).
Over a century of research efforts have been directed toward the development of materials to improve the efficiency of vulcanizing processes by adding activators, ultra-accelerators and retarders.

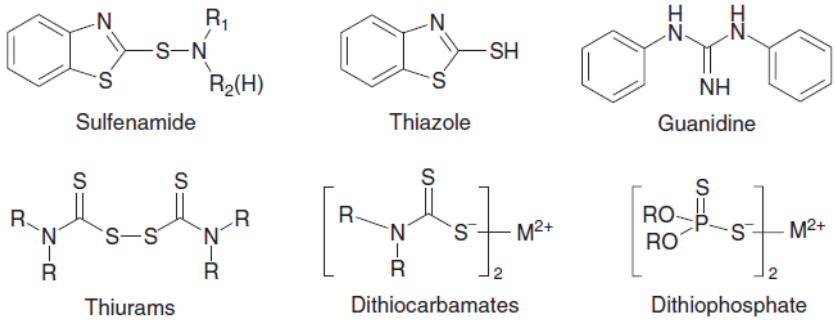

Figure 23: Chemical structure of accelerators.

Inorganic and organic *activators* are used to activate the accelerator.

Zinc oxide is the most important inorganic activator.

As reported by Heideman[90] the addition of zinc oxide increases the vulcanization rate and cross-linking efficiency. However, only the zinc oxide action is not enough to activate the vulcanization process.

In fact, ZnO is best used in combination with other organic activators: fatty acids, although weak amines, guanidines, ureas, thioureas, amides, polyalcohols.

The most important and popular type of organic activator is stearic acid.

The large preponderance of rubber compounds, today use a combination of zinc oxide and stearic acid as the activating system.

Fatty acid is needed to dissolve the oxide coordinating Zn^{2+} with a carboxylic acid as shown below:

$$ZnO + 2\ C_{17}H_{35}COOH \rightarrow Zn\ (OOCC_{17}H_{35})_2 + H_2O$$

The efficiency of the polysulfide cross-links during vulcanization can be controlled by the complex formed by activators (zinc and carboxylic acid), sulfur, and accelerators as shown in Figure 24 where the scheme of vulcanization process is reported[91].

The formation of the complex of zinc with accelerator, and stearic acid and sulphur weakens the polysulfide bridge giving rise to sulphur radical species able to react with the polymer.

To conclude, the cross-linking of rubber is affected, not only by the chemical reagent, but also by the thermal treatment it is subjected to during the compounding.

Typical vulcanization system includes, sulfur (0.5-4 phr), an accelerator (0.5-2 phr), zinc oxide (2-10 phr), and stearic acid (1-4 phr).

The *retarders* are the ingredients used to reduce the scorchiness of a compound in order to improve the processability in the early stage of the vulcanization process.

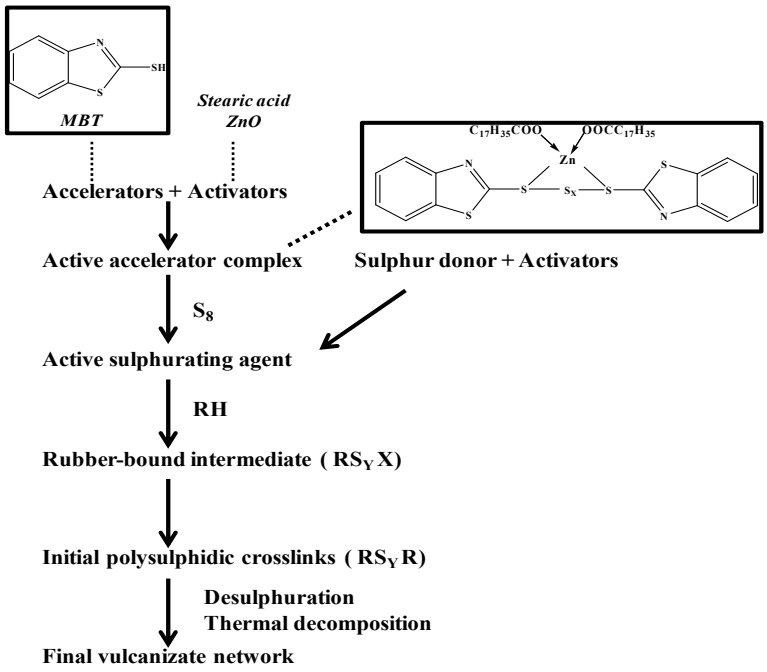

Figure 24: Reaction scheme of suphur vulcanization.

The most common used retarder is cyclohexyl-N-thiophthalimide. It makes a sulfenamide or thiazole accelerated compound, much less scorchable with higher processing safety without affecting significantly the cure rate and vulcanize properties.

The vulcanization can be characterized by measuring the evolution of its dynamic properties as a function of time, commonly called the cure curve.

More detail where will be given in chapter 3.3.1.

2.4.3. Effect of filler addition on tire compounds properties

The reinforcement of the elastomers occurs from the addition of inorganic fillers and consequently, the composite obtained shows non-linear viscoelastic behavior.

For a better understanding of the meaning of nonlinear viscoelastic behavior of the compound, in tire application, dynamic-mechanical tests will be illustrated.

In particular, mechanical analysis shows the response of the materials after stress application[92].

Mechanical tests at fixed temperature, report the behavior of a material when it is subjected to a stress (σ, applied force), and consequently it exhibits a deformation or strain (γ).

In the graph, where the data obtained are reported, the slope of the line (the modulus) gives the relationship of the stress to strain and is reported in Figure 25.

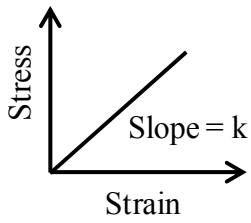

Figure 25: Stress-strain curve.

This modulus value is a measure of the material's stiffness and indicates how well the material will work in a specific condition. It depends on the applied stress and working temperature.

The stress σ applied is the product of a force (F) across an area (A), and is given from the International System for Units as a pressure (Pascal, pa), which is equivalent to one Newton (force) per square meter (area). It can be applied in static or in dynamic modes.

The static stress can be applied constant in time and in temperature (normal stress strain curve); or constant in time but varying the temperature (while watching the material change); or change the force applied in different times and temperatures (creep recovery test).

The stress can be applied in different orientations as shown in Figure 26[93].

Therefore, different appearing stress-strain curves can be obtained from these different geometries. It is obvious that the moduli obtained from compressive, flexural, extensile, shear and bulk mechanical analysis are not the same. The dimensions of the sample have to be precise in all the geometries. In particular, the ratio of the sample length, to width to thickness need to be controlled and fixed.

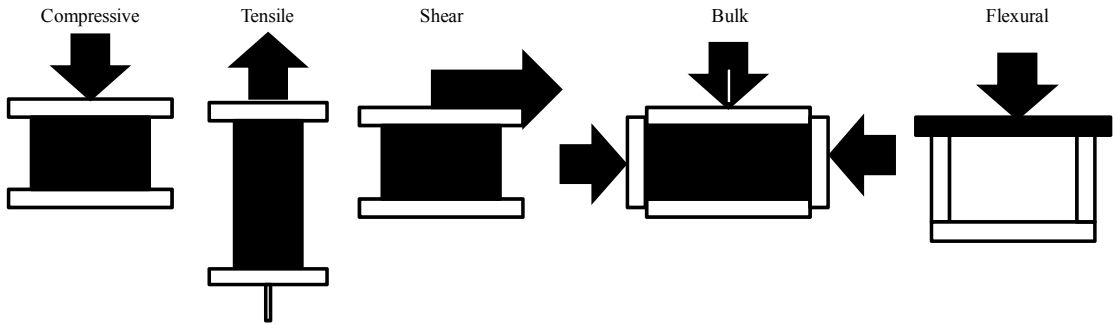

Figure 26: Methods for applying stress.

The rubber composite material, is a viscoelastic material[94] because its behavior is intermediate between that of solid elastic springs (Elastic material) and that of a viscous liquid (Viscous material).

Hooke's law model describes the ideal reversible behavior of completely elastic material, where the relationship between stress and strain is constant:

$$\sigma = k * \gamma$$

Therefore the deformation of the spring is linearly related to the force applied to the spring, by a specific constant. The material alters its shape instantly, and remains constant for all the time in which the stress is applied. When the stress is removed, the material goes back to its original shape as a spring. In this case the supplied energy to the material is given back completely after removing the stress (see Figure 27a).

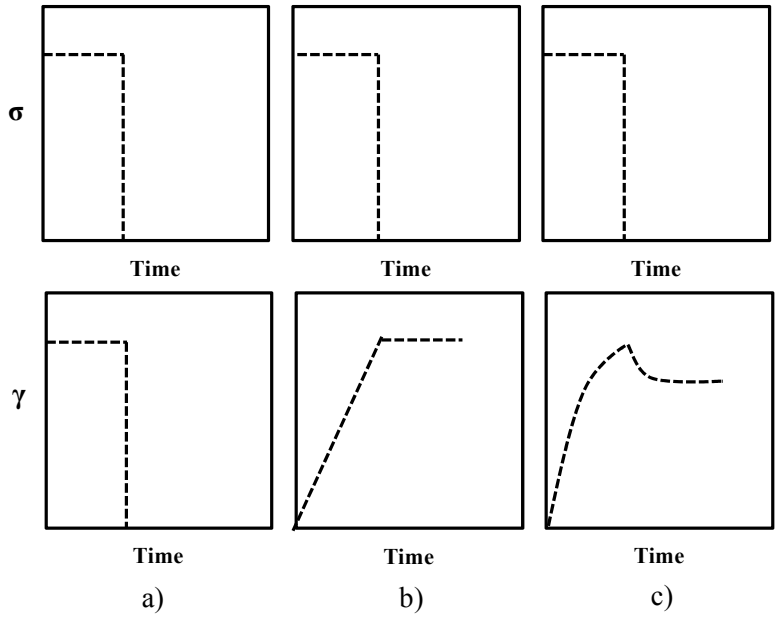

Figure 27: Over time, strain materials reply: a) elastic, b) viscous and c) viscoelastic.

As the spring constant increases, the material becomes stiffer and the slope of the stress-strain curve increases[95]. Therefore, the modulus (ratio between stress and strain) obtained for compressive, tensile and flexural analysis will be written as E, for shear mode G, and for bulk mode B.

$$E = \frac{d\sigma}{d\gamma}$$

Through Poisson's ratio (ν, measure of the material volume changes with the deformation when it is in extension) is possible to convert the modulus in the modulus G (shear mode) of B (bulk mode):

$$E = 2G\,(1 - \nu) = 3B\,(1 - \nu)$$

In most cases, we are interested in the first part of the graph stress-strain (initial slope), before the rupture of the material, where the material shows a stiffness behavior (Young's

modulus). In addition, from the graph we are also interested to know how much stress is needed to deform the material[95], and this value can be achieved after looking at the behavior until the deformation and the final rupture. The area under the stress-strain curve is proportional to the energy needed to break the material.

Another limiting extreme of the behavior of the material is the viscous liquid (like a flow), which is described from a Newtonian model. Viscous flow behavior describes the irreversible deformation of the material polymer associated with irreversible slippage of the molecular chains through each other. The Newtonian model describes the behavior with a relationship between stress and strain, as dependent from the proportional coefficient viscosity (η) of the material as follows:

$$\sigma = \eta * \gamma$$

In this case the strain is defined as the gradient of the velocity (v) of the flowing liquid:

$$\gamma = \frac{dv}{dx}$$

where x is the direction perpendicular to the flow. Therefore, the measure of the resistance of the fluid which is being deformed by the applied stress is the viscosity (η).

In detail, viscous liquid changes the original shape during the time in linear mode or rather the rate of the material strain instantly modifies in a constant way for constant applied stress. When the stress is removed, the strain remains in the shape obtained until that moment (see Figure 27b).

In this case all the energy supplied to the material is not given back and will be dissipated as heat in a hysteretic manner.

Composite or viscoelastic material shows a behavior in the middle of elastic and viscous perfect models (see Figure 28).

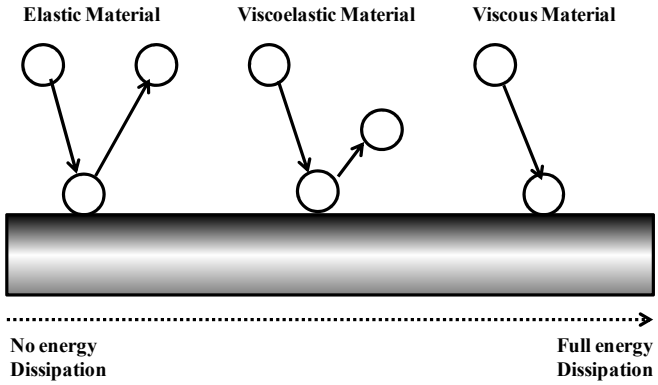

Figure 28: Three different material behaviors.

The strain increases rapidly (as elastic model) and then slows down, archiving a linear equilibrium in the time (as viscous model). When the stress is removed, the material partially return to its original shape. Therefore, the strain recovery is partial and requires a finite length of time (see Figure 27c).

Many models try to describe the behavior of viscoelastic material starting from the well known Hooke and Newton models. In detail, most of the studies report a combination of the two simple elements (elastic and viscous). In the Voigt o Kelvin models, the stress is applied in parallel to a spring and a viscous liquid:

$$\sigma = \mathrm{K} * \gamma + \eta * \frac{\mathrm{d}\nu}{\mathrm{dt}}$$

In the Maxwell model, the stress is applied in series to a viscous liquid and a spring. In order to simplify the model, it is considered that the area, in which the stress is applied, is the same for both elements.

The stress applied to the elastic material can be dynamic or rather sinusoidal oscillation of the applied stress:

$$\sigma\,(t) = \sigma_0 * \sin \omega t$$

where ω is the frequency of oscillation, σ is the stress at time t and σ_0 is the maximum stress.

In addition, the stress can have a rate of application:

$$\frac{d\sigma}{dt} = \omega\,\sigma_0 * \cos \omega t$$

The relative strain will be :

$$\gamma\,(t) = \gamma_0 * \sin \omega t$$

where γ_0 is the strain at the maximum stress.

The curve which represents both, stress and strain, shows no time difference from the stress curve to strain (no phase lag) and is called the in-phase portion of the curve (see Figure 29).

In the case of dynamic stress applied to viscous material, the strain will be:

$$\gamma\,(t) = \eta\omega\sigma_0\,\sin\left(\omega t + \frac{\pi}{2}\right)$$

which report the out-phase portion (90°) of the curve.

The intermediate case of both behaviors (elastic and viscous) shows a difference between the applied stress and the resultant strain as an angle δ and is reported in the following two equations:

$$\sigma(t) = \sigma_0 \sin(\omega t + \delta)$$

$$\gamma\,(t) = \gamma_0 \sin(\omega t)$$

Developing the first of these equations can easily obtain:

$$\sigma(t) = \sigma_0\ [\sin(\omega t)\cos\delta\ + cos(\omega t)\sin\delta]$$

The strain that is applied on the sample is the addition of two contributions: the in-phase and out-of-phase components.

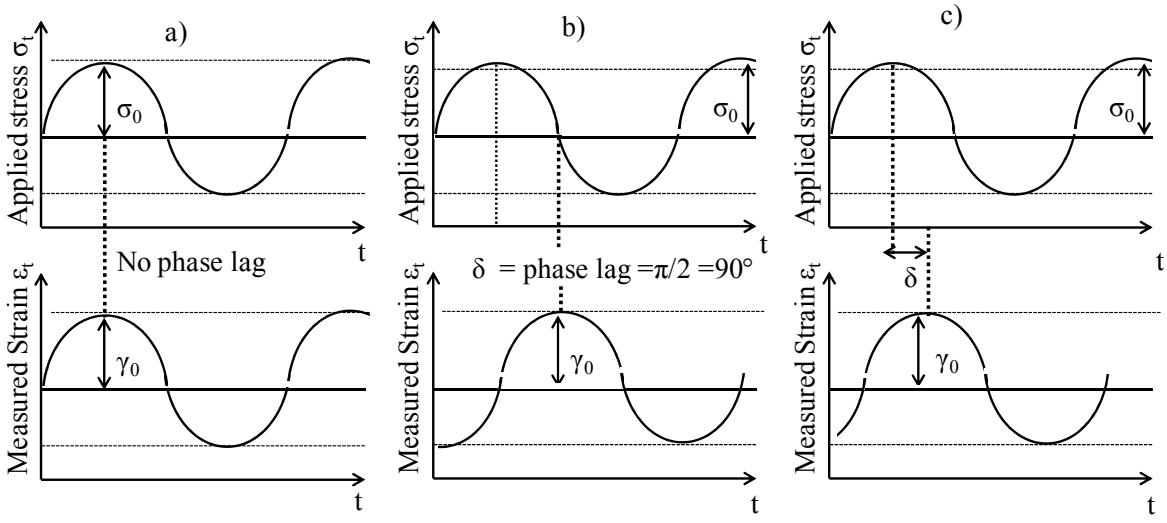

Figure 29: Response of the material to the applied wave: a) elastic, b) viscous and c) viscoelastic.

If the strain applied is small, it is possible to specify two different moduli E' and E'', independent from γ_0. In this condition the material is linear viscoelastic because the modulus depends only on the frequency (ω):

$$E'(\omega) = \left(\frac{\sigma_0}{\varepsilon_0}\right)\cos\delta$$

$$E''(\omega) = \left(\frac{\sigma_0}{\varepsilon_0}\right)\sin\delta$$

The modulus E', regarding the in-phase component, is a conservative modulus because the amount of strain applied does not involve the energy dissipation.

The second modulus, E'', regarding the out-of-phase component, is a dissipative modulus because the stress applied to the materials give a dissipation of energy.

The ratio between E'' and E' modulus corresponds to a number between 0 and 1:

$$\tan\delta = \frac{\sin\delta}{\cos\delta} = \frac{E''}{E'} = \frac{G''}{G'}$$

Therefore, the tangent of the phase angle is one of the most basic properties measured by mechanical analysis.

Tan δ is the damping and is an indicator of the amount of energy lost by the material upon deformation.

Moreover, Tan δ is also the ratio between loss and storage modulus, and is independent from the geometry of the sample.

Within the viscoelastic materials, linear and non linear behaviors of the materials[95] can be distinguished.

Linear viscoelastic material behavior allows the description of the rubber behavior in a small range of use: only when the shear stress is applied giving a small deformation of the material or when compression and traction stresses are applied to rubber without filler.

In this case, the relationship between stress to strain depends on temperature, time (frequency), and not from strain amplitude. If there is a dependence of strain amplitude beyond temperature and time, the behavior shown describes typical non linear viscoelasticity material, followed after the changes of the sample's geometry. This is the case of composites, where the filler is present in the rubber and the uncured rubbers.

Moreover in filled composites the relationship between stress and strain depends also from the strain amplitude. After this explanation, it is possible to understand better the influence of the filler adding in rubber for tire applications.

The tire can be considered today a mature and fully developed primary engineering component of transport vehicles. The tire has undergone a series of functional changes over the decades improving a number of key performances, such as dry and wet grip, lower rolling resistance (RR), abrasion resistance, comfort and esthetics.

Progress in the tire technology is continuous on many fronts, in order to meet never-ending customer demands and to accommodate new applications by supporting and meeting the demand of all-around development.

Therefore, innovation is related on the material front with new formulations exploiting specific elastomers, new nanofillers or tailored modifications of the filler surface, or new accelerators and retarder materials.

From the filler point of view, carbon black has been incorporated into the polymer to achieve several performances; among others, low rolling resistance, good abrasion resistance and wet grip are sometimes assigned to a so-called magic triangle (see Figure 30).

In recent years, the world's leading carbon black manufacturers have been searching for innovations to meet worldwide demands.

Therefore, many developments have recently taken place in the reinforcing-filler technology.

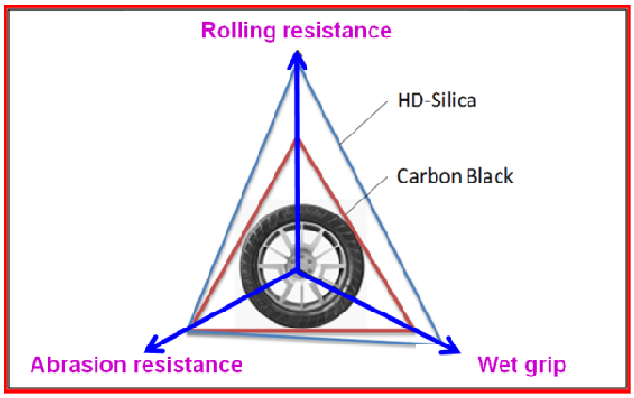

Figure 30: Magic Triangle.

These advances include the usage and the introduction of silica filler with the application of highly dispersible silica and the use of silane as a coupling agent and compatibilizer. In tire applications, rolling resistance and wet to grip have been improved without changing abrasion resistance.

The tire magic triangle[96] can be extended to a polygon with more sides, where every angle is assigned to a specific characteristic.

The same concept can be applied to compound properties, representing particular behaviors in a particular condition of the composite such as hardness, rebound resilience, tear, elongation at break, strength, Mooney viscosity etc.. Some of these properties will be explained in the next paragraphs.

2.4.3.1. Rolling resistance

Rolling friction or rolling resistance[97] is defined as the energy consumed by a tire under load for a unit of distance covered and consists in the motion resisting force due to a body movement on a surface. Consequently, energy divided by a distance expresses the rolling resistance.

As reported before, when rubber is reinforced with filler[6], during the dynamic deformation, it shows, a typical nonlinear viscoelastic behavior.

Therefore, the main source which contributes to rolling resistance is the viscoelasticity or non elasticity of tire rubber compounds which allows to explain the phenomenon that happens during the deformation of the tire.

In fact, during the contact of the tire under load with the ground, not all the energy used to deform the tire will be recovered when the pressure is removed.

During the deformation of this kind of material, return to the initial shape occurs after a certain time and is associated to energy dissipation in the form of heat.

This phenomenon which takes place is called hysteresis.

The factors which affect the energy dissipation are modulus (or the rigidity/flexibility of the materials), deformation frequencies, operating temperature, strain levels, desorption or adsorption of rubber ingredient, and inter-aggregate distance between particles.

The last aspect, of significant relevance, is related to the dispersion of filler particles and aggregates in rubber matrix.

From an experimental point of view, the presence of closer aggregates of filler leads to a non-linearity of modulus[98, 99]. This explains that the dynamic deformation of the composites is mainly due to the filler presence.

Besides, strain independent contributions come from hydrodynamic effect, polymer network cross-linkage and in-rubber structure.

These effects correspond to the amount of filler-rubber interaction (G'_{∞}) or better the mobility of the polymer chain, due to the presence of filler particles.

Therefore, at low strains, a significant sigmoid decrease of storage modulus (response of elastic behavior) occurs from zero strain value G'_0 to high amplitude plateau value G'_{∞}, while the viscous modulus G'' passes through a maximum. This phenomenon is known as Payne effect[98] and measured by $\Delta G' = G'_0 - G'_{\infty}$.

This viscoelastic behavior is of great practical importance in tire essential application where it affects the rolling resistance and heat generation. A lot of work has been reported on the interpretation of this effect [100,101,102].

The mechanism responsible for the Payne effect, according to the most commonly accepted opinion, is the destruction of filler networking with breakage of physical bonds between filler particles (for example Van der Waals or London forces) during a periodic sinusoidal shear strain condition ($\Delta G'$ has been shown to depend on several parameters).

It increases with increasing concentration of filler and with particle aggregation, while it decreases with increasing temperature and with improving the dispersion (see Figure 31).

In order to reduce a tire's energy dissipation, it is better to choose a polymer or a blend of polymers characterized by a low hysteretic nature for the nanocomposite preparation, and/or increase the distance between reinforcing filler aggregates.

Hysteresis depends on the temperature or frequencies of elastomeric composite.

With regard to filler aggregate, reducing energy dissipation is possible by using lower amounts of filler, and/or increase the distance between reinforcing filler aggregates.

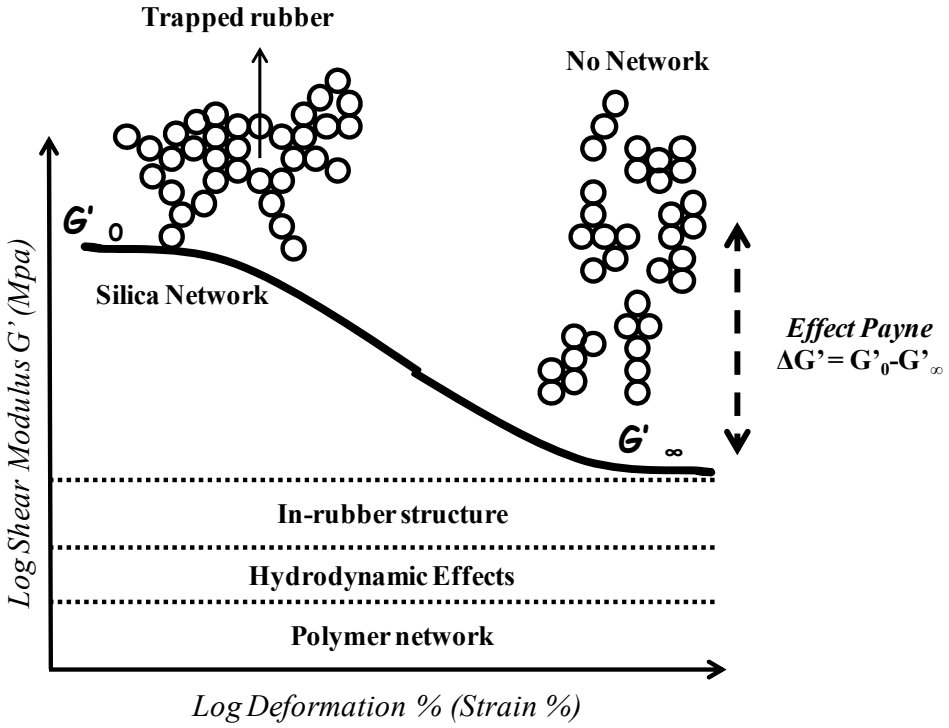

Figure 31: Strain-dependent breakdown of the filler network (Payne effect).

Therefore, an improvement of the distribution of filler in rubber matrix, including also the distance between particles, may be achieved by increasing the starting material's mixing time or by grafting, suitable chemical groups at the end of polymer chains.

Bonding the such chemical groups to the filler aggregates avoids that they come too close to each other.

Consequently, the rolling resistance affects the fuel consumption, and hence costs, and perseveres the environment.

Moreover, reducing a vehicle's fuel consumption means decreasing the use of fossil fuels and releasing less exhaust gases in the atmosphere, by reducing the amount of pollution in the air.

With the intention of reducing rolling resistance, it is necessary to understand the mechanisms involved during the deformation of the tire rolling under load.

In general there are five forces which resist the movement of the vehicle: inertial forces (depend on the vehicle's mass and variations in speed), gravitational forces (depend on the slope and mass), aerodynamic forces (depend on the wind, speed, and vehicle's shape), tire rolling resistance and internal friction of rotating parts (see Figure 32).

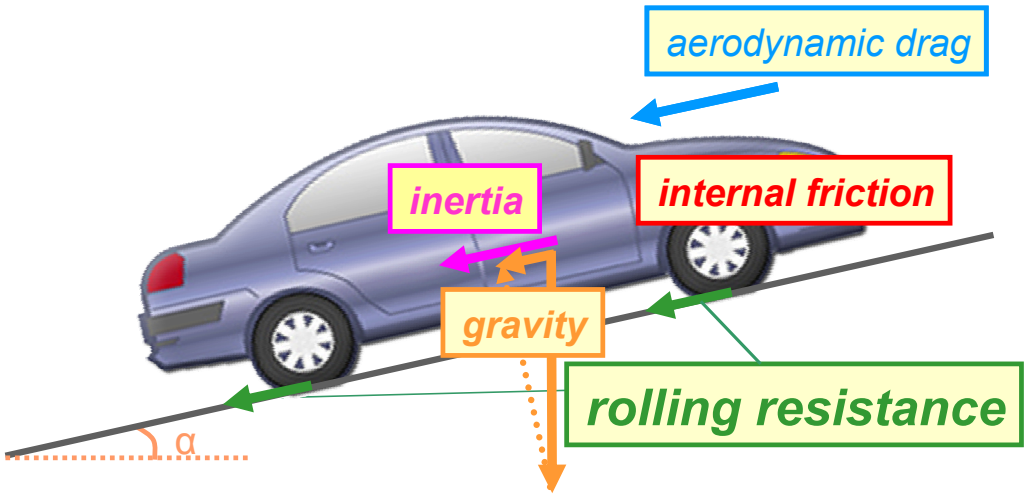

Figure 32: The different contributions of resistance to movement.

The mechanical manifestation of energy dissipation due to tire deformation takes place when it is in contact with the ground at only one point around its circumference.

Therefore, the value of rolling resistant coefficient is practically constant, and depends on the speed acceleration, type of road and rubber compound; the other forces are not dependent on these factors.

From the physical point of view, there are two causes of rolling resistance.

The first one, that covers approximately 80-95 %, is the deformation of a tire when it flattens out in contact patch.

The remaining amount of rolling resistance, consists in aerodynamic resistance of the rotating tire and micro-slippage between the tread and the road surface.

Tire flattening in contact patch causes three main kinds of deformation: bending, compression and shearing of the tread.

As a result, the rolling resistance depends primarily on the physical and chemical behavior of the tread rubber composite.

2.4.3.2. Abrasion resistance

Abrasion or wear occurs every time two bodies slide against each other. Material is transferred from one body to the other.

Abrasion resistance is the ability of a material compound to resist mechanical action such as friction or erosion that tends progressively to remove material from its surface. Wear is therefore associated with friction.

Abrasion resistance is measured under defined conditions of load, speed and type of abrasive surface.

It is usually reported as an Abrasion Resistance Index, which is a ratio of the abrasion resistance of the test compound compared to that of a reference standard measured under the same test conditions.

Abrasion[103] appears to involve a competition between two different mechanisms: one is the removal of microscopic particles of composites by fracture process and the other is chemical deterioration of rubber in the surface region, initiated by mechanical stress and also promoted by the oxygen in the atmosphere.

Research tries to find ways to retain high friction while minimizing wear. The abrasion method is useful in making quality control checks on rubber products intended for rough service.

A more basic approach is to consider the dependence of the abrasion loss on the energy dissipation[104] U caused by the frictional force F. For sliding experiments this is:

$$U = F \times s$$

where s is the distance covered.

Wear is associated with friction. Dissipation of frictional energy leads to increase the temperature in the contact area, increasing the rate of oxidation and/or thermal decomposition; at the same time it weakens the resistance of the rubber to cut growth, thus further increasing the rate of abrasion.

Hence, abrasion is not purely a physical phenomenon, but is strongly influenced by chemical processes, which depend on the chemical structure of the polymer and any protective agents added to the compound.

For tire materials, the rate of abrasion is clearly important because it determines the product life.

Rubber, due to its elastomeric properties, usually, has a low abrasion resistance. Fillers, such as carbon black and silica, can be added to impart abrasion resistance.

Decreasing the interaggregate[105] distance between filler particles decreases the abrasion loss.

Moreover, increasing the filler concentration decreases abrasion loss.

Increased adhesion between the filler and the matrix by adding a multifunctional additive and compatibilizer, contributes to an increase in abrasion resistance.

2.4.3.3. Friction and grip

In general, adherence is a friction force against skidding of the vehicle on ground. Therefore, the adherence of the tire on the ground may be considered as a synonymous of car safety.

Two different processes contribute to the total friction: adhesion and internal energy losses during repeated deformation[104].

Adhesion is a process similar to the cohesion of two liquids and does not usually play a significant role for standard tires.

The viscoelastic properties of tread compounds play a dominating role in the tire friction.

As a result, adherence depends on the composition of the tread compound and temperature.

The friction of these viscoelastic materials, is generated by contact between the tread and the road.

In fact, the roughness of the road produces tread deformations at a high frequency from 10^4 to 10^8 Hz: it is necessary have high hysteresis values at these frequencies for good grip.

The master curve of a polymer contains practically all of the frictional information.

This could become an interesting area of research, since every possibility of increasing friction on the road without simultaneously enhancing the internal friction, will hence increase the rolling resistance of the tire.

2.4.3.4. Tensile strength and elongation at break

Tensile strength and elongation at break, set by tensile strength testing, are considered the most common parameters of evaluation of filled elastomers.

Particles size and shape, interaction with rubber matrix and concentration of filler (or volume fraction of the filler) in composites are important factors which contribute to the improvement of tensile strength[106].

In addition, the distribution of filler network has an influence on the maximum strength which composites can support. In fact, an increment of interparticle spacing actively contributes to the strength.

Tensile strength is usually inversely proportional to elongation at break, which indicates that increasing the tensile strength of filler materials decreases the elongation at break.

Therefore, the determination of tensile stress is one of the preferred methods of composite testing because it gives an indication about the filler-rubber interaction.
High adhesion and filler rubber interaction allow to increase the tensile strength.
In fact, in silica filled elastomeric nanocomposites, in the presence of the coupling agent, which improves the filler-rubber interaction, filler-rubber adhesion is improved and brings to good tensile strength.
Therefore, tensile strength can be improved by surface treatment of the filler with functional moieties able to change the interaction between organic and inorganic parts.
Thus, these methods should be regarded as quality control tests because the results obtained allow to predict the range of fracture and the composition of the composites material and thus the characteristics which the tire can support.

2.4.3.5. Hardness

The hardness of tire material is defined by ASTM as the resistance to indentation as measured under specified conditions.
Hardness of rubber composites is measured by pressing the indenter against the sample and reading the scale.
It appears in almost every specification and is widely used by rubber goods manufacturers for quality control.
Determination of hardness is probably the most often-measured property of vulcanized elastomer. It is well known, from the literature, that the addition of filler to rubber increases the hardness.
Fillers which have relatively large particle sizes do not interact, and therefore their effect on hardness is due to their higher hardness.
However, the increase in hardness is very small because these particles are surrounded by an elastic matrix, which moderates the effect of their hardness.
A much larger increase in value is observed with semi-reinforcing grades[107] due to the formation of an interlayer with mechanical properties more similar to the filler than to the matrix.
In this case, the actual size of the particle is increased by the thickness of its adsorbed layer, therefore even small particles occupy a substantial space in composites.

Reinforcing fillers introduce another variable related to the formation of physical cross-links which can be very numerous because of the small size of the particles.

These physical cross-links further reinforce the rubber resulting in its increased hardness. The following graph reports the trend of variation of the hardness as a function of the surface area of the filler particles at fixed filler loading and vulcanization (see Figure 33).

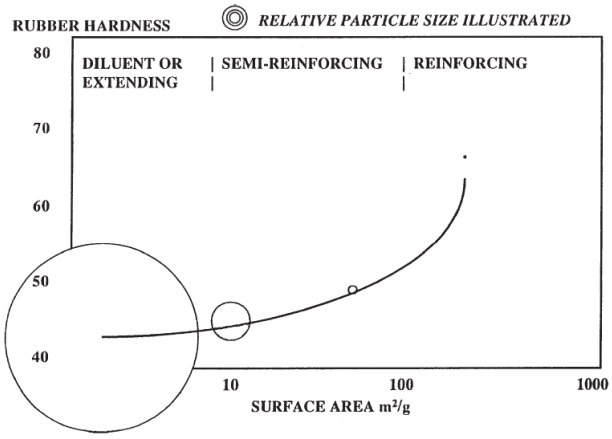

Figure 33: Rubber hardness vs. surface area of silica filler.

[1] C. Sanchez, B. Julian, P. Belleville and M. Popall, *Journal of Materials Chemistry*; 2005, **15**, 3559-3592.

[2] G. Wypych; *Handbook of fillers, 2nd edition*; Chem. Tec. Publishing, 2000; Canada.

[3] C. Sanchez and F. Ribot, *New J. Chem.;* 1994, **18**, 1007.

[4] L. Bokobza; *Macromol. Mater. Eng.* 2004, **289**, 607–621.

[5] T. Sabu and S. Ranimol; *In Rubber Nanocomposites: Preparation, Properties and Application, 1st ed.*; Wiley-Interscience, 2010, New York.

[6] L. Bokobza and O. Rapoport; *Journal of Applied Polymer Science*; 2002, **85**, 2301-2316.

[7] H. Zou, S. Wu and J. Shen; *Chem. Rev.,* 2008, **108**, 3893–3957.

[8] C. Sanchez and P. Gomez-Romero, *Functional Hybrid Materials*, Wiley VCH, Weinheim, 2004.

[9] C.Sanchez, P. Belleville,M. Popalld and L. Nicole; *Chem. Soc. Rev*., 2011, **40**, 696–753.

[10] *SusChem Hybrid Materials Workshop Report,* March 2010.

[11] K. Nakamura and K. Nakanara, *P.C.T Int. Appl*. 2004, **26**.

[12] V. M. Rotello, *Adv Drug Deliv Rev.;* 2008, **60** (11), 1225.

[13] M. Maiti, M. Bhattacharya and A. K. Bhowmick, *Rubber Chemistry and Technology*; 2008, **81** (3), 384-469.

[14] G. Kraus, *Reinforcement of Elastomers*; Wiley-Interscience,1965; New York.

[15] J. L. Leblanc, *Filled polymers: Science and Industrial Applications*, CRC Press Taylor & Francis Group, 2010.

[16] M. López-Manchado, B. Herrero, and M. Arroyo, *Polym. Int*., 2003, **52**, 1070.

[17] S. Varghese and J. Karger-Kocsis, *J. Appl. Polym. Sci.*, 2004, **91**, 813.

[18] M.A. López-Manchado, M. Arroyo, B. Herrero, and J. Biagiotti, *J. App. Polym. Sci.*, 2003, **89**, 1.

[19] S. Poomradub, B. Chaichua, C. Kanchanaamporn, T. Boosalee and P. Prasassarakich, *KGK Kautschuk Gummi Kunststoffe*; 2008, **61** (4), 152-155.

[20] J. Siramanont, V. Tangpasuthadol, A. Intasiri, N. Na-Ranong and S. Kiatkamjornwong, *Polymer engineering and Science*; 2009, **49**, 1099-1106.

[21] Y. I keda, *KGK Kautschuk Gummi Kunststoffe*; 2005, **58** (9), 455-460.

[22] Y. Tanaka and L. Tarachiwin, *Rubber Chemistry and Technology*; **2009**, 82 (3), 283-314.

[23] C.Gooyear, US Patent 3.633 (1844).

[24] T. Hancock, *Personal Narrative of the Origin and Progress of the India Rubber Manufacture in England, Longman, Brown Green, Longmans and Roberts*, London (1857).

[25] M. Akiba and A. S. Hashim, *Prog. Polym. Sci;* 1997, **22**, 475-521.

[26] J. L. White, *Rubber Processing: Technology, Materials and Principles*; Hanser Gardner Publications, Inc Cincinnati, 1995.

[27] EPOBIO: *Realising the Economic Potential of Sustainable Resources – Bioproducts from Non-food Crops*: CLP Press 2006.

[28] J.E.Mark, B. Erman and F. R. Eirich, *Science and technology of Rubber; Third Edition;* Elsevier Academic Press, San Diego, California, 2005.

[29] A. N. Gent, *Engineering with rubber: how to design rubber components 2nd edition*; Hanser publishers, Munich, 2001.

[30] J. L. Halary, F. Laupretre and L. Monnerie; *Polymer materials: macroscopic properties and molecular interpretations;* Wiley-Interscience, 2011; New York.

[31] E. A. Gorrepati, P. Wongthahan, S. Raha and H. S. Fogler, *Langmuir*; 2010, **26** (13), 10467-10474.

[32] C. Y. Jung, J. S. Kim, T. S. Chang, S. T. Kim, H. J. Lim and S. M. Koo, *Langmuir*; 2010, **26** (8), 5456-5461.

[33] J. Schlomach and M. Kind, *Journal of Colloid and Interface Science*; 2004, **277**, 316-326.

[34] S. Ek, A. Root, M. Peussa and L. Niinisto, *Thermochimica Acta*; 2001, **379**, 201-212.

[35] R. Mueller, H. K. Kammler, K. Wegner and S. E. Pratsinis, *Langmuir*, 2003, **19**, 160-165.

[36] J. M. Kim, S. M. Chang, S. M. Kong, K. S. Kim, J. Kim, W. S. Kim, *Ceramics International*, 2009, **35**, 1015-1019.

[37] Y. H. Wen, P.-C. Lin, C.Y. Lee, C. C. Hua and T.-C. Lee, *Journal of Colloid and Interface Science*; 2010, **349**, 134–141.

[38] B. Zhao and W.J. Brittain, *Prog. Polym. Sci.,* 2000, **25**, 677–710.

[39] A. I. Isayev, *Encyclopedia of Polymer Blends, Vol.2: Processing*; Wiley-Interscience: New York, 2011.

[40] G. Tillet, B. Boutevin and B. Ameduri, *Progress in Polymer Science*; 2011, **36**, 191-217.

[41] B. Rodgers, *Rubber compounding: chemistry and applications*; CRC Press Taylor & Francis Group: Broken Sound Parkway NW, 2004.

[42] J. W. ten Brike, S.C. Debnath, L.A.E.M. Reuvekamp and J. W. M. Noordermeer, *Composites Science and Technology*; 2003, **63**, 1165-1174.

[43] R. Scotti, L. Wahba, M. Crippa, M. D'Arienzo, R. Donetti, N. Santo and F. Morazzoni, *Soft Matter*, 2012, **8**, 2131-2143.

[44] A. A. Ward, A.I. Khalf, C. Dokki, *KGK Kautschuk Gummi Kunststoffe* ; 2009, **62**, 650-656.

[45] O. Klockmann, A. Hasse, H. D. Luginsland, *KGK Kautschuk Gummi Kunststoffe* ; 2003, **56**, 471-477.

[46] J. W. Ten Brinke, S.C. Debnath, L. A. E. M. Reuvekamp, J. W. M. Noordermeer, *Composites Science and Technology*; 2003, **63**, 1165-1174.

[47] J. R. White and S.K. De, *Rubber technologist's Handbook*, Rapra Technology, 2001.

[48] C.J. Brinker and G.W. Scherer, *Sol-Gel Science: The Physics and Chemistry of Sol-Gel Processing*. Academic Press (1990).

[49] L. L. Hench and J. K. West, *Chemical Reviews*, 1990, **90** (1), 33-72.

[50] A. S. Poyraz and O. Dag, *J. Phys. Chem, C*; 2009, **113**, 18596-18607.

[51] U. Schubert and N. Husing, *Synthesis of Inorganic Materials*; Wiley-Interscience,; New York, 2000.

[52] M. Niederberger and N. Pinna, Metal *oxide nanoparticles in organic solvents: synthesis, formation, assembly and application*; Springer, London, 2009.

[53] G. Kickelbick, *Hybrid Materials: synthesis, characterization and applications*; Wiley-Interscience,; New York, 2007.

[54] W. Stöber , A. Fink and E. Bohn, *Journal of Colloid and Interface Science*; 1968, **26** (1), 62-69.

[55] S. Huh, J. W. Wiench, J. C. Yoo, M. Pruski and V. S.Y. Lin, *Chem. Mater.;* 2003, **15**, 4247-4256.

[56] Y. Ikeda and S. Kohjiya, *Polymer*, 1997, **38**, 4417-4423.

[57] Y. Ikeda, A. Katoh, and S. Kohjiya, *J. Mater. Chem.,* 1997, *7* (3), 455-458.

[58] S. Kohjya and Y. Ikeda, *Rubber Chemistry and Technology*; 2000, **73**(3), 534-550.

[59] S. Kohjiya, K. Murakami, S. Ito, T. Tanahashi, and Y. Ikeda, *Rubber Chemistry and Technology*; 2001, **74**(1), 16-27.

[60] S. Kohjiya and Y. Ikeda, *J. Sol-Gel Sci. Technol*; 2003, **26**, 495-498.

[61] K. Murakami, S. Ito, Y. Ikeda, H. Ito, M. Tosaka and S. Kohjiya; *Journal of Materials Science*, 2003, **38**, 1447-1455.

[62] Y. Ikeda and Y. Kameda, *J. Sol-Gel Sci. Technol*; 2004, **31**, 137-142.

[63] Y. Ikeda, A. Katoh, J. Shimanuki and S. Kohjiya, *Macromol. Rapid Comm*.; 2004, **25**, 1186-1190.

[64] S. Kohjiya, A. Katoh, J. Shimanuki, T. Hasegawa and Y. Ikeda, *Polymer*, 2005, **46**, 4440-4446.

[65] Y. Ikeda, S. Poompradub, Y. Morita and S. Kohjiya, *J. Sol-Gel Sci. Technol*; 2008, **45**, 299-306.

[66] M. Messori, F. Bignotti, R. De Santis and R. Taurino, *Polym. Int*, 2009, **58**, 880-887.

[67] M. Messori and M. Fiorini; *Journal of Applied Polymer Science*; 2011, **119**, 3422-3428.

[68] B. Chaichua, P. Prasassarakich and S. Poompradub, *J. Sol-Gel Sci. Technol*; 2009, **52**, 219-227.

[69] T. Sittiphan, P. Prasassarakich and S. Poompradub, *Advanced Materials Research*; 2010, **93-94** , 525-528.

[70] A. Bandyopadhyay, M. De Sarkar and A.K. Bhowmick , *Journal of Materials Science;* 2005, **40**, 53-62.

[71] A. Bandyopadhyay, M. De Sarkar and A.K. Bhowmick, *J. Applied Polymer Science: Part B: polymer physics;* 2005, **43**, 2399-2412.

[72] V. Tangpasuthadol, A. Intasiri, D. Nuntivanich, N. Niyompanich S. Kiatkamjornwong, *Journal of Applied Polymer Science*, 2008, **109**, 424–433.

[73] N. Watcharakul, S. Pooradub and P. Prasassarakich, *J. Sol-Gel Sci. Technol*; 2011, **58**, 407- 418.

[74] P. H. Mutin and A. Vioux, *Chem. Mater.*; 2009, **21**, 582-596.

[75] L. Bouget, R. J. P. Corriu, D. Leclercq, P. H. Mutin and A. Vioux, *Journal of Non-Crystalline Solids*; 1998, **242**, 81-91.

[76] A. Vioux, *Chem. Mater.;* 1997, **9**, 2292-2299.

[77] A. Aboulaich, O. Loreet, B. Boury and P. H. Mutin, *Chemistry of Materials Communication*; 2009, **21**, 2577-2579.

[78] D. C. Bradley, R. C. Mehrotra and D. P. Gaul, *Metal alkoxides*; Academic Press, New York, 1978.

[79] R. J. P. Corriu, D. Leclercq, P. Lefevre, P. H. Mutin and A. Vioux, *Journal of Non-Crystalline Solids*; 1992, **146**, 301-303.

[80] R. J. P. Corriu, D. Leclercq, P. Lefevre, P. H. Mutin and A. Vioux, *Materials Chemistry Communication;* 1992, **2** (6) 673-674.

[81] M. Niederberger and G. Garnweitner, *Chem. European Journal*; 2006, **12**, 7282-7302.

[82] A. M. Cojocariu, P. H. Mutin, E. Dumitriu, F. Fajula, A. Vioux and V. Hulea, *Chem. Commun.;* 2008, 5357-5359.

[83] L. Wei, N. Hu and Y. Zhang; *Materials* 2010, **3**, 4066, 4079.

[84] J. N. Hay and H. M. Raval, *Chem. Mater.;* 2001, **13**, 3396-3403.

[85] K. G. Sharp, *J. Sol-Gel Sci. Technol*; 1994, **2**, 35-41.

[86] A. Bhattacharya, J. W. Rawlins and P. Ray, *Polymer Grafting and Crosslinking*; Wiley-Interscience, New York, 2009.

[87] A. Lechtenboehmer, H. G. Moneypenny and F. Mersch; *British Polymer Journal;*1990, **22**, 265-301.

[88] R.N. Datta, N.M. Huntink, S. Datta and A.G.Talma, *Rubber Chemistry and Technology*; 2007, **80** (3), 436-480.

[89] Z. Cibulkova, P. Simon, P. Lehocky and J. Balko, *Journal of Thermal Analysis and Calorimetry;* 2005, **80**, 357-361.

[90] G. Heideman, N. Datta and J.W.M. Noordermeer; *Rubber Chemistry and Technology*; 2004, **77** (3), 512-541.

[91] A. N. Wilkinson and A.J. Ryan, *Polymer processing and structure development*; Kluwer Academic Publisher, Netherlands, 1998.

[92] M. Farina, P. Giusti and S. Cesca, *Macromolecole Scienza e Tecnologia*, Pacini Editore, Pisa, 1982.

[93] H. P. Menard, *Dynamic Mechanical Analyis, A practical Introduction*; CRC Press, Taylor & Francis Group 2008.

[94] E. Riande, R. Diaz- Calleya, M. G. Prolongo, R. M. Masegosa and C. Salom, Polymer viscoelasticity: stress and strain in practice; Marcell Deker, 2000.

[95]A.I.M. Associazione Italiana di Scienza e tecnologia delle Macromolecole*, Caratterizzazione meccanico-dinamica di materiali polimerici*; 26-27 maggio 2005.

[96] A. K. Bhowmick, *Current Topics in Elastomers Research*, CRC Press Taylor & Francis Group, 2008.

[97] The Tyre, rolling resistance and fuel saving, Societé de Technologie Michelin.

[98] A. R. Payne, *Journal of Applied Polymer Science*; 1962, **6** (19), 57-63.

[99] P. G. Maier and D. Goritz, *KGK Kautschuk Gummi Kunststoffe;* 1996, **49** (1), 18-21.

[100] M. Rendek and A. Lion, *Z. Angew. Math. Mech.,*2010, 1-23.

[101] J. Ramier, C. Gauthier, L. Chazeau, L. Stelandre and L. Guy, *Journal of Polymer Science: Part B: Polymer Physics*, 2007, **45**, 286–298.

[102] I. M.-Zloczower, *Mixing and Compounding of Polymers: Theory and Practice,* Hanser Verlag, Munich 2009.

[103] A. N. Gent and C. T. R. Pulford, *Journal of applied polymer science*;1983, **28,** 943-960.

[104] *Mechanics of Pneumatic Tires*, U.S. Department of Transportation, National Highway Traffic Safety Administration, February 2006.

[105] A. C. Patel, *KGK Kautschuk Gummi Kunststoffe;* 1994, **47** (8), 556-570.

[106] S. Hashemi, M. T. Hodgkinson and J. Gilbride, *J. Mat. Sci.;* 1996, **19**, 5017-5025.

[107] Di P. A. Ciullo, *Industrial Minerals and Their Uses: A Handbook and Formulary*; Noyes publications, USA, 1996.

Chapter 3

Characterization techniques

This chapter aims to report the experimental technique and the method used for analyzing fillers, composites and compounding/curing processes.
In particular, all compound were characterized from morphological, thermal and mechanical points of view.
Fillers were analyzed to better understand the mechanism of particles growing in rubber matrix; composites were investigated to evaluate filler and rubber influence on morphological and mechanical properties.
In the last part of the chapter, uncured and cured compounds were mechanically tested in order to check how the properties of the composites before curing determine the performance in tire application.

3.1. Filler characterization

In the first part of this section, the basic principles and methodologies of inorganic particle characterization are discussed.
In particular, structural and morphological characterization methods are reported: Thermogravimetric analysis (TGA), Transmission Electron Microscopy (TEM), Specific Surface Area measurement (BET), density and Fourier Transform Infrared Spectroscopy (FTIR).
The experimental parameters and instrumental details of all the characterization tools are also reported.

3.1.1. Thermal analysis (TGA)

Thermo-gravimetric analysis (TGA)[1] is a technique that allows the measurement of the weight changes of sample materials as a function of the temperature in a controlled atmosphere.
During a thermal treatment of the filler it is possible to determine the amount of functionalizing molecules allocated on the surface, the amount of solvent and humidity physically adsorbed on the surface and in the pores, and its thermal stability.
The instrument used for doing this kind of analysis is composed of four parts: analytic thermo-balance, heating oven, gas injector (inert or reactive gases) and a computer for instrument control in order to collect and process the data obtained.

The heart of the instrument consists in a light horizontal arm (balance) immersed in a magnetic field on which the sample pan is allocated. A special optical sensor controls the position of the pan where the samples are positioned.

For each mass sample loss, the arm moves inducing an electric current which is recorded as a signal by the machine.

In detail, the instrument records a graph which reports the loss of the mass (normalized or not) as a function of time or temperature and the first derivative curve of the mass loss (DTGA).

A thorough understanding of the result provided by the instrument allows to explain the processes, which take place in the sample, during the thermal treatment. For every small mass loss, it is possible to determine the correspondent temperature at which the sample loses the maximum amount and then hypothesize the kind of reaction which occurs. Thermogravimetric analysis was used to characterize the silica obtained from the sol gel method. The determination of powder characteristics was carried out by Thermo Gravimetric Analysis (TGA) on MettlerToledo TGA/DSC1 Star^e System.

The thermal profile was obtained at a constant N_2 flow (50 ml min^{-1}) by heating rate 5°C min^{-1} in the range 30-150°C and 10°C min^{-1} in the range 150-1000°C.

The reasons for the slowness of the first step is due to the presence of large amounts of solvent and water physisorbed which require a long thermal treatment for their removal. In the second step, the loss weight quantifies the amount of OH group[2, 3], organic moieties and surfactant present in the sample. In addition, with these methods, it is possible to determine the amount of functional group allocated on silica surface by subtracting the weight loss (between 150-100°C) of the silica, without functionalizing molecules (see paragraph 4.3), according to the following equation:

$$\left(\frac{n_{OH} - yn_f}{2}\right) \times MW_{H2O} + n_f \times MW_f = \Delta w_{150°C-1000°C}$$

Where n_{OH} are the OH moles on silica surface without functionalization evaluated by TGA, normalized to the mass of the analyzed sample; n_f the moles of functionalizing molecules on silica; (n_{OH}-yn_f) the effective OH moles on modified silica, taking into account that each functionalizing group substitutes one OH[4] unit; y can be 2 if functionalizing molecules are generated from bisilane precursor and 1 for the silane monosubstituted precursor; ΔW 150–

1000 is the weight loss in the interval 150°C<T<1000°C; MW_{H2O} and MW_f are the molecular weight of water and the functionalizing group.

3.1.2. Transmission electron microscopy (TEM)

Structural analysis of the inorganic particles, over a wide range of resolutions (from 10 µm to 2 Å), were carried out with electron microscopy, working in transmission mode (TEM)[5]. Through this technique it is possible to investigate, under ultra-vacuum conditions, the morphology of the materials, by analyzing the electrical signals from the samples after the electron beam hit them. In detail, it is possible to investigate the structure and the distribution of the particles which have diameters in the order of nanometers. Primarily, an electron microscope is composted of 4 sections: the electrons beam source, the device to accelerate the electron beam, the ultra-vacuum apparatus formed by different pumps, and finally the electromagnetic lenses which focus and scan the surface of the sample.

TEM analysis utilizes two different kinds of electrons produced by the electron beam: unscattered electrons (incident electrons which are transmitted through the thin specimen, without any interaction) and elastically scattered electrons (incident electrons which are deflected from their original path in an elastic fashion by atoms in the specimen and then transmitted through the remaining portions of the sample).

The use of unscattered and elastic electrons (see Figure 1) is allowed by the thin layer of the sample (in the range of 70 nm).

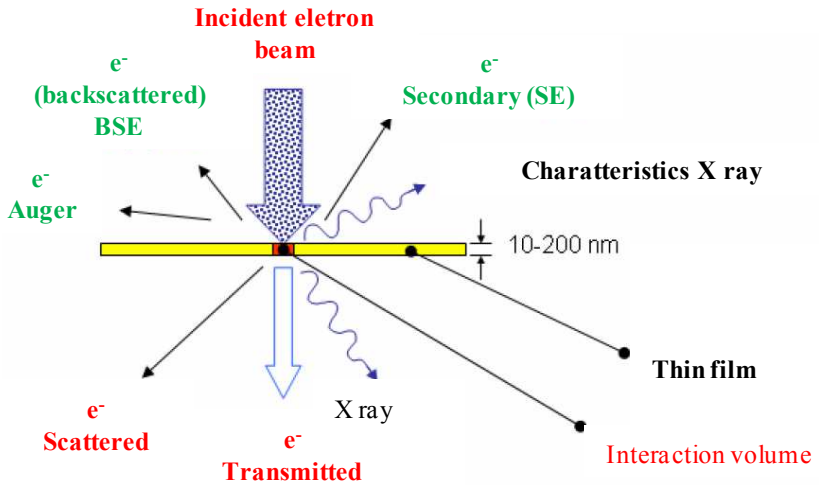

Figure 1: Electron beam – specimen interaction diagram.

The morphological investigation of inorganic filler powders was carried out by Transmission Electron Microscopy (TEM) by using a Zeiss EFTEM Leo 912AB

transmission electron microscope, working at 80 kV. Digital images were acquired by a charge coupled device (CCD) Esi Vision Proscan camera. Powder analysis was performed on ≈10 μg of silica or functionalized silica suspended by sonication for 10 min in 0.5 ml in ethanol. Afterwards, 100μL drop of this suspension was deposited on a holey carbon film supported on a nickel grid (300 mesh) for the investigation.

3.1.3. Nitrogen physisorption (BET)

Specific surface area, external surface area and porosity[6] (pore volume and pore size distribution) was measured out by physical adsorption of N_2.

Regarding the porosity, in particular for pore diameter, an official classification was proposed by the International Union of Pure and Applied Chemistry (IUPAC)[7]: micropores (pore size < 2 nm), mesopores (pore size between 2 nm and 50 nm) and micropores (pore size > 50)[8].

Adsorption[9] is a phenomenon in which a fluid interacts with the surface atoms of solid by Van der Waals or weak forces (energies of interaction between adsorbent and adsorbed is in the order of 20 kJ/mol).

Among the fluids used for the physical adsorption measurements, N_2 is the most chosen because it is chemically inert and condenses at –196°C.

The increase of the amount of adsorbed fluid corresponds to a variation of pressure in dynamic equilibrium. Isotherm function represents the change of the equilibrium expressed as volume of the adsorbed gas as function of the relative pressure p/p_0, where p is the pressure of the vapor and p_0 is its saturation pressure.

At low relative pressure the smallest pores are filled with nitrogen. As the pressure is increased further, larger pores are filled; near the saturation pressure, all pores are filled. The total pore volume is determined by the quantity of gas adsorbed near the saturation pressure. Desorption occurs when the pressure is decreased from the saturation pressure downward[10].

The desorption isotherm rarely overlaps with that of adsorption, creating an hysteresis, due to the presence of pores in the adsorbent material.

By studying the hysteresis shape it is possible to determine the total pore volume and size distribution of the pores.

The IUPAC classification recognizes six basic types of isothermes and four different types of hysteresis (see Figure 2)[11]: I isotherm is typical for microporous solids and chemisorption isotherms; type II is observed on finely divided non-porous solids, type III and type V are typical for vapor adsorption (e.g. water vapour on hydrophobic materials) and type IV and V feature a hysteresis loop, finally, the rare type VI steplike isotherm is seen on special types of carbons. Regarding the hysteresis, it is due to desorption on mesopores which occurs at lower pressures than those at which adsorption in similar-sized pores would take place.

There are 4 types of hysteresis shape,: H1(associated with solid homogeneous pore size), H2 (porous solids in which the distribution of the shape and size of the pores is not uniform and pores are not intersected with each other), H3 (solid pore forming flat shape (cracks) of non-uniform size); H4 (solid pore forming flat shape (cracks) of uniform size).

Different models can be applied to different regions of the adsorption isotherms to evaluate the specific surface area (e.g. BET method, Dubinin method, Langmuir adsorption isotherm, etc.), or the micro-and mesopore volume and pore size distributions (e.g. BJH method, Horvath and Kawazoe method, Saito- Foley method, etc.)[12,13,14].

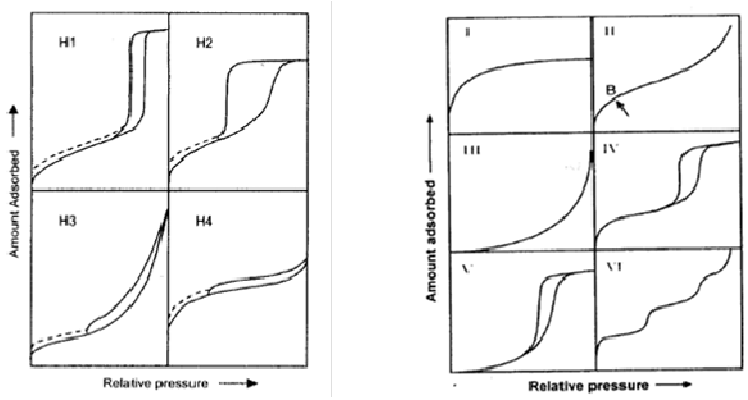

Figure 2: Classification of gas adsorption hysteresis and isotherms.

The microporous volume is determined by the t-plot method of de Boer, while mesopore size and volume are determined by the Kelvin equation.

Nitrogen physisorption measurements of the synthesized samples were carried out on Quantachrome Autosorb-1.

The specific surface area (SSA, BET method[15]), pore volume (desorption cumulative pore volume, DCPV), and pore size distribution (BJH method[16]) of selected samples were measured after evacuation at 200 K for 16 h.

3.1.4. Density

Fillers occupy the full spectrum of density of known materials, but most tire filler density is in the range between 1.5 to 3 g/cm^3. Density[6] of the filler has to be known for formulation calculations[17], for mixing chamber filling of the internal mixer and for the calculation of composite cross-link density[18].

The silica density was measured on 2 g of powder by using a Micromeritics Accupy C 1330 gas pycnometer, the result utilized was an average on five measurements.

3.1.5. Fourier transform infrared spectroscopy (FT-IR)

Infrared spectroscopy is an analysis based on the vibration of the atoms of the molecules.

By passing infrared radiation through a sample (liquids, solutions, pastes, powders, films, gases and surfaces) it is possible to determine what fraction of the incident radiation is adsorbed at a particular energy, and these values are shown in the infrared spectrum.

The interaction of infrared radiation with matter is associated to the change of the molecular dipoles associated to vibration and rotation movements.

FTIR spectroscopy is based on the radiation interference between two beams in order to produce a signal (interferogram) which is a function of the change of pathlength between two beams. By mathematical method (Fourier-Transformation) it is possible to convert the two domains of distance and frequency.

The infrared radiation emerging from the source passes through an interferometer and then through the sample before reaching a detector. In order to increase the signal, the high frequency component was eliminated by a filter. The most common interferometer is the Michelson one, which consists of two perpendicularly plane mirrors, one of which can move in a perpendicular direction to the other[19].

ATR (Attenuated total reflectance) spectroscopy uses the phenomenon of total internal reflection in a crystal. The radiation undergoes a total internal reflection when the angle of incidence at the interface between the crystal and the material is greater than the critical angle (it is a function of the refractive indices of the two surfaces) see Figure 3.

However, the beam penetrates a fraction of a wavelength beyond the reflecting surface. When the material is in close contact with the reflecting surface, the beam loses energy at the wavelength where the material absorbs. The radiation resultant is measured (absorption

energy) and plotted as a function of the wavelength[20]. The penetration depth is a function of the wavelength, the angle of incident radiation and the refractive index of the crystal.

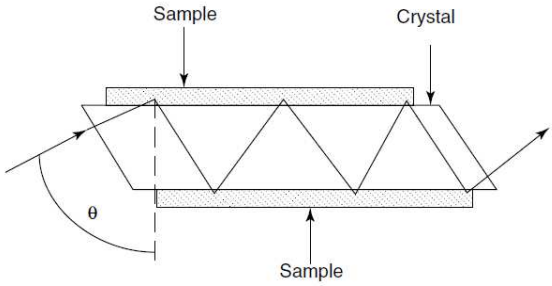

Figure 3: Typical attenuated total reflectance cell.

The Attenuated Total Refletance Fourier Transform Infrared spectroscopy (ATR-FTIR) in the range 4000-600 cm^{-1} was used to check the effective functionalization of silica particles and the presence of adsorbed molecules of starting reagent.

In addition, ATR-FTIR was also used to check the stability and the reactivity of the functional groups, the hydrolysis rate of the alkoxy groups of the trialkoxysilanes in the early stage of the sol-gel reaction of the silica formation and the real functionalization of silica surface by chemical groups. The measurements were performed by a Perkin Elmer Spectrum 100 instrument (1 cm^{-1} resolution spectra, 650-4000 cm^{-1} region, 16 scan).

3.2. Uncured and cured composite characterization

This section of the chapter discusses the basic principles and methodologies for characterizing uncured and cured nanocomposites.

Thermal and morphological characterizations were performed by Density measurement, Termogravimetric Analysis (TGA), Differential Scanning Calorimetry (DSC), Transmission Electron Microscopy (TEM) and Scanning Electron Microscopy (FE-SEM).

The interaction between the inorganic and the organic part within the composite was determined with swelling, bound rubber and cross-link density measurements.

The mechanical analysis of the uncured composites was carried out in a dynamic mode with two different applied stresses: shear (at fixed temperature), tension (at varying temperature). While, for cured composite static tension mechanical analysis, dynamical analysis in compression and in shear stresses were carried out.

All the mechanical analyses were described by reporting the experiment parameters, instrument detail and basic principles.

In order to find the optimal way to vulcanize the compound Mooney viscosity and curing kinetics were checked.

In addition, the vulcanized compounds were characterize from hardness, abrasion and rebound resilience aspects.

3.2.1. Density

Adding fillers to polymer increases density value in comparison to unfilled polymer. The density of the composite, can be calculated according to the linear rule of mixture, where ρ_c, ρ_f and ρ_p are the densities of the composite, filler and matrix, respectively, and m_f is the mass fraction of filler.

$$p_c = \frac{p_p p_f}{p_p m_f + p_f (1 - m_f)}$$

The results thus obtained usually agree with the measured values. A lower value of density than expected may be due to an error of the amount of ingredient, or to inclusions of air resulting from poor mixing or poor wetting of the filler. It is a simple test, considered as a quality check. In addition, the density was determined in order to calculate the crosslink density of the composite.

The density (ρ_c, g cm^{-3}) was determined on 45 g approximately of composite by using ELATEST® BRABENDER®.

The sample material is compressed in the measuring cylinder in order to remove by compression any gas contained in the composite. The moving piston reaches a position which is specific for each individual sample at a well defined pressure.

The final position of the piston is measured by a transducer and transmitted to the computer which correlates the value to a specific volume. Thus, with the weight and the volume it is possible to calculate the density. The measurement was repeated five times.

3.2.2. Thermal analysis (TGA)

The principle of the thermogravimetric analysis has already discussed in section 3.1.1.

The analysis of the composite was carried out in order to determine the amount of filler. Therefore, quantitative determination of silica content in composites[21,22], blending or sol gel prepared, was carried out by Thermo Gravimetric Analysis (TGA), at constant gas flow (50 $cm^3\ min^{-1}$).

The sample (20 mg) was placed in an alumina pan and heated under flowing gas up to 1000°C at a heating rate of 10°C/min.

The silica content was calculated by the following expression:

$$SiO_2 \text{ content (phr)} = (W_1/W_2) \times 100$$

where W_1 is the weight of remaining ash, W_2 is the composite weight. The conversion of SiO_2 precursor was calculated by the expression:

$$\text{Conversion (\%)} = (W_3/W_4) \times 100$$

where W_3 is the amount of SiO_2 calculated from the first equation and W_4 is the theoretical amount of SiO_2, assuming quantitative conversion of SiO_2 precursor.

3.2.3. Differential Scanning Calorimetry (DSC)

The differential scanning calorimetry[23] (DSC) is a thermo-analytical technique which measures, under a controlled atmosphere, the difference in the amount of heat required to increase the temperature of a sample and reference as a function of the temperature.

The information that can be obtained from these analyses, is not only about the temperatures of phase transitions, but also the degree of crystallinity, the specific heat, and the characterization of endothermic and exotermic processes.

The DSC instrument relates, by Ohm equation, the temperature change dT of the composite with the heat flow dQ, where R is electrical resistance of the thermoelectric disc, as reported hereafter:

$$\frac{dQ}{dt} = \frac{dT}{R}$$

Inside the furnace, two hermetically closed aluminum pans were allocated: one with the sample the other one empty (in order to not find any exo or endo phenomenon). Pans are electrically heated in the same way to emanate heat fluxes.

The tests are performed under an inert atmosphere (usually N_2) in order to avoid, during the analysis, possible oxidation of the samples. DSC of the prepared composites was performed in order to determine the T_g (glass transition).

The aim of this analysis is to determine the temperature below which it is possible to cut the composite for TEM. The DSC thermal analysis of composites was performed with DSC1 MettlerToledo Star^e Thermal Analysis System equipped with N_2 low temperature apparatus

by using Al crucible. Between 0.05 to 5 mg of samples were heated from -100°C to 100°C at 2 °C/min.

3.2.4. Transmission electron microscopy (TEM)

The principle of TEM has already discussed in section 3.1.2.

TEM investigation on rubber composite was performed to study in depth the morphology of the particles (size and shape) and the distribution and homogeneity of the particle network[24]. Specimens for the analysis were prepared by cutting the samples into slices, of ≈ 70 nm thickness, using an ultra-microtome (KLB 4800A Ultrotome) equipped with a cryo-system (LKB14800 Cryokit) at a temperature near the glass transition (between -65°C and -50°C). The sections were placed on a nickel grid (300 mesh), covered with a Folmvar® film, and coated with evaporated carbon.

3.2.5. Scanning electron microscopy (FE-SEM)

Evaluation of size and shape of filler aggregates and their distribution in the matrix can be investigated by using FE-SEM (Field Emission Scanning Electron Microscopy)[25,26]. Among the different types of scanning electron microscopy available, which differ from each other from the type of electronic source, field emission shows the best resolution and magnification.

The electron microscope is composed of a: source that generates a beam of electrons, which is followed by a device which can, through the imposition of high values of potential, accelerate the beam; a combination of different types of pumps to obtain an ultra-vacuum condition; electromagnetic lenses, capable of focusing and scanning the surface of the sample. The interaction between the sample and the beam generate the emission of particles and electromagnetic radiation, whose number depends on the morphology of the sample.

These emissions are converted to electrical signals and then in pixels and images. The electron bean source is a cathode, formed by a single tungsten crystal, with a curvature radius in the range of 20-200 nm. This cathode is situated after two anodes, which accelerate the electron emission.

The morphological investigation of uncured and vulcanized composites was performed by Field Emission Scanning Electron Microscopy (FE-SEM) Ultra Plus Gemini Zeiss having an accelerating voltage of 15 kV and in-lens beam. Before FE-SEM analysis, the rubber composites were cryogenically fractured into slices of ≈ 1 mm thickness under liquid

nitrogen, and the surface was gold sputtered by electro-deposition using an Edwards Sputter Coater S150B (deposition time, 0.5 min; current set, 30 mA; electric potential, 1 kV) to impart electrical conductivity.

3.2.6. Swelling, bound rubber and cross-link density

Swelling tests were performed by dipping the composite in an appropriate organic solvent. During swelling, absorption and diffusion of the solvent into the polymer matrix occurs[27, 28] and the uncured polymer is able to dissolve totally or partially in the solvent to form a homogeneous polymer solution. The degree of liquid swelling depends on the nature of the solvent, time of immersion of the rubber composite and on the thickness of the specimen: an equilibrium condition can be reached after sufficient exposure time. If the polymer has cross-links and its chains form an extended network, it cannot dissolve [29,30,31].

Therefore swelling experiments were performed to investigate the degree of cross-links of the composite macroscopically.

Generally, the incorporation of fillers in composite creates a partial loss of polymer solubility [32,33]. Therefore, the solubility of the uncured composite results lower than that of pure polymer.

Swollen elastomers have a more elastic behavior than a viscous one. The equilibrium is reached when the swelling degree is maximum that is when the force of the network swollen is equal to the solvent diffusion. Therefore, by weighting the sample before, after swelling[34], and after solvent removal it is possible to determine the swelling ratio (Q%), the absolute swelling ratio (q) and the extractable fraction (f). They are calculated according to the following equations :

$$Q\% = \frac{m_s - m_0}{m_0} \times 100$$

$$q = \frac{m_s}{\mathrm{m_d}}$$

$$f = \frac{m_0 - m_d}{m_0} \times 100$$

where m_0 is the weight of the composite before swelling, m_s the weight of the swollen mass and m_d the weight of the dried mass.

The swelling tests of the synthesized composites were performed by using toluene as a solvent.

Samples of size 10 x 10 x 2 mm^3 (0.20 ± 0.02 g) were immersed in 20 ml of toluene at 40°C for three days in closed vessels in dark (in order to avoid photo-degradation reactions of the compounds). Toluene was replaced daily with fresh solvent to eliminate all the uncrosslinked fractions. Finally, the swollen mass was weighted and dried to constant mass in vacuum at 70°C for 12 h.

Swelling applied to uncured filled composites can also be used as a method to determine the filler-bound rubber[35]. It is defined as the amount of rubber trapped by the filler aggregate after the mixing[36] and is strongly adsorbed on filler particles surface[37], which resists to the desorbtive action of the solvent. Different models try to explain the different ways in which rubber is excluded from the rubber matrix and incorporated with the filler; Figure 4 illustrate schematically such models:

a) the rubber chain is attracted either physically or chemically to form a rubber shell on the surface of the particle;

b) the rubber shell on individual particles extends throughout the particle aggregate;

c) the rubber collects around the aggregate and the rubber shell to form an outer layer of occluded rubber;

d) the rubber is trapped between aggregates which form agglomerates.

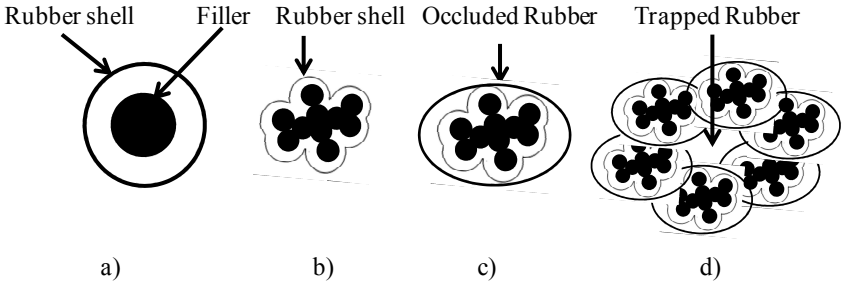

Figure 4: Models of filler-bound rubber.

There are many factors influencing the bound rubber formation. They can be classified[37] according to filler variables (concentration, aggregate size, surface area, chemical composition, surface activity), elastomer variables (chemical composition, unsaturation, thermal, mechanical and oxidative stability), effect of chemical additives (coupling agents), mixing variable (mixing energy, time and temperature) and test method.

Toluene swelling combined with TGA measurement was used to determine the fraction of rubber strongly adsorbed on the filler surface. Bound rubber content was determined in uncured composites by extracting the unbound materials, such as ingredients and free rubber

with toluene for three days at room temperature. The weights of the samples before and after the extraction were measured, and the bound rubber contents were calculated as [38,39]:

$$B_r\% = \frac{\left[m_d - m_0\left(\frac{m_f}{m_f + m_r}\right)\right]}{m_0\left(\frac{m_r}{m_f + m_r}\right)} \times 100$$

where m_f and m_r are the fractions of the filler and the rubber in the compound previously determined by TGA in air flow.

Toluene swelling on composites prepared by using the sol-gel method show that they are partially cross-linked. The easiest method for checking these characteristics is the swelling of toluene.

Crosslink density (η) can be calculated using Flory-Rehner equation[40,41,42] as shown in the equation:

$$\eta = \frac{-[\ln(1 - V_r) - V_r - \chi V_r^2]}{V_s\left(V_r^{\frac{1}{3}} - \frac{V_r}{2}\right)}$$

where V_s is the molar volume of the solvent (106.2 $cm^3\ mol^{-1}$ for toluene), V_r is the volume fraction of rubber in the swollen gel, χ the rubber solvent interaction parameter (χ = 0.3795 for the NR-toluene system). The value of V_r was calculated by the following equation:

$$V_r = \frac{\left(\frac{m_0}{\rho_{cr}} - \frac{m_f}{\rho_f}\right)}{\left(\frac{m_0}{\rho_{cr}} - \frac{m_f}{\rho_f}\right) + \left(\frac{m_s - m_0}{\rho_{toluene}}\right)}$$

where ρ_{cr} is the density of the cross-linked rubber (g cm^{-3}), ρ_f is the density of silica prepared by sol-gel method and $\rho_{toluene}$ is the density of toluene (0.862 g cm^{-3}).

This theory assumes that all the cross-links have the same length, and the network is without defect.

3.2.7. Electron Spin Resonance (ESR)

Electron Spin Resonance was performed in order to study the cross-linking extent of the rubber matrix in the presence of differently functionalized silica fillers. In detail, the behavior of the nitroxide radical was investigated introducing it as a spin probe to check the rigidity of the rubber chains in presence of the reinforcing filler.

The radicals were incorporated into uncured NR composites by swelling the samples in a toluene TEMPOL solution.

The samples of 10 x 10 x 2 mm^3 size, 0.20±0.02 g weight, were immersed in 20 ml of TEMPOL/toluene solution (1.3 x 10^{-4} M) in closed vessels, at 40°C in dark for three days. It was assumed that TEMPOL molecules dissolved in toluene and entered the swollen NR matrix. After three days, the supernatant solution containing the unlinked NR chains extracted from the composites, was removed.

In order to eliminate the small amount of residual solvent trapped in NR matrix, samples were further dried to constant mass under vacuum at 70°C for 12 h before ESR analysis.

As TEMPOL may act as spin-trapping of reactive radical species, eventually formed during the swelling procedure, the stability of nitroxide radical in the presence of the thiol groups of TMSPM and the polysulfide groups of TESPD and TESPT was evaluated. ESR spin-probe blank tests were performed by solving in 20 ml of TEMPOL/toluene solution (1.3 x 10^{-4} M) suitable amounts of TMSPM, TESPD, TESPT and TEOS, equimolar to the substituted silanes present in NR-TMSPM-2, NR-TESPD-2 and NR-TESPT-2 composites. The solutions were maintained in closed vessels at 40°C in dark for three days, before ESR analysis.

The ESR investigation was performed by a Bruker EMX spectrometer working at the X-band frequency, equipped with an Oxford temperature control unit, at 25°C. Spectra were recorded on 10 x 2 x 2 mm^3 specimen, put in a ESR quartz tube (inner diameter 3 mm). Typical ESR spectrometer settings were: microwave frequency: 9.8 GHz; microwave power: 1 mW; sweep width: 2 mT; modulation amplitude: 0.1 mT; scan time: 41.94; time constant: 81.92.

Care was taken in order that the most sensitive part of the EPR cavity (1 cm length) was filled by the samples. The g values were calculated by standardization with α,α'- diphenyl-β-picryl hydrazyl (DPPH). The spin concentration was obtained by double integration of the resonance lines, referring the area to that of the standard Bruker weak pitch (9.7 x 1012 ± 5% spins cm^{-1}). Accuracy on double integration was ± 20%.

3.2.8. Dynamic mechanical analysis (DMA)

Dynamic mechanical analysis (DMA) of the composites is carried out with the shearing stress mode, which allows to determine flow properties[43].

The basic principle of mechanical analysis were reported in paragraph 2.4.3.

Parameters G'_0, G'_∞, $\Delta G'$, G'' and Tan δ were determines with the intention to study the viscoelatic properties of the filler-rubber nanocomposites[44].

There are various types of polymer shearing[45,46] : a) laminar flow, b) Co-axial flow (Mooney viscosimeter), c) telescopic flow (capillary rheometer) or d) torsional flow (plate-plate, cone -plate rheometer RPA) (see Figure 5).

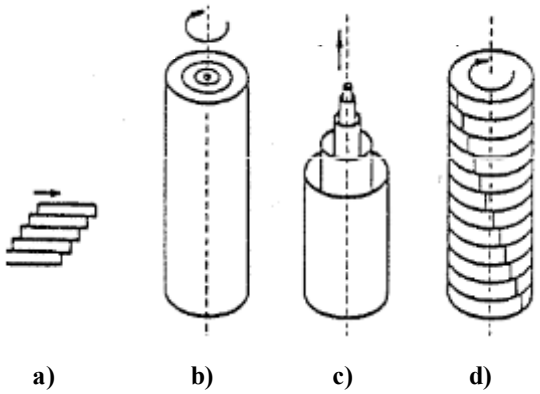

Figure 5: Different flow properties.

Within the torsional plate, parallel and cone geometries can be used (see Figure 6).

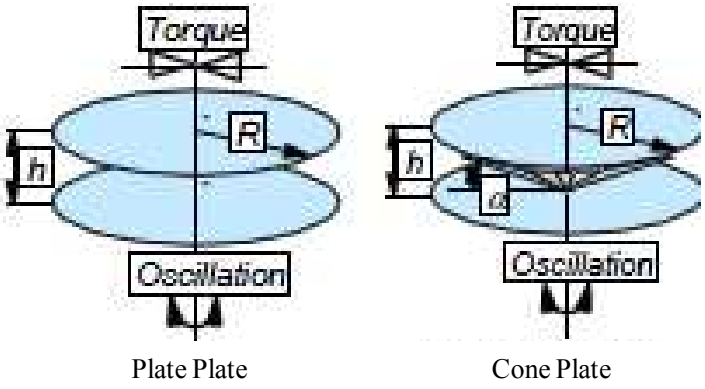

Figure 6: Torsional plate geometries.

In the parallel plates rubber test, the gap between two plates is determined by the viscosity of the composite.

The cone geometry uses a cone in the upper plate which is set at a specific angle.

A very small angle corresponds to a homogeneous strain across the sample. While the gap between the plates is decided before and does not vary with the material used.

This geometry is the most used today.

Dynamic mechanical characterization of composite samples was performed by Rubber Process Analyzer (RPA2000, Alpha Technologies) on the appropriate composite samples.

Specimens for RPA analysis were cut by a Constant Volume Rubber Sample Cutter (CUTTER 2000, Alpha Technologies) from the uncured vulcanized composite sheets (see composite preparation) and were 3.5 cm in diameter and ≈ 0.2 cm thick, weight 4.5±0.3 g (see Figure 7).

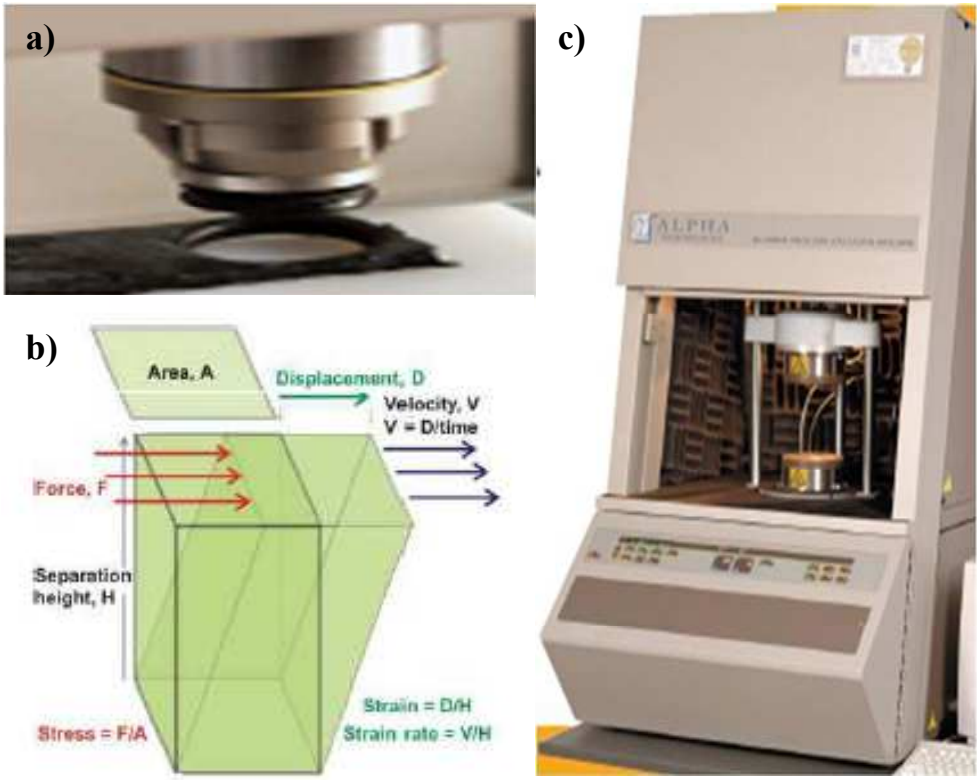

Figure 7: a) Rubber cutter, b) material shearing and c) RPA.

Two measurements were made for each sample, and the averages were reported.

The strain sweep tests were carried out at T = 70°C and 1 Hz from 2.0 % to 100 % of elongation (strain %).

In order to verify the effect of the temperature on the dynamic mechanical properties of the uncured composites, the samples were heated at 150°C for 10 min (corresponding to vulcanization temperature), then cooled down to 70°C before performing a new strain sweep test. Dynamic mechanical analysis carried out in shear stress mode of cured samples was made in the same machine used for uncured samples. In this case the strain sweep was carried out at 70 °C and 10 Hz.

3.2.9. Dynamic mechanical thermoanalysis (DMTA)

Dynamic mechanical thermo analysis (DTMA)[46,47] is one of the methods which allow to measure the response of polymer in a broad range of temperature and frequency of dynamic deformation. From this analysis one can receive a pattern of changes for dynamic Young modulus and the loss tangent. The knowledge of these patterns enables to establish relationships between molecular parameters and mechanical properties of polymeric materials that affect materials performance[48].

DTMA can be simply described as applying, during a temperature program, an oscillatory traction force to a sample and analyzing the material's response to that force [49].

In detail, the trends of Tan δ, E' and E'' were obtained as a function of temperature or time as reported (see Figure 8).

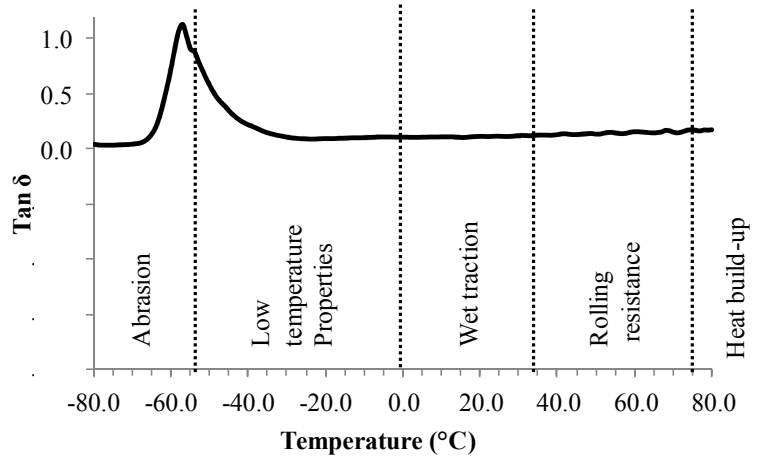

Figure 8: Tan δ as a function of temperature (tread rubber evaluation).

As shown in this plot, the test temperature modifies the modulus and Tan δ[50]. In addition, the maximum temperature of the Tan δ shows the glass transition temperature of the composite.

The trend of Tan δ is indicative of the behavior of the most important properties of the tire tread.

Tan δ at low temperature is indicative of the tire tread behavior for winter use, indicating skidding behavior (grip, traction) on ice. In addition, Tang δ at 0°C was used as a predictor of tread compound wet traction.

The tread compound contribution to tire rolling resistance is predicted by Tang δ at 70°C.

DMTA characterization was performed on uncured composite by using Explexor® DMA/DMTS 150 Gabo.

The samples were cooled to -80 °C by using liquid nitrogen and equilibrated for 3 min at that temperature and then heated to +80 °C at a frequency of 1 Hz with a constant heating rate of 2°C/min also under nitrogen atmosphere.

These analyses were performed on rectangular samples of 1 mm thickness, 10 mm width and 29 mm of useful length.

The shape of the sample, with a small ratio between the weight and the exposed surface, was chosen because it can cool rapidly.

3.2.10. Curing kinetic

Uncured composites in generally are not very strong. When a force is applied to these materials, they do not maintain their shape after a large deformation[51,52].

Therefore, the vulcanization process applied to uncured compound, increases the elasticity of the material while decreasing its plasticity. During this process, the polymer interactions at molecular level of the rubber change[53].

The vulcanization process can be followed by measuring torque variation as a function of the time at fixed temperatures.

The plot obtained at the end of vulcanization is called kinetic vulcanization curve and can be divided in to three parts indicative of: processing, curing and physical properties (see Figure 9). Different parameters can be seen in the plot:

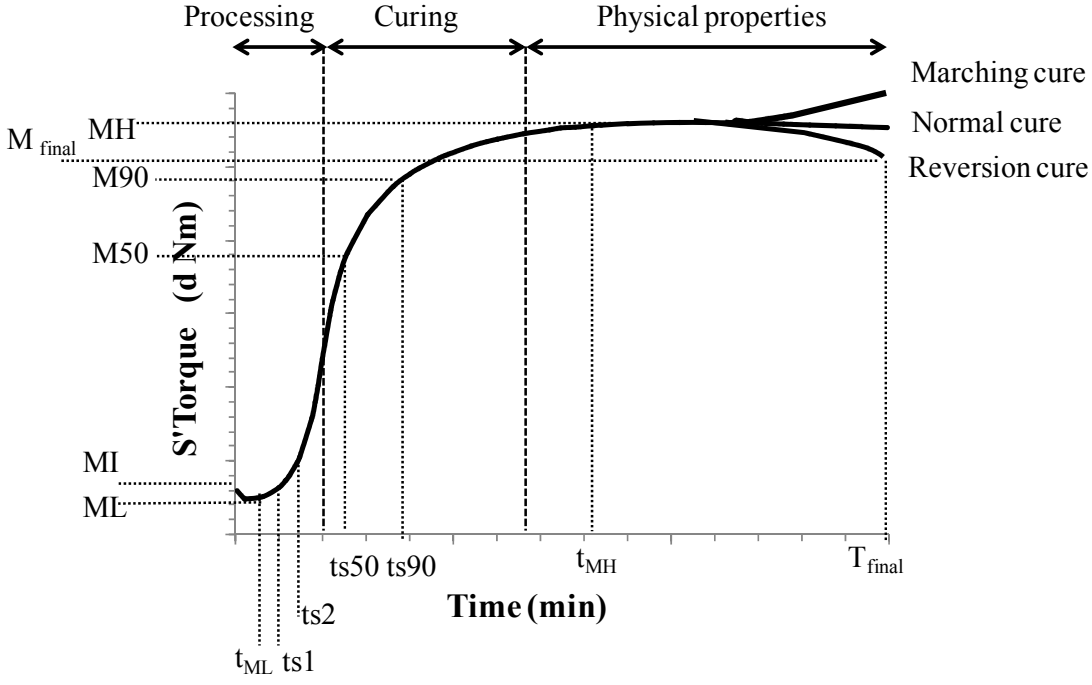

Figure 9: Rheometer cure curve.

MI, initial torque.

ML, minimum torque, a measure of the viscosity of uncured composite correlated with Mooney viscosity.

MH, maximum torque, the maximum torque achieved during the cure.

ts1, the time necessary for the cure state to increase of one torque unit above the minimum at the given cure temperature, it is a measure of the scorch time or processing safety.

Scorch time is the time in which a three dimensional network develops to make the rubber more elastic.

Scorch safety is the length of time which the rubber can be kept at high temperature and still remain plastic. At this time the plastic material starts to became elastic.

ts2, the time necessary to increase of two torque units above the minimum at the given cure temperature.

t50, the time to reach 50 % of the maximum torque, it is a measure of the cure rate.

The cure rate describes the rate at which cross-links in rubber form, and determines how long a compound has to be cured.

t90, the time to reach 90% of the full cure defined as (MH-ML). It can be considered the state of cure at which the physical properties reach an optimal result and is called cure time. The shorter the time is, the faster the cure rate is.

Sometimes after the optimum cure time and torque, reversion of cross-link density can occur.

This phenomenon is always combined by a drop in torque and can be quantified by the following formula:

$$R\ \% = \frac{MH - M_{final}}{MH - ML} \times 100$$

Therefore the kinetics of curing can be studied by using a rheometer which measures the variation of the torque as a function of the time at a fixed temperature.

A Moving Die Rheometer (RPA 2000, Alpha Technological) was used under following conditions: oscillation angle = ± 1°, temperature = 150°C, pressure 4.3 bar and running time = 30 min.

Before the analysis the rubber specimens were cut by a Constant Volume Rubber Sample Cutter (CUTTER 2000, Alpha Technologies) from compound sheets (see composite preparation) and were 3.5 cm in diameter and ≈ 0.2 cm thick, weight 4.5±0.3 g.

3.2.11. Mooney viscosity

The Mooney viscosimeter[54] determines the relative viscosity and scorch time of rubber and composites in the uncured state. The viscometer measures the force, or torque, required to rotate a metal disk, or rotor, within a shallow cylindrical cavity filled with rubber compound. Mooney viscosity is reported in Mooney units, which are related to the torque required to rotate the disk (rotor). The value reported is not a true viscosity, but it indicates relative viscosity, or resistance to flow, of compounds measured under the same conditions. Time and temperature for viscosity measurement have to be defined. Mooney scorch time is the total running time to reach a viscosity of five or ten units above the minimum (t_5 or t_{10})[55]. It is used as an index of the processable life of the compound; the greater the scorch time, the longer the processable life.

A typical curve of the trend of Mooney viscosity is reported (see Figure 10).

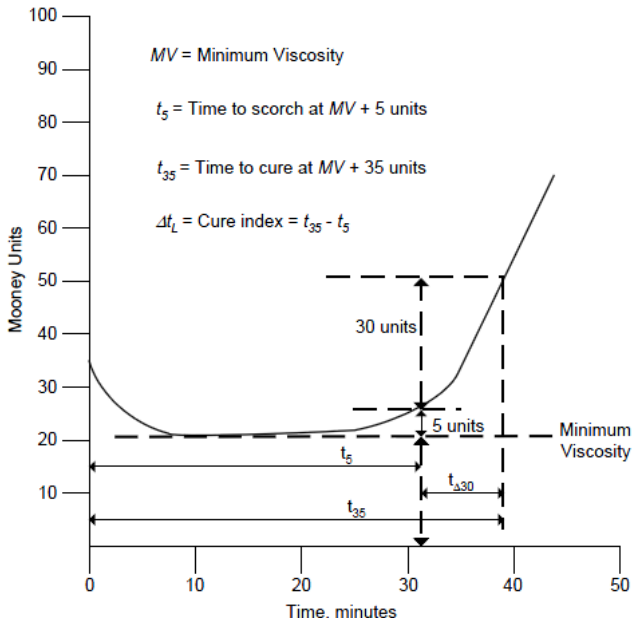

Figure 10: Typical Mooney viscosity curve

Viscosity of uncured compounds was investigated by using a shearing disk viscometer. A Mooney MV 2000 E Viscometer from Alpha Technologies was used adopting the experimental procedure described by ASTM D1646. Scorch tests were run at 121°C, using a large rotor with a 37 mm in diameter rotating clockwise at 0.209 rad/s (2 rpm). Viscosity tests were performed preheating rubber specimens in the viscometer for 1 min at 100°C at

stopped rotor and the viscosity value was then measured upon allowing the rotor to rotate for 4 min (ML_{1+4}). Viscosity is expressed in MU and 1MU corresponds to 0.083 Nm.

3.2.12. Tensile properties

Static tensile mechanical characterization was performed on vulcanized samples. From the stress-strain curve[46] the elongation at break, tensile strength and the modulus at different strain % (50%, 100%, 300%) were obtained. In addition as index of reinforcement can be calculated as the ratio between the modulus 300%/modulus 100% (see Figure 11).

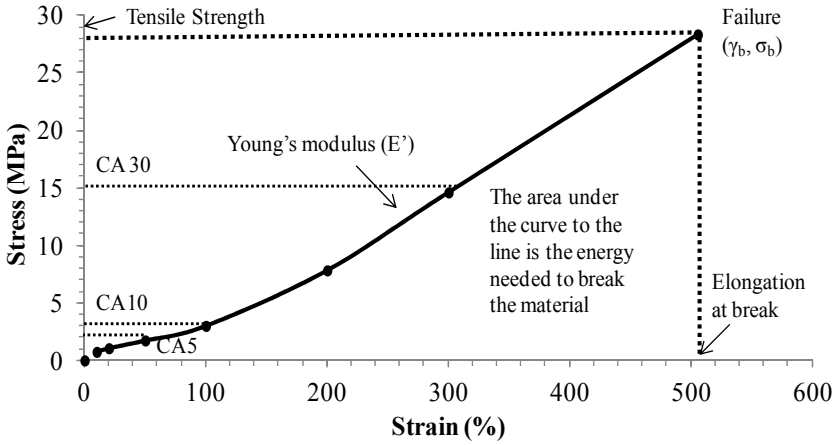

Figure 11: Typical stress strain curve for elastomer material.

The tests were performed on a homemade Control system testing machine on ring type specimens (Schopper ring) of 50 mm of inner diameter, 60 mm of outer diameter and 4 mm in thickness according ASTM D421. During the test, the ring specimen rotates at 15 rpm rate speed, a crosshead speed of 500 mm/min, and a load cell of 5 kN. The values reported for each sample were based on the average of the three measurements.

3.2.13. Compression dynamic mechanical characterization

Dynamic mechanical characterization carried out in compression, was performed on vulcanized samples at three different temperatures (10, 23 and 70°C) and three different oscillation frequencies (1, 10 and 100 Hz). The tests were performed by using Instron apparatus on cylindrical specimen of 1.4 cm diameter and 25 mm of length. Before the analysis, the specimen was heated for 3 min at testing temperature. In addition, the sample was compressed until 25% of the initial length, and the strain amplitude adopted was 3.5 %. Through this test it is possible to determine the thermo-mechanical properties of cured

composites in different use conditions. In fact, by using this analysis, elastic modulus (E'), viscous Modulus (E'') and Tan δ are obtained as three fixed temperatures and frequencies; hence there are 9 elastic modulus, 9 viscous modulus and 9 tan delta for every sample.
In this way it is possible to characterize the sample in most of the use conditions and to check the frequency-temperature dependency of the material.

3.2.14. Hardness

The Hardness of a compound is its resistance to indentation under specified conditions[28]. Hardness is probably the most often-measured property of elastomer vulcanizates[56]. All the factories which control the product use this characterization because it is quick to analyze. It is measured with a durometer. The analysis is carried out by pressing the indenter against the sample and reading the corresponding scale. The force imposed on the indenter is constant and the detection of the sinking is carried out after application of the load (30 sec).
Therefore, the hardness obtained of cured compounds is evaluated by using an International Rubber Hardness Durometer (IRHD) and was determined with an automatic durometer (Monsanto Duratron 2000I). The procedure adopted was ISO 48 for measures at 23°C and 100°C. Specimens used for hardness analysis are composite disks of 4.9 cm in diameter and 0.8 cm thick (for hardness test at 23°C) or 0.4 cm (for hardness test at 100°C). Five measurements were made for each sample.

3.2.15. Abrasion resistance

Abrasion[48] or wear occurs every time two bodies slide against each other under friction. Material is transferred from one body to the other. Abrasion resistance is the ability of a material composition to resist mechanical action, such as friction or erosion that tends progressively to remove material from its surface. Consequently, the surface of the compound heats. The more heat is produced the more the air tendency to oxidize the rubber will be. Different factors influence the compound abrasion: abrasive surface, contact pressure, frequency and length of the contact, temperature and rate of relative motion[28].
Abrasion resistance of the compounds was measured by using a rotating drum abradimeter (from Zwick Instrument) on cylindrical specimens of 17 mm in diameter and 10 mm in height according[57] to DIN 53516. The specimen slide on cylinder covered which abrasive paper with rolls at 40 rpm, under 10 N load, for 40 m in distance. The values are reported on

the "volume loss" basis, calculated from the weight loss and the density of the compound. The results are the average of the three measurements.

---

[1] P. Gabbott, *Principles and Applications of Thermal Analysis*; Blackwell Publishing Ltd, 2008.

[2] S. Ek, A. Root, M. Peussa and L. Niinistro, *Thermochimica Acta*; 2001, **379** (1-2), 201-212.

[3] L. T. Zhuravlev, *Langmuir*, 1987, **3** (3), pp 316–318.

[4] R. Mueller, H. K. Kammler, K.Wegner and S. E. Pratsins, *Langmuir*; 2003, **19**, 160–165.

[5] D.A. Skoog and J. J. Leary, *Chimica analitica strumentale*; EdiSES, Napoli, Italy, 2000.

[6] S. Lowell, J. E. Shields, M. A. Thomas and M. Thommes, *Characterization of porous solids and powders: surface area, pore size and density*; Kluwer Academic Publishers, 2004.

[7] IUPAC, *Pure and Applied Chemistry*; 1972, **31**, 578.

[8] S. Lowell and J.E. Shield, *Powder Surface Area and Porosity*; 2 nd B. Scarlett, Powder Technology Series London, 1984.

[9] S.J. Gregg and K.S.W Sing, *Adsorption, Surface Area and Porosity-2nd Edition*; Academic Press Limited. United Kingdom., 1997.

[10] K.S.W. Sing, D.H. Everett, R.A.W. Haul, L. Moscou, R.A. Poerotto, J. Rouquerol and T. Siemieniewska, *Pure Appl. Chem.;* 1985, **57**, 603.

[11] L. Forni, *Introduzione alla catalisi aspetti applicative*; Cooperativa Universitaria Studio e Lavoro, 1982.

[12] R.G. Avery, J.D.F. Ramsay, *J. Colloid. Interface Sci.* 1973, **42** , 597.

[13] G. Horvath, K. Kawazoe*, J. Chem. Eng. Jpn*.; 1983, **16**, 470.

[14] A. Saito, H.C. Foley, "*Curvature and parametric sensitivity in models for adsorption in microporous*, AIChE J", 1991, **37**, 429.

[15] S. Brunauer, P. H. Emmet and E. Teller, *J. Am. Chem. Soc.*; 1938, **60**, 309.

[16] L. G. Joyner and P. P. Halenda, *J. Am. Chem. Soc*.; 1951, **73**, 373.

[17] B. Rodgers, *Rubber Compounding*; Taylor and Francis Marcell Dekker, 2004.

[18] J.E. Mark, *Rubber Chemistry and Technology*; 1982, **55**, 762-768.

[19] H. Gunzler and H. U. Gremlich, *IR Spectroscopy: an introduction*; Wiley-Interscience: New York, 2002.

[20] B. Stuart, *Infrared spectroscopy: Fundamentals and applications*, Wiley-Interscience: New York, 2004.

[21] J. Siramanont, V. Tangpasuthadol, A. Intrasiri, N. Na-Ranong and S. Kiatkamjornwong, *Polymer Engineering and Science* 2009, **49**, 1099-1106.

[22] V. Tangpasuthadol, A. Intasiri, D. Nuntivanich, N. Niyompanich and S. Kiatkamjornwong, *Journal Applied Polymer Science* 2008, **109**, 424-433.

[23] D. J. D. Menczel and R. B. Prime, *Thermal Analysis of Polymers, Fundamentals and Applications*; Wiley, New Jersey, 2009.

[24] R. Scotti, L. Wahba, M. Crippa, M. D'Arienzo, R. Donetti, N. Santo and F. Morazzoni, *Soft Matter*, 2012, **8**, 2131-2143.

[25] D. L. Reimer, *Scanning Electron Microscopy: Physics of Image Formation and Microanalysis* 2nd; Springer, optical Science, 1998.

[26] AIM, Associazione Italiana di Scienza e Tecnologia delle Macromolecole, *Materiali Polimerici Ibridi e Nanostrutturati*; Atti del Convegno Scuola AIM XXVIII, Gargnano (Italy) 2007.

[27] V. M. Litvinov and P. D. Prajma, *Spectroscopy of Rubber and Rubbery Materials*; Rapra Technology Limited, UK, 2002.

[28] Alan N. Gent, *Engineering With Rubber: How to Design Rubber Components*, 2nd ; Carl Hanser Verlag, Munich 2001.

[29] M. T. Shaw and W. J. MacKnight, Introduction to Polymer Viscoelasticity, Third Edition; John Wiley & Sons, Inc., Hoboken, New Jersey, Canada, 2005.

[30] M.A. Lopez-Manchado, J.L. Valentın, J. Carretero, F. Barroso and M. Arroyo, *European Polymer Journal*, 2007, **43**, 4143–4150.

[31] J. L. Valentín, J. Carretero-González, I. Mora-Barrantes, W. Chassé and K. Saalwächter; *Macromolecules,* 2008, **41** (13), 4717–4729.

[32] J. L. Valentín, I. Mora-Barrantes, J. Carretero-González, M. A. López-Manchado, P. Sotta, D. R. Long and K. Saalwächter, *Macromolecules*, 2010, **43** (1), 334–346.

[33] I. Mora-Barrantes, A. Rodrıguez, L. Ibarra, L. Gonzalez and J.L. Valentin*, J. Mater. Chem.,* 2011, **21**, 7381-7392.

[34] M. Messori and M. Fiorini, *Journal Applied Polymer Science*, 2011, **119**, 3422-3428.

[35] J.L. Leblanc, *Prog. Polym. Sci.;* 2002, **27**, 627-687.

[36] D.J. Kohls, G. Beaucage, *Current Opinion in Solid State and Materials Science*; 2002, **6**, 183–194.

[37] L. Karasek and M. Sumita, *Journal of materials science*; 1996, **31**, 281-289.

[38] Sung-Seen Choi, *Journal of Applied Polymer Science*, 2004, **93**, 1001–1006.

[39] C. Sirisinha and W. Sittichokchucha, Journal of Applied Polymer Science, 2000,**76**, 1542–1548.

[40] P. J. Flory, *Journal of Chemical physics*, 1942, **10,** 51-61.

[41] P. J. Flory and J. Rehner, *Journal of Chemical physics;*1942, **11**, 521-526.

[42] P. J. Flory and J. Rehner, *Journal of Chemical physics;*1943, **11**, 521-520.

[43] Barbara H. Stuart, *Polymer Analysis*; John Wiley & Sons, 2002.

[44] A.V. Shenoy, *Rheology of filler Polymer Systems*; Kluwer Academic Publisher, Great Britain, 1999.

[45] J. M. Dealy and R. G. Larson, *Structure and Rheology of Molten Polymers: From Structure To Flow Behavior and Back Again*; Hanser Verlag, Munich 2006.

[46] H. P. Menard, *Dynamic Mechanical Analyis, A practical Introduction*; CRC Press, Taylor & Francis Group 2008.

[47] S. N. Bhattacharya, M. R. Kamal, R. K. Gupta, *Polymeric Nanocomposites: Theory and Practice*; Hanser Verlag, Munich 2008.

[48] A.K. Bhowmick, *Current Topics in Elastomers Research;* CRC Press, Taylor & Francis Group 2008.

[49] Y.-J. Lin and S.-J. Hwang, *Mathematics and Computers in Simulation*; 2004, **67**, 235–249.

[50] A.I.M. Associazione Italiana di Scienza e tecnologia delle Macromolecole*,Caratterizzazione meccanico-dinamica di materiali polimerici*; 26-27 maggio 2005.

[51] J. E. Mark, B. Erman and F. R. Eirich, *Science and Technology of Rubber;* Elselvier Academic Press, Usa 2005.

[52] J.-M. Vergnaud and I.-D. Rosca; *Rubber curing and properties*; CRC Press, Taylor & Francis Group 2009.

[53] B. Rodgers, *Rubber compounding: Chemistry and application*; CRC Press, Taylor & Francis Group 2004.

[54] C. Lin Jr., W. L. Hergenrother and A. S. Hilton, *Rubber chemistry and technology*; 2002, **75**(2), 215-245.

[55] D. N. Hewitt, *Compounding Precipitated Silica in Elastomers*; William Andew Publishing, Norwich, NY, U.S.A.

[56] V.C. Chandrasekaran, *Essential Rubber Formulary, Formulas for practitioners*; William Andrew Publishing, NY, 2007.

[57] K. Nagdi, Rubber *as a Engineering Material: Guideline for users*; Hanser Verlag, Munich 1993.

Chapter 4

Synthesis of *in situ* Silica-NR composites by sol-gel aqueous method

In this chapter the preparation of silica and functionalized silica in rubber by *in situ* sol-gel method is reported.

The synthesis of silica and functionalized silica powders with the same procedure but not in rubber is also described in order to study in depth the morphology of the nanoparticles. Afterwards, composites are compounded and vulcanized in order to study their performance properties in a real application.

4.1. Materials

Silica and functionalized silica, as powders and in composites, are synthesized by sol-gel hydrolysis and condensation of alkoxysilane in a water environment.

In detail bare silica is prepared starting from TEOS (tetraethoxysilane) and functionalized silica are prepared by adding to TEOS a suitable amount of trialkoxysilane containing the functionalizing molecules.

The presence of functionalizing groups on the particle surface can significantly influence the interaction between the particles, aggregate and agglomerate (filler-filler) and vary the interaction between the silica particles with the rubber. Consequently, functionalized silica particles modify the reinforcing level of the composite.

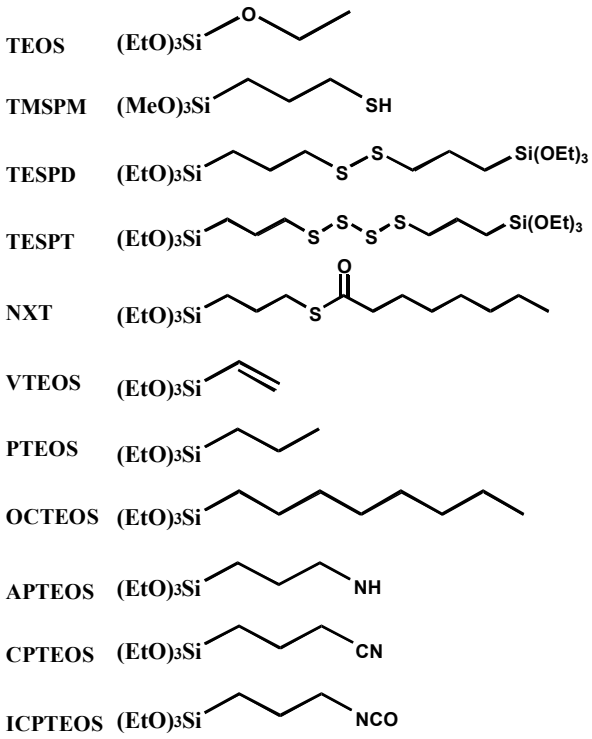

Figure 1: Chemical structures of silica precursor.

Therefore, the different categories of functionalized silica have been chosen:

i) sulfur containing alkyl groups (alkylthiol, alkyldisulfide, alkyltetrasulfide and alkylthiocaboxilate chains),

ii) alkyl and alkenil groups (vinyl, propyl and octyl chains),

iii) nitrogen containing alkyl groups (alkylamine, alkylcyanate and alkylisocianate chains).

Figure 1 reports the chemical structure of tetraethylorthosilicate (TEOS, 99 %); (3-mercaptopropy)trimethoxysilane, (TMSPM, 95 %); bis(3-triethoxysilylpropyl)disulfide, (TESPD, 100%); bis(3-triethoxysilylpropyl)tetrasulfide, (TESPT, 100%); vinyltriethoxysilane, (VTEOS, 98%); triethoxy(propyl)silane, (PTEOS, 99%); triethoxy(octyl)silane, (OCTEOS, 97.5%); (3-aminopropyl)triethoxysilane, (APTEOS, 99%); 3-cyanopropyltriethoxysilane, (CPTEOS, 98%); 3-(triethoxysilyl)propylisocyanate, (ICPTEOS, 99%); they are used for the synthesis.

The alkoxysilanes were purchased from Aldrich and were used without further purification.

Natural Rubber Latex (NR-latex) was Latex 60% from Latex Plan-Hevea Ind. (latex from *Hevea brasiliensis* containing 60.0 % dried rubber, 39.3 % water, 0.7 % ammonia as a stabilizer).

In order to have better control on the size and the porosity of the silica particles, to improve the compatibility of the filler with the rubber and to increase the amount of the silica grown in rubber, a surfactant was used during the synthesis: cetyltrimethylammonium bromide (CTAB) (see Figure 2).

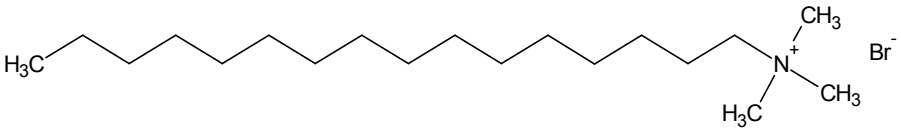

Figure 2: Chemical structure of CTAB.

Typically, this amphiphilic surfactant molecule, used for the synthesis of the inorganic part, is a structure-directing agent that organizes itself through polar head groups in microcavities containing the solvent. Therefore, the structure of micelles is different depending on the nature of the solvent.

In particular, in water the hydrophobic tails interact with each other and fill the interior of the micelle, while the hydrophilic head groups stick in the water phase. It is obvious that their function is obtained only during the synthesis. Therefore, after the formation of the

particles, the template has to be removed from the porosity of the particles by washing in a solvent where it is soluble (such us alcohols with acid).

As a result of this method, by adapting the synthesis parameters, it is possible to prepare nanocomposites and to use small amounts of surfactant to reduce the difference of polarity of inorganic and organic parts and at the same time to increase the porosity of the final materials.

6PPD, N-(1,3-dimethylbutyl)-N'-phenyl-p-phenylenediamine, was the antidegradant used and was purchased from Flexsys. Following the chemical structure is reported (see Figure 3):

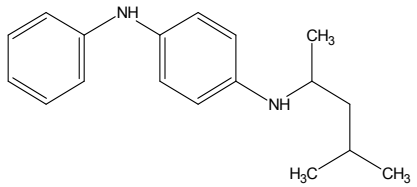

Figure 3: Chemical structure of 6 PPD.

For the reference samples precipitated silica Rhodia Zeosil MP1165, (BET specific surface area 160 $m^2\ g^{-1}$) and dried natural rubber (FFB) supplied from Cau Casulbor was used.

For the compounding preparation we used stearic acid (Stearina TP8) from Undesa; wax (Cera SER AO 54) from SER; carbon black (N 234) from Degussa (specific surface area 120 m^2g^{-1}, average particle size 20–25 nm); sulphur from Zolfoindustria; zinc oxide from Zincol Ossidi; N-tbutyl-2-benzothiazylsulphenamide, TBBS was Vulkacit NZ/EG-C from Lanxess.

4.2. Synthesis of silica and functionalized silica composites

Silica-rubber composites were prepared by the following *in situ* aqueous sol-gel procedure. A solution of CTAB in H_2O (molar ratio H_2O/CTAB = 4857) was added to 100 g of NR latex under mechanical stirring at 900 rpm at room temperature in a 500 ml PE container[1]. The solution of CTAB was added in order to stabilize the formation of silica particles in a rubber/water environment, avoiding particle agglomeration[2]. The total amount of H_2O was fixed at H_2O/SiO_2 molar ratio = 20. Afterwards, silica precursor was added to the previous solution and homogeneous milky mixture was obtained after 10 min of stirring (see Figure 4). After, 10 min, 0.605 g of finely grounded 6 PPD antioxidant were successively mixed to the previous solution.

The reactor was closed to avoid rapid evaporation of the solution and heated at 50°C for 5 days. The sol-gel transition occurred and the silane-latex brown mixture hardened. Finally, the reactor was opened and the composite was dried at 50°C for other 5 days (see Figure 4).

In order to better disperse the filler, sheets of uncured silica-rubber of about 1 mm thickness were prepared by using an open two-roll mill (roll diameters 470 mm; working distance 20 mm).

The temperature of the rolls was set to 50°C by means of a thermostated water recirculation circuit. The mixing time was 2 min at 1.5 mm roll distance and 1 min at 0.5 mm. The speed of the frictional rolls was fixed to 24 rpm and the friction ratio was 1.4:1.

Figure 4: Aqueous scheme synthesis.

Three different silica concentration composites were prepared: 16.65 wt% (20.18 phr, parts per hundred of rubber), 22.93 wt% (30.27 phr) and 30.95 wt% (45.26 phr).

Therefore, 0.2032, 0.3048 or 0.4558 mol of silica precursor were added to the previous solution.

The following table reports all the amounts of the reactants for the three silica concentrations of the composites.

The samples were labeled NR-TEOS-20, NR-TEOS and NR-TEOS-45 (see Table 1).

Composite	NR_{dried}	6PPD	SiO_2	SiO_2	SiO_2	TEOS	CTAB	H_2O
	phr	phr	%	mol	phr	phr	phr	ml
NR-TEOS-20	100	1	16.65	0.2032	20.18	70	0.50	34.24
NR-TEOS	100	1	22.93	0.3048	30.27	105	0.75	70.81
NR-TEOS-45	100	1	45.26	0.4558	45.26	157	1.13	125.16

Table 1: Composition of the composites and amount of reactants.

In order to modify the filler-filler and the filler-rubber interactions and to promote the formation of differently shaped silica particles, the surface was functionalized.

Therefore rubber composites were prepared containing silica modified by alkylthiol, thiocarboxylate, alkyldisulfide, alkyltetrasulfide, vinyl, propyl, octyl chains, alkylamine, alkylcyanate and alkylisocyanate groups [3].

Functionalized silica rubber composites were prepared following the previously described procedure, mixing TEOS with suitable amounts of the organotrialkoxysilane silica precursors TMSPM, TESPD, TESPT, NXT, VTEOS, PTEOS, OCTEOS, APTEOS, CPTEOS, ICPTEOS, to have the same total content of silica and modified silica in rubber (30.3 phr, corresponding to 22.9 wt % of silica).

The organotrialkoxysilane/SiO_2 molar ratios were 0.0184 in the case of TMSPM, NXT, VTEOS, PTEOS, OCTEOS, APTEOS, CPTEOS and 0.0092 for TESPD and TESPT (corresponding to 0.0056 and 0.0028 mol of silane, respectively)[3].

Hereafter, the uncured rubber silica composites are labeled NR-TMSPM-2, NR-NXT, NR-VTEOS, NR-PTEOS, NR-OCTEOS, NR-APTEOS, NR-CPTEOS, NR-TESPD-2 and NR-TESPT-2.

The amount of precursors of silica in phr (considering 100 % purity of the precursor) were reported in table 2.

Samples	Silica Precursor (phr)	
	TEOS	Silane funz.
NR-TEOS	105.00	-
NR-TMSPM-2	101.14	1.82
NR-TESPD-2		2.20
NR-TESPT-2		2.46
NR-NXT		3.39
NR-VTEOS		1.76
NR-PTEOS		1.92
NR-OCTEOS		2.56
NR-APTEOS		2.05
NR-CPTEOS		2.14
NR-ICPTEOS		2.29

Table 2: The amount of silica precursors in phr and in weight in silica composites.

In addition, in order to study the effect of the amount of functionalizing molecules on silica surface, only for TMSPM, TESPT and TESPD different organotrialkoxysilane/SiO_2 molar ratios were used[1].

Sample	X[a]	Silane/SiO_2	Mol						phr[b]			
		molar ratio	TEOS	TMSPM	TESPD	TESPT	NR	Antiox	TEOS	TMSPM	TESPD	TESPT
NR-TEOS	-	-	0.3048	-	-	-	100	1	105.00	-	-	-
NR-TMSPM	1	0.0092	0.3020	0.0028	-	-	100	1	104.04	0.91	-	-
	2	0.0184	0.2992	0.0056	-	-	100	1	103.07	1.82	-	-
	3	0.0367	0.2936	0.0112	-	-	100	1	101.14	3.64	-	-
	4	0.0735	0.2824	0.0224	-	-	100	1	97.28	7.27	-	-
NR-TESPD	1	0.0046	0.3020	-	0.0014	-	100	1	104.04	-	1.10	-
	2	0.0092	0.2992	-	0.0028	-	100	1	103.07	-	2.20	-
	3	0.0184	0.2936	-	0.0056	-	100	1	101.14	-	4.40	-
	4	0.0367	0.2824	-	0.0112	-	100	1	97.28	-	8.79	-
NR-TESPT	1	0.0046	0.3020	-	-	0.0014	100	1	104.04	-	-	1.23
	2	0.0092	0.2992	-	-	0.0028	100	1	103.07	-	-	2.46
	3	0.0184	0.2936	-	-	0.0056	100	1	101.14	-	-	4.93
	4	0.0367	0.2824	-	-	0.0112	100	1	97.28	-	-	9.85

[a] X refers to different concentrations of the same precursor. [b] phr parts per hundred of rubber.

Table 3: Compositions and reactant molar ratios of silica-rubber composites (30.27 phr).

In particular, 30 phr silica-composites were prepared with four different concentrations of functionalizing molecules.

In detail, for 30 phr composite, the TMSPM/SiO_2 molar ratios were 0.0092, 0.0184, 0.0367, 0.0735, the TESPD/SiO_2 and TESPT/SiO_2 ones were 0.0046, 0.0092, 0.0184 and 0.0367. Composition and reactant molar ratios of the prepared samples are summarized in Table 3.

Additionally, in order to study the effect of a larger amount of functionalized silica, 45 phr samples for a selected numbers of precursors (TMSPM, TESPD, TESPT) were prepared[1]. The detailing of 45 phr composites are reported following (see Table 4).

Sample	Silane/SiO_2	Mol						phr[b]			
	molar ratio	TEOS	TMSPM	TESPD	TESPT	NR	Antiox	TEOS	TMSPM	TESPD	TESPT
NR-TEOS-45	-	0.4558	-	-	-	100	1	157.00	-	-	-
NR-TMSPM-45	0.0184	0.4474	0.0084			100	1	154.12	2.72		
NR-TESPD-45	0.0092	0.4474		0.0042		100	1	154.12		3.29	
NR-TESPT-45	0.0092	0.4474			0.0042	100	1	154.12			3.68

[a] X refers to different concentrations of the same precursor. [b] phr parts per hundred of rubber.

Table 4: Compositions and reactant molar ratios of silica-rubber composites (45.26 phr).

Reference master batches were prepared by mixing dry NR, 20.18, 30.27 phr or 45.26 phr of commercial silica Zeosil MP1165 and 1 phr of finely grounded antioxidant 6 PPD in a Brabender Plasti-corder lab station.

The aim was to compare the properties of *in situ* aqueous sol-gel synthesized silica rubber composites with those of a composite prepared by conventional ex-situ blending process. The reactants were mixed at 90°C and 20 rpm for 12 min and, finally, at 90°C and 40 rpm for 3 min.

Sheets of about 2 mm thickness were obtained by 2 min mixing in an open two-roll mill. These reference samples were labeled NR-SiO_2-20, NR-SiO_2 and NR-SiO_2-45.

4.3. Compounding

In order to study the final properties of the composite used in a real application, compounding has to be done.

Therefore, vulcanization system ingredients were added to the composites prepared by mechanical mixing or *in situ* sol gel method.

The list of the compounds prepared in three steps by a Thermo Haake Reomix lab station (mixing chamber of 250 ml, fill factor of 0.7) is reported in Table 5.

The amount of vulcanization reactants and the recipe in phr were detailed for the reference samples and for *in situ* composites containing 30 phr of silica.

	V-NR-C_{black}	V-NR-SiO_2	V-NR-TEOS, -TMSPM, -TESPD, -TESPT, -NXT, -VTEOS, -PTEOS, -OCTEOS, -APTEOS, -CPTEOS, -ICPTEOS.	V-NR-TEOS+C8
NR latex	-	-	100	100
NR	100	100	-	-
In situ - SiO_2	-	-	30	30 (NR-TEOS)
SiO_2 Rhodia	-	30	-	-
TESPT	2.40	2.40	-	2.40
6 PPD	2	2	2	2
Stearic Acid	2	2	2	2
Wax	1	1	1	1
Carbon Black	20	20	20	20
Zinc oxide	3.5	3.5	3.5	3.5
Sulphur	1.2	1.2	1.2	1.2
TBBS	1.8	1.8	1.8	1.8

Table 5: Recipe for the vulcanization of (30 phr) silica rubber composite (phr, parts per hundred rubber).

In depth, for composites containing 22.9 % of silica two reference samples were prepared: V-NR-C_{black} and V-NR-SiO_2.

The first one was prepared in order to separate the contribution of the vulcanization system and additional filler (C_{black}) from the silica.

The second reference was prepared to compare the *in situ* compound with a real compound used.

Therefore, a master batch reference was prepared by using commercial NR and silica.

These compounds were prepared in 3 stages in Thermo Haake Reomix at a temperature of 90°C and at a rotor speed of 70 rpm for 6 min.

In first step, at 0.75 min ½ of the amount of silica and TESPT were added to NR, followed at 1.25 min, by the remaining silica and TESPT and 3.00 min by stearic acid, waxes and carbon black. Successively, after 16 h, the compound was re-worked in Thermo Haake Reomix at 90°C and 60 rpm for 4 min by adding ZnO and 6 PPD.

In the third step, sulphur and the accelerator TBBS were added to the composite at 50 °C and 15 rpm in 4 min in two-roll mill.

Composites were further molded for 5 min to produce sheets of about 2 mm thickness and then undergo the vulcanization process.

Regarding the composites prepared by the *in situ* sol gel method, the compounds were prepared in three steps, modifying the procedure used for blending compounds.

In detail, in the first step *in situ* composites, carbon black (90 % of the amount), stearic acid and waxes were mixed at 90°C and 70 rpm for 6 min.

The first 3 min were used to heat up the *in situ* composite, and masticate and break down the rubber. The sequences of ingredient addition and their progressive time are reported in Table 6.

Stage	Step	Operation	Progressive time
1	0	Composite	0 min
1	1	Carbon black, wax, stearic acid	3 min
1	1	Removal	6 min

Table 6: Sequences of ingredient addition and time for the first step of *in situ* compound preparation.

After 16 h, Carbon black (10 % of the amount), ZnO and 6 PPD were added to the compound at 90°C and 60 rpm for 4 min (see Table 7).

Stage	Step	Operation	Progressive time
2	0	Composite step 1	0 min
2	1	Carbon black, ZnO, 6 PPD	2 min
2	1	Removal	4 min

Table 7: Sequences of ingredient addition and time for the second step of *in situ* compound preparation.

In the third step, sulphur and the accelerator TBBS were added to the composite at 50 ± 3 °C and 15 rpm in 4 min in two-roll mill.

The addition of the vulcanization ingredient was performed at 1.5 mm rolls distance. During the first min, the compounds were worked in order to reach the optimal temperature.

Following, during the second min the accelerator powder (previously grounded) was dropped into the mill tray. Then, during the third min sulphur was added.

During the fourth minute, powders which had not been incorporated in the composite were collected and added back to the mix.

In addition, in order to promote uniform dispersion of the ingredients, cutting and folding were continuously carried out.

The rubber composite was collected preparing a roll and was later worked by using 0.8 mm of roll distance.

During this step the rubber was continuously formed in a sheet and rolled three times. After obtaining a roll of composite, it was worked again by using 0.3 mm of roll distance in order to obtain a sheet.

The procedure used is the same for all the composites prepared by the *in situ* sol gel method, which contained 30 phr of total silica, and did not vary for the composite which had different amounts of functionalizing molecules on silica surface.

Vulcanization of sheets was performed by using an electrically heated hydraulic press[1,3] (BM Biraghi), under the following conditions: temperature 150°C, pressure 4.3 bar, running time 30 min.

Hereafter, the vulcanized silica-rubber composites are labeled V-NR-X, where X is the acronym of the silane.

V-NR-TEOS+C8 was another composite prepared in order to estimate the effect of the addition of TESPT as a compatibilizer during the compounding to V-NR-TEOS.

The procedure adopted was the same used for uncured *in situ* silica–rubber composites when mixed to the vulcanization chemicals.

4.4. Synthesis of silica and functionalized silica

Silica and modified silica powders were prepared following the procedure previously reported for uncured *in situ* silica-rubber composites, in the absence of rubber and the antioxidant.

The aim was to more easily evaluate the modification, the specific surface area (SSA), the shape and size of silica particles.

0.3048 mol of TEOS or a mixture of 0.2992 mol of TEOS and the suitable amount of organotrialkoxysilane[3] (0.0056 mol of TMSPM, NXT, VTEOS, PTEOS, OCTEOS, APTEOS, CPTEOS, ICPTEOS or 0.0028 mol of TESPD, TESPT) were mixed at room

temperature under stirring (900 rpm) to a solution of CTAB in NH_3/H_2O (H_2O/SiO_2 molar ratio = 20) in a 250 ml PE container.

In detail, 0.456 g of CTAB was dissolved in 107.75 ml of water and 2.85 ml of NH_3 (25% v/v). The total amount of NH_3 was the same as in NR latex. The clear solution of the mixture becomes milky after a few minutes.

After 15 min, the powder suspension was heated in a closed reactor at 50°C for 5 days, it was dried in an open reactor at 50°C for 5 days and successively at 120°C for another 2 days. The obtained samples were grounded in a mortar and suspended in a methanol/water solution of HCl 37% v/v (for 1 g of silica, 200 ml methanol and 1 ml HCl) for 6 hours at 80°C under stirring at reflux, in order to eliminate the surfactant CTAB traces[4]. The powder was hot filtered, washed with water and acetone and finally dried under vacuum until constant weight. Hereafter, the powder samples were labeled SiO_2-TEOS and SiO_2-TMSPM, SiO_2-TESPD, SiO_2-TESPT, SiO_2-NXT, SiO_2-VTEOS, SiO_2-PTEOS, SiO_2-OCTEOS, SiO_2-APTEOS, SiO_2-CPTEOS and SiO_2-ICPTEOS.

---

[1] R. Scotti, L. Wahba, M. Crippa, M. D'Arienzo, R. Donetti, N. Santo and F. Morazzoni, *Soft Matter*, 2012, **8**, 2131-2143.

[2] V. Uskokovic and M. Drofenik, *Surf. Rev. Lett.*; 2005, **12**(5), 239–277.

[3] L. Wahba, M. D'Arienzo, R. Donetti, T. Hanel, F. Morazzoni, R. Scotti and L. Tadiello; *In situ sol-gel obtained silica-rubber nanocomposites: influence of the filler precursors on the improvement of the mechanical properties,* Accepted *RSC Advantaces.*

[4] S. Huh, J. W. Wiench, J.-C. Yoo, M. Pruski and S.-Y. V. Lin, *Chem. Mater.;* 2003, **15**, 4247–4256.

Chapter 5

In situ aqueous sol-gel obtained nanocomposites: influence of the sol-gel precursor on the reinforcing properties of *in situ* prepared silica fillers

This chapter discusses silica-rubber nanocomposites obtained by *in situ* aqueous sol-gel synthesis, by using trialkoxysilane with different amounts of functional groups as a precursor. In particular, the first paragraph reports the conversion of precursors to create silica. A detailed morphological characterization of silica rubber composites follows with the aim to understand filler-filler and filler-rubber interactions.

Hereafter, there is a discussion on the efficacy of the filler network in reinforcing the rubber matrix, which was assisted by swelling measurements and the Electron Spin Resonance spectroscopy. Thereafter, dynamic mechanical properties of uncured silica-natural rubber composites were investigated and discussed, in order to find a relationship between the morphology obtained, the degree of network dispersion and the mechanical behavior.

In the last part of the chapter the curing kinetic study and the characterization of the vulcanized composites is reported with a description of mechanical, abrasion, hardness, rebound property results.

5.1. Conversion of silica precursors and properties of silica powders

The conversion of silica precursor to silica in uncured silica rubber composite was determined by TGA in air. Following TGA profiles of NR-TEOS-20, NR-TEOS [1] and NR-TEOS-45 are reported in order to determine the amount of silica in the composites (see Figure 1).

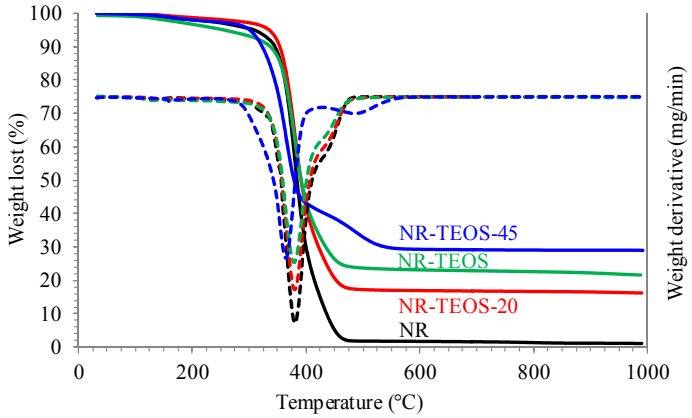

Figure 1: TGA profiles and related derivatives curves of natural rubber (NR) and *in situ* silica composites containing different silica amounts: NR-TEOS-20, NR-TEOS and NR-TEOS-45.

TGA thermograms of NR-TEOS-20, NR-TEOS and NR-TEOS-45 show that after rubber combustion at T > 500°C, the sample weight remains constant, the residual sample at 800°C was assumed to be the amount of *in situ* generated silica. According to the equations reported in the paragraph 3.2.2. the conversion of TEOS precursor to silica particles always

resulted > 98 %, and the filler contents for NR-TEOS-20, NR-TEOS and NR-TEOS-45 were respectively 20.0 ± 0.2 phr, 30.0 ± 0.3 phr and 44.82 ± 0.45 phr which are very similar to the nominal ones.

Also the conversion of functionalized precursor to silica resulted > 98 % and the silica content similar to the nominal one, as shown by the TGA thermogram of NR-TESPT reported as an example (see Figure 2).

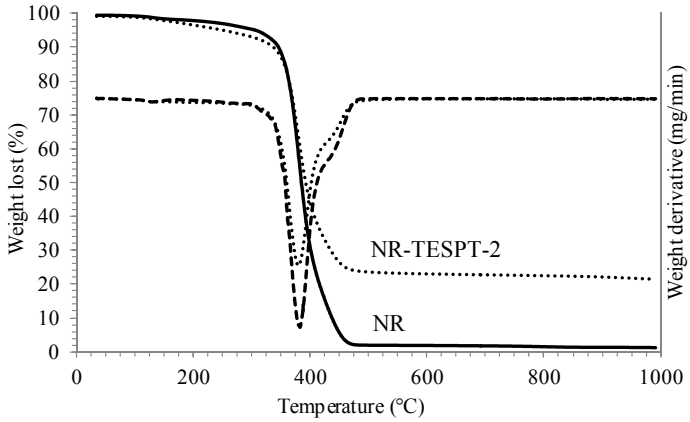

Figure 2: TGA profiles and related derivatives curves of Natural Rubber (NR) and NR-TESPT composite.

TGA analyses demonstrate that no silica precursor loss occurred during sol-gel synthesis. TGA measurements were also carried out under nitrogen on SiO_2-TEOS and SiO_2-X samples in order to evaluate the effective functionalization of SiO_2 fillers. Hereafter, the TGA profiles are reported, carried out in nitrogen flow, of SiO_2-TEOS in comparison to SiO_2-TESPT (see Figure 3a) and SiO_2-TESPD (see Figure 3b) as an example.

The amount of the grafted molecules, expressed as silane/SiO_2 molar ratio, was calculated by the equation reported in paragraph 3.1.1..

The results demonstrated the presence of grafted molecules on the silica surface, and that the amount of organic molecules on silica surface ranged from 0.005 to 0.007 for TESPD and TESPT (TGA profiles in Figure 3) and between 0.010 to 0.015 for the other monosubtituited silane. The results are roughly in agreement with the nominal content.

Nitrogen physisorption analyses were performed on SiO_2-TEOS and SiO_2-X powders. Some examples of nitrogen adsorption-desorption isotherms and pore size distributions are reported in Figure 4.

Specific surface area (SSA), external surface area (S_{ext}) desorption cumulative pore volume (DCPV) and average pore size distribution are reported in Table 1.

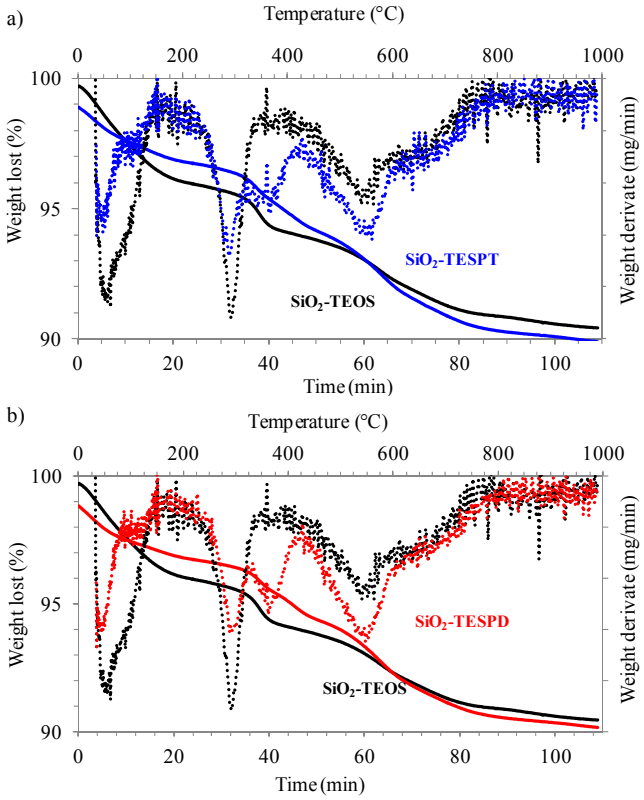

Figure 3: TGA profiles in nitrogen flow and related derivative curves of SiO_2-TEOS in comparison with a) SiO_2-TESPT and b) SiO_2-TESPD.

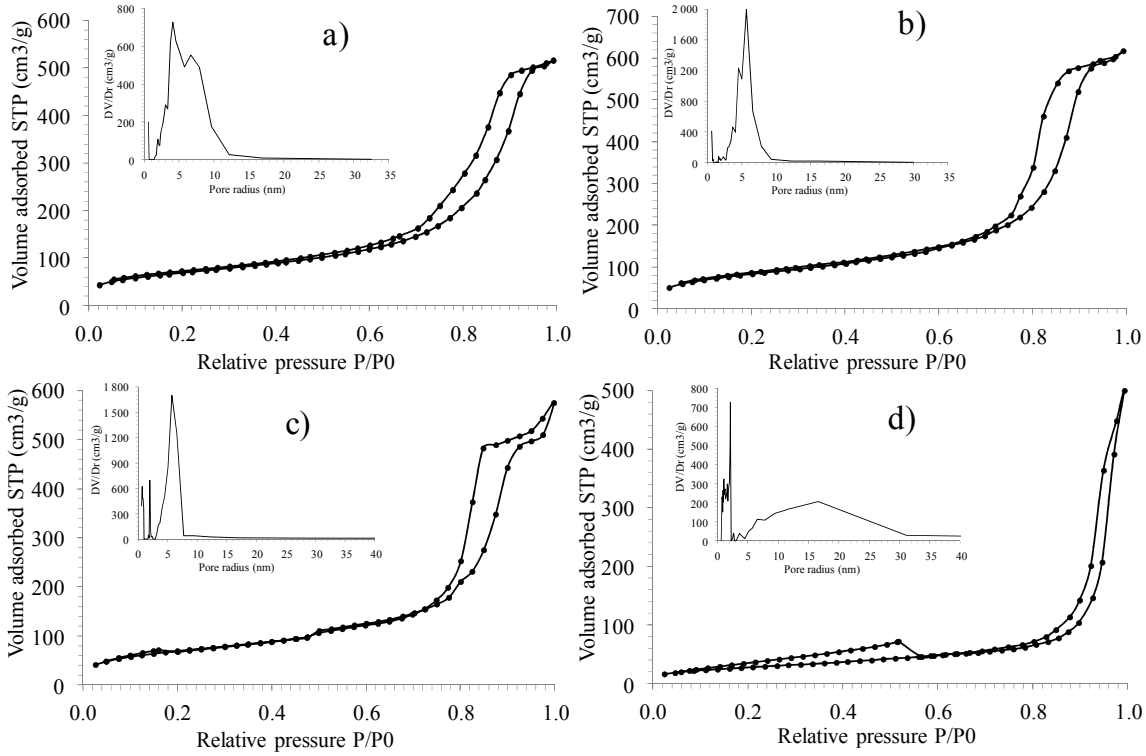

Figure 4: Nitrogen adsorption-desorption isotherms and pore size distribution for a) SiO_2-TEOS, b) SiO_2-TESPT, c) SiO_2-OCTEOS and d) SiO_2-APTEOS.

All silica powders have typical cylindrical meso-scale pores as shown by IV Brunauer[2] shape type isotherm and pore size distribution in the range 10-16 nm, except SiO_2-APTEOS which exhibits a broader distribution centered at a larger size (≈ 30 nm) and a typical non porous isotherm shape.

According to the t-plot and considering the small differences between SSA and S_{ext}, the contribution of micropores to SSA is estimated at 3-5%.

In general, both surface area and pore volume increased in functionalized silica particles, except in SiO_2-APTEOS which exhibits less uniform pore dimension and larger mesopores (see Figure 4 d).

Samples	SSA m^2/g	S_{ext} m^2/g	DCVP cm^3/g	Average pore diameter nm
SiO_2-TEOS	245.0	238.3	0.7999	13.1
SiO_2 -TMSPM	294.7	292.7	0.8721	11.8
SiO_2 -TESPD	300.7	296.7	0.9915	13.2
SiO_2 -TESPT	297.4	295.4	0.9573	12.9
SiO_2-NXT	318.9	318.9	0.9532	11.9
SiO_2-VTEOS	415.4	415.4	1.2010	11.6
SiO_2-PTEOS	294.0	294.0	0.9089	12.4
SiO_2-OCTEOS	249.7	225.2	0.8917	14.3
SiO_2-APTEOS	102.1	102.1	0.7753	30.4
SiO_2-CPTEOS	300.8	300.8	0.8438	11.2
SiO_2-ICPTEOS	300.2	285.9	1.2290	16.2

Table 1: Properties of silica and functionalized silica[3].

This is probably related to the fast rates of the hydrolysis and condensation induced by the amino group, which prevents the formation of small and size controlled nanoparticles (see later).

The TEM images of SiO_2-TEOS and SiO_2-APTEOS particles are reported in Figure 5 and confirm the large particle size of SiO_2-APTEOS compared to the uniform nanoparticles of SiO_2-TEOS.

Regarding SiO_2-TMSPM, SiO_2-TESPD, SiO_2-TESPT and SiO_2-NXT, or rather silicas functionalized with a group containing S, they show similar isotherm shape, pore size distribution and range of specific surface area (see Figure 4 b).

The least pore volume was shown for SiO_2-TMSPM which has a surface thiol function group which can interact both with the oxide silanol group and with other thiol groups (see later) increasing the particle dimensions and reducing the amount of pores.

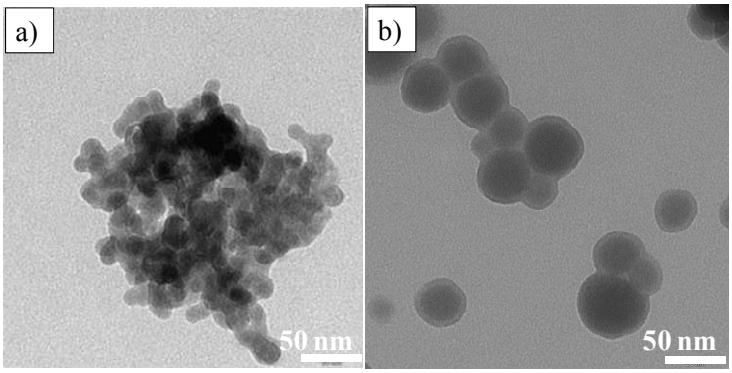

Figure 5: TEM images of a) SiO_2-TEOS and b) SiO_2-APTEOS.

The higher surface area of SiO_2-NXT is probably due to the presence of the protecting group as explained later.

The following TEM images of SiO_2-TMSPM, SiO_2-TESPD, SiO_2-TESPT and SiO_2-NXT confirm the nanodimensions of the powders and the differences reported for SiO_2-TMSPM (see Figure 6).

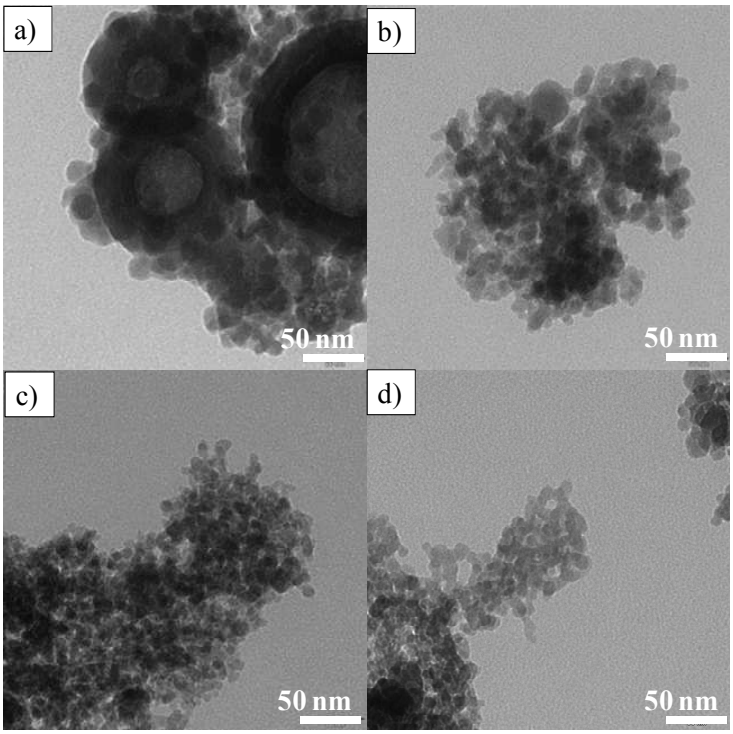

Figure 6: TEM images of a) SiO_2-TMSPM, b) SiO_2-TESPD, c) SiO_2-TESPT and d) SiO_2-NXT.

Interestingly, regarding SiO_2-VTEOS, SiO_2-PTEOS and SiO_2-OCTEOS, as the aliphatic chain length increases the specific surface area decreases (see Table 1) and the pore size increases.

This is particularly evident for SiO_2-OCTEOS, where the largest particles were observed as confirmed by the TEM images (Figure 7).

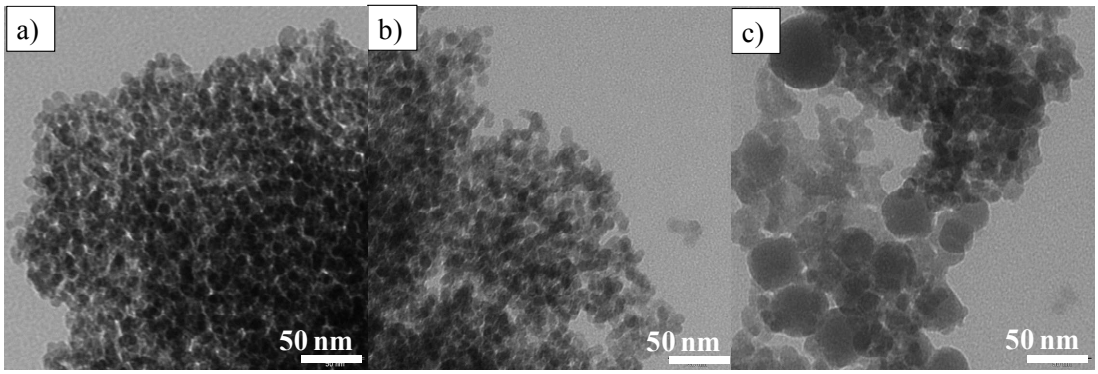

Figure 7: TEM images of a) SiO_2-VTEOS, b) SiO_2-PTEOS and c) SiO_2-OCTEOS.

This behavior can be related to the rate of the hydrolysis/condensation reaction of OCTEOS, which is slower compared to TEOS and to the other substituted silanes.

In fact, the long OCTEOS alkyl chain hinders the interaction between the triethoxy and silanol groups[4].

Thus, OCTEOS did not interact with the silica surface at the early stages of hydrolysis and condensation reactions, leading to the growth of large nanoparticles[5].

The slow kinetics of OCTEOS hydrolysis was confirmed by the FTIR analysis performed on latex suspensions containing the alkoxide precursor (see paragraph 5.2).

Regarding SiO_2-CPTEOS and SiO_2-ICPTEOS, they exhibit similar surface areas and isotherm shapes. In addition, their TEM images show the same nanoparticles morphology (see Figure 8).

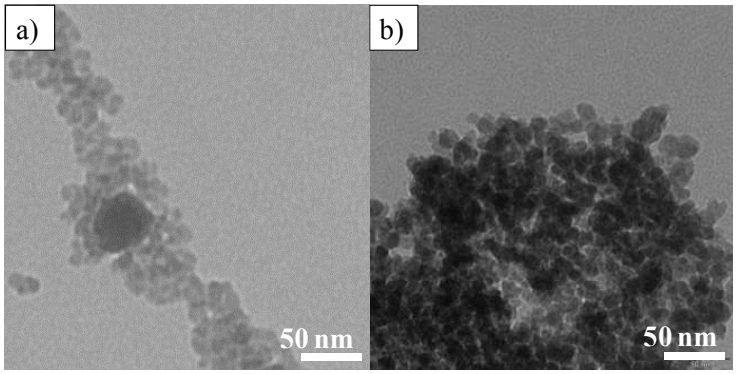

Figure 8: TEM images of a) SiO_2-CPTEOS and b) SiO_2-ICPTEOS.

FTIR analysis was also performed to evaluate the stability and the possible reactions of the functional groups of the silanes during the process.

FTIR spectra demonstrated that the functional groups –NCO and –CN from ICPTEOS and CPTEOS silanes easily hydrolyze[6,7] in the synthesis solution (NR latex), which consists predominantly of water.

No reactions of the other functional groups have been detected in these synthesis conditions.

In order to determine what kind of product can form after hydrolysis of ICPTEOS and CPTEOS in synthesis condition, FTIR spectra of pure reagents[8] (NR latex, TEOS, ICPTEOS and CPTEOS) were acquired (see Figure 9).

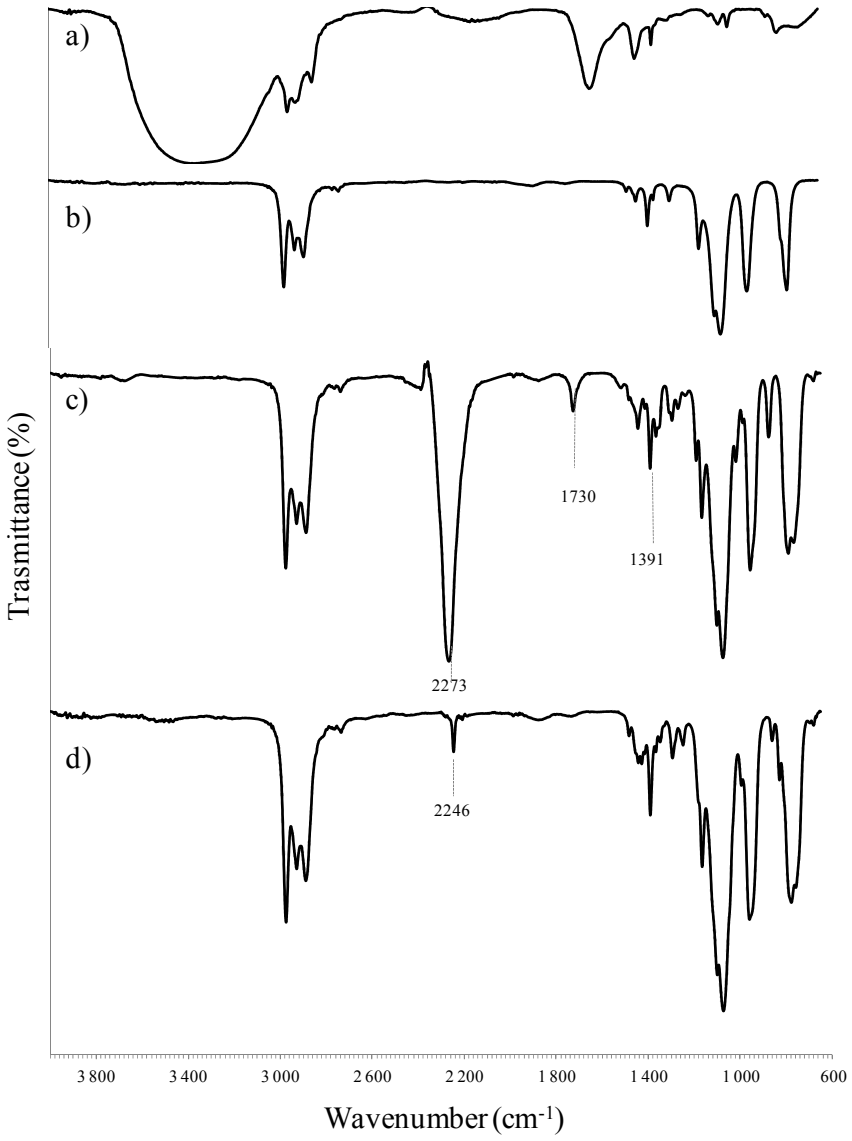

Figure 9: FTIR spectra of pure reagents: a) NR latex, b) TEOS, c) ICPTEOS and d) CPTEOS.

FTIR spectrum of NR latex (see Figure 9 a) shows absorption bands at 3500-3000 cm^{-1} due to O-H and N-H stretching of water and ammonia present in latex; 2963 and 2855 cm^{-1} ascribed to the vibrations of C-H asymmetric and symmetric stretching of 1,4 *cis* polyisoprene; 1449 cm^{-1} corresponds to the characteristic vibrations of CH_2 stretching; 1653 cm^{-1} attributed to C=C stretching and 829 cm^{-1} to C-H bending respectively.

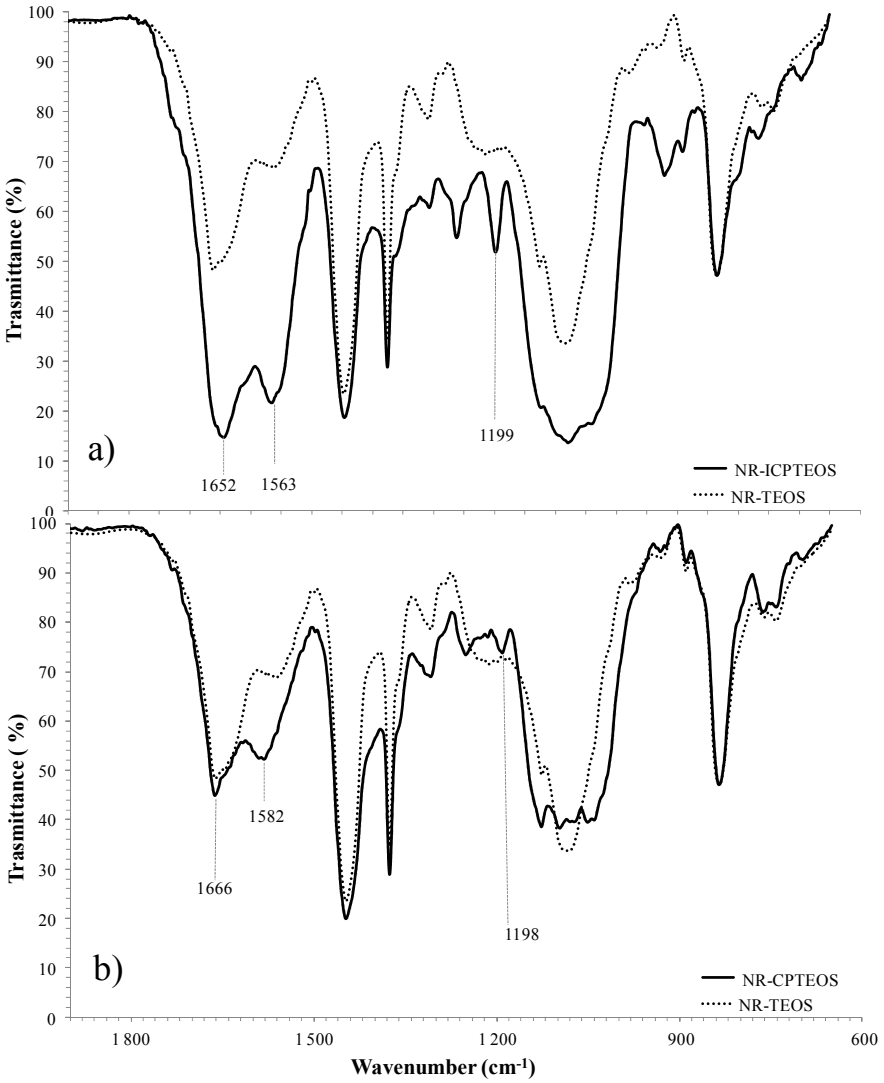

Figure 10: FTIR spectra of a suspension of NR with a) ICPTEOS and b) CPTEOS (H_2O/silane molar ratio = 2) after the same treatment (70°C for 1 h) of the sol-gel synthesis. FTIR spectra are compared with that of a suspension of NR and TEOS under the same conditions (dotted lines).

The TEOS FTIR spectra (see Figure 9 b) shows strong bands at 1078 and 783 cm^{-1} which are attributed to the asymmetric and symmetric Si–O–Si and C-O stretching; at 1106 cm^{-1} were present asymmetric stretching of C-C and C-O; 1170 cm^{-1} -CH_3 rock; 1297 cm^{-1} CH_2 twist; 1391 cm^{-1} -CH_2- wag; 1365 cm^{-1} symmetric bending of -CH_3;1443 cm^{-1} asymmetric

bending of -CH_3; 1484 cm^{-1} symmetric bending of -CH_2-; 2975 cm^{-1} and 2880 cm^{-1} C-H asymmetric and symmetric stretching of -CH_3; 2930 cm^{-1} vibrations of C-H symmetric stretching of -CH_2-, correspondingly.

Regarding the ICPTEOS FTIR spectra, all the bands of the ethoxysilane groups are present, along with the absorption bands of the alkylisocyanate group. ICPTEOS FTIR spectra shows ν_{as} and ν_s of –N=C=O group at 2273 and 1391 cm^{-1} vibration frequency, absorption band of C=O stretching vibration at 1730 cm^{-1} and C-N stretching vibration at 1168 cm^{-1} respectively (see Figure 9 c).

Considering the CPTEOS FTIR spectra, along with the absorption bands of the alkylcyanate group all the bands of the ethoxysilane groups are present.

The spectra shows medium intensity vibration at 2246 cm^{-1} corresponding to nitriles saturated alkyl stretching; at 1248 cm^{-1} frequency with medium intensity, twisting and wagging vibration mode was attributed to the -CH_2- chain linked to Si; at 861 cm^{-1} frequency the band was attributed to Si-CH_2-, at 756 cm^{-1} frequency the band was attributed to the rocking vibration mode of metilene when more than two are present.

Thereafter, FTIR spectra was collected on suspensions of NR latex and suitable amounts of TEOS, ICPTEOS and CPTEOS precursors (H_2O/silane molar ratio = 2), after the same thermal treatment (70°C for 1 h) of the synthesis conditions (see Figure 10).

FTIR analysis demonstrated that the functional group of –NCO of NR-ICPTEOS easily hydrolyzes in the latex basic solution, forming carbamate, urea or amine groups respectively (see Figure 10 a).

Due to electrophiles characteristics of the alkylisocyanate group, it can react with a variety of nucleophiles (such as water, ammonia and alcohols).

The following figure reports the reactions which occurred between the alkylisocyanate group with the water and ammonia (present in NR latex), with the ethanol formed after the hydrolysis of the silica precursor and with the OH groups present on silica surface (see Figure 11).

In detail, in the first reaction the alkylisocyanate group reacts with water to form instable carbamic acid, which evolves to amine and carbon dioxide (reaction entropically favored because from one reagent two products are formed, one of which is gas).

The second reaction forms urea from the reaction between the alkylisocyanate group with ammonia present in NR latex.

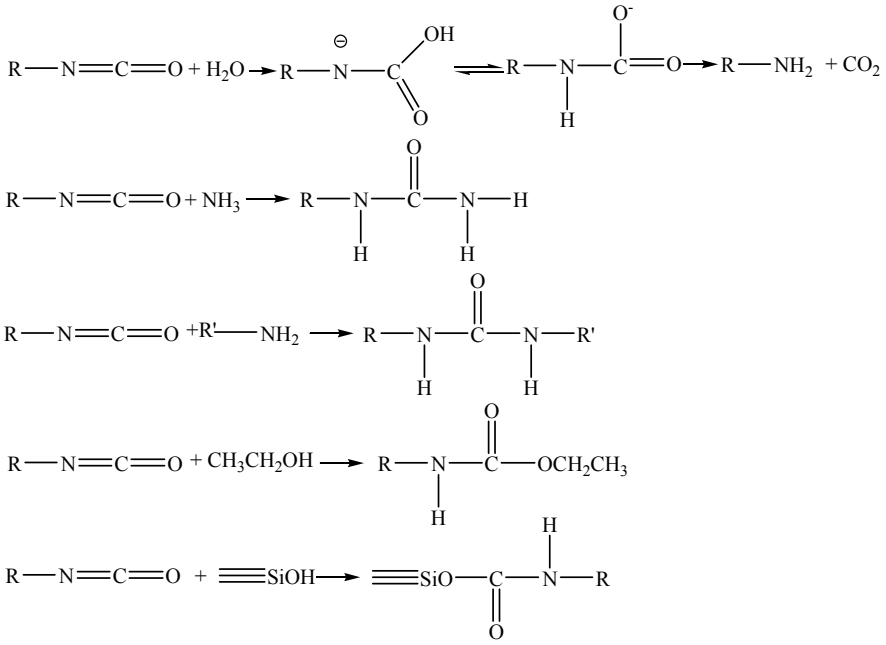

Figure 11: Alkylisocyanate group reactions.

In the third reaction urea derivates are formed from the reaction between amine (product of the first reaction) and the alkylisocyanate group.

Moreover, the alkylisocyanate group can react with ethanol (formed after hydrolysis of the silica precursor) or with the hydroxyl group allocated on the silica surface to form a stable urethane or carbamate[9, 10].

The easily hydrolysis of –NCO group with the formation of the product explained above is demonstrated by the FTIR analysis (see Figure 10 a).

In particular, in the FTIR spectra is evidenced: a) the disappearance in NR-ICPTEOS of the -N=C=O asymmetric and symmetric stretching bands at 2273 and 1391 cm^{-1} and of the CO stretching band at 1730 cm^{-1} of the precursor ICPTEOS (see Figure 9 c); b) the presence in NR-ICPTEOS of new bands ascribe to carbamate group: at 1652 cm^{-1} the band of CO asymmetric stretching and 1563 cm^{-1} of C-N-H bending, partially superimposed to the bands of the hydrolyzed silicon alkoxyde groups; at 1199 cm^{-1} the band of C-N stretching of carbamate group.

Regarding the –CN group of NR-CPTEOS, the FTIR spectra also demonstrated that the functional group easily hydrolyzes in latex basic solution to form the carboxylate group respectively.

Following two reactions are reported of the cyanate group, which reacts with water and ethanol (see Figure 12).

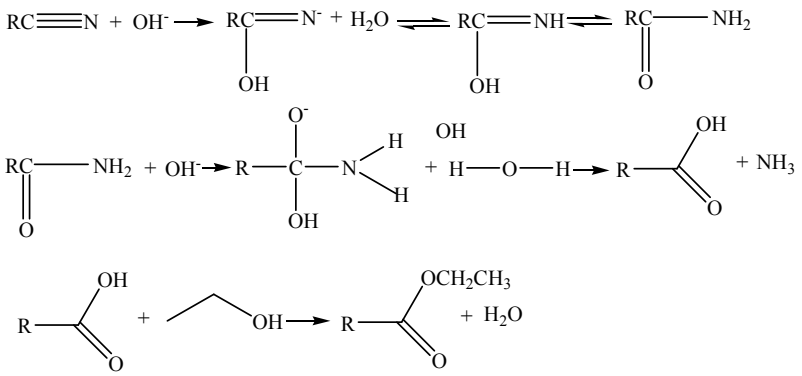

Figure 12: Alkylcyanate group reactions.

The hydrolysis of the alkylcyanate group can continue, under acid or base environmental, to achieve carboxamides $RC(=O)NH_2$, which is in equilibrium with an enolic form.

In excess of a base environment this stable carboxyamide reacts to give carboxylic acid or to create ester in the presence of ethanol.

The behavior of the alkylcyanate group was evidenced a) by the disappearance in NR-CPTEOS of the CN stretching band at 2264 cm^{-1} of the precursor (see Figure 9d) and b) by the presence in NR-CPTEOS of a new band of the C=O stretching at 1582 cm^{-1} ascribed to the carboxylate group (see Figure 10 b) the formation of a small amount of amide due to the presence of a small band at 1198 cm^{-1} and due to -C-N stretching even if cannot also be excluded (see Figure 10b).

5.2. Morphology of silica-rubber composites

The FE-SEM investigation allowed us to evaluate the size and shape of silica aggregates and their distribution in the rubber matrix.

FE-SEM micrographs for some of the fractured uncured composites NR-TEOS, NR-TMSPM-2, NR-TESPD-2 and NR-TESPT-2, are shown in Figure 13.

Silica appears as white spots in the dark area of the rubber matrix, and no relevant differences can be observed among the differently functionalized fillers.

In all the *in situ* sol–gel samples silica particles remain well dispersed on a large scale in the NR matrix, with particle aggregation in the range 50–100 nm and with a good adhesion between the filler and the matrix, as evidenced by the absence of voids at the interface.

FE-SEM micrographs of samples after vulcanization confirmed that silica particles are still well dispersed on a large scale with an increase in the dimension of the particle aggregates (see Figure 14).

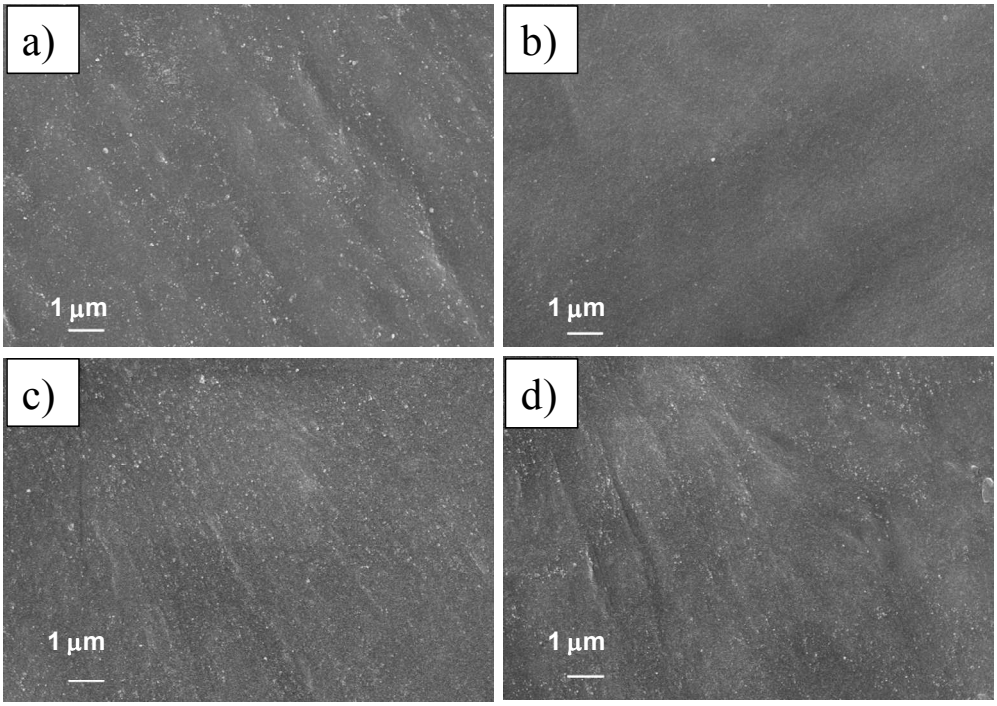

Figure 13: FE-SEM micrographs of uncured composites (a) NR-TEOS; (b) NR-TMSPM-2; (c) NR-TESPD-2; (d) NR-TESPT-2.

The size and shape of silica particles of the *in situ* sol-gel composites, their aggregation and their distribution in the rubber matrix were evaluated by a deep investigation performed by TEM.

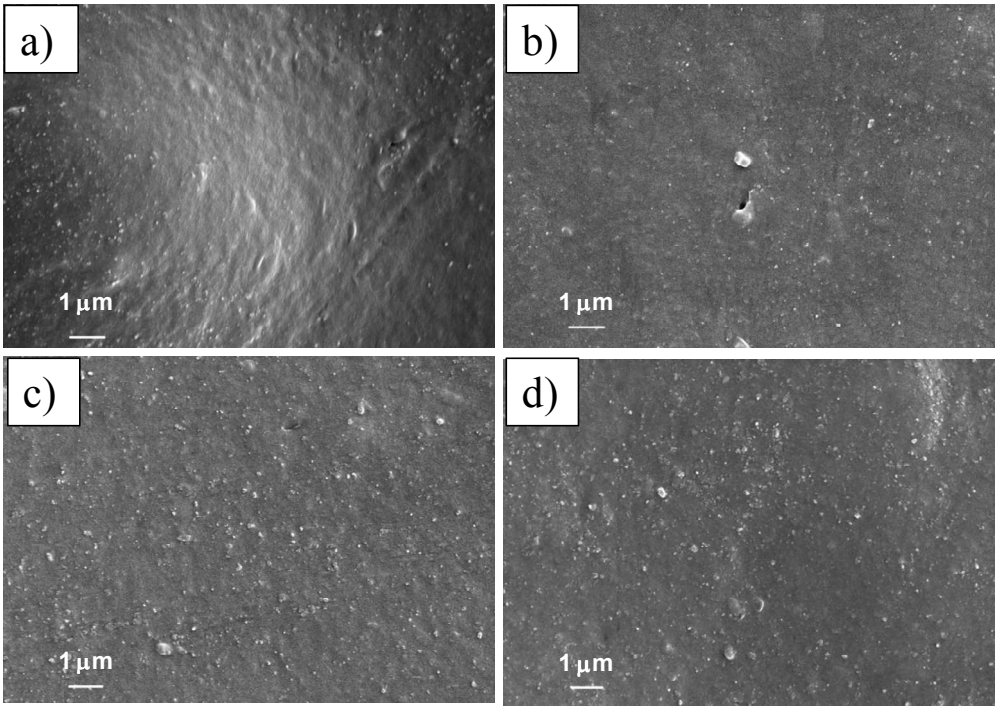

Figure 14: FE-SEM micrographs of vulcanized composites (a) V-NR-TEOS; (b) V-NR-TMSPM-2; (c) V-NR-TESPD-2; (d) V-NR-TESPT-2.

The morphological investigation showed that the filler morphology is strongly dependent on the silica precursors, both in uncured and vulcanized composites.
In the following the TEM images of the different silica/rubber composites are shown and discussed in details.

Masterbatch NR-SiO_2

Figure 15 shows the image of the uncured master batch reference sample NR-SiO_2, with irregularly distributed aggregates of silica particles where the regular spherical shape of filler moieties is difficult to distinguish.

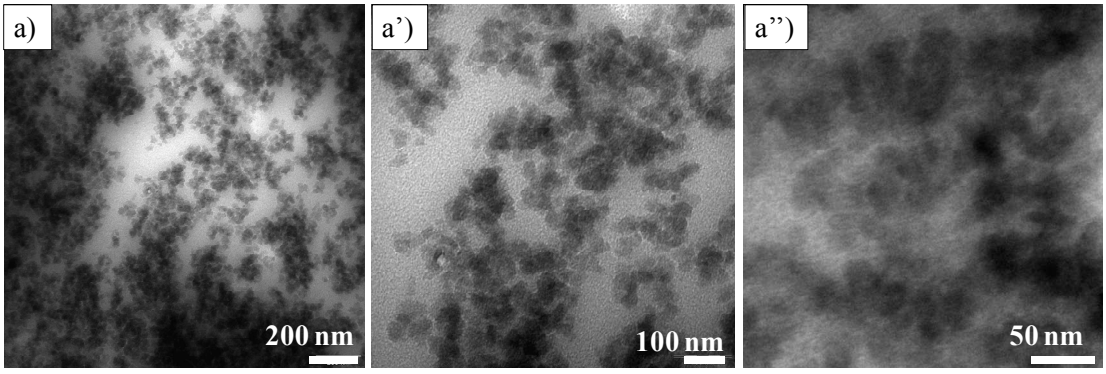

Figure 15: TEM images of NR-SiO_2 master batch at different magnifications.

NR-TEOS

Uncured NR-TEOS shows well assembled and compact aggregates (50–100 nm) of spherical silica particles with sizes 15–20 nm (see Figure 16 a'-a''), which form a homogeneous filler network that is well distributed throughout the rubber matrix (see Figure 16 a).

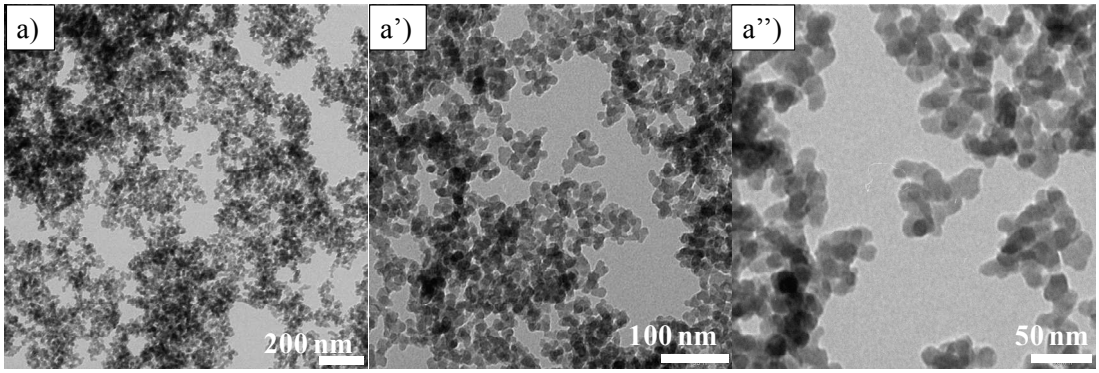

Figure 16: TEM image of uncured NR-TEOS composite at different magnifications).

No rubber layers surround SiO_2 particles and a strong filler-filler interaction is evident, favored by the isotropic shape of particles.

The spherical particles can be well recognized before curing and allow homogeneous self-assembling also after vulcanization.

NR-TESPD, NR-TESPT, NR-TMSPM, NR-NXT

Regarding silica filler functionalized with a sulphur containing group, NR-TESPD-2 and NR-TESPT-2 a have similar morphology with particle size distribution of 5-20 nm and anisotropic shape (see Figures 17a' and 17b').

Particles are surrounded by rubber layers (see Figures 17a'' and 17b'').

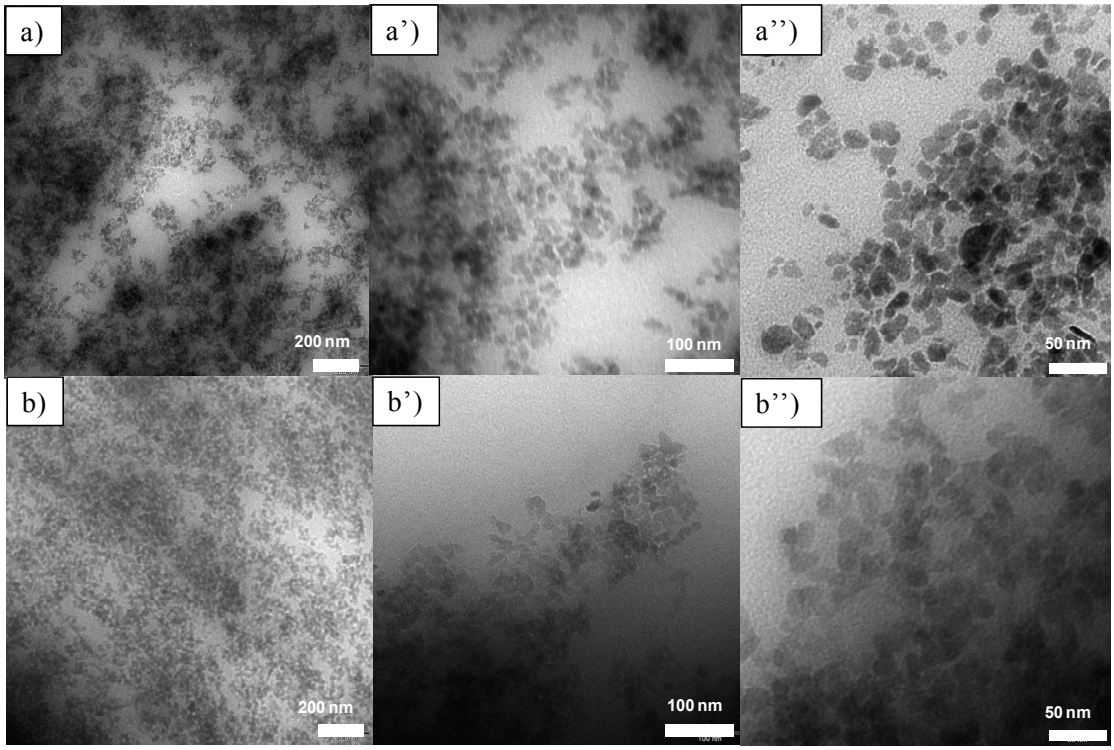

Figure 17: TEM images of uncured a) NR-TESPD-2 and b) NR-TESPT-2 (the superscription ' stands for the higher magnification).

The well distributed filler network is continuous within the rubber (see Figures 17a and 17b), but the aggregates are less compact than in NR-TEOS due to the polymer layer.

This is relatable to the stronger filler-rubber interaction, due both to the presence of functional alkylsulphide groups interacting with rubber and to the anisotropic particle shape which increases the interface with rubber.

Regarding NR-TMSPM-2, the filler particles show size distribution of 15–30 nm (see Figure 18a''). Particles have an irregular shape, also showing a number of elongated ones with a high aspect ratio of 2–2.5.

Aggregates are large and irregular (see Figure 18a') and as a consequence, the filler network is not continuous and homogeneously distributed throughout the rubber matrix (see Figure 18a).

Although the irregular shapes do not assist the particle assembly as much as the spherical ones, the aggregates in NRTMSPM-2 are large and compact (see Figure 18a), with the particles closely linked together and a very small amount of rubber layer surrounding them.

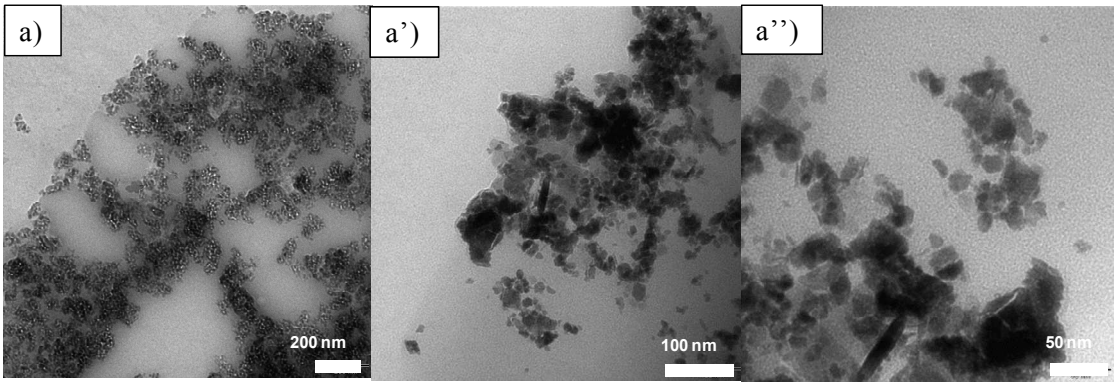

Figure 18: TEM images of uncured NR-TMSPM-2 (the superscription ' stands for the higher magnification).

This can be associated with the silica functionalization by thiol groups, which interacts with both the oxide silanol groups and the polymer units.

This causes both a very strong filler–filler and filler–rubber interaction.

In order to study the effect of the amount of silica modifier on the dimension of the particles and the aggregates in the rubber composites TESPT, TESPD and TMSPM were selected to prepared composites with different silane/silica ratios (see Table 3 in chapter 4).

TEM analysis shows that increasing TESPT/SiO_2 and TESPD/SiO_2 ratios, the size of anisotropic particles and of their aggregates decreases and the filler network becomes less compact, due to the strong filler–rubber interaction, also evidenced by the thicker rubber layers surrounding particles (see sample NR-TESPD-4 in Figures 19a and 19a').

On the contrary, large and compact aggregates of irregularly shaped particles are still present after the increase of the TMSPM/SiO_2 ratio, confirming the strong filler–filler interaction induced by the thiol groups (see sample NR-TMSPM-4 in Figures 19b and 19b').

The TEM images of the composite NR-NXT show the presence of silica particles (20-40 nm), having an elongated shape with an aspect ratio of ~ 3 (see Figure 20).

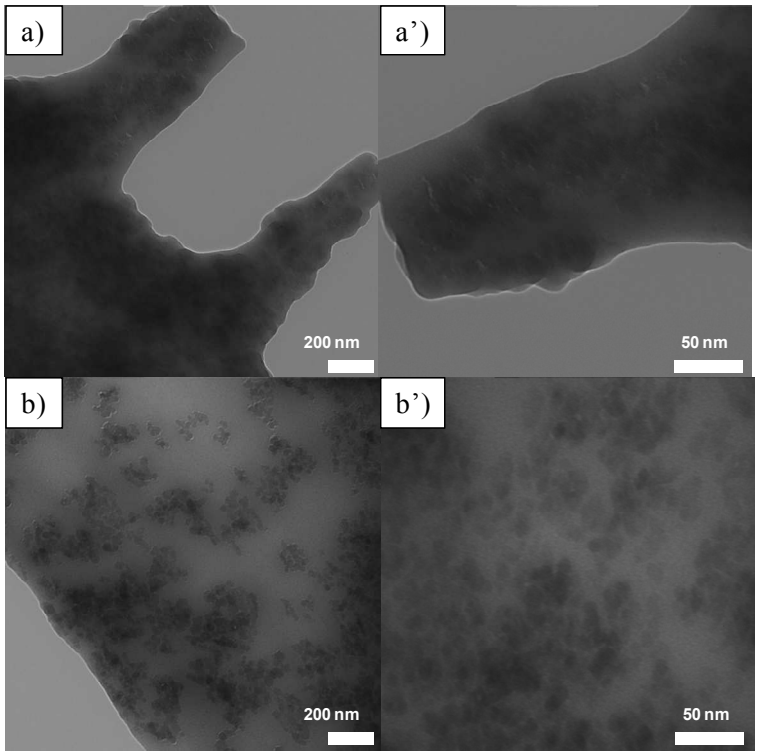

Figure 19:TEM micrographs of (a) NR-TESPT-4 and (b) NR-TMSPM-4 samples (the superscript ' stands for the higher magnification).

They form aggregates of different dimensions (100-300 nm), where the particles are surrounded by a rubber layer.

The filler network is continuous throughout the matrix.

Also in this case, analogously to NR-TESPT and NR-TESPD, there is a strong filler-rubber interaction, allowed by the presence of the alkyl chain.

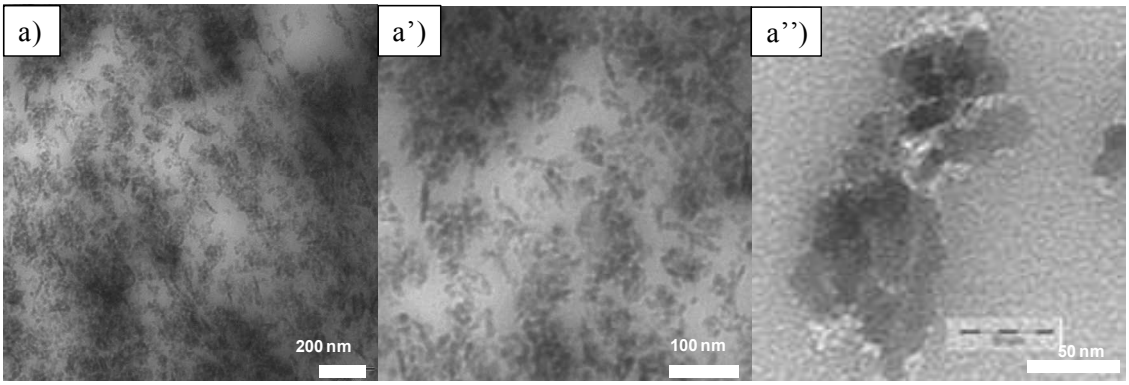

Figure 20: TEM images of NR-NXT composite (the superscript ' stands for the higher magnification).

NR-VTEOS, NR-PTEOS, NR-OCTEOS

Regarding the alkyl and alkenyl substituted silica fillers, NR-PTEOS and NR-VTEOS, they show morphological analogies (see Figure 21a and 21b).

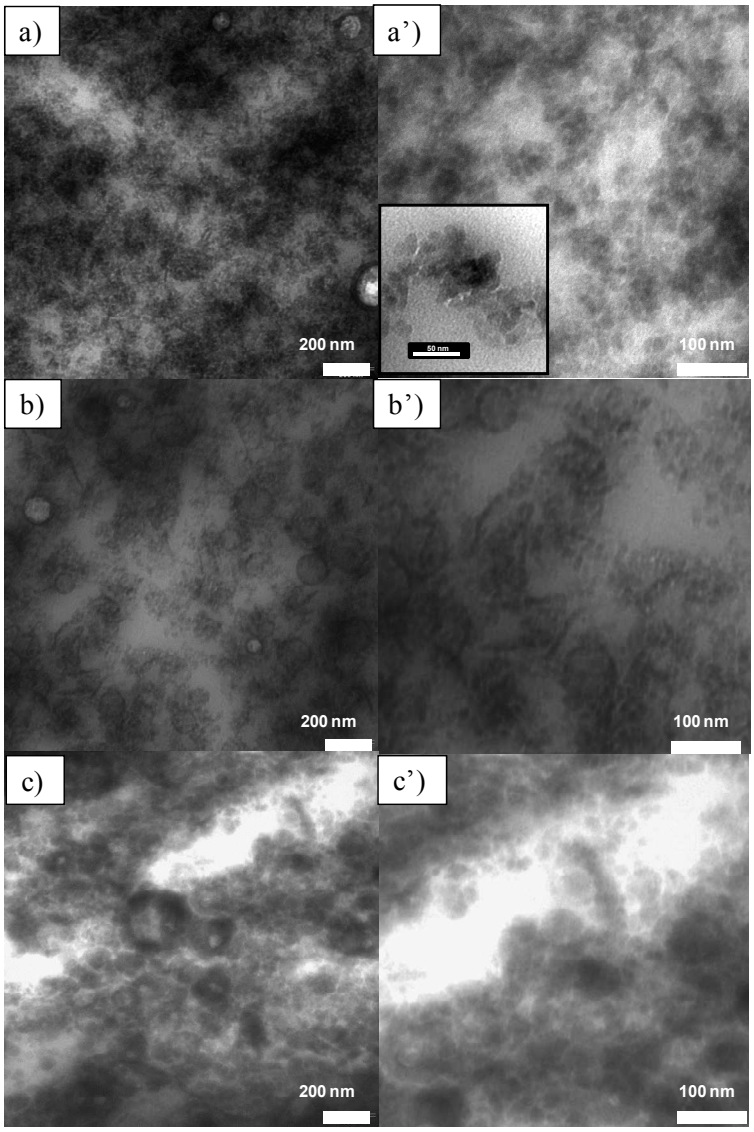

Figure 21: TEM images of uncured composites: a) NR-VTEOS; b) NR-PTEOS; c) NR-OCTEOS; (the superscript ' stands for the higher magnification).

Particles have a size of 10-20 nm and an evident anisotropic shape, especially NR-VTEOS, where some particles show an aspect ratio ~ 3 (see Figure 21 a').

The filler network is continuous throughout the rubber (see Figures 21a and 21b); nevertheless, the aggregates are less compact than those observed in NR-TEOS (see Figure 16) due to the presence of a rubber layer which surrounds all particles and lowers the filler-filler interaction.

The different network morphology in NR-VTEOS and NR-PTEOS, compared to NR-TEOS, can be related to a stronger filler-rubber interaction, due to the presence of vinyl or propyl groups interacting with rubber by weak chemical bond and to the anisotropic shape less favorable to physical self assembling.

Interestingly, the morphology of NR-OCTEOS (see Figure 21c) is quite different from that of the other alkyl substituted composites.

Silica particles appear large (20-50 nm) and irregularly shaped (see Figure 21c and 21c'), forming aggregates of different dimensions.

The filler network is highly discontinuous even if the presence of rubber layers surrounding particles suggests filler-rubber interaction.

The origin of the large particles and the irregular network may be associated to the presence of the long octyl chains on the silica surface. In fact, as reported in paragraph 5.1 the slow kinetics of the OCTEOS induces the growth of large and irregular silica particles, functionalized with long alkyl chains, which favors the interaction with rubber but hinders that with the other filler particles.

Both these effects prevent the formation of a homogeneous and continuous network, favoring the formation of extended rubber regions lacking inorganic particles.

A similar effect was observed by Ito[11] et al. for decyl functionalized silica filled polyisoprene systems.

The FTIR analysis was used in order to confirm the slow hydrolysis kinetic shown by OCTEOS, and give an explanation of the different composite filler morphology shown in NR-OCTEOS and NR- NXT, both filler functionalization containing a long hydrocarbon chain.

FTIR spectra (range 600-1200 cm^{-1}) of NR latex suspensions and of suitable amounts of TEOS, OCTEOS and NXT precursors (H_2O/silane molar ratio = 2), taken after the same treatment (70°C for 1 h) as the *in situ* synthesis, are reported in Figure 22 and compared with the spectra of the silanes before the reaction.

The spectra demonstrated that after 1 hour of reaction at 70°C the ethoxy groups of the OCTEOS only partially reacted, unlike TEOS and the other substituted silanes which completely hydrolyzed.

In detail, TEOS spectra recorded after reaction, showed that the bands related to ethoxy groups, the (Si-O + C-O) stretching at 783 cm^{-1} and the (H_3CC or H_2CO) bending at 956 cm^{-1}, are completely absent, while the band at 840 cm^{-1}, due to the symmetric stretching (C-C + C-O) of the ethanol, which is a product of the hydrolysis/condensation reaction is easily detectable (see Figure 22a).

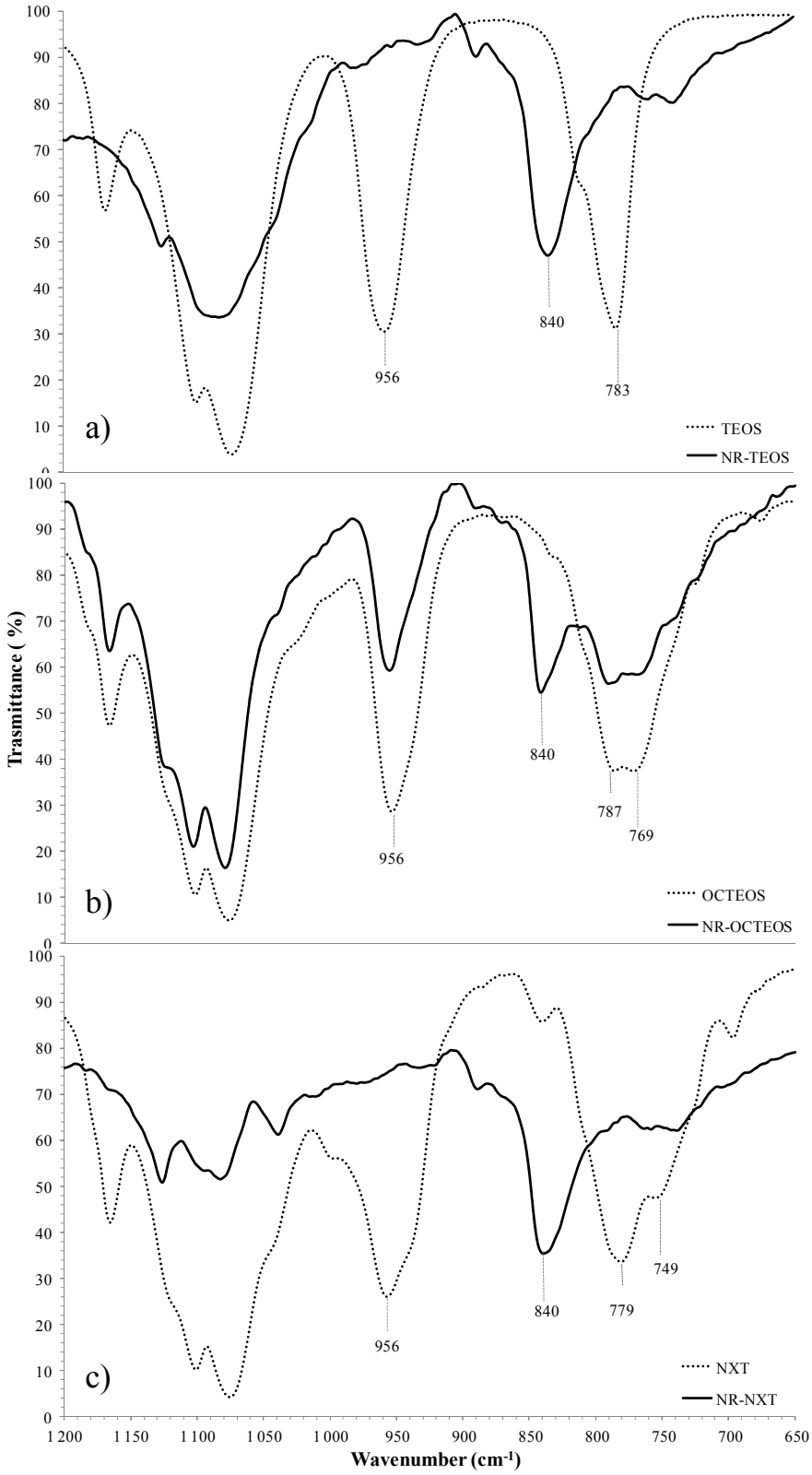

Figure 22: FTIR spectra of a suspension of NR and a) TEOS, b) OCTEOS and c) NXT (H_2O/silane molar ratio = 2) after the same treatment (70°C for 1 h) of the sol-gel synthesis (bold lines). FTIR spectra are compared with those of silanes before reaction (dotted lines).

In the case of OCTEOS, the same bands of the alkoxy groups at 787 cm^{-1} and 956 cm^{-1} were still present after the reaction, though less strong and superimposed to the ethanol band at 840 cm^{-1} (see Figure 22b).

Regarding NXT, the behavior is similar to that of TEOS. The alkoxy groups at 779 cm^{-1} and 956 cm^{-1} disappeared after reaction, and the ethanol band at 840 cm^{-1} was detectable (see Figure 22c).

In summary, the spectra showed that the alkoxy groups of the OCTEOS did not fully hydrolize, as evidenced by the residual intensities of the vibrational bands [12,13,14]; conversely in the spectra of TEOS and NXT, these bands completely disappear.

Therefore, NR-NXT composite, in comparison with NR-OCTEOS, does not show network voids, due to the fast kinetics of NXT silane. Thereafter, the fast rate of hydrolysis reaction allows the growth of smaller and more homogeneous nanoparticles and, consequently, the formation of an almost continuous network within the rubber.

Briefly, the kinetic rate influences the morphology of the particles, their aggregation degree and their distribution in rubber matrix.

NR-ICPTEOS, NR-CPTEOS, NR-APTEOS

The morphology of silica filler functionalized with N containing groups is different from those described before. The TEM images better explain the reasons for this difference (see Figure 23).

NR-ICPTEOS and NR-CPTEOS show some morphological analogies.

The range of the filler particle size of both samples is 10-20 nm and the particle shape is almost spherical or slightly elongated (see Figure 23a' and 23b').

The aggregates are constituted by well assembled particles forming a continuous network throughout the rubber (Figures 23a and 23b).

As in the case of NR-TEOS (see Figure 16), only rarely very small rubber layers surrounding SiO_2 particles are present, suggesting that the filler-filler interaction is prevalent.

The reason for this network morphology is related to –CN and –NCO groups which react in the basic environment of the *in situ* sol-gel synthesis forming carboxylate and carbamate groups, as evidenced by FTIR measurements and explained in paragraph 5.1.

The polarity of these groups hinders the interaction with the rubber, while allowing the chemical interaction between the surface hydroxyl groups.

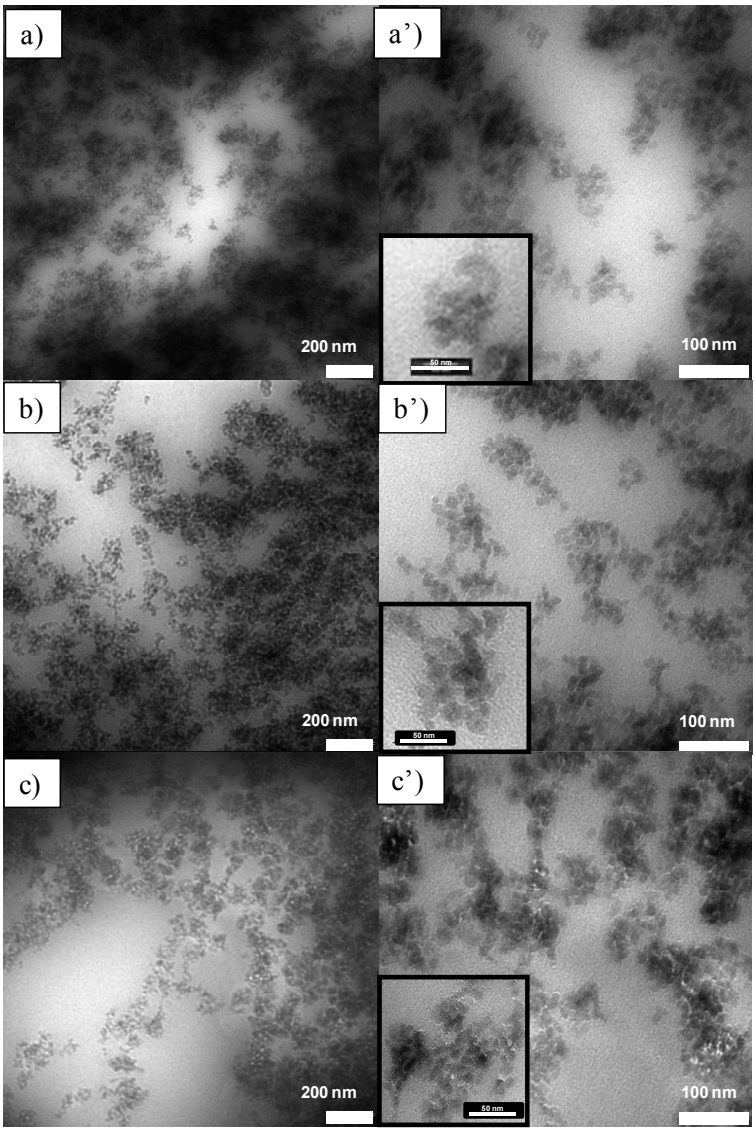

Figure 23: TEM images of uncured composites: a) NR-ICPTEOS; b) NR-CPTEOS; c) NR-APTEOS; (the superscript ' stands for the higher magnification).

The morphology of NR-APTEOS network is relatable to the presence of the amino groups which strongly increase the rate of hydrolysis-condensation process during the material synthesis, as evidenced by the fast and quite immediate gelation of the samples.

The fast reaction rate influences the particle aggregation and their distribution in the rubber matrix. In fact, silica particles show small sizes (10-25 nm) but irregular shapes (see Figure 23c'). They form large, compact and irregular aggregates without rubber layers surrounding the nanoparticles. This suggests a strong filler-filler interaction assisted by the interaction between surface amino groups; however, the filler network is not continuous and contains large parts of rubber without filler (see Figure 23c).

Cured composites

After curing the aggregation and the irregular shape of silica nanoparticles are much more evident in cured V-NR-SiO_2 masterbatch, though the TEM images is less clear due to the presence of carbon black particles (see Figure 24).

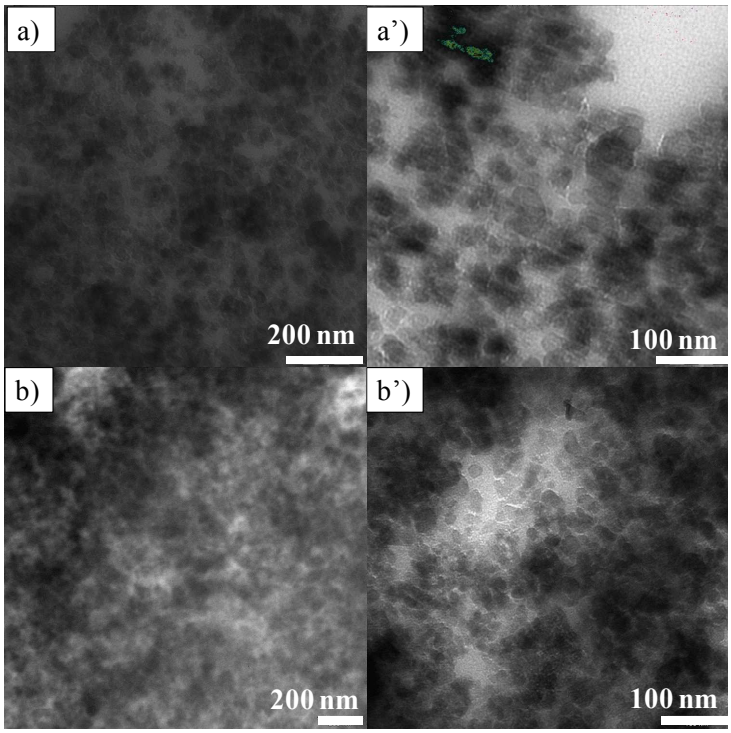

Figure 24: TEM images of a) V-NR-SiO_2 vulcanized master batch and b) of V-NR-TEOS (the superscription ' stands for the higher magnification).

Regarding the morphology of the *in situ* composites, no substantial changes occur even if carbon black particles mixed to the composites makes TEM images interpretation more difficult. Following selected examples are reported.

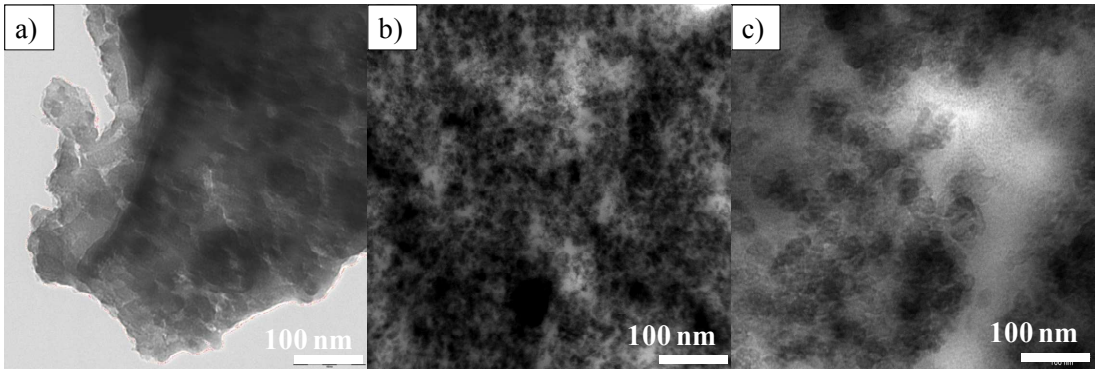

Figure 25: TEM images of cured composites: a) V-NR-TESPD-2, b) V-NR-TESPT-2 and c) V-NR-TMSPM-2.

V-NR-TEOS is shown in Figure 24a and 24b presents a slight increase of the degree of aggregation. The same observation can be done for V-NR-TESPD-2, V-NR-TESPT-2 and V-NR-TMSPM-2 (see Figure 25).

5.3. Swelling measurements

Swelling ratios (Q%), absolute swelling ratios (q), extractable fractions (f), bound rubber (B_r %) and cross-link density (η) calculated according to equations reported in paragraph 3.2.6 are shown in Table 2 for uncured composites containing different amounts of functional groups on filler surfaces and for different functional groups.

Samples	X[a]	Q %	q (w/w)	f (%)	B_r %	η mol cm^{-3}
NR_d-SiO_2	-	n.d.	n.d.	n.d.	n.d.	n.d.
NR-TEOS	-	398	12.0	58.6	25.14	0.00676
NR-TMSPM	1	451	11.7	53.0	31.71	-
	2	769	14.8	42.5	46.59	0.00420
	3	899	15.3	34.5	55.52	-
	4	605	8.1	13.2	83.04	-
NR-TESPD	1	502	14.0	56.9	26.52	-
	2	645	15.8	52.9	31.71	0.00476
	3	798	17.0	47.2	39.17	-
	4	818	16.9	45.7	41.12	-
NR-TESPT	1	706	15.9	49.3	36.65	-
	2	925	19.6	47.7	38.62	0.00368
	3	913	16.3	37.7	51.47	-
	4	568	9.2	27.6	64.49	-
NR-NXT	-	1060	19.7	41.0	47.34	0.00335
NR-VTEOS	-	791	15.9	43.9	43.62	0.00413
NR-PTEOS	-	748	17.5	51.5	33.50	0.00429
NR-OCTEOS	-	931	22.2	53.7	30.63	0.00366
NR-APTEOS	-	312	12.6	67.3	13.42	0.00805
NR-CPTEOS	-	596	14.6	52.2	32.70	0.00501
NR-ICPTEOS	-	526	12.1	48.4	37.70	0.00548

X[a] refers to different concentrations of the same precursor, n.d. not determined

Table 2: Swelling, bound rubber and cross-link density on uncured composites.

Swelling measurements for uncured NR-SiO_2 sample were not performed as the sample was almost completely swollen in toluene because it was not cross-linked.

The results demonstrate that all uncured composites are significantly cross-linked.

The cross-linking is generally more effective in composites containing silica particles modified by sulphur or alkyl/alkenyl functionalities than in those derived from the unsubstituted TEOS and silica functionalized with alkylamine.

The results show lower Q% value for composites containing silica functionalized with nitrogen containing alkyl groups probably due to the nature of the functionalizing molecules which form a barrier which reduces the penetration of the toluene inside the composites.

In particular, NR-APTEOS, similarly to TEOS, showed the lowest less Q% value due to the presence of alkylamine and hydroxyl groups on the silica surface, both with a different chemical nature in comparison with toluene.

This behavior in also evident in NR-ICPTEOS and NR-CPTEOS.

Regarding composites containing silica functionalized with propyl and octyl groups, Q% value increases with the increase of the aliphatic chain length.

Instead, NR-TEOS and NR-APTEOS showed less Q% value due to the presence of hydroxyl and alkylamine groups on the silica surface, both with a different chemical nature in comparison with toluene, as well as less steric hindrance characters than other functionalizing molecules. This behavior in also lesser evident in NR-ICPTEOS and NR-CPTEOS.

Considering only NR-TMSPM, NR-TESPD and NR-TESPT, the results suggested higher cross-link degree by the general decrease of the *f* value (corresponds to high strength and adhesion of filler with the rubber link) and the increase of Q% and *q* values with respect to TEOS derivatives and by the increase of the amount of substituent molecules in TEOS (compare samples 1-4 for NR-TMSPM, NR-TESPD and NR-TESPT in Table 2).

Moreover, for these composites the Br% increases with the increase of the amount of functionalizing molecules on the silica surface.

Swelling ratios (*Q%*), absolute swelling ratios (*q*) and extractable fractions (*f*) were calculated for vulcanized composites containing different functional groups and are shown in Table 3.

A similar trend, though less evident, is observed after vulcanization, although Q %, q and f values are much lower than in uncured samples.

The differences between composites are less significant, as expected from the increased reticulation of the polymer chains after the vulcanization process.

The values suggest that the silica modifying molecules also modify the rubber cross-linking and in general increase the filler-rubber interaction.

Cured samples	Q%	q (w/w)	f (%)
V-NR_d-SiO_2	207	3.2	5.8
V-NR-TEOS	208	3.2	4.1
V-NR-TMSPM	223	3.3	4.2
V-NR-TESPD	176	2.9	4.1
V-NR-TESPT	186	3.0	4.2
V-NR-NXT	182	3.0	4.6
V-NR-VTEOS	209	3.2	4.0
V-NR-PTEOS	226	3.4	4.3
V-NR-OCTEOS	232	3.5	4.2
V-NR-APTEOS	188	3.0	4.5
V-NR-CPTEOS	203	3.2	4.4
V-NR-ICPTEOS	236	3.5	4.3

Table 3: Swelling of cured samples.

5.4. Electron spin resonance (ESR) measurements

ESR (Electron Spin Resonance) investigation was performed by using the nitroxide radical TEMPOL as spin probe in a selected number of composites: NR-TEOS, NR-TESPT-2, NR-TESPD-2, NR-TMSPM-2 and NR-SiO_2.

The introduction of the spin probe TEMPOL[15] in rubber composites was performed by using a toluene swelling procedure[16, 17, 18, 19].

The aim was to study the cross-linking extent of the rubber matrix in the presence of differently functionalized silica fillers.

To do this the matrix embedding the spin probe was investigated after the elimination of the toluene phase, which contained the unlinked NR chains, and after drying it (see paragraph 3.2.8).

The room temperature ESR spectrum of TEMPOL is sensitive to the dynamics of the nitroxide molecules, which are determined by the rotational correlation time τ_R, the time required for a complete radical rotation around its axis[20].

τ_R can vary from fast motion (10^{-11}-10^{-9} s) to slow motion (10^{-8}-10^{-7} s).

Fast motion occurs when nitroxide has no or very few mobility restrictions, as in solution. The motion averages the anisotropic g and A tensors components[20].

The resulting isotropic spectrum is characterized by three well resolved resonances with small hyperfine coupling, due to interaction with the nuclear spin of nitrogen (I=1), and has a small line width.

When the nitroxide mobility is limited by physical or chemical interaction with the surroundings, the line width and the hyperfine coupling increase. If the motion is fully hindered, the ESR anisotropic lines resemble those of a powder.

The spectra of NR-TEOS, NR-TESPT-2, NR-TESPD-2, NR-TMSPM-2 and NR-SiO_2 samples show the very intense broad anisotropic signals of nitroxide (g_1=2.023 g_2= 2.005 g_3= 1.981), associable to spin-probe slow motion in a high density matrix. The resonances overlap the much less intense narrow isotropic signals due to fast motion spin probe units; is the ESR spectrum for NR-TMSPM is shown as an example in Figure 26.

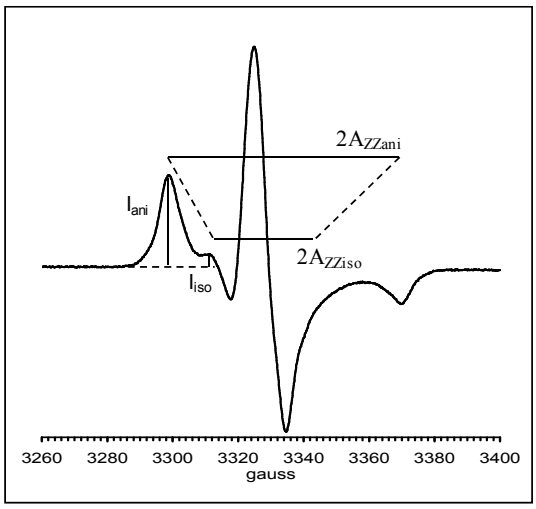

Figure 26: ESR spetctrum of TEMPOL spin probe in NR-TMSPM composite after swelling in toluene (the peak hights of anisotropic, I_{ani}, and isotropic, I_{iso}, species are indicated).

The separation between the outer components of the signals ($2A_{zz}$) increases from ≈ 30 gauss for the isotropic signal to 72 gauss for the anisotropic one.

The results clearly evidence that after the extraction of uncured polymer by toluene, the spin mobility in the cross-linked composite part is very low, due to the high density of the rubber matrix and to the very limited presence of free volume holes.

Similar spin probe investigations performed by different authors on vulcanized rubber showed a much higher contribution of the isotropic signal, however in those cases the

swelled rubber chains were not removed from the sample before drying [16, 17, 18, 19].

In our investigation, the small amount of fast-motion signal is truly related to the presence of residual free volumes in the cross-linked matrix.

In order to estimate the contribution of the two overlapped species, the intensities (estimated from the peak high) of the anisotropic (I_{ani}) and isotropic (I_{iso}) signals (see Figure 27) were evaluated[16, 17] .

The calculated intensity ratio I_{ani}/I_{iso} was taken as a measure of the probe motion in the composite matrix. Higher I_{ani}/I_{iso} values indicate the prevalence of the slow motion component and were related to high rubber cross-linking and low free volume size.

The ratios I_{ani}/ I_{iso} of NR-SiO_2, NR-TEOS, NR-TESPT-2, NR-TESPD-2, NR-TMSPM-2 are reported in Figure 27.

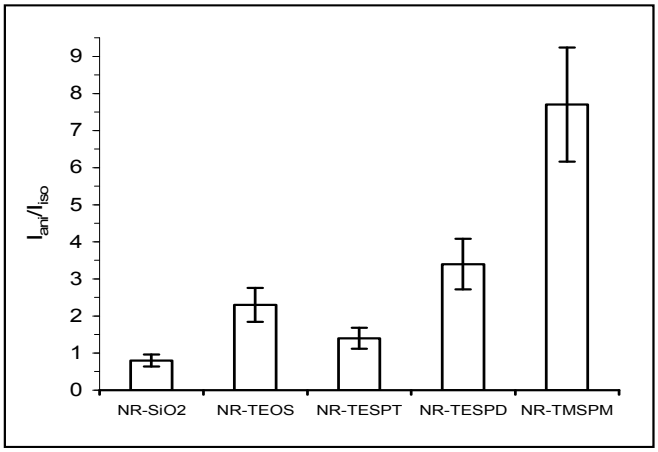

Figure 27: I_{ani}/I_{iso} ratios of the uncured composites NR-SiO_2, NR-TEOS, NR-TESPT-2, NR-TESPD-2, NR-TMSPM-2.

The uncertainty of I_{ani}/ I_{iso} ratio (± 20%), evaluated on three ESR samples, was related to the presence of an isotropic signal at g≈2, superimposed to the nitroxide lines in composite samples.

This signal was detected in samples before toluene swelling (see as an example NR-TMSPM-2 of Figure 28) and may be likely attributed to artifact radicals created during the two-roll mill mixing operations [21] and/or to traces of C_{black} introduced during two-roll mill operation.

Based on the previous observation, all *in situ* composites have I_{ani}/ I_{iso} values higher than the reference NR-SiO_2. NR-TMSPM-2 and NR-TESPD-2 have the highest ratio values I_{ani}/I_{iso}, confirming that the highest cross-linking resulted from their swelling parameters.

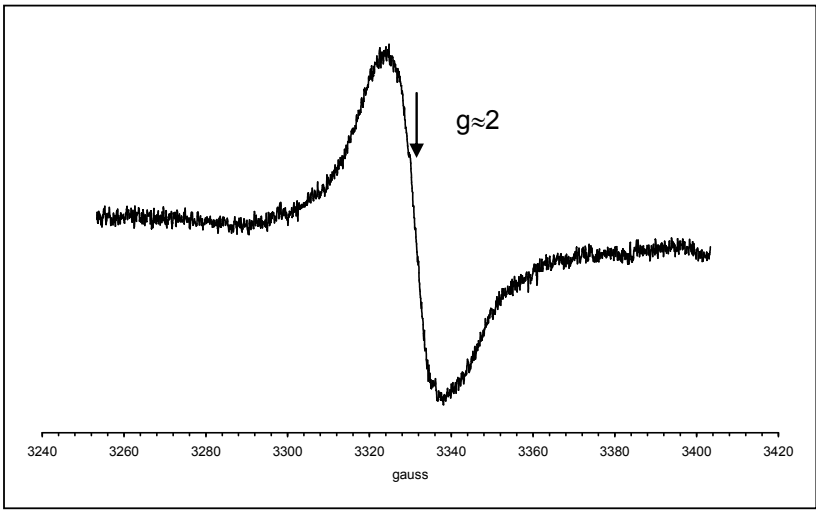

Figure 28: ESR spectrum of NR-TMSPM-2 composite.

NR-TESPT-2 shows a very unexpected lower ratio; however the interference of the artifact radicals, evidenced in the spectrum, hinders in this case a correct relationship with the cross-linking properties. Blank tests were performed on TEMPOL/toluene solutions of TMSPM, TESPD, TESPT and TEOS in order to check the stability of nitroxide radical in the presence of the different silane groups.

TEMPOL may act indeed as spin-trapping agent [22] of the reactive radical species eventually formed during the swelling procedure.

The ESR spectrum of the TEMPOL/toluene solution shows an isotropic signal with three well resolved lines due to nitrogen hyperfine coupling[23,24] (not shown in the figure).

The nitroxide stability in the presence of TMSPM, TESPD, TESPT and TEOS was investigated by monitoring the decrease of the ESR signal**,** maintaining the toluene solutions at the same temperature, 40°C, of the swelling treatment.

The plot of nitroxide concentration vs time in toluene solution is reported for the different silanes in Figure 29. TEOS does not react with nitroxide radicals, whose concentration remains unvaried after three days.

On the other hand, in the presence of TMSPM, nitroxide radicals disappeared after three hours. Nitroxide radicals decreased also in the presence of TESPD and TESPT, even if less rapidly, and they fully disappeared after three days.

These results demonstrate that disulfide/tetrasulfide groups of TESPD/TESPT and, particularly, thiol groups of TMSPM are able to reduce nitroxide[23,24], in toluene solution. Nevertheless nitroxide radicals do not undergo total reduction in NR-TESPT-2, NR-TESPD-2, NR-TMSPM-2 after swelling and drying treatments.

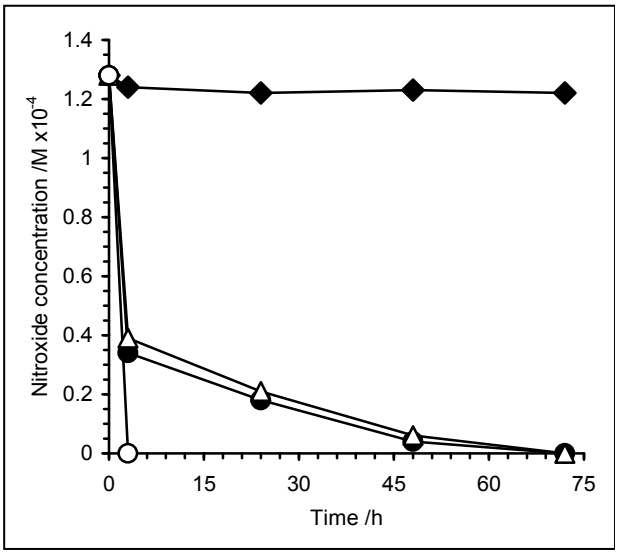

Figure 29: Plot of TEMPOL concentration vs time in toluene solutions of the different silanes: ♦TEOS, ●TESPD, ΔTESPT and ○TMSPM.

Their amount is in the range 1-2 x 10^{16} spin/g, being maximum in NR-TMSPM.

Thus in the rubber composites before vulcanization, part of alkyldisulfide, alkyltetrasulfide and alkylthiol groups, grafted to silica particles, can no longer freely interact with TEMPOL molecules.

In fact, during the *in situ* sol-gel process the functional groups lost their freedom, interacting with the polymer chains and/or with the hydroxyl groups of neighbor silica particles.

This agrees either with the high cross-linking of NR-TESPT-2, NR-TESPD-2, NR-TMSPM-2, since it results from the swelling measurements, or with the different filler-filler and filler-polymer interactions as evidenced in the TEM analysis.

ESR spin-probe measurements were not performed on vulcanized composites, as the presence of the very intense resonance at g≈2, due to carbon black, hinders the detection of the less intense overlapped lines of nitroxide.

5.5. Dynamic mechanical analysis of uncured composites

In order to appreciate the dynamical mechanical behavior of uncured composites, two different tests were carried out: DMA by RPA (Rubber Process Analyzer) and DMTA.

In the first method the strain sweep tests were carried out at T = 70 °C (at fixed temperature) and 1 Hz from 2 % to 100% of elongation. Low frequency was chosen to maximize the differences between the various composites and the fixed temperature was chosen in order to understand the rolling resistance characteristics.

After the strain sweep, in order to study the effect of the thermal treatment on the dynamic-mechanical properties, the uncured samples were heated at 150°C for 10 min, then cooled down to 70°C before performing a new strain sweep test.

DMTA was carried out by applying a traction force at 1 Hz at variable temperature (-80°C to +80°C).

The aim was to evaluate the temperature dependent dynamic behaviors with the three regions: glass (near the glass transition, from -80°C to -60°C), transition region (where abrupt changes in the modulus take place due to the mobility gain of the rubber segment from glassy state to the rubbery state, from -60°C to 30°C) and rubbery regions (where the modulus is constant up to +30°C). The addition of silica filler is expected to provide the rubber with viscoelastic behavior[25, 26], characterized by non linear dependence of the storage modulus G' value on the applied strain.

Therefore, the dynamic stress strain behavior of silica-rubber composites was expressed by the elastic or storage modulus G', and by the viscous or loss modulus G''[27].

In fact, during the analysis, the storage modulus G′ at low strain (G'_0 at 2%) decreases rapidly by increasing strain amplitude, and at large strain amplitude (G'_∞ at 100%) approaches the lowest value, since the stress softening is attributable to the breakdown of the filler inter-aggregate network (Payne effect)[28, 29].

G'' is related to the energy loss of the filled rubber during the dynamic strain, determined by the breakdown and reformation of the filler network[25].

The discussion reported of G' and G'' trends of *in situ* composites were subdivided into three parts:

- Tests on 30 phr composites containing silica functionalized with the different silanes.
- Tests on a selected number of 30 phr composites containing sulphur group, in order to study the effect of the amount of functionalizing molecules on silica particles.
- Tests on a selected number of composites containing different amount of silica (20 or 30 or 45 phr) or functionalized silica in order to study the effect of the filler amount.

RPA analyses were performed on all rubber composites synthesized by *in situ* sol-gel method containing 30 phr of silica and silica modified by alkylthiol, thiocarboxylate, alkyldisulfide, alkyltetrasulfide, vinyl, propyl, octyl chains, alkylamine, alkylcyanate and

alkylisocyanate groups. The trends of G' for all *in situ* silica-rubber composites compared with those of the reference sample NR-SiO_2 and of pure NR are shown in Figure 30.

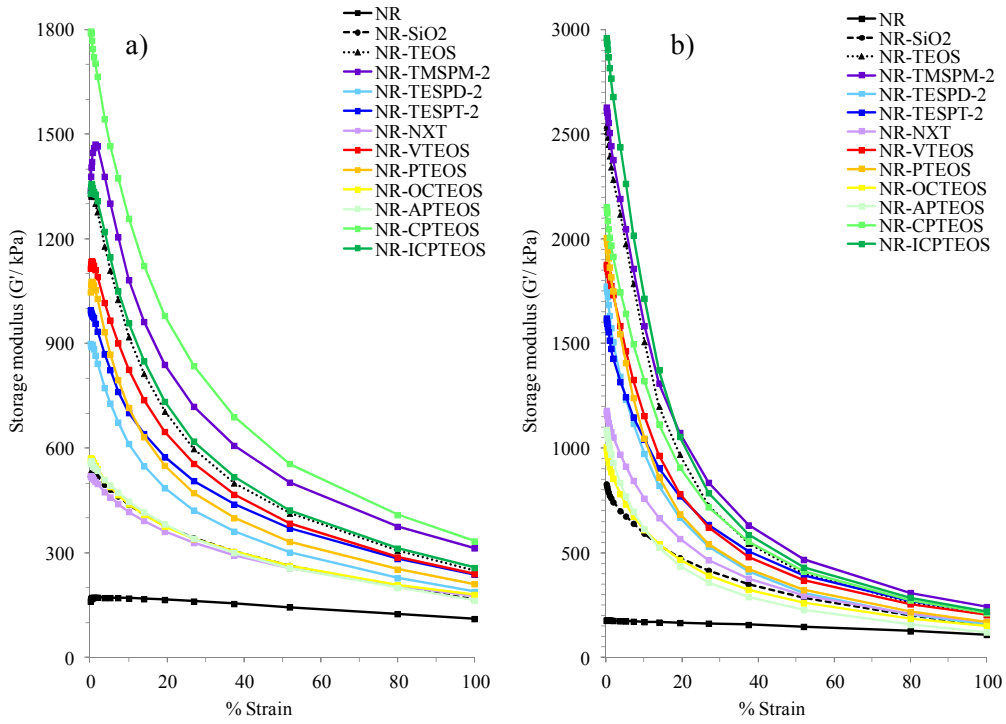

Figure 30: Storage modulus G´ vs strain of the uncured *in situ* silica-rubber composites NR-TEOS, NR-TMSPM, NR-TESPD, NR-TESPT, NR-NXT, NR-VTEOS, NR-PTEOS, NR-OCTEOS, NR-APTEOS, NR-CPTEOS, NR-ICPTEOS compared with NR-SiO_2 and pure NR, a) before and b) after the thermal treatment at 150°C.

In order to simplify the discussion of the various composites containing functionalized silica, the results (G'_∞ and $\Delta G'$) obtained are reported in the following graph (see Figure 31).

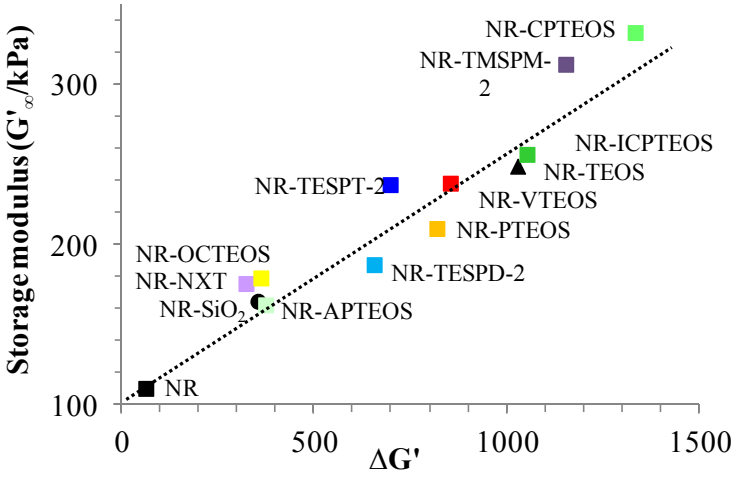

Figure 31: Filler-rubber interaction vs filler-filler interaction of *in situ* composites.

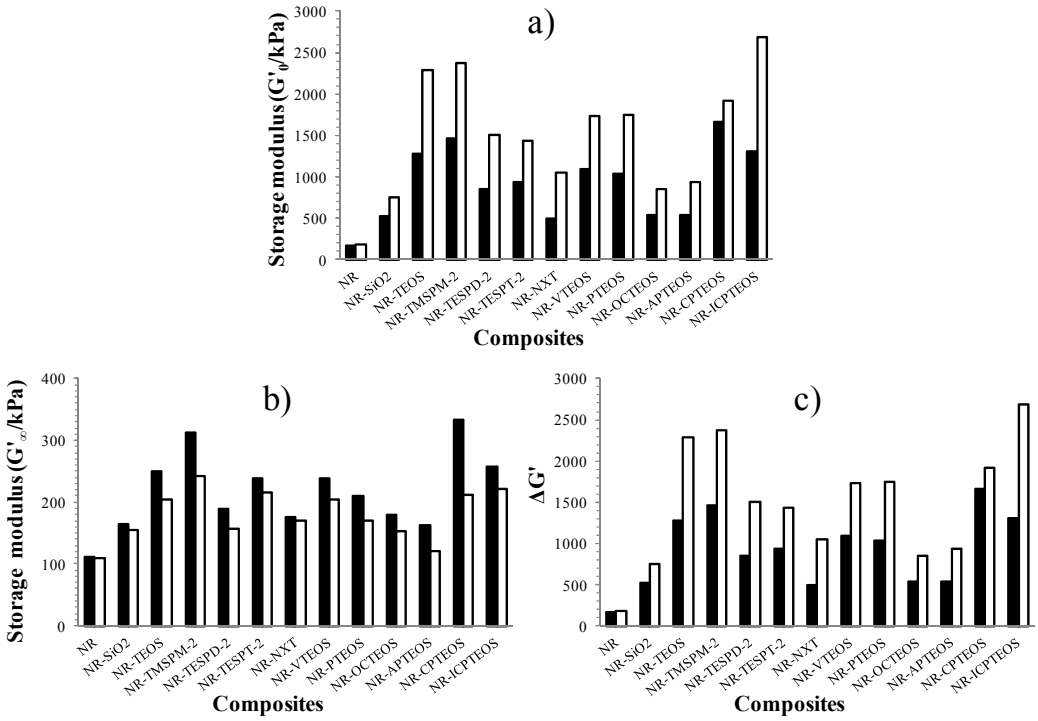

Figure 32: Histograms of *in situ* silica-rubber composites NR-TEOS, NR-TMSPM-2, NR-TESPD-2, NR-TESPT-2, NR-NXT, NR-VTEOS, NR-PTEOS, NR-OCTEOS, NR-APTEOS, NR-CPTEOS, NR-ICPTEOS in comparison with reference sample NR-SiO_2 of a) G'_0 at low strain; b) G'_∞ at high strain; c) $\Delta G' = (G'_0 - G'_\infty)$; the black column of the chart reports the values of DMA at 70°C; the white column the values of DMA at 70°C after a thermal treatment of 150°C.

In addition, in order to compare all the *in situ* composites containing different silica functionalizations, the values G'_0, G'_∞ and $\Delta G'$ are reported in Figure 31.

All the samples prepared by *in situ* sol-gel procedure showed G' values higher or similar to that of NR-SiO_2 both before and after the thermal treatment and, in general, G′ increased after thermal treatment at 150°C.

The filler-filler and filler-rubber interactions of all *in situ* composites containing functionalized silica with different molecules can be considered to belong to a hypothetical line.

Therefore, by varying the kind of functional molecules on silica, it is possible to vary the dynamic mechanical properties and the filler-filer and filler-rubber interactions.

All the *in situ* composites, from mechanical point of view, can be divided into three groups. The first group composed of NR-CPTEOS, NR-ICPTEOS, NR-TEOS and NR-TMSPM-2, showed high filler-filler and filler rubber interactions.

The second group composed of NR-VTEOS, NR-PTEOS, NR-TESPT-2 and NR-TESPD-2 samples showed and high filler-rubber interaction and a moderate filler-filler interaction.
Regarding the last group, NR-OCTEOS, NR-APTEOS, NR-NXT composites show less filler-filler and filler-rubber interactions.
Therefore, following each category will be discussed, taking into account the morphology previously examined. In detail, NR-CPTEOS, NR-ICPTEOS, NR-TEOS and NR-TMSPM-2 have the highest G' values and, consequently, the highest difference $\Delta G' = G'_0 - G'_\infty$ (G'_0 is the G′ value at low strain amplitude (2%) and G'_∞ is the G' value at large strain amplitude (100%).
NR-VTEOS, NR-PTEOS, NR-TESPD and NR-TESPT show significant G' and ΔG' values but lower than the previous ones and, finally, NR-APTEOS, NR-OCTEOS and NR-NXT have the lowest G' values, similar to those of the reference sample NR-SiO_2.
The dynamic-mechanical behavior of the silica-rubber composites is relatable to the different morphologies of the composites, as evidenced by TEM analysis.
According to the mechanistic interpretation of the Payne effect, as related to the breakdown of the filler network upon oscillatory shear, the higher the values of G' and ΔG', the stronger is the reinforcing effect of the filler desirable only in cured composites.
The formation of the filler network is due either to filler-filler interaction, associated to the continuous interaction among filler particles or to the immobilization of the elastomeric chains consequent to filler-polymer interaction.
The *in situ* grown silica or modified silica particles generally undergo both effective filler-filler and filler-rubber interactions due to the continuous filler network throughout rubber and to the small particle size.
However, the different trialkoxysilane precursors modify silica particles with surface functional groups, which change the filler-rubber interaction.
Moreover, they change the shape of the particles from the spherical one of TEOS, due to the functionalizing chain, which hinders the isotropic growth of the particles.
Both these effects can in principle strongly affect the filler-filler and filler-rubber interactions.
In fact, the highest G' value of NR-CPTEOS, NR-ICPTEOS and NR-TEOS can be associated to a strong filler-filler interaction, due to the formation of continuous networks of

well assembled spherical or slightly anisotropic silica nanoparticles and to a chemical interactions, between the surface hydroxyl groups.

As reported before in NR-TMSPM, the particles are larger with irregular shapes, and the network is less homogeneous but continuous.

This is caused by the presence of thiol groups, which interact both with the silanol groups and with the rubber matrix. Thus, although the network is inhomogeneous, the filler-filler interaction is strong and the G' value is high.

The lower G' and ΔG' values of NR-VTEOS, NR-PTEOS, NR-TESPD-2 and NR-TESPT-2 can be associated to a weaker filler-filler interaction in comparison to the previous samples. In fact, these compounds present filler networks continuous throughout the rubber, constituted by anisotropic shaped particles, surrounded by extended rubber layers lowering the filler-filler interaction.

This is a consequence of the alkyl or alkylsulfide chains present in alkoxide precursors, which make the silica surface less hydrophilic and more compatible with rubber, as well as of the particle anisotropic shape which is less favorable to compact self assembling.

In the cases of NR-APTEOS and NR-OCTEOS, the dynamic-mechanical properties are strongly affected by the formation of not continuous and not homogeneous filler networks with large regions of rubber without filler.

These results explain the very low G' values, similar to those of the reference sample NR-SiO_2 obtained by mechanical blending.

Regarding NR-NXT, the low G' values seem apparently unexpected, as the filler network, constituted by anisotropic nanoparticles, appears homogeneous and continuous.

It could be suggested that the presence of the octyl chain, similar to the NR-OCTEOS substituent, strongly improves the interaction with the rubber hindering that between the filler particles.

The presence of the continuous network in NR-NXT allows the significant increase of G' and ΔG' values after thermal treatment at 150°C (see Figure 30 b), where the sulphur groups react with the rubber matrix and strongly enhance the filler rubber interaction.

The previous results demonstrate that the alkoxysilane substituents modify the silica surface and influence particle size/shape and continuity of the network, allowing to modulate the dynamic mechanical properties of filler-rubber composites.

The G'' strain dependence of *in situ* silica-rubber composites before and after the thermal treatment at 150°C is shown in Figure 33. In general, G'' increases after thermal treatment at 150°C.

The trend of G'' is similar to that of G'.

NR-CPTEOS, NR-ICPTEOS, NR-TEOS and NR-TMSPM-2 have the highest G'', and the curves show maximum values at moderate strain amplitude (12-18 %). NR-VTEOS, NR-PTEOS, NR-TESPD-2 and NR-TESPT-2 have lower G'' and maxima at lower strain amplitude (5-10 %).

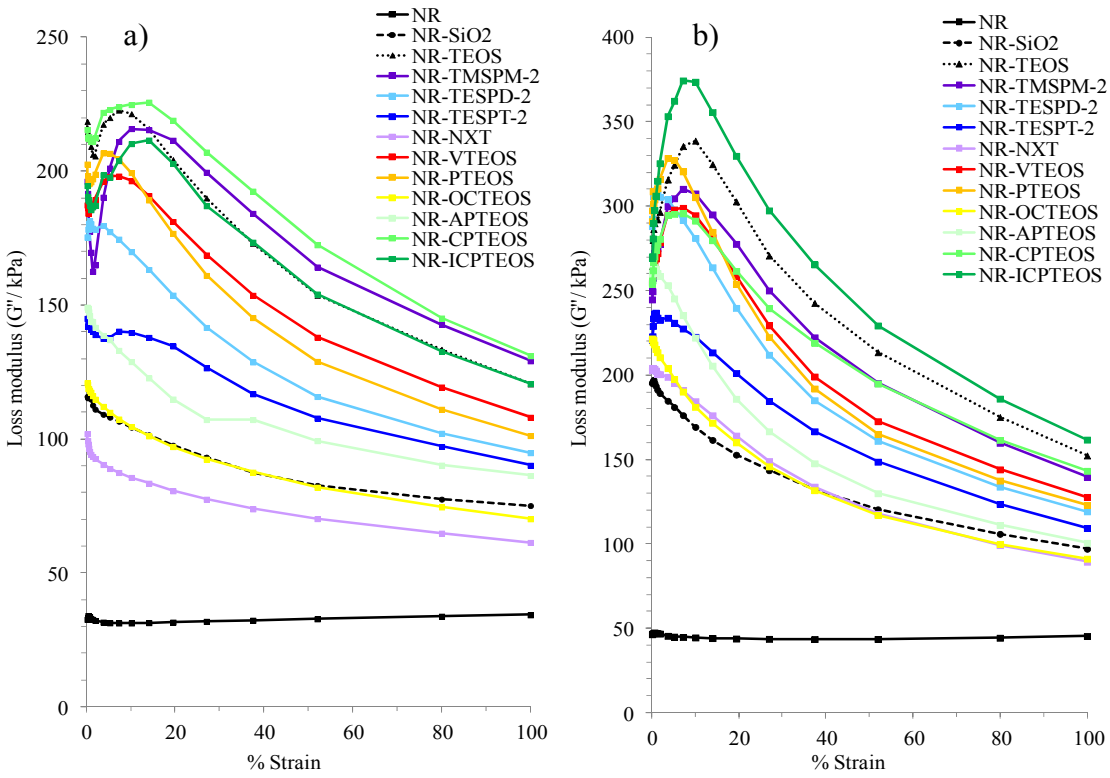

Figure 33: modulus G'' vs strain of the uncured in situ silica-rubber composites NR-TEOS, NR-TMSPM, NR-TESPD, NR-TESPT, NR-NXT, NR-VTEOS, NR-PTEOS, NR-OCTEOS, NR-APTEOS, NR-CPTEOS, NR-ICPTEOS compared with NR-SiO_2 and pure NR a) before and b) after thermal treatment at 150°C.

NR-APTEOS, NR-OCTEOS and, in particular, NR-NXT have the lowest G'' and no maximum in the curves.

The loss modulus G'' depends on the rates of network breakdown and reformation, due to the strain amplitudes. Increasing the strain amplitude, the filler breakdown would increase, and its reformation rate would diminish more rapidly than it would disrupt.

Once the strain amplitude is high enough for the filler network to be destroyed, and it cannot reform in the time scale of the dynamic strain, the effect of filler network on G'' disappears. Similarly, if the strain is small enough that the network cannot be broken, G'' depends only on the hydrodynamic effect of the filler, and the strain dependence is eliminated.

Since in the investigated silica-rubber composites the amount of filler is the same, the higher the G'' values and the strain at which G'' is maximum, the stronger is the network.

The curves with the lowest G'' values without a maximum are due to the formation of weak networks in uncured composites.

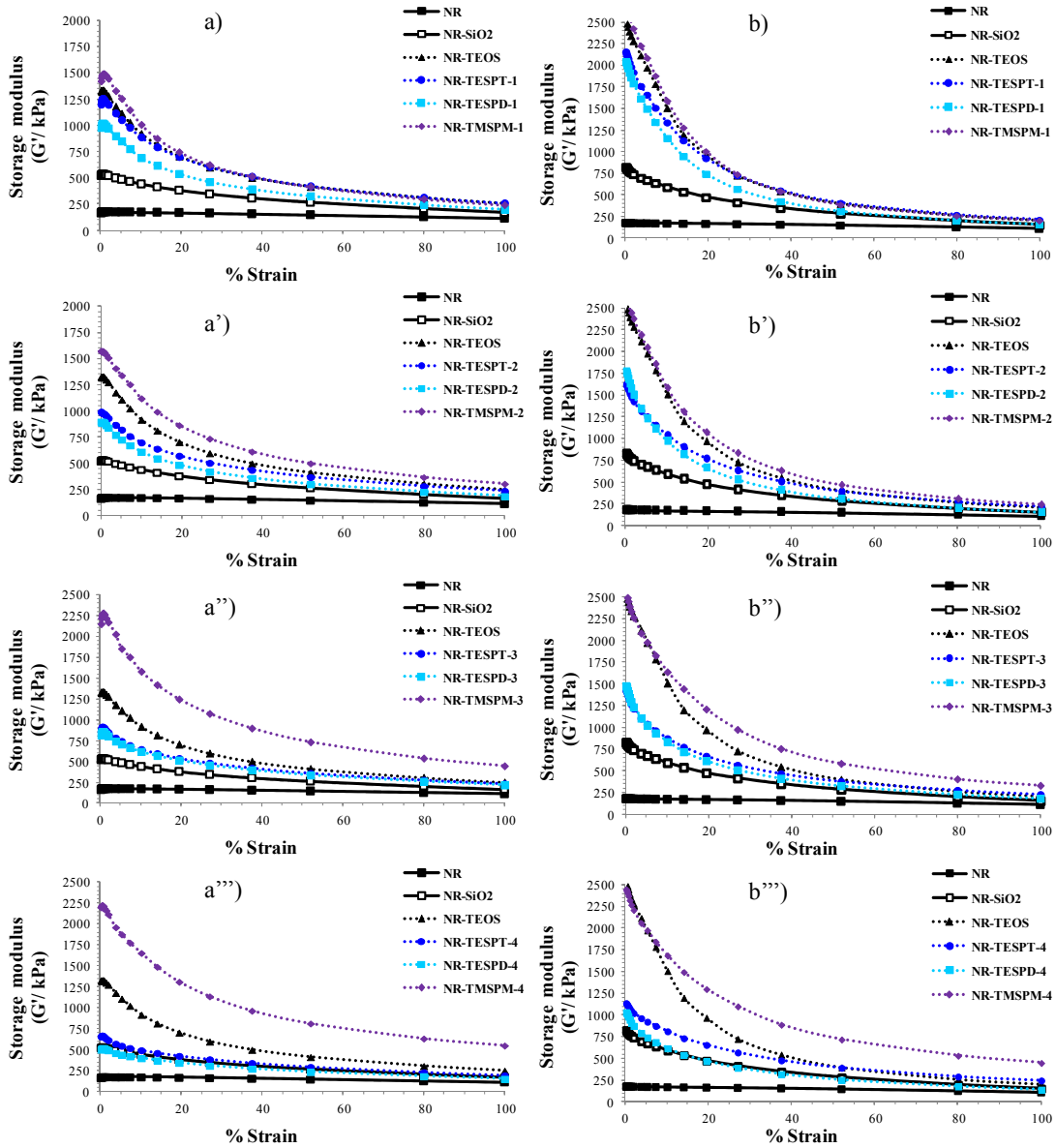

Figure 34: modulus G´ vs strain of the uncured *in situ* silica-rubber composites NR-TEOS, NR-TESPT-1/4, NR-TESPD-1/4, NR-TMSPM-1/4 compared with NR-SiO_2 and pure NR (a) before and (b) after the thermal treatment at 150°C.

These results are in agreement with the indications obtained by G' measurements and support the previous conclusions regarding the relations between the morphology of the composites and the dynamic-mechanical properties.

In order to study the effect of the amount of functionalizing molecules on silica particles RPA analysis was performed on a selected number of composites.

G´ trends for 30 phr *in situ* silica-rubber composites and silica-rubber composites containing different amounts of alkylthiol, alkyldisulphide and alkyltetrasuphide (see Table 3 chapter 4) are shown in Figure 34a and 34b before and after the thermal treatment at 150°C, compared with those of the reference samples NR-SiO_2 and of pure NR.

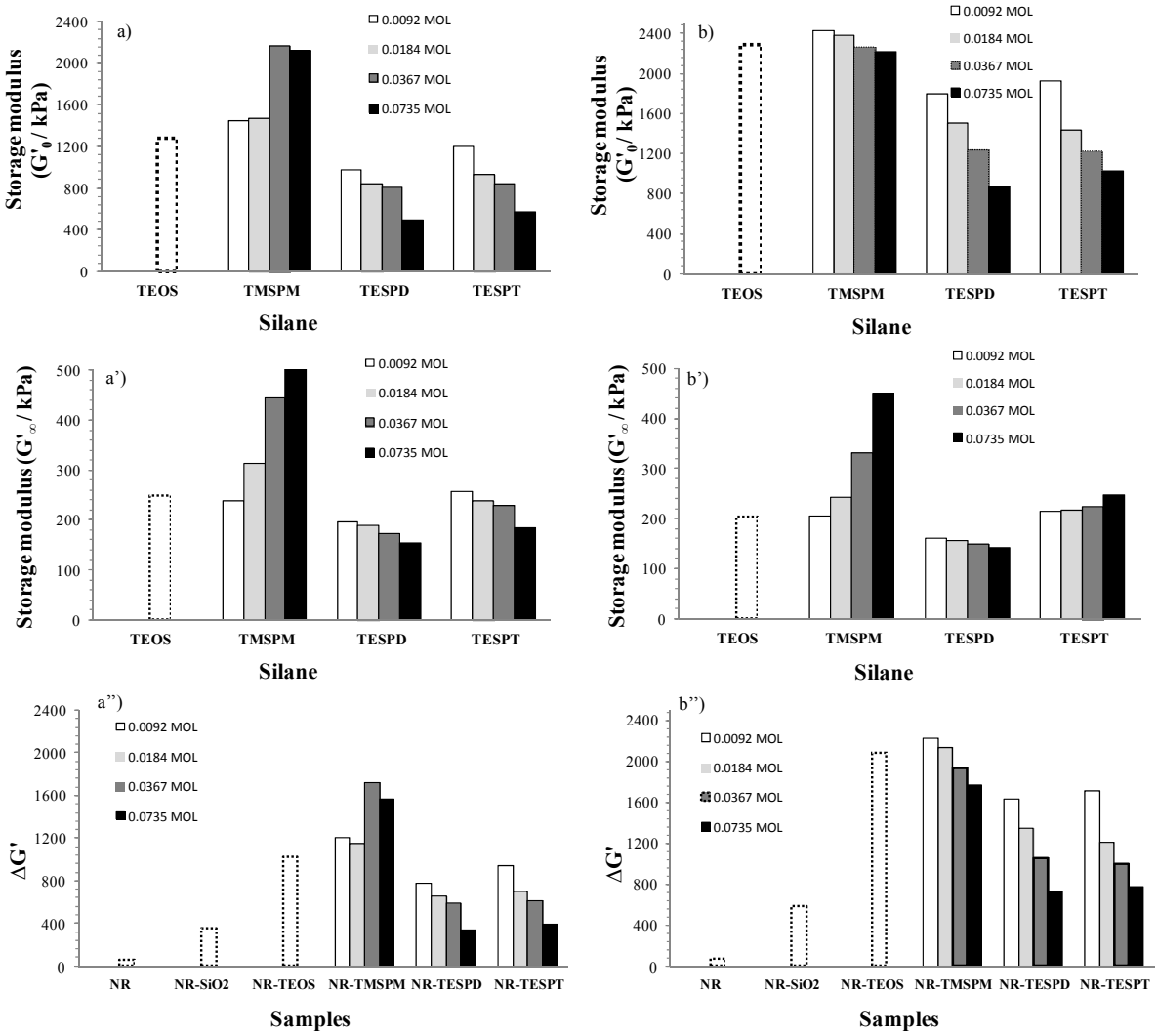

Figure 35: Storage modulus G´$_0$ at low strain (a, b), G'$_\infty$ at high strain (a', b'), and difference ΔG´= G´$_0$-G´$_\infty$ (a'', b'') of NR, NR-SiO_2, NR-TEOS and of NR-TESPT, NR-TESPD, NR-TMSPM with different modifier molecule/silica ratios, and (a) before and (b) after the thermal treatment at 150°C.

All these samples prepared the by *in situ* sol-gel procedure show G'_0 values higher than NR-SiO_2, both before and after the thermal treatment and, in general, G′ increases after thermal treatment at 150°C.

In Figure 35 the storage modulus G'_0 at low strain, G'_∞ at high strain, and the difference $\Delta G' = G'_0 - G'_\infty$, relative to the composites before and after the thermal treatment, are reported for various modifier silane/SiO_2 ratios.

ΔG′ values of NR-TMSPM and NR-TEOS samples are always higher than those of NR-TESPD and NR-TESPT samples before and after thermal treatment, due to their higher G'_0 and G'_∞.

Surprisingly, at variance with TMSPM, the G'_0 and ΔG′ values decrease by increasing the amount of the modifier groups in NR-TESPD and NR-TESPT.

The graph below clearly shows our interpretation of the relationship between the values of ΔG′ (interaction between filler-filler) and G'_∞ (interaction between filler- rubber) (see Figure 36) after thermal treatment.

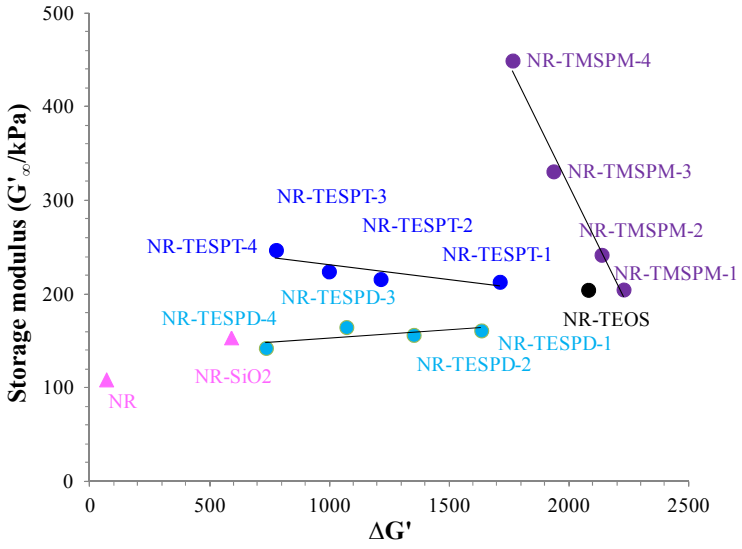

Figure 36: Filler-filler interaction vs filler-rubber interaction after thermal treatment for 30 phr silica rubber composites containing different amounts of functionalizing molecules on silica particles.

Therefore the dynamic mechanical behavior may be commented as follows.

The construction of the filler network can be achieved and reinforced either by filler-filler interaction, associated to the diffuse and homogeneous interaction between filler particles, or by filler-polymer interaction, associated to the immobilization of the elastomeric chains under filler-polymer interaction.

The *in situ* grown silica or modified silica fillers generally undergo stronger interactions both among them and with the polymer matrix, due to the lower size and more homogeneous dispersion of the filler aggregates throughout rubber, with respect to a mechanically mixed silica blend.

Increasing the amount of substituted SiO_2, G′ values increase in the case of TMSPM, but decrease in the case of TESPT and TESPD composites.

In fact, as suggested by TEM analysis, in the former case the filler-filler interaction remains strong even at high amounts of functionalizing molecules, while in the latter case the filler network becomes less compact due to the increase of filler-rubber interaction.

These results demonstrate that the type of TEOS substituent influences shape and dispersion of silica aggregates/agglomerates, allowing to modulate the dynamic mechanical properties of filler-rubber composites. The increase in the amount of silica modifiers increases the G'_0 value in NR-TMSPM, while in the case of NR-TESPD and NR-TESPT the higher the amount, the lower the dynamic property.

Thus, the effects of the filler-filler interaction prevail in NR-TMSPM composite, while those of the filler-rubber interaction prevail in NR-TESPD and NR-TESPT derivatives.

In order to study the effect of the filler amount on the nanocomposite RPA analysis was performed on a selected number of samples of bare and functionalized silica.

Regarding silica-rubber composites containing 31% silica, NR-TEOS-45, NR-TMSPM-45, NR-TESPD-45 and NR-TESPT-45 show similar G' and ΔG' values trends to those with 23% silica (30 phr) and the same molar amount of functional molecules, corresponding to that of NR-TMSPM-2, NR-TESPD-2 and NR-TESPT-2).

The curves of G' vs strain for these composites are shown in Figure 37.

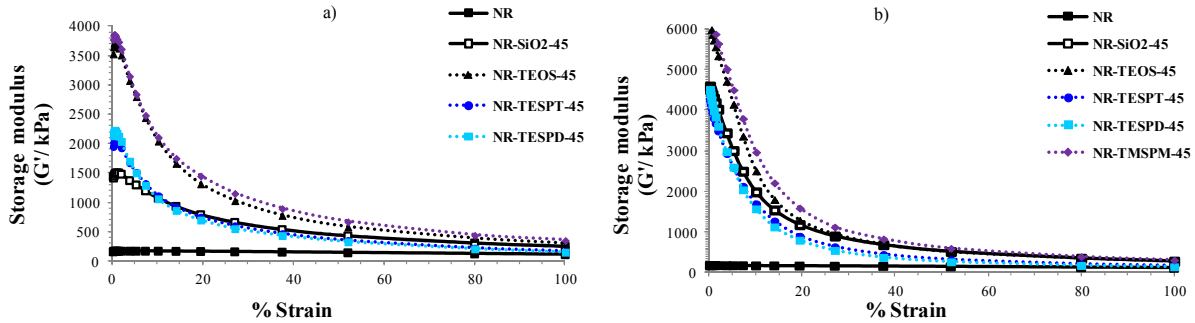

Figure 37: modulus G´ vs strain of the uncured 45 phr *in situ* silica-rubber composites NR-TEOS-45, NR-TESPT-45, NR-TESPD-45, NR-TMSPM-45 compared with NR-SiO_2-45 and pure NR (a) before and (b) after the thermal treatment at 150°C.

The graphs show an increase of the G'_0 and G'_∞ in comparison to those of composite containing 30 phr of silica. In addition, G'_0 and G'_∞ increase after thermal treatment. Therefore, the dynamic mechanical analysis of *in situ* silica rubber composite containing this large amount of filler show a higher reinforcing effect in comparison to those containing 30 phr.

In order to understand the degree of reinforcing effect due to the addition of only bare silica, without any functionalizing molecules on the particle surface, the dynamical mechanical analyses were carried out on three composites containing 16.65% (20.18 phr), 22.93% (30.27 phr) 30.95 % (45.26 phr) silica amount before and after thermal treatment (see Figure 38).

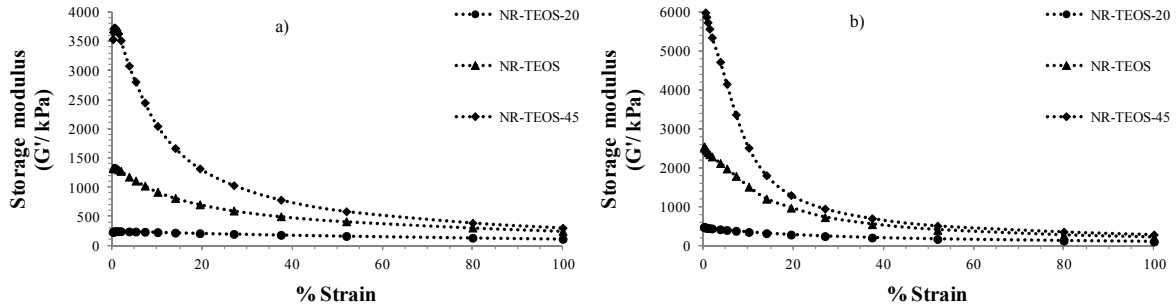

Figure 38: Storage curves of *in situ* silica-rubber composite at different concentration of silica before (a) and after (b) thermal treatment.

It is evident that increasing the amount of silica increases the storage modulus due to the increase of filler-filler interaction, therefore the amount of filler influences the mechanical properties

The DMTA results show again that the dynamic mechanical properties (E', E'' and Tan δ) of the uncured silica rubber composites were affected by the kind of functionaling molecules on silica surface. The results show that the glass transition temperature was not affected by the presence of silica and silica functionalized *in situ* in rubber composite, and the value ranging between -58.2°C and -55.6°C.

5.6. Curing

Uncured samples were vulcanized[30] according to the procedure reported in the paragraph 3.2.10. The vulcanization kinetic was studied by measuring the variation of torque with time, using the torque requested to keep the rotor rotating at the constant rate.

In order to find the optimal cure condition, the curing kinetic was monitored at two different condition: 170°C for 15 min and 151°C for 30 min as reported in Figure 39 for V-NR-TEOS sample.

Short scorch time and high reversion degree are visible for vulcanization process performed at 170°C for 15 min.

Therefore the preferred condition to vulcanize these composites at151°C for 30 min.

In fact, medium scorch time and low reversion degree were showed by NR-TEOS during the vulcanization kinetic performed at 151°C for 30 min. Vulcanization curves for aqueous *in situ* sol-gel composites containing silica functionalized and reference samples are shown in Figure 40 and the parameters are reported in Table 5.

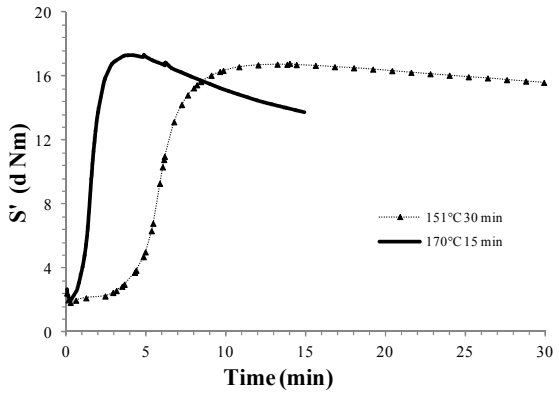

Figure 39: Cure kinetic of NR-TEOS at 151°C for 30 min and at 170°C for 15 min.

The scorch time t_{S1} is the time during which the rubber composite can be manipulated before curing; the minimum torque ML is the torque measured at the scorch time; the curing time t_{MH} is the time to completely cure the composite; the maximum torque MH is the torque measured when the reticulation can be considered complete.

All *in situ* prepared samples show curing time and maximum torque values higher than V-NR-SiO_2 and NR-C_{black} samples, suggesting a higher degree of rubber reticulation, except NR-OCTEOS whose curing characteristics are due to poorly homogeneous filler dispersion and bad reinforcement.

Besides, NR-OCTEOS composite contain silica particles with 10% of micropores (see Table 1) which during the vulcanization process could trap and hydrolyze the accelerator, leading to shorter scorch time and higher reversion.

During the compounding of all our composites the curing package and carbon black were added. In order to separate the contributions of 20 phr of carbon black from NR-SiO_2 sample, NR-C_{black} sample was prepared.

In detail, the addition of Rhodia silica increases about 73% the minimum and the maximum torque, doubles the scorch and the curing times with respect to the values of the composite containing only carbon black.

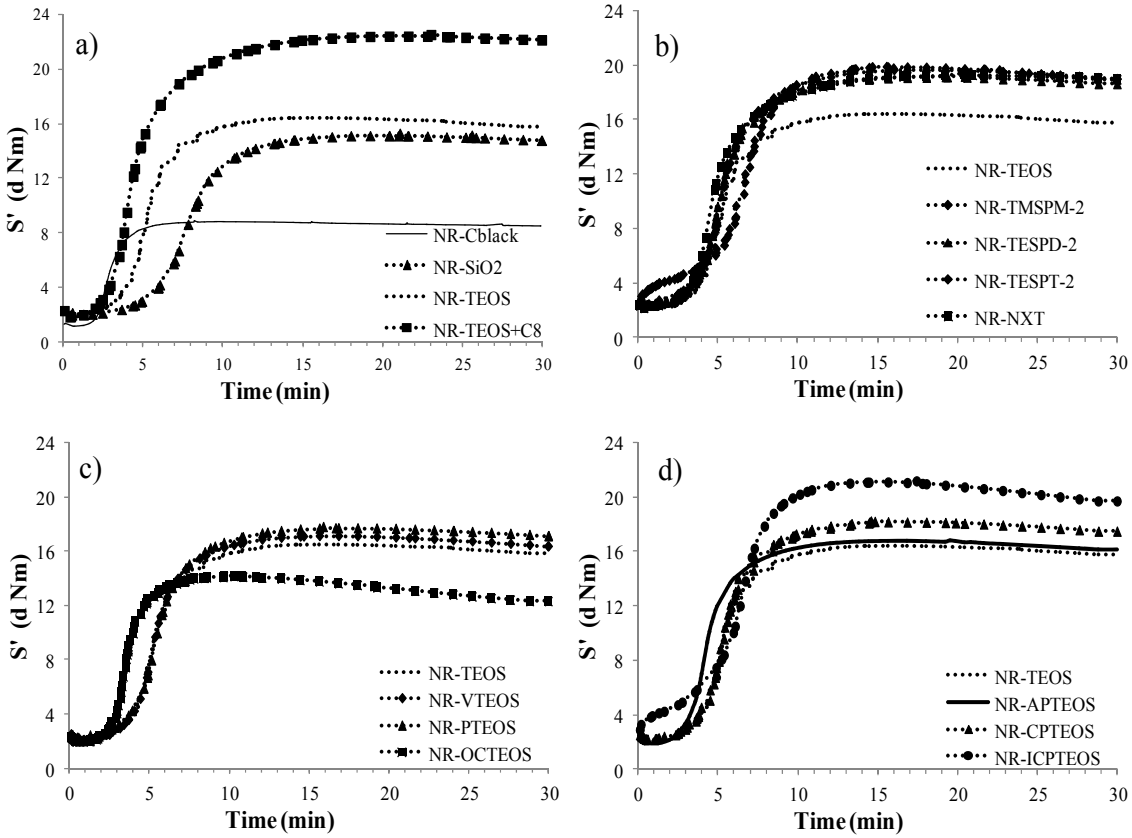

Figure 40: Cure kinetics a) reference samples, b) composites containing silica functionalized with sulphur groups, c) composites containing silica functionalized with alkyl and alkenil groups, d) composites containing silica functionalized with nitrogen groups, compared with composite containing bare silica from TEOS.

In particular, all composites containing sulphur functionalized silica (V-NR-NXT, V-NR-TESPT, V-NR-TESPD, V-NR-TMSPM) have similar curing behavior, the highest values of curing time and maximum torque in comparison with the other compounds.

This demonstrates that the functionalizing units affect the curing process.

In detail, low scorch time was showed by V-NR-TMSPM whose beginning of curing curve illustrate the typical behavior attributable to the filler flocculation (when the rubber network is not yet densified).

In addition scorch and curing times of V-NR-TESPT and V-NR-TESPD show a decreasing time for composite containing silica functionalized with alkyltetrasulphide in comparison to disulfide, because the polysulfide act as a sulphur donors during the cross-linking process.
Considering always these two samples a small increase in maximum torque for V-NR-TESPT is due to a more efficient reticulation of the composite acted by the alkyltetrasulphide that functionalize the silica surface.

Samples	Minimum torque ML (dNm)	Scorch time T_{S1} (min)	Maximum torque MH (dNm)	Curing time t_{MH} (min)	Rev. %
V-NR-C_{black}	1.17	2.24	8.90	8.22	5.0
V-NR-SiO_2	2.02	4.92	15.30	21.07	3.9
V-NR-TEOS	2.03	3.29	16.55	14.42	5.1
V-NR-TMSPM-2	2.47	0.53	19.98	15.51	5.6
V-NR-TESPD-2	2.37	3.01	19.24	20.41	3.6
V-NR-TESPT-2	2.46	2.79	19.78	18.01	4.5
V-NR-NXT	2.16	2.75	19.43	20.36	2.8
V-NR-VTEOS	2.21	3.37	17.23	14.52	5.7
V-NR-PTEOS	2.23	3.07	17.80	15.86	4.3
V-NR-OCTEOS	1.95	2.50	14.23	10.27	15.7
V-NR-APTEOS	1.91	2.69	16.84	19.51	4.5
V-NR-CPTEOS	2.19	3.16	18.24	14.55	4.5
V-NR-ICPTEOS	2.92	0.84	21.18	17.39	8.1
V-NR-TEOS+C8	1.89	2.30	22.52	23.02	1.9

Table 4: Cure characteristics.

Regarding the difference showed by V-NR-TESPT, V-NR-TEOS and V-NR-TEOS+C8, it is evident that the last sample shows the best curing properties than the other two.
The reasons of this behavior showed by V-NR-TEOS+C8 is due to the addition of TESPT on composite which contain the silica well dispersed in the network, therefore the role of this silane is not only to functionalize the silica particle but to compatibilize a composite.
Regarding V-NR-PTEOS, V-NR-VTEOS, V-NR-APTEOS show only slightly higher curing properties than NR-TEOS.
Besides, the low scorch times of the *in situ* sol-gel samples evidence that they are partially cured before vulcanization, in agreement with the swelling measurements.

The effect is particularly evident in NR-TMSPM and NR-ICPTEOS, whose curing curves show a very fast torque increase in the early stage of vulcanization.

This behavior is attributable to the filler flocculation occurring when the rubber network is not yet densified, and confirms the high tendency of the thiol groups to link both with the filler and the rubber.

Also for NR-ICPTEOS, as for NR-OCTEOS, the high reversion tendency during the curing kinetics may be due to the presence of 5% of micropores (see Table 1) in the silica which affect the behavior of accelerator during the curing kinetic.

5.7. Vulcanized composites properties

In this paragraph are reported all the vulcanized composites characterization.

The properties of the aqueous *in situ* sol gel silica and functionalized silica composites are discussed taking into account the morphology characteristics showed in the beginning of this chapter. Analogously to the uncured silica and functionalized silica master batches, the dynamic mechanical analysis in shear stress mode were carried out on the vulcanized silica and functionalized silica full compounds.

Therefore this mechanical characterization on vulcanized composites was performed by RPA instrument at 70°C and at constant frequency (10 Hz), higher than in the case of uncured samples.

The reasons of the choice of this analysis parameter is that this condition allows to appreciate the mechanical behavior of the vulcanized composites in a situation near the rolling resistance performance of the tire.

The trends of the storage modulus G' and loss modulus G'' of all composites prepared by *in situ* procedure and compared with the reference sample are reported in Figure 41.

G′, ΔG′ and G'' values for all *in situ* composites are higher than those of V-NR-SiO_2 confirming that *in situ* prepared silica is more homogeneously dispersed in NR matrix even after vulcanization.

In general, the trends of G', ΔG′ and G' are similar to those of uncured samples confirming that the influence of functionalizing molecules on the silica filling properties is maintained even after the curing process, with the exception of silica functionalized with sulphur containing group, V-NR-TESPT, V-NR-TESPD and, in particular, V-NR-NXT, whose G'

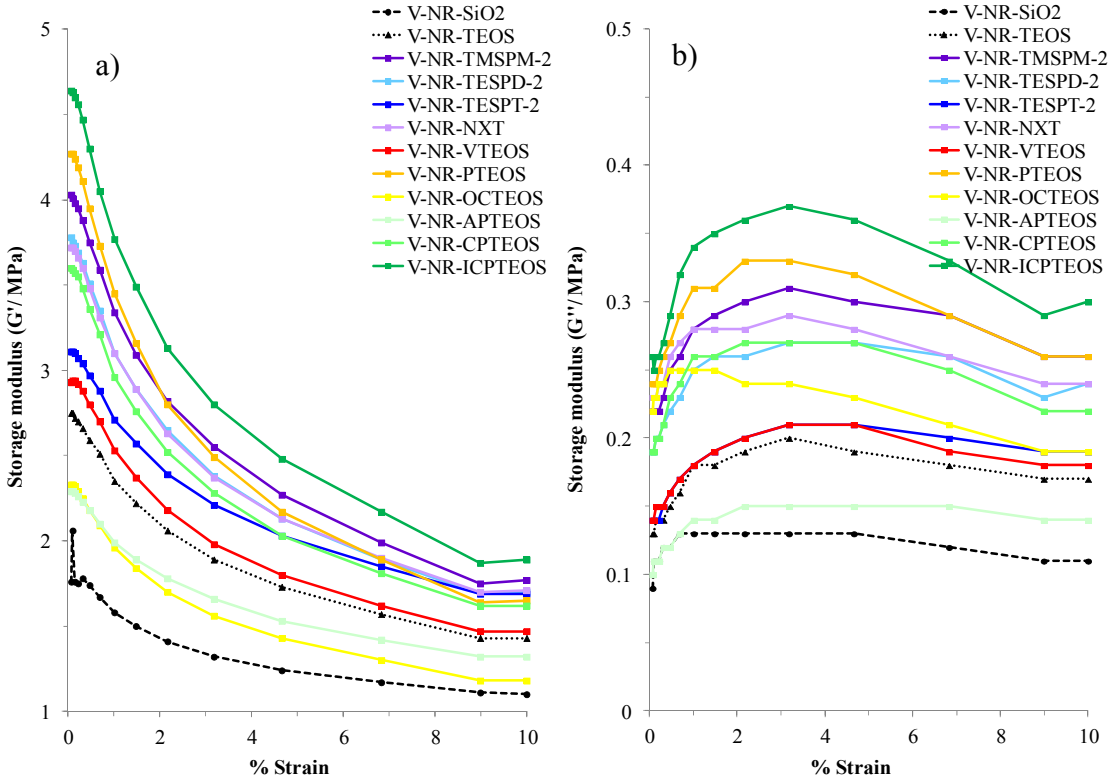

Figure 41: Storage modulus G´ (a) and loss modulus G'' (b) vs strain of the vulcanized *in situ* silica-rubber composites V- NR-TMSPM-2, V-NR-TESPD-2, V-NR-TESPT-2, V-NR-NXT, V-NR-VTEOS, V-NR-PTEOS, V-NR-OCTEOS, V-NR-APTEOS, V-NR-CPTEOS, V-NR-ICPTEOS compared with V-NR-SiO_2.

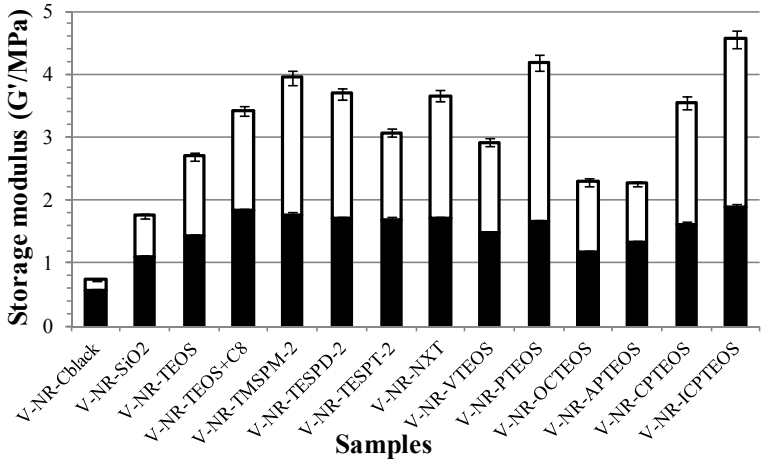

Figure 42: Histograms of the variation of storage modulus G' vs strain: Full column chart indicates the magnitude of G'_0 (storage modulus at low strain); inside the black column chart shows the amount of G'_∞ (storage modulus at high strain) and the white column chart reports the quantity of $\Delta G' = (G'_0 - G'_\infty)$. The graph report the trend of the vulcanized rubber composites V-NR-TEOS, V-NR-TEOS+C8, V-NR-TMSPM, V-NR-TESPD, V-NR-TESPT, V-NR-NXT, V-NR-VTEOS, V-NR-PTEOS, V-NR-OCTEOS, V-NR-APTEOS, V-NR-CPTEOS, V-NR-ICPTEOS compared with V-NR-C_{black} and V-NR-SiO_2.

values are higher than those expected taking into account the G' trend of uncured samples (see Figure 42).

This is due to the reactions of polysulphide and thioester groups with the rubber during the curing treatment at 150°C, which strongly improves the filler-rubber interaction and the rubber reticulation, as already observed in the vulcanization curves.

Therefore this analysis on vulcanized samples reports and confirms the dynamical mechanical properties showed in uncured composites and justifies the morphological characterization presented before.

Other characterizations

Hardness, abrasion, tensile strength, elongation at break, elastic modulus were determined on the vulcanized silica and functionalized silica compounds in order to understand better, from technological point of view, the relationship between the morphology and the final properties in the real application.

Mooney viscosity was also measured on the compounds before curing process.

All these techniques and the related instruments, methods and procedures have been described in the chapter 3 (pharagraphs from 3.2.11 to 3.2.15).

Table 5 reports, for all the *in situ* composites and for the mechanical mixed reference sample V-NR-SiO_2 the Mooney viscosity, the abrasion values, the hardness values acquired at 23°C and at 100°C and relative variation of the hardness as a function of the temperature ($\Delta H/\Delta T$ %).

The Mooney viscosity indicates the behavior of the compound at the beginning of the vulcanization process and during the processing.

High Mooney viscosity means low processability, besides a possible high filler flocculation within the composite.

A lower Mooney viscosity suggests an effective hydrophobization of the filler surface and a higher compability with the polymer.

The hardness is related to the reinforcing effect of the filler addition.

The variation of the hardness as a function of the temperature indicates the dependence of the rigidity upon temperature.

Regarding the abrasion value, it is related to the strength of the filler-rubber interaction in the compounds and it is fundamental for the long-lasting of the tire.

Samples	Mooney viscosity ML_{1+4} (M.U.)	Hardness (23°C)	Hardness (100°C)	ΔH/ΔT %	Abrasion mm^3
V-NR-SiO_2	62.6	64.4	59.0	7.01	95.4
V-NR-TEOS	62.5	66.3	59.7	8.57	142.8
V-NR-TEOS+C8	58.9	74.9	68.4	8.44	95.1
V-NR-TMSPM	76.9	67.9	59.8	10.52	144.6
V-NR-TESPD	67.9	71.4	63.9	9.74	119.4
V-NR-TESPT	68.7	72.3	64.5	10.13	111.5
V-NR-NXT	67.4	74.6	63.5	14.41	109.8
V-NR-VTEOS	65.5	68.0	60.3	10.00	138.0
V-NR-PTEOS	65.7	72.0	60.1	15.46	150.2
V-NR-OCTEOS	57.4	63.5	51.0	16.23	169.8
V-NR-APTEOS	56.7	67.2	59.6	9.87	137.2
V-NR-CPTEOS	66.1	70.2	59.3	14.15	146.1
V-NR-ICPTEOS	77.5	68.7	58.8	12.85	158.1

Table 5: Mooney viscosity, hardness at 23°C and 100°C and abrasion for all *in situ* silica-rubber composites and compared with V-NR-SiO_2.

In fact, increasing the filler-rubber interaction, the abrasion loss of the compounds reduces and the tire life increases.

Table 6 reports the tensile mechanical analysis of the vulcanized compounds carried out at room temperature (23°C).

In details, the tensile strength, the value of the modulus at three different percentages of composite elongation and the elongation at break are reported.

In general, high tensile strength indicates that the vulcanized compounds have a high resistance to the rupture while low tensile strength means a less homogeneous rubber network.

Regarding the modulus value, it is related to the strength and the effectiveness of the filler-filler network.

The elongation at break is related to the tensile strength and modulus. A decreasing of elongation at break corresponds either to bad filler dispersion (corresponding also to low tensile strength) or to effective filler dispersion but high modulus and hardness of the vulcanized compounds.

Therefore the tensile mechanical analysis is indicative of the quality of the compounds processing as well as the dispersion of the ingredients.

Samples	Tensile strength MPa	Modulus 50 % MPa	Modulus 100 % MPa	Modulus 300 % MPa	Modulus 300 % / 100%	Elongation at break %
V-NR-SiO_2	27.05	1.21	2.18	13.54	6.21	534.26
V-NR-TEOS	23.21	1.21	1.98	10.23	5.17	553.13
V-NR-TEOS+C8	27.62	1.96	3.99	19.57	4.91	457.16
V-NR-TMSPM	23.10	1.11	1.73	9.70	5.60	551.96
V-NR-TESPD	25.41	1.48	2.58	13.92	5.40	516.85
V-NR-TESPT	25.69	1.58	2.79	14.98	5.37	493.44
V-NR-NXT	27.79	1.61	2.86	15.37	5.37	525.77
V-NR-VTEOS	23.44	1.23	2.01	10.35	5.15	553.42
V-NR-PTEOS	23.82	1.26	1.94	9.21	4.75	581.80
V-NR-OCTEOS	22.07	1.03	1.50	7.04	4.69	615.44
V-NR-APTEOS	23.60	1.32	2.30	11.48	5.00	536.01
V-NR-CPTEOS	21.55	1.28	2.02	10.23	5.07	527.09
V-NR-ICPTEOS	24.04	1.05	1.58	8.61	5.45	600.96

Table 6: Static mechanical analysis of vulcanized silica and functionalized silica rubber composites.

In order to compare all the properties of the silica-rubber composites and predict the behavior in the tire application, dynamic mechanical tests were carried out in compression stress mode on vulcanized composites.

In particular the mechanical analysis were performed at three different frequencies (1,10, 100 Hz) and three different temperatures (10, 23, 70 °C) in order to obtain for every test the elastic and viscous moduli (E' and E'') and the tanδ (see Table 7).

Hereafter the elastic and viscous moduli and tanδ will be discussed for the tests at 100 Hz and at 10, 23, 70 °C as these conditions are more similar to the working condition of a tire and as the results obtained at 10Hz are complementary to those obtained in dynamic mechanical analysis performed in shear stress mode (RPA) before presented.

Also in this case, the higher the elastic modulus, the better reinforcing, hardness and strength of the vulcanized composites.

Besides, a low viscous modulus determines a quick destruction and reformation of the filler network during the tire movement, tan δ is related to the energy dissipation during tire use; this parameter has to be low to save energy with less tire and fuel consumption and lower air pollution.

Samples	E'			E''			tan δ		
	10°C	23°C	70°C	10°C	23°C	70°C	10°C	23°C	70°C
V-NR-SiO_2	6.576	6.119	5.198	1.282	0.886	0.453	0.195	0.145	0.087
V-NR-TEOS	7.256	6.659	5.621	1.529	1.096	0.568	0.211	0.165	0.101
V-NR-TEOS+C8	11.331	10.332	8.405	2.107	1.442	0.658	0.186	0.140	0.078
V-NR-TMSPM	7.867	7.156	6.075	1.895	1.371	0.768	0.241	0.192	0.126
V-NR-TESPD	9.475	8.599	6.923	2.081	1.471	0.742	0.220	0.171	0.107
V-NR-TESPT	9.695	8.768	7.159	2.033	1.385	0.754	0.210	0.158	0.105
V-NR-NXT	10.43	9.409	7.155	2.234	1.605	0.784	0.214	0.171	0.110
V-NR-VTEOS	7.586	6.936	5.870	1.690	1.155	0.599	0.223	0.166	0.102
V-NR-PTEOS	8.578	7.768	6.289	2.029	1.498	0.748	0.237	0.193	0.119
V-NR-OCTEOS	8.086	7.172	4.912	2.024	1.493	0.698	0.250	0.208	0.142
V-NR-APTEOS	7.017	6.493	5.482	1.347	0.957	0.453	0.192	0.147	0.083
V-NR-CPTEOS	8.378	7.579	6.190	1.950	1.350	0.722	0.233	0.178	0.117
V-NR-ICPTEOS	6.117	5.532	4.660	1.470	1.024	0.600	0.240	0.185	0.129

Table 7: Compression set of all the vulcanized compounds

Comparing the results obtained from the vulcanized composites it is possible find out some information which confirm and deepen the previous results, allowing to find the relationship between the final properties and the morphology.

V-NR-TEOS, V-NR-TEOS+C8 and V-NR-SiO_2

In order to understand which are the advantages of the preparation of the silica *in situ* by aqueous sol-gel method the proprieties of V-NR-TEOS, V-NR-TEOS+C8 and V-NR-SiO_2 samples were compared.

V-NR-TEOS was prepared by *in situ* aqueous sol-gel method while V-NR-TEOS+C8 is the same sample with the addition of TESPT as a compatibilizer during the compounding; V-NR-SiO_2 is a mechanical blending of silica and NR with TESPT as compatibilizer.

All the three composites contains the same amount of silica.

The Mooney viscosity of V-NR-TEOS+C8 (58.9 M.U.) is lower than V-NR-TEOS and V-NR-SiO_2 (62.6 M.U.) due to a better and effective hydrophobization of silica surface prepared *in situ* which make easier the processability of the compound.

Regarding the hardness tests at both temperatures, the ΔH/ΔT % is slightly higher for the compounds which contains the silica grown *in situ* possibly due to the presence of silica with high surface area, interaction between the particles and well dispersed in rubber matrix. The addition of TESPT to the compounds increases the hardness values, due to the alkyltetrasulphide action which enhances the link between silica and rubber.

Abrasion tests of V-NR-TEOS+C8 and V-NR-TEOS confirms that the addition of TESPT improves the interaction of the filler with the rubber creating stable links which make difficult to lose materials by abrasion.

The preparation of the silica *in situ* improve the rigidity and the hardness of the composite as shown by the comparison of V-NR-TEOS+C8 and V-NR-SiO_2 tensile strength (2% or ≈ 1 MPa of improvement).

In addition mechanical analysis carried out in tensile stress mode reports an improvement of elastic modulus for *in situ* silica (correspond to 44%), due to a stronger filler-rubber interaction, and, consequently, the elongation at break of these composites is lower (reduction of ≈ 14%).

Regarding the addition of TESPT as a compatibilizer, the static mechanical analysis reports an increase of the tensile strength value (19 % or ≈ 4.5 MPa) due to improvement of filler-rubber interaction, and an increase of the elastic modulus at 300% of strain.

Comparing the compression for V-NR-TEOS+C8 and V-NR-SiO_2, it is evident that the elastic moduli of the former at 10°C, 23°C and 70°C (in the conditions of tire use) almost doubles due to higher filler distribution and networking in rubber matrix.

Consequently the composite which contains the silica growth *in situ* has a lower tan δ (from 0.087 to 0.078) which means an improvement in rolling resistance of the tire.

In details, the energy dissipation for V-NR-TEOS is reduced at 10°C of 4.6 %, at 23°C of 3.5% and at 70°C of 10.3% and for V-NR-TEOS+C8 at 10°C of 12 %, at 23°C of 15% and at 70°C of 23% due to the addition of TESPT as compatibilizer.

V-NR-TMSPM, V-NR-TESPD, V-NR-TESPT and V-NR-NXT.

V-NR-TMSPM composite shows higher Mooney viscosity in comparison with V-NR-TEOS.

This result confirms that thiol group does not act as an effective compatibilizer of the silica due to the strong filler-filler interaction with causes a not homogeneous distribution of the filler in the rubber.

Consequences are difficult processing of the compounds, filler flocculation and low scorch time.

V-NR-TMSPM hardness show similar values in comparison with V-NR-TEOS, as well as $\Delta H/\Delta T$ % and abrasion, due to high filler-filler and low filler-polymer interaction.

Analogously, the low tensile strength, medium modulus at 300% of elongation and elongation at break are similar to those reported for V-NR-TEOS and also the compression results with increases of the energy dissipation 14% at 10°C, 16% at 23°C and 24% at 70°C.

Regarding V-NR-TESPD, V-NR-TESPT and V-NR-NXT, their behaviors are similar. Mooney viscosity are lower than V-NR-TMSPM, therefore the sulphur functionalization on silica surface does not substantially influence the viscosity of the compound, as confirmed also by the curing kinetics.

Anyway functionalization molecules increase viscosity in comparison with V-NR-TEOS, possibly due to the higher silica-rubber interaction and higher bound rubber.

The hardness of the V-NR-TESPD, V-NR-TESPT and V-NR-NXT are similar both at 23°C and at 100°C and higher than that reported for V-NR-TEOS. In particular, the increasing number of sulphur in alkylpolysulphide functionalization allows a slightly increase of hardness.

V-NR-TESPD, V-NR-TESPT, V-NR-NXT samples show also a similar abrasion, lower (about 30%) that that of V-NR-TEOS due to the high filler-polymer interaction and to the link which allow to reduce the amount of compound lost during the abrasion tests.

Tensile strength, elastic modulus and elongation at break are very different from V-NR-TEOS.

In particular V-NR-TESPT shows higher tensile strength and elastic modulus at 300% than V-NR-TESPD and lower elongation at break as alkyltetrasulphide has higher amount of sulphur. V-NR-NXT shows higher modulus and tensile strength due to the higher reinforcing effect than V-NR-TESPD and V-NR-TESPT.

The reasons of this results is probably due to the presence of silica filler with smaller particles and higher surface area.

In comparison with V-NR-TEOS, V-NR-TESPD, V-NR-TESPT and V-NR-NXT improve hardness, abrasion, the tensile strength; also compression measurement present higher moduli due high reinforcing effect.

The amount of improvement in elastic modulus in compression stress mode is approximately 36% at 10°C, 34% at 23°C and 26% at 70°C. In addition, V-NR-NXT shows a slightly higher elastic modulus at low temperature confirming again the results of tensile stress analysis and of hardness test.

Regarding the energy dissipation V-NR-TESPD, V-NR-TESPT and V-NR-NXT show low tan δ.

V-NR-VTEOS, V-NR-PTEOS and V-NR-OCTEOS

Mooney viscosity of V-NR-VTEOS and V-NR-PTEOS is slightly higher than V-NR-TEOS. Probably, the hydrophobation of the silica surface is not so effective to balance the networking effect of polar functionalizing moieties.

The hardness of V-NR-PTEOS is higher than V-NR-VTEOS, and both are harder than V-NR-TEOS, due to the high filler-polymer interaction.

However, their hardness is lower than that of composites containing silica functionalized with sulphur.

The abrasion resistance is low because no strong links between polymer and functionalized silica occur.

V-NR-VTEOS and V-NR-PTEOS show similar tensile and compression properties than V-NR-TEOS, with a slight increase in dissipation energy of V-NR-PTEOS probably due to a worse dispersion.

V-NR-OCTEOS composite shows completely different behavior in comparison to V-NR-VTEOS and V-NR-PTEOS, justified by the irregular and discontinued network of large and not uniform silica particles, showed by TEM, and also by the presence of long alkyl chains on silica surface which probably may act as lubricants for the composite reducing the hardness and the tensile strength.

In fact, the curing kinetics show bad composite properties and high reversion degree (15.7 %) related to a not effective surface hydrophobation at microscopic scale and to the presence of a small amount of micropores in silica, which are able to adsorb the accelerator and hydrolyze it, by reducing its efficiency during the vulcanization process.

Consequently, V-NR-OCTEOS shows low hardness and the highest abrasion value respect to all the other *in situ* silica composites.

Tensile measurements show low modulus and tensile strength due to the low filler-filler and filler-rubber interaction; elongation at break is high, despite all above consideration on dispersion and weak filler-rubber interaction, simply because modulus is very low.
The very low reinforcing is evidenced also by the low elastic modulus and, therefore, by the high tan δ, high energy dissipation and high hysteresis.

V-NR-APTEOS, V-NR-CPTEOS and V-NR-ICPTEOS

The Mooney viscosity of V-NR-APTEOS is low due to the presence on silica surface of a functionalizing molecules which do not improve the compability with rubber, leading to poor dispersion.
The slight improvement in the hardness in comparison to V-NR-VTEOS, V-NR-PTEOS and V-NR-OCTEOS, is probably due to the presence of larger silica particles and low surface area, even if the value is comparable with the V-NR-SiO_2.
Also tensile strength, modulus at 300% elongation at break and compression properties are similar to those of V-NR-SiO_2 due to the present of low filler rubber interaction.
Both V-NR-CPTEOS and V-NR-ICPTEOS show high Mooney viscosity and, in particular, V-NR-ICPTEOS shows the highest Mooney viscosity evidenced by the filler flocculation in the early stage of the curing process.
The hardness values of both composites are high.
Also abrasion is high due to the low interaction with the polymer, particularly for V-NR-ICPTEOS, which shows also filler flocculation at the first stage of curing process.
V-NR-ICPTEOS elongation at break is higher than that of V-NR-CPTEOS and the trend of the elastic modulus in compression mechanical test is similar. Consequently V-NR-CPTEOS composite dissipate less energy that V-NR-ICPTEOS as evidenced by tan δ.

[1] R. Scotti, L. Wahba, M. Crippa, M. D'Arienzo, R. Donetti, N. Santo and F. Morazzoni, *Soft Matter*, 2012, **8**, 2131-2143.

[2] S. Lowell, E. J. A. Shields, M. Thomas and M. Thommes, *Characterization of Porous Solid and Powders: Surface Area, Pore Size and Density*, 1st ed; Kluwer Academic Publishers, Springer, 2004, p.10-55.

[3] L. Wahba, M. D'Arienzo, R. Donetti, T. Hanel, F. Morazzoni, R. Scotti and L. Tadiello; *In situ sol-gel obtained silica-rubber nanocomposites: influence of the filler precursors on the improvement of the mechanical properties,* Accepted *RSC Advantaces.*

[4] A. Koln, *KGK Kautschuk Gummi Kunststoffe*; 2011, **64** (4), 38-43.

[5] M. Messori and M. Fiorini, *Journal of Applied Polymer Science*; 2011, **119**, 3422-3428.

[6] S. Ozaki, *Chem. Rev.*; 1972, **72** (5), 457–496.

[7] R. G. Arnold, J. A. Nelson and J. J. Verbanc; *Chem. Rev.*; 1957, **57** (1), 47–76.

[8] H. Gunzler and H. U. Gremlich, *IR Spectroscopy: an introduction*; Wiley-Interscience: New York, 2002.

[9] I. C. Hisatsune, *J.Chem.;* 1984, **62**, 945-948.

[10] D. L. Frasco, *J.Chem. Phys.;* 1964, **41**, 2143-2140.

[11] N. Suzuki, F. Yatsuyanagy, M. Ito and H. Kaidou, *Journal of Applied Polymer Science*; 2002, **86**, 1622-1629.

[12]C. Canevali, N. Chiodini, F. Morazzoni, J. Padovani, A. Paleari, R. Scotti and G. Spinolo, *J. of Non-Crystalline Solids*; 2001, **293-295**, 32-38.

[13] W. Nie, *Advance Materials;* 1993, **5**, 520.

[14] J. Gnado, P. Dhamelincourt, C. Pelegris, M. Traisnel and A. Le Maguer Mayot, *J. of Non-Crystalline Solids*; 1996, **208**, 247.

[15] G. I. Likhtenshtein, J. Yamauchi, S. Nakatsuji, A. I. Smirnov and R. Tamura, *Nitroxides: Applications in Chemistry, Biomedicine, and Materials Science*, 1st ed.; Wiley-Interscience: New York, 2008.

[16] I. Dubrovic, D. Klepac, S. Valic and G. Zauhar, *Radiation Physics and Chemistry* 2008, **77**, 811-817.

[17] M. Didovic, D. Klepac and S. Valic, *Macromolecular Symposia* 2008, **265**, 144-147.

[18] Z. Veksli, M. S. Andreis and D. Campbell, *Polymer* 1998, **39**, 2083-2088.

[19] M. M. Borgohain, D. Banerjee, L. Korecz and S.V. Bhat, Applied Magnetic Resonance 2009, **36**, 149-156.

[20] B. Ranby and J. F. Rabek, *ESR Spectroscopy in Polymer Research*, 1st ed.; Kluwer Academic Publishers, Springer, 1977, p.297.

[21] M. Ito, H. Isago, N. Suzuki, *Journal Applied Polymer Science* 2008, **108**, 1385-1392.

[22] V. Brezova, D. Dvoranova and A. Stasko, *Research on Chemical Intermediates* 2007, **33**, 251-268.

[23] S. Goldstein, A. Samuni and G. Merenyi, *Journal of Physical Chemistry A*. 2008, **112**, 8600-8605.

[24] J. Zakrzewski, J. Hupko and K. Kryczka, *Monatshefte für Chemie* 2003, **134**, 843-850.

[25] M.-J. Wang, *Rubber Chemistry and Technology*; 1997, **71**, 520-589.

[26] A. V. Shenoy, *Rheology of fillerd polymer system;* Kluwer Academic Publisher, Netherlands, 1999.

[27] A. N. Gent, *Engineering with rubber: how to design rubber components 2nd edition*; Hanser publishers, Munich, 2001.

[28] P. G. Maier and D. Goritz, *KGK Kautschuk Gummi Kunststoffe*; 1996, **49**, 18-21.

[29] A. R. Payne, *Journal of Applied Polymer Science*; 1962, **6** (19), 57-63.

[30] M. Akiba and A. S. Hashim, *Prog. Polymer Sci.;*1997, **22**, 475-521.

Chapter 6

Synthesis of SiO_2 and *in situ* Silica-NR composites by the sol-gel non-aqueous method

In this chapter a novel non-aqueous *in situ* sol-gel preparation of silica-composites in different silica concentrations is reported, in order to find the relationship between the amount of silica particles and the formation of a continuous filler network, their morphology and the enhancement of mechanical properties of the composite.

Afterwards, silica-natural rubber composites were compounded and vulcanized in order to study their performance properties in a real application.

In the last part of the chapter the three procedures of non-aqueous sol-gel preparations of silica nanoparticles are reported.

6.1 Materials

Silica was synthesized by sol-gel hydrolysis and condensation of tetraethylorthosilicate (TEOS, 99 %), from Aldrich. Dried natural rubber (NR) was FFB from Cau Casulbor; tetraethylorthosilicate and toluene puriss. p.a (> 99.7 %) were from Fluka, formic acid (98-100%) was from Merck and ethanol absolute anhydrous (99.9%) was from Scharlau.

For the reference samples, precipitated silica Rhodia Zeosil MP1165, (BET specific surface area 160 $m^2\ g^{-1}$) was used.

For the compounding preparation, the materials used were: 6PPD, as the antidegradant N-(1,3-dimethylbutyl)-N'-phenyl-p-phenylenediamine, purchased from Flexsys; stearic acid (Stearina TP8) from Undesa; wax (Cera SER AO 54) from SER; carbon black (N 234) from Degussa (specific surface area 120 m^2g^{-1}, average particle size 20–25 nm); sulphur from Zolfoindustria; zinc oxide from Zincol Ossidi; N-tbutyl-2-benzothiazylsulphenamide, TBBS was Vulkacit NZ/EG-C from Lanxess.

For the synthesis of silica powder: silicon (IV) tetrachloride (99%), anhydrous benzyl alcohol (BzOH) (99+ %) from Sigma Aldrich; n-Hexane (96% HPLC grade) from Scharlau was used to wash the powders.

All chemicals were used without further purification.

6.2 Synthesis of non-aqueous *in situ* sol-gel silica-rubber composites

Silica-natural rubber nanocomposites were prepared by the following *in situ* non-aqueous sol-gel procedure.

Before using, NR sheets of 2 mm thickness were obtained by using an open two-roll mill (roll diameters 470 mm; working distance 20 mm). The temperature of the rolls was set to 50°C by means of a thermostated water recirculation circuit.

In a 500 ml round bottom flask at room temperature and in dark, about 12 g of dried NR sheets were swelled for 1 night in 240 ml of toluene (weight ratio 1:17.4) and a suitable amount of silica precursor (TEOS) (see Figure 1 a).

To improve the swelling of all the rubber, the flask was immersed in an oil bath at 80°C and stirred at reflux at 1000 rpm with magnetic stirring bar for 30 min. Successively a suitable amount of alcohol (ethanol or benzylalcohol) was added to the brown solution.

After 30 min the appropriate amount of formic acid (HCOOH) was added to the solution and reacted for 5 hours at 80°C at vigorous stirring (1000 rpm) (see Figure 1b).

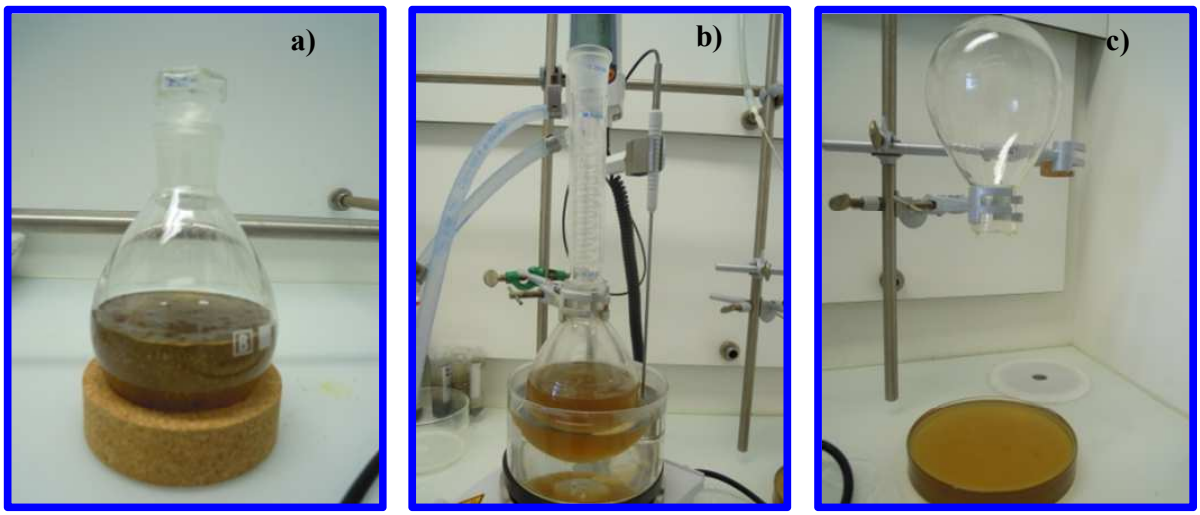

Figure 1: The steps of non-aqueous silica-rubber composite preparation.

The choice of HCOOH, as a carboxylic acid for this synthesis, is related to its highest acidic character (pKa 3.77) showed in comparison with the other carboxylic acids (as an example acetic acid has pKa 4.76).

Regarding the choice of the type of alcohol, it is well known that their reactivity towards esterification reaction decreases with the linearity of the chain linked to the OH group[1]. Moreover, the use of a primary alcohol with an aromatic ring (Benzyl alcohols, BzOH) can act as a capping agent and steric stabilizator for metal oxide particle growth[2, 3, 4].

Obviously, the speed of the esterification reaction will be slow in comparison with alcohols with small ethyl or methyl chains (ethanol or methanol).

As a result, the speed of the esterification reaction *in situ* can be controlled, choosing an alcohol less branched which has a high steric hindrance[1]. The reaction between alcohol and carboxylic acid forms an ester and water, which starts the hydrolysis and condensation of the silica precursor (see Figure 2). The molar ratio TEOS: alcohol: carboxylic acid used for the

synthesis is 1:2:3. The small excess of HCOOH with respect to the alcohol is added in order to improve the thermodynamics of the reaction and to change the equilibrium.

The esterification reaction is reversible and generally reaches an equilibrium when there are appreciable amounts of both reactants. Therefore, if either alcohols or carboxylic acid are economical and readily available, they can be used in large excess to shift the equilibrium toward the products and thus to increase the yield of ester and water.

Esterification reaction

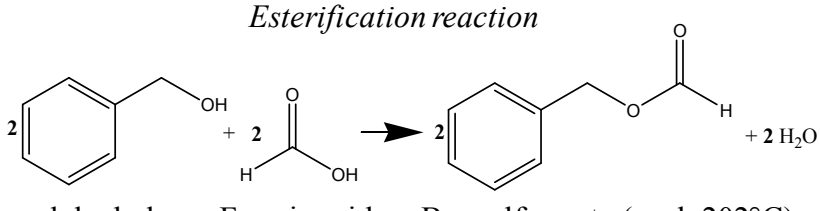

Benzylalcohol Formic acid Benzylformate (p. eb.202°C)

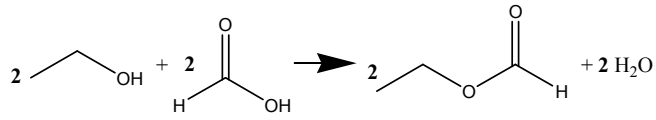

Ethylalcohol Formic acid Ethylformate (p. eb.54°C)

Hydrolysis and condensation of TEOS

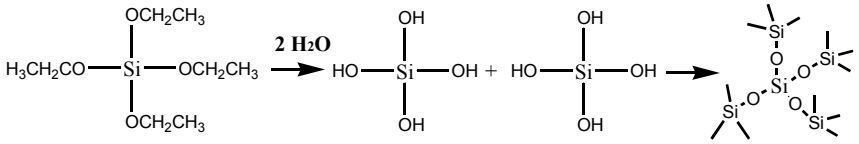

Figure 2: Scheme of the reaction involved in silica rubber composite preparation by the non-aqueous *in situ* sol-gel method.

The suspension obtained was cast into a Petri dish and the volatiles were removed by maintaining the system under an aspiration hood overnight (see Figure 1c).

Sample	NR	SiO_2	SiO_2	SiO_2	TEOS	EtOH	BzOH	HCOOH
	phr		% wt	% vol	moli			
NR-EtOH_15	100	15	13.04	5.90	0.03	0.06		0.09
NR-EtOH_30	100	30	23.08	11.15	0.06	0.12		0.18
NR-EtOH_45	100	45	31.03	15.84	0.09	0.18		0.27
NR-EtOH_60	100	60	37.50	20.06	0.12	0.24		0.36
NR-EtOH_75	100	75	42.86	23.88	0.15	0.30		0.45
NR-BzOH_30	100	30	23.08	11.15	0.06		0.12	0.18
NR-BzOH_45	100	45	31.03	15.84	0.09		0.18	0.27

Table 1: Composition and reactants amount of non-aqueous *in situ* silica-rubber composites.

The complete elimination of the sub products inside the composites was done in an oven at 70°C at 12 mbar of vacuum for 1 hour.

The composites were reprocessed in order to form a sheet of about 1 mm thickness in a two roll mill, in the same condition as before used.

Silica-rubber composites were prepared in five different concentrations of silica by using ethanol and two concentrations of silica by using benzylalcohol.

Hereafter, the uncured rubber silica composites are labelled NR-X-Y, where X is the acronym of the kind of alcohol used (EtOH for ethylalcohol or BzOH for benzylalcohol), and Y is the amount of phr of silica present in the silica-rubber composite.

In Table 1, all the samples prepared by non-aqueous *in situ* sol gel silica rubber composites are reported. In particular it shows the amount of SiO_2 in weight and in volume, and the reactant molar ratio for 12 g of dried natural rubber.

Reference master batches were also prepared by mixing NR, with 15 or 30 or 45 phr of commercial silica Zeosil MP1165 (corresponding to 13.04, 23.08, 31.03 wt % of SiO_2) and 1 phr of finely ground antioxidant 6 PPD in a Haake Reomix station.

The aim was to compare properties of non-aqueous *in situ* synthesized silica rubber composites with those of composites prepared by the conventional *ex-situ* blending process.

Reference master batches with silica concentration higher that 45 phr, were not carried out due to the high amount of poorly dispersed silica that was added to the rubber matrix without using a coupling agent.

Silica and dried natural rubber were mixed at 90°C and 60 rpm for 8 min. Sheets of about 2 mm thickness were obtained by 2 min mixing in an open two-roll mill. These samples were labelled NR-SiO_2-15, NR-SiO_2-30 and NR-SiO_2-45.

6.3 Compounding

In order to study the final properties of the non-aqueous *in situ* silica-rubber composites compounding had to be done. Therefore, vulcanization system ingredients were added to the composites prepared by *in situ* sol-gel method and to master batches.

In situ silica composites up to 45 phr were used to produce compounds. The list of the compounds prepared in three steps by a Thermo Haake Reomix lab station (mixing chamber of 250 ml, fill factor of 0.7) is reported in Table 2. The amount of vulcanization reactants and the recipe in phr are shown for the references samples and for *in situ* composites containing 15, 30 and 45 phr of silica.

	V-NR-SiO_2-15	V-NR-SiO_2-30	V-NR-SiO_2-45	V-NR-EtOH-15	V-NR-EtOH- 30 V-NR-BzOH-30	V-NR-EtOH-45 V-NR-BzOH-45
NR swelled	-	-	-	100	100	100
NR	100	100	100	-	-	-
In situ - SiO_2	-	-	-	**15**	**30**	**45**
SiO_2 Rhodia	15	30	45	-	-	-
TESPT	**1.2**	**2.4**	**3.6**	**1.2**	**2.4**	**3.6**
6 PPD	2	2	2	2	2	2
Stearic Acid	2	2	2	2	2	2
Wax	1	1	1	1	1	1
Carbon Black	20	20	20	20	20	20
Zinc oxide	3.5	3.5	3.5	3.5	3.5	3.5
Sulfur	1.2	1.2	1.2	1.2	1.2	1.2
TBBS	1.8	1.8	1.8	1.8	1.8	1.8

Table 2: Recipe for the vulcanization of non aqueous *in situ* silica-rubber composites (phr, parts per hundred rubber).

The three master batch reference samples (13.04, 23.08, 31.03 % wt silica) were prepared in 3 stages in Thermo Haake Reomix at a temperature of 90°C and at a rotor speed of 70 rpm. In the first step, at 0.75 min ½ of the amount of silica and TESPT were added to NR, followed at 1.25 min by the remaining silica and at 3.00 min by stearic acid, waxes and carbon black; all additions were carried out within 6 min. Successively, after 16 h, compounding was re-worked in Thermo Haake Reomix at 90°C and 60 rpm for 4 min by adding ZnO and 6 PPD. In the third step, sulphur and the accelerator TBBS were added to the composite at 50°C and 15 rpm in 4 min in a two-roll mill. Composites were further molded for 5 min to produce sheets of about 2 mm thickness and then underwent the vulcanization process.

The reference samples were labelled V-NR-SiO_2-15, V-NR-SiO_2-30 and V-NR-SiO_2-45.

Regarding the composites prepared by the non-aqueous *in situ* sol-gel method, the compounds were prepared in three steps, modifying the previous procedure.

In detail, in the first step *in situ* composites, carbon black (90 % of the amount), stearic acid and waxes were mixed at 90°C and 70 rpm for 6 min. The first 3 min were used to heat up the *in situ* composite, and masticate and break down the rubber.

After 16 h, carbon black (10 % of the amount), ZnO and 6 PPD were added to the compound at 90°C and 60 rpm for 4 min.

In the third step, sulphur and the accelerator TBBS were added to the composite at 50 ± 3 °C and 15 rpm in 4 min in two-roll mill.

The addition of the vulcanization ingredient was performed at 1.5 mm roll distance. During the first min, the compounds were worked in order to reach the optimal temperature. Following, during the second min the accelerator powder (previously grounded) was dropped into the mill tray. Hence, during the third min the sulphur was added.

During the fourth minute, powders which had not been incorporated in the composite were collected and added back to the mix.

In addition, in order to promote uniform dispersion of the ingredients, cutting and folding were continuously carried out.

The rubber composite was collected preparing a roll and was later worked by using 0.8 mm of rotor distance. During this step the rubber was continuously formed in sheet and rolled three times. After obtaining a roll of composite, it was worked again by using 0.3 mm roll distance in order to obtain a sheet.

Vulcanization of sheets was performed by using an electrically heated hydraulic press (BM Biraghi), under the following conditions: temperature 150°C, pressure 4.3 bar, running time 30 min. Hereafter, the vulcanized silica-rubber composites are labeled V-NR-X-Y, where X is the acronym of the alcohols used for esterification reaction and Y is the amount in phr of the silica present in the composite.

6.4 Synthesis of non-aqueous silica sol-gel powder

The aim for the preparation of silica powders by the same non aqueous sol-gel methods used for the composites was to more easily evaluate the effective shape, size and specific surface area (SSA) and the amount of OH group on the surface of silica nanoparticles.

Three different methods were tested in order to find the more suitable non aqueous route to produce the composites and two of them were used for this purpose, as described in 6.2.

Silica prepared from Ethanol

SiO_2-EtOH powder was prepared following the procedure previously reported for uncured non-aqueous *in situ* composites in the absence of swollen rubber.

In a 500 ml round bottom flask at room temperature 240 ml of toluene were added to 11.78 ml of silica precursor (TEOS, 99%) and the flask was immersed in an oil bath at 80°C and

stirred at reflux at 1000 rpm for 30 min. Successively, 7.07 ml of ethylalcohol was added to the previous solution.

After 30 min, 6.85 ml of formic acid was added to the clear solution.

After 5 hours at 80°C at vigorous stirring (1000 rpm), the milky mixture was cast into Petri dish (20 cm of diameter) and volatiles were partially removed by maintaining the system under an aspiration hood overnight. The powders were separated from the solvent after centrifugation for 10 min at 4000 rpm and washed three times with 20 ml of fresh ethanol. Therefore, particles were separated from the solvent and dried in air for one night at 120°C, in other to completely remove any excess of ethylformate (p. eb 54°C) and water.

Silica prepared from benzylalcohol

SiO_2-BzOH powder was prepared following the procedure previously reported for uncured non-aqueous *in situ* composites in the absence of swollen rubber.

In a 500 ml round bottom flask at room temperature 240 ml of toluene were added to 11.78 ml of silica precursor (TEOS, 99%) and the flask was immersed in an oil bath at 80°C and stirred at reflux at 1000 rpm for 30 min. Successively 12.57 ml of benzylalcohol was added to the previous solution. After 30 min, 6.85 ml of formic acid was added to the clear solution.

After 5 hours at 80°C at vigorous stirring (1000 rpm), the milky mixture was cast a into Petri dish (20 cm of diameter) and volatiles were partially removal of the by maintaining the system under an aspiration hood overnight. The powders were separated from the solvent after centrifugation for 10 min at 4000 rpm and washed three times with 20 ml of fresh ethanol. Therefore particles were separated from the solvent and dried in air for one night at 220°C in order to completely remove any excess of benzylformate (p. b. 202°C) and water and benzylalcohol (p. eb. 205°C).

Silica prepared from silicon tetrachloride and benzylalcohol

SiO_2-$SiCl_4$ powder was an explorative approach synthesis used in order to prepare silica by non aqueous route. In addition, the SiO_2-$SiCl_4$ morphology obtained can be used in order to compare with those obtained by the previous non-aqueous method, which involves the esterification *in situ*.

In a typical preparation procedure 0.80 ml silicon (IV) tetrachloride was added to 14.21 ml of anhydrous benzylalcohol (SiO_2/BzOH molar ratio corresponding to 1:20) in a Schlenck tube equipped with a magnetic stirring bar and connected to a nitrogen line at room temperature.

After addition of the silica precursor, the clear solution was stirred for 1 hour in order to remove the hydrocloridric acid produced.

The reaction mixture was transferred into a Teflon cup of 45 ml inner volume performed by Parr, slid into a steel autoclave, and carefully sealed.

The autoclave was heated in a furnace at 150°C for 24 hours. The monolith obtained was washed three times with 20 ml of Hexane and the particles were separated by centrifugation at 4000 rpm for 10 min in order to remove BzOH. The wet powder obtained was air dried for one night at 80°C, and for 5 hours at 150°C.

Silica synthesized with this route shows spherical silica particles with diameters in the range between 5-10 nm (see Figure 3), with lower tendency to aggregate in comparison with silica from aqueous sol-gel method (see paragraph 5.1) due to a lower amount of OH surface groups, as demonstrated by the TEM analysis.

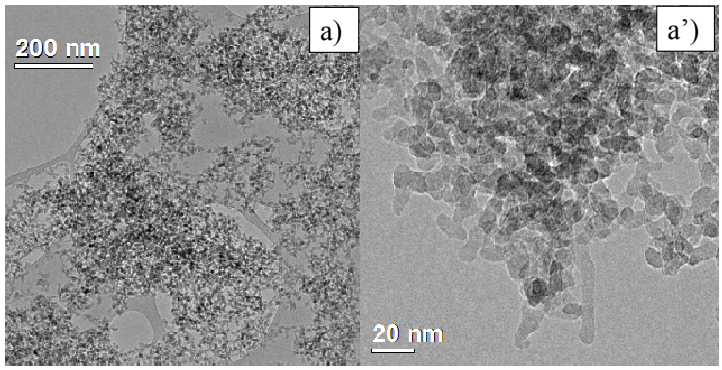

Figure 3: TEM images of SiO_2-$SiCl_4$.

TGA analysis in nitrogen (about 5-6 % in weight due to OH) (see Figure 4).

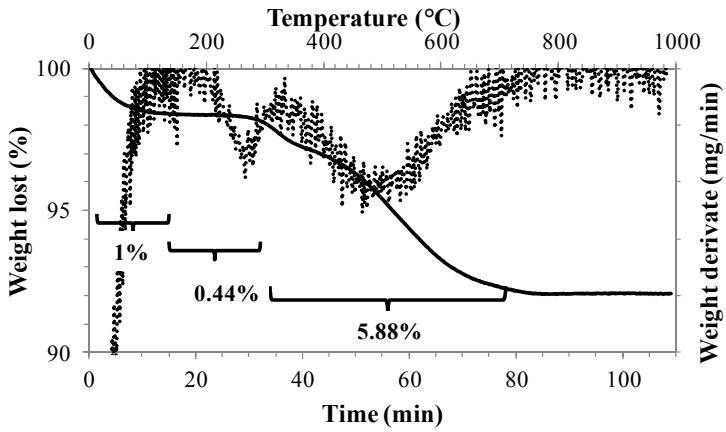

Figure 4: TGA profile and derivative curves of SiO_2-$SiCl_4$.

This method allows to prepare a large amount of nanosized silica which is suitable to prepare natural rubber composite by mechanical blending. The compounds with this silica will be prepared in the future.

Unfortunately, modify this synthetic procedure, in order to introduce the rubber and grow the silica within as a non-aqueous preparation method, isn't possible because during the synthesis hydrochloric acid forms as by product which can lead to possible rubber degradation.

---

[1] J. Otera and J. Nishikido, Esterification: Methods, Reactions, and Applications,2nd ed., Wiley-Interscience: New York, 2010.

[2] N. Pinna and M. Niederberger, *Angew. Chem. Int. Ed.;* 2008, **47**, 5292-5304.

[3] M. Niederberger and G. Garnweitner, *Chem. Eur. J.*; 2006, **12**, 7282-7302.

[4] M. Niederberger and N. Pinna; *Metal Oxide Nanoparticles in Organic Solvents: Synthesis, Formation, Assembly and Applications*; Springer 2009.

Chapter 7

Non-aqueous *in situ* sol-gel silica-natural rubber nanocomposites

This chapter discusses non-aqueous *in situ* sol-gel silica-rubber nanocomposites obtained by *in situ* esterification reaction followed by hydrolysis and condensation of the silica precursor.

A detailed morphological characterization of silica-rubber nanocomposites by TEM was performed in order to investigate the efficacy of the filler networking in reinforcing the rubber matrix.

Thereafter, dynamic mechanical properties of uncured silica-rubber composites were investigated and discussed, in order to find a possible relationship between the morphology obtained, the degree of filler network dispersion and the dynamic-mechanical behavior.

7.1. Conversion of silica precursors and properties of silica powders

The conversion of TEOS to silica in uncured non-aqueous *in situ* sol-gel silica-natural rubber nanocomposite was determined by TGA in air. Following, TGA profiles of the NR-EtOH and NR-BzOH nanocomposites for different silica concentrations are reported (see Figure 1).

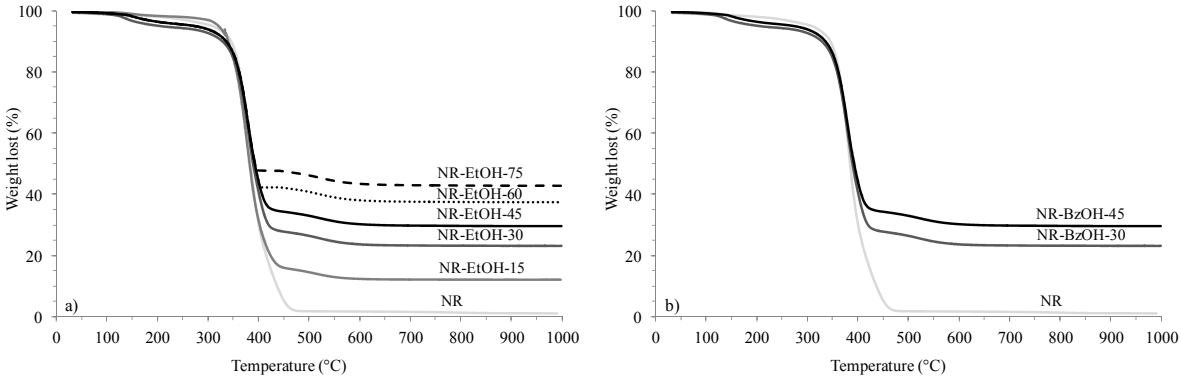

Figure 1: Tga profiles on non aqueous *in situ* sol gel silica-natural rubber composites prepared by *in situ* esterification by using a) ethanol and b) benzylalcohol.

TGA thermograms show that after rubber combustion at T > 580°C, the sample weight remains constant. The residual sample at 900°C was assumed to be the amount of *in situ* generated silica. According to the equations reported in the paragraph 3.2.2. the conversion of TEOS precursor to silica particles always resulted > 99 %, and the filler content is similar to the nominal value demonstrating that no silica precursor loss occurred during sol-gel synthesis.

In order to characterize better the morphology of silica particles produced *in situ* from the esterification of two different alcohols (ethanol or benzylalcohol), silica particles

synthesized with the same procedure of composite preparation without using the rubber, were characterized by BET and TEM. Nitrogen physisorption analyses were performed on pure SiO_2-EtOH and SiO_2-BzOH silica powders. Their adsorption-desorption isotherms and pore size distributions are reported in Figure 2.

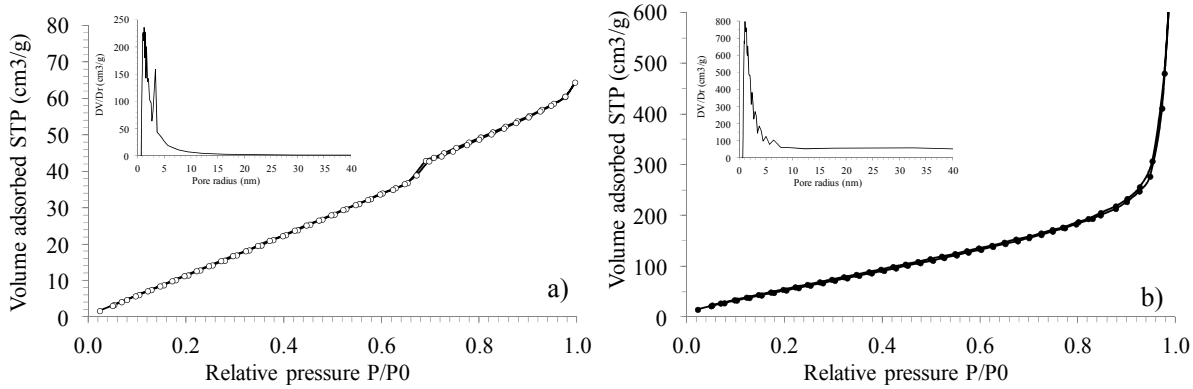

Figure 2: Nitrogen adsorption-desorption isotherms and insert pore size distribution for a) SiO_2-EtOH and b) SiO_2-BzOH.

Specific surface area (SSA), external surface area (S_{ext}) desorption cumulative pore volume (DCPV) and average pore size distribution are reported in Table 1.

Sample	SSA m^2/g	S_{ext} m^2/g	DCVP cm^3/g	Average pore diameter nm
SiO_2-EtOH	87.86	87.86	0.0998	4.54
SiO_2 -BzOH	281.30	281.30	1.0818	15.37

Table 1: Properties of non-aqueous silica produced by esterification *in situ* by a) ethanol and b) benzylalcohol.

SiO_2-EtOH silica powder is a typical finely divided non-porous solid as shown by II Brunauer shape type isotherm and monomodal pore size distribution in the range of 5 nm. SiO_2-BzOH silica powder has typical cylindrical meso-scale pores as shown by IV Brunauer[1] shape type isotherm and monomodal pore size distribution in the range of 15 nm. In both silica there are no micropores due to the absence of differences between SSA and S_{ext}.

These characteristics suggest that the kind of alcohol, which reacts with formic acid during the esterification reaction[2], influences the silica particles growth. In addition, the nitrogen physisorption analysis shows that the smallest silica particles are obtained by using

benzylalcohool. In fact, SiO_2-BzOH grew slowly in comparison to SiO_2-EtOH, which after 3 h of reaction was completely formed. The characteristics of SiO_2-BzOH is due to BzOH which acts as a capping agent which sterically stabilizes the formation of the silica particles[3]. Regarding the morphology of both silica powders, TEM images showed, homogeneous spherical shape particles, with diameter ≈ 20 nm for SiO_2-BzOH and ≈ 50 nm SiO_2-EtOH.

7.2. Morphology of silica-rubber composites

The different morphologies of SiO_2-EtOH and SiO_2-BzOH are found even within the composites. FE-SEM and TEM allowed to evaluate the size and the shape of the silica particles, their aggregation and agglomeration within the rubber matrix.

In particular, FE-SEM micrographs allowed to see the distribution of the silica aggregate in NR. The micrographs did not show appreciable differences between nanocomposites containing the same amount of silica. Moreover, only a few differences were observed between NR-EtOH and NR-BzOH at 15, 30 and 45 phr, as shown for NR-EtOH as example in Figure 3.

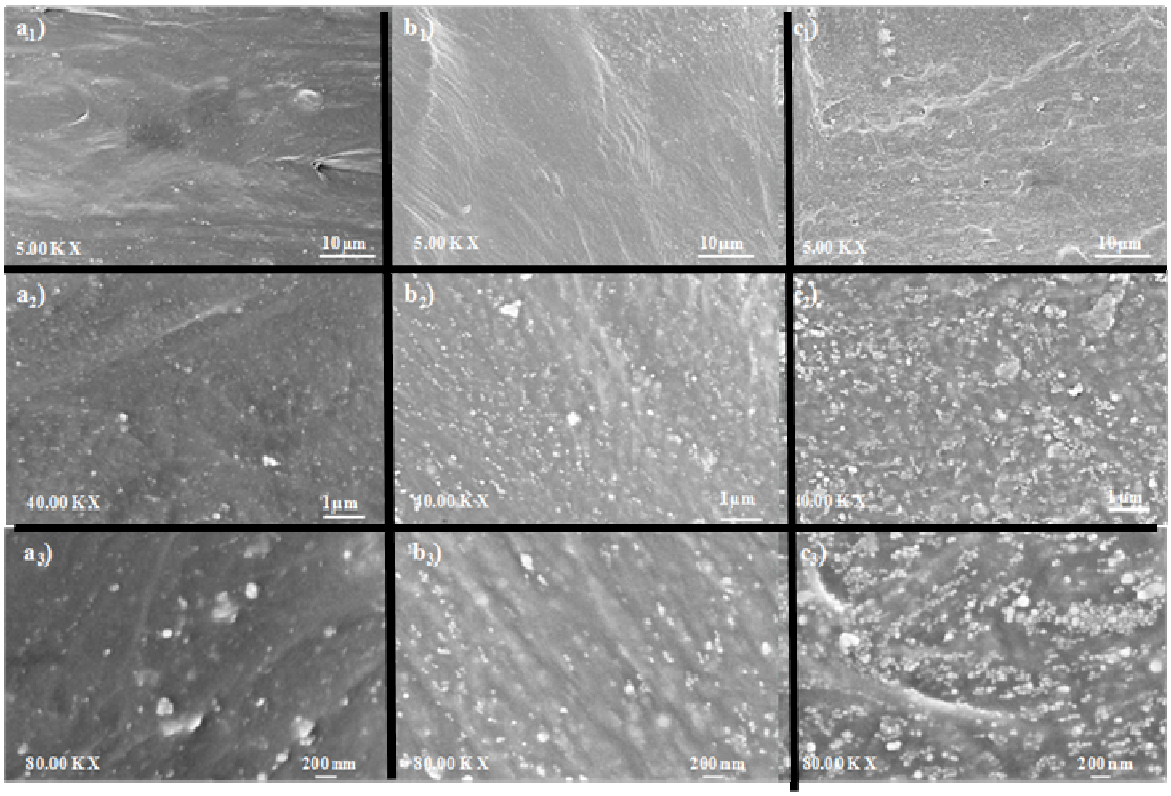

Figure 3: FE-SEM micrographs of uncured non-aqueous *in situ* composites prepared by EtOH esterification: a) NR-EtOH-15, b) NR-EtOH-30 and c) NR-EtOH-45.

Moreover the micrographs of all nanocomposites showed the absence of voids at the silica-rubber interface, indicating good dispersion of silica and good adhesion between the silica and the natural rubber. At high resolution, it is evident that the dimension and the number of the silica aggregates increase with the amount of filler. For all the samples the dimension of the silica aggregate is ≈ 80-100 nm.

Figure 4 reports the TEM images of uncured non aqueous *in situ* sol-gel nanocomposites, which contain 45 phr of silica prepared by using benzylalcohol and ethanol in order to compare the silica morphology obtained with two different alcohols.

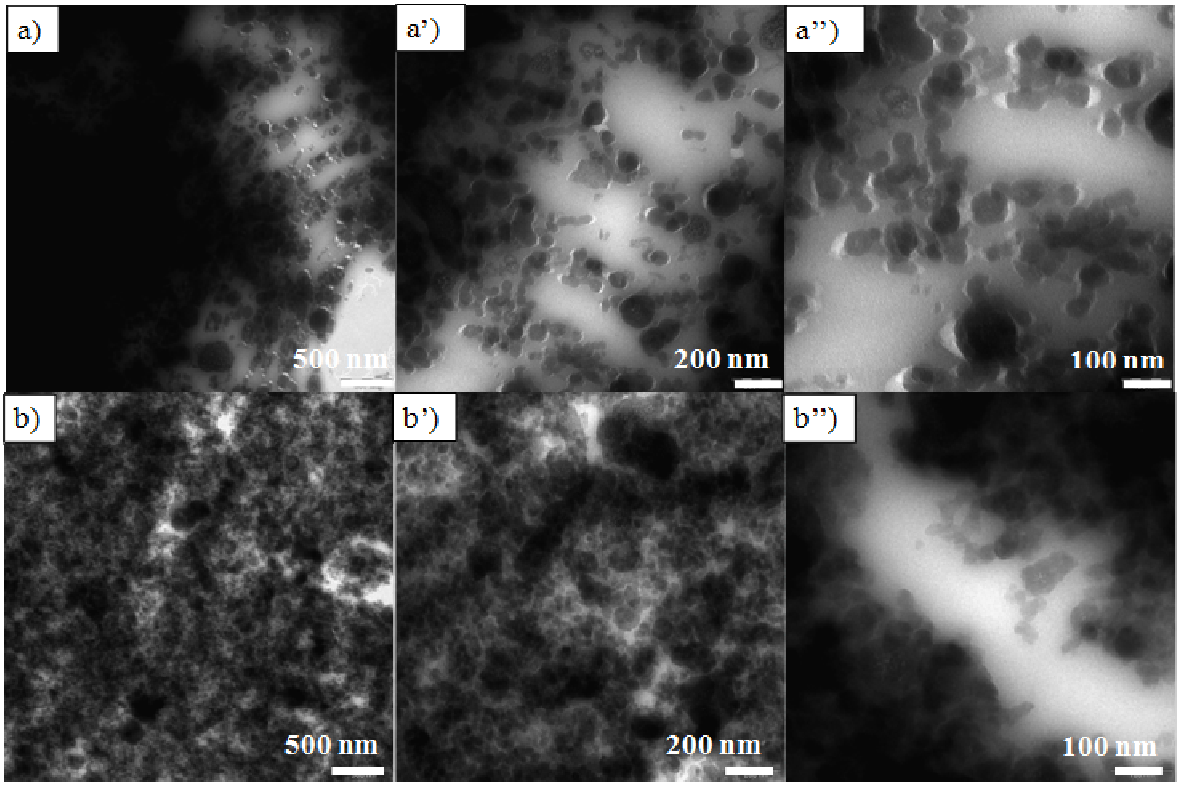

Figure 4: TEM images of uncured a) NR-EtOH-45 and b) NR- BzOH-45; the superscript ' stands for the high magnification.

TEM images of uncured composites with lower silica concentration (not reported in figure) are similar to those of 45 phr sample.

Micrographs of the non aqueous *in situ* sol-gel composites under investigation again show that the silica morphology is strongly dependent on the composite preparation method. As reported for the silica powders, the particles in NR-BzOH-45 composite are smaller than in NR-EtOH-45, and both have a spherical silica shape.

Moreover, NR-EtOH-45 shows well assembled and distributed aggregates in the range 150-200 nm of spherical particles with different sizes in the diameter range of 20-50 nm.

In addition, the filler network is not homogeneously formed, with the presence of non interacting silica particles surrounded by rubber.

NR-BzOH-45 shows higher assembled and distributed aggregates than NR-EtOH-45, with spherical particles in the range of 10-15 nm. Also in this case the particles are not directly interacting as they are surrounded by a rubber layer.

Regarding the two composites containing a high amount of silica filler (NR-EtOH-60 and NR-EtOH-75), the TEM images are not showed, report the same silica shape and dimension previously shown from NR-EtOH-45.

The TEM image of NR-EtOH-60 and NR-EtOH-75 reports an increasing of aggregates dimension respect to NR-EtOH-45 sample (see Figure 5). In addition NR-EtOH-60 sample shows aggregates that are well distributed that are forming the network, while the NR-EtOH-75 shows a well distributed network.

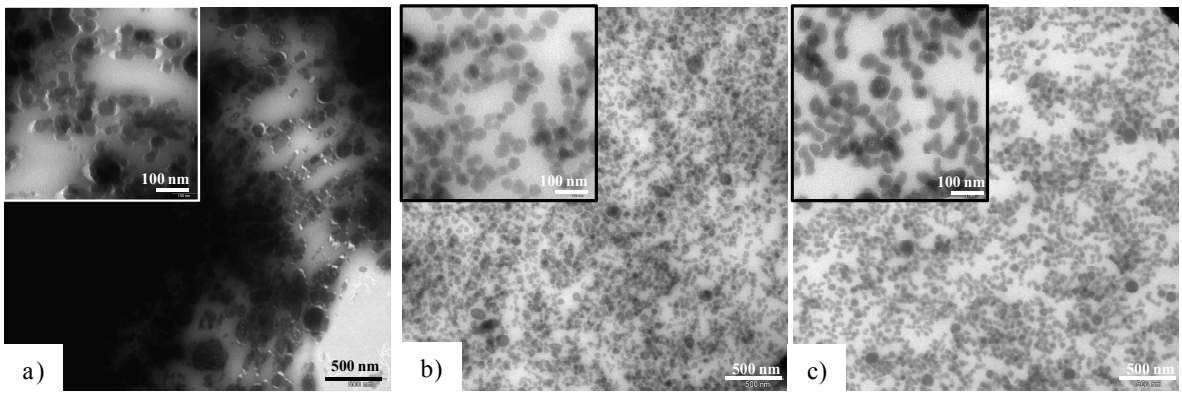

Figure 5: TEM images of a) NR-EtOH-45, b) NR-EtOH-60 and c) NR-EtOH-75.

Therefore, the high dispersion of the silica particles in the rubber matrix is related to the *in situ* non-aqueous synthesis method which produce particle with lower amount of surface hydroxyl groups and lower tendency to aggregate.

7.3. Dynamic mechanical analysis of uncured composites

The dynamic mechanical analyses of uncured composites were carried out by RPA (Rubber Process Analyzer). The strain sweep tests were carried out at T = 70 °C and 1 Hz from 2 % to 100% of elongation.

Low frequency was chosen to maximize the differences between the various composites.

After the strain sweep, in order to study the effect of the thermal treatment on the dynamic-mechanical properties of samples containing different amount of silica, the uncured samples

were heated at 170°C for 10 min, then cooled down to 70°C before performing a new strain sweep test.

The dynamic stress strain behavior of silica-rubber nanocomposites was expressed by the elastic or storage modulus G', and by the viscous or loss modulus G''(see paragraph 5.5).

The trends G' for NR-BzOH and NR-EtOH composites, reference sample and pure NR are shown in Figure 6.

In addition, the trend of the samples after thermal treatment is also reported.

All the samples prepared by *in situ* non aqueous sol-gel procedure show G' values lower that the reference sample at the same silica content, before and after thermal treatment, due to the high dispersion of the silica particles in rubber matrix.

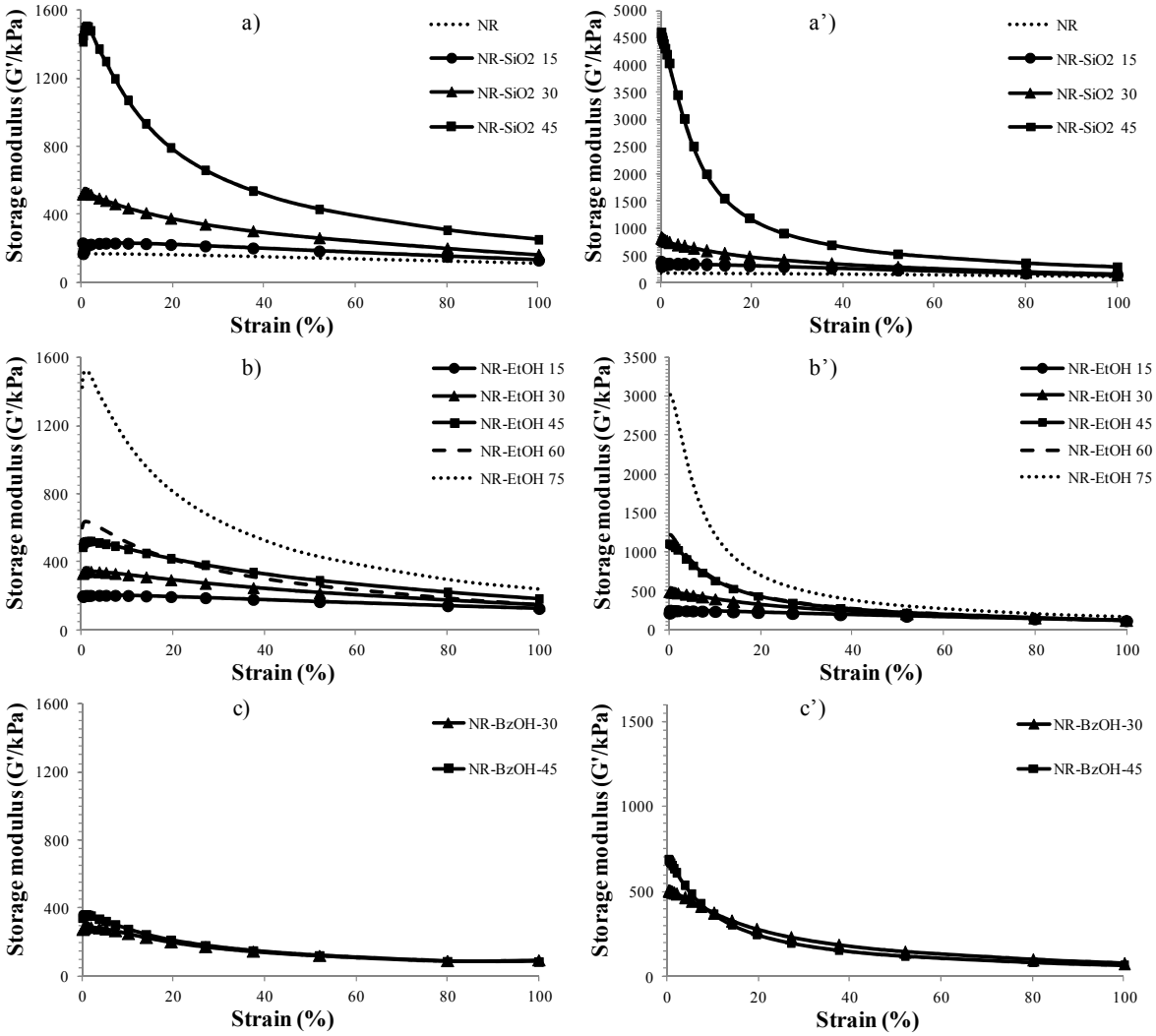

Figure 6: Storage modulus G' vs strain of the uncured reference samples (a) and non-aqueous silica rubber composites prepare prepared by *in situ* esterification by using (b) ethanol and (c) benzylalcohol for the different silica concentrations.

Up to 45 phr of silica, the trend of G'_0 is NR-SiO_2 >> NR-EtOH > NR-BzOH due to the formation of an efficacious filler network of silica which is absent in NR-EtOH and NR-BzOH, where particles are highly dispersed and less aggregated.

It is obvious that the composites showed the same G'_0 trend also for $\Delta G'=G'_0-G'_\infty$ (G'_0 is the G′ value at low strain amplitude (2%) and G'_∞ that at large strain amplitude (100%)).

The dynamic-mechanical behavior of the silica-rubber composites is relatable to the different morphologies of the nanocomposites, which depend on the amount of silica as evidenced by TEM.

In fact, NR-EtOH-30, NR-EtOH-45, NR-BzOH-30 and NR-BzOH-45 showed low storage modulus at low strain amplitude, due to high particle dispersion and the absence of a well homogeneous filler network.

Whereas NR-EtOH-60 and NR-EtOH-75, showed a high G' values due to the higher filler content which creates a well distributed filler network in rubber matrix as shown by the histograms of the G'_0, G'_∞ and $\Delta G'$ magnitudes in Figure 7.

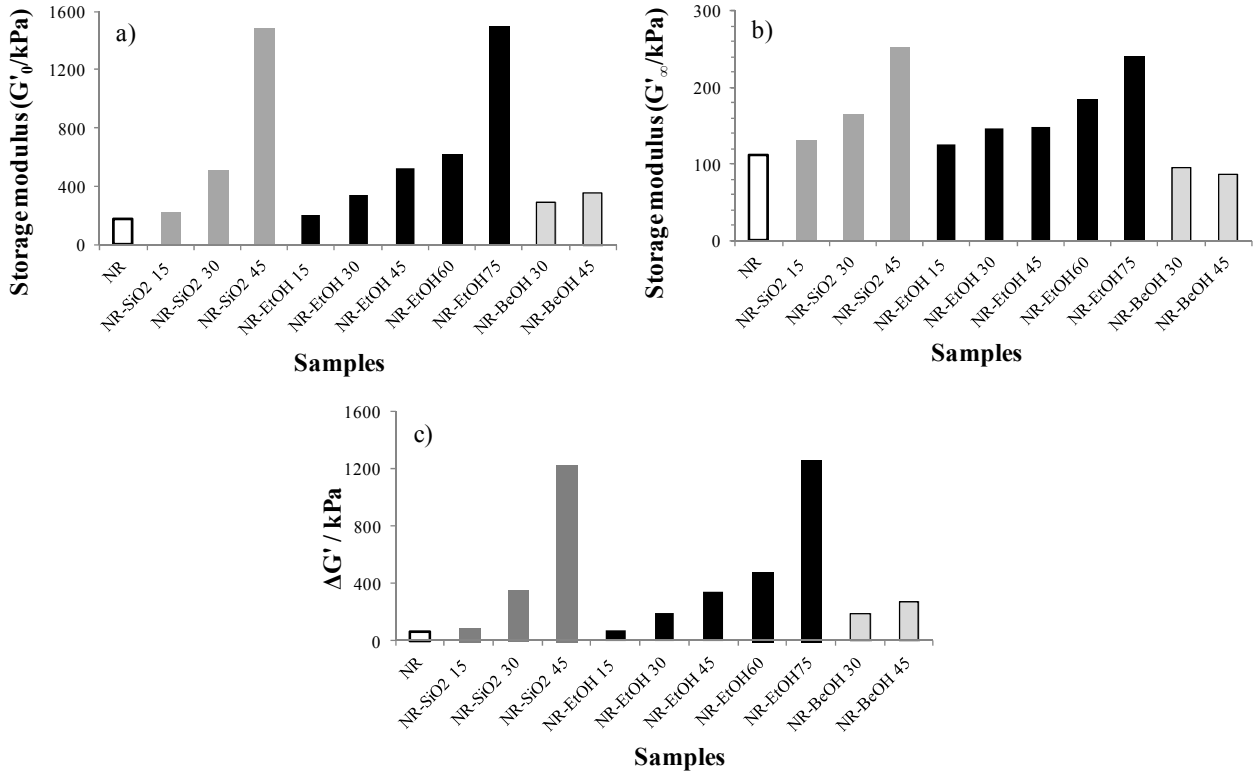

Figure 7: Comparison of the storage modulus G'_0 at low strain amplitude (a), G'_∞ at high strain amplitude (filler-rubber interaction) (b) and $\Delta G'= G'_0 - G'_\infty$ (filler-filler interaction) (c) for blending and non aqueous *in situ* sol gel composites.

Also in the samples prepared by mechanical mixing, increasing the silica amount increases the shear modulus, the interaction between filler particles and the interaction with the rubber.

Summing up the results obtained from the dynamical mechanical analysis, it is evident that the mechanical properties depend on the nanocomposite preparation.

The preparation of the non-aqueous *in situ* sol-gel method is devoted to obtaining the nanocomposite with the best dispersion of the filler in elastomer matrix.

Therefore, the resulting dispersion and networking of silica particles strongly depend on the filler/matrix compability due to the surface chemistry of the filler, on the filler morphology and on the filler amount.

In fact, in spite of the different particle dimensions, silica produced from the two different esterification routes are equally highly dispersed in the rubber matrix, due to the lower hydrophilicity of the surface. Consequently, a large amount of filler is required to form an efficient silica network able to reinforce the composite.

High dispersion degree involves a large variation of the reinforcing effect of the elastomer matrix, which appears to be dependent on the nanocomposite preparation method.

Plotting the values of the shear modulus vs the volume of the filler contained in the rubber matrix allows to evaluate the optimal concentration of the filler which is able to modify the mechanical properties (see Figure 8).

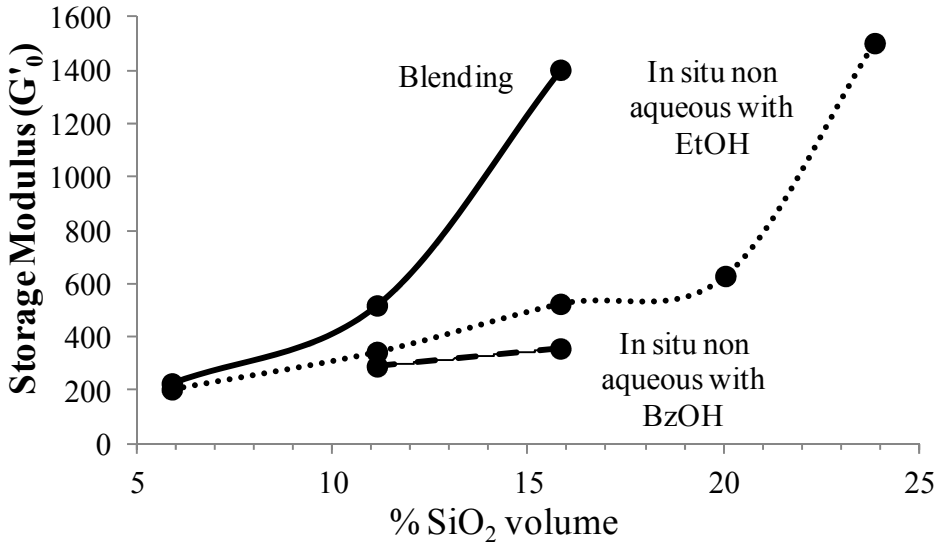

Figure 8: Plot of volume % of silica vs storage modulus for blending and non aqueous *in situ* sol gel composites.

At silica volume lower than 20.06% (60 phr) the filler shows a random dispersion in the rubber without a large amount of aggregation and networking. In addition for these samples, the mechanical properties only slightly increase with the increasing of the amount of filler.

At silica volume of 23.88% (75 phr), the formation of filler network occurs and the mechanical properties of the composite strongly increases, as shown by the high value of G'.

The amount of silica required to obtain the strong increase of G' is very high if compared with silica-rubber composites produce by mechanical mixing of commercial silica (see Figure 8) or by *in situ* aqueous sol-gel method (see paragraph 5.5).

This is a peculiar behavior of the silica particles prepared by non aqueous *in situ* method and confirms that in order to obtain an efficient and strong reinforcement of the rubber, a homogeneous distribution of the particles in the matrix is required but the full separation of the particles should be avoided as the network formation is fundamental.

On the other side the non aqueous synthesis allows to load a large amount of silica in the rubber, which could not be loaded with the traditional blending method without using a compatibilizer or disperdent agent.

Dynamic mechanical analysis also provides the trend of G'' vs strain (as seen also for composites prepared by aqueous *in situ* sol gel preparation see paragraph 5.5).

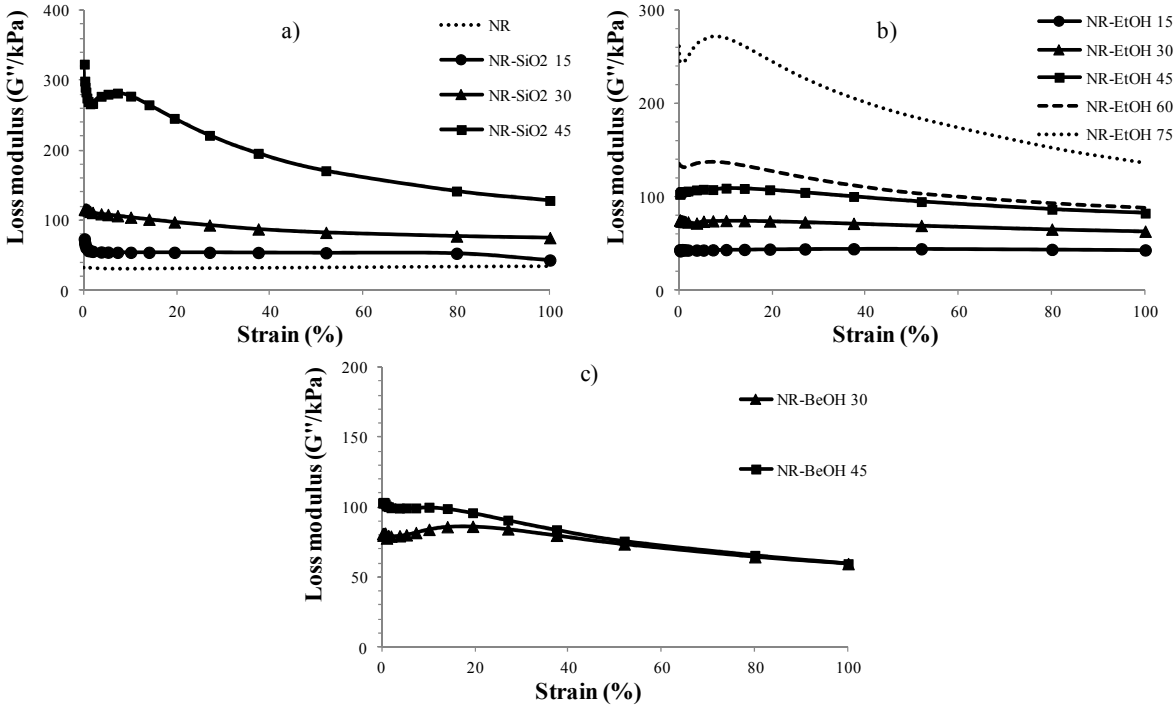

Figure 9: Loss modulus G'' vs strain of the uncured blending (a) and non aqueous *in situ* sol gel composites prepared by esterification by using (b) ethanol and (c) benzylalcohol.

The plots of G'' for NR-BzOH composites, NR-EtOH composites, reference samples and pure NR are reported in Figure 9 and confirm the trend of G', as described before in Figure 7.

Vulcanization curves for non aqueous *in situ* sol-gel composites prepared by esterification and compared with mechanical blending samples are shown in Figure 10.

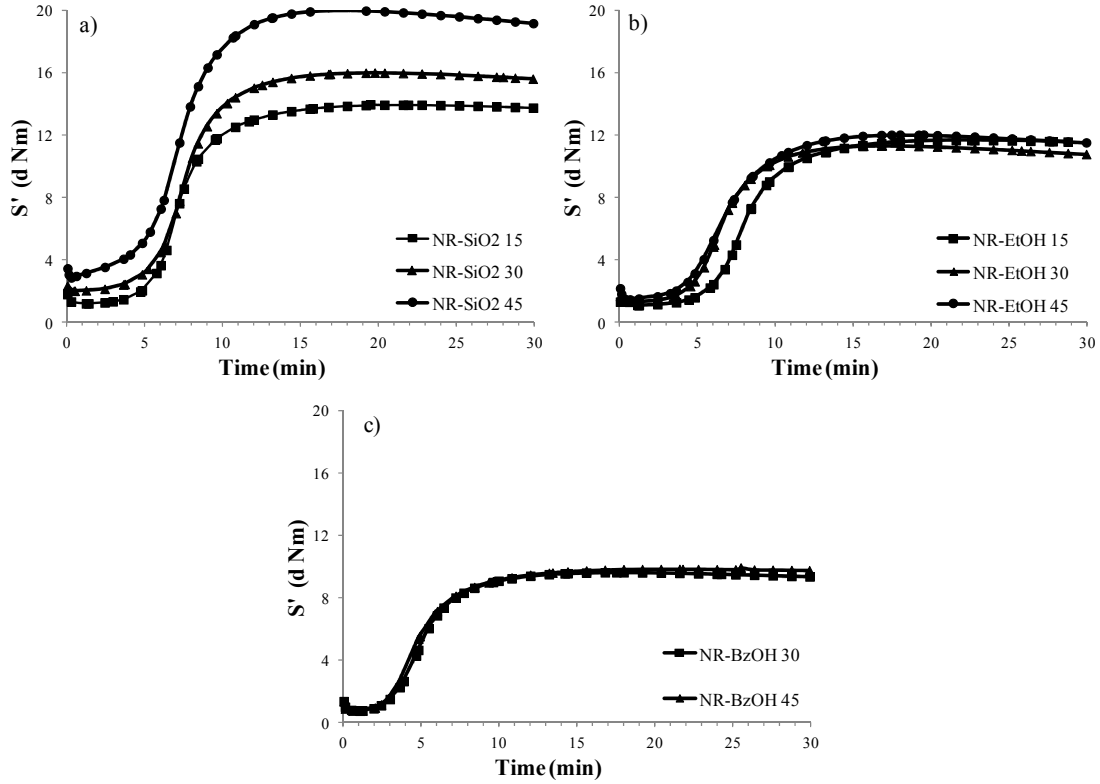

Figure 10: Cure kinetics of the uncured blending (a) and non aqueous *in situ* sol gel composites prepared by esterification by using (b) ethanol and (c) benzylalcohol.

Mechanical blending of silica Rhodia and NR shows an increasing of the maximum torque with the increasing of the amount of silica network.

Regarding the composites prepared by non-aqueous *in situ* method, it is evident that the amount of silica randomly dispersed does not influence the vulcanization process.

Slightly difference in maximum torque is evident between NR-EtOH and NR-BzOH composites due to different silica particles dimension.

Moreover, from curing kinetic is visible that for the non-aqueous *in situ* composites containing silica at concentration less that 45 phr, no network is formed and no significant change in strength of the composites is evident.

Probably at concentration higher of 60 phr of silica filler in non aqueous composites, it is possible to appreciate the filler networking with the improvement of the mechanical proprieties.

---

[1] S. Lowell, E. J. A. Shields, M. Thomas and M. Thommes, *Characterization of Porous Solid and Powders: Surface Area, Pore Size and Density*, 1st ed; Kluwer Academic Publishers, Springer, 2004, p.10-55.

[2] J. Otera and J. Nishikido, Esterification: Methods, Reactions, and Applications,2nd ed., Wiley-Interscience: New York, 2010.

[3] M. Niederberger and N. Pinna; *Metal Oxide Nanoparticles in Organic Solvents: Synthesis, Formation, Assembly and Applications*; Springer 2009.

Chapter 8

Conclusion

Silica-natural rubber composites for tire applications with a controlled composition and morphology was obtained by *in situ* sol-gel method and compared with conventional mechanical blending prepared by using silica Rhodia and dried NR.

Regarding the *in situ* sol-gel method of nanocomposite preparation, two different synthetic approaches were carried out by starting from the same silica precursor: aqueous and non aqueous methods.

Deep investigation on the relationship between composition, size and morphology of the silica particles, dispersion network degree and dynamic mechanical behavior of uncured composites allowed to rationalize the final performance of the cured composites.

In fact, the efficacy of silica filler to improve the mechanical properties of the tires for the automotive industry is related both to the interaction among the silica particles and aggregates (filler-filler interaction) and to their capability to interact with the rubber matrix (filler-rubber interaction). Therefore, the characteristics of the silica such as shape, size, surface area, nature of the surface (OH group, functional molecules and amount), degree of aggregation lead to modify the nature of the interface with the rubber and also the homogenous distribution of the filler network.

The obtained results for aqueous *in situ* sol-gel silica-natural rubber preparation led to the following conclusions:

- The aqueous sol-gel method is a promising procedure to prepare nanocomposites from silica precursor TEOS mixed to trialkoxisilanes having different functional groups when the filler precursor doesn't react quickly through hydrolysis and condensation reactions in water environment and allow to control the filler-filler and filler-rubber interactions.

- The functional groups from different substituted silicon alkoxide precursors promote during the sol-gel process the formation of different silica particle shapes and modify the filler-filler and filler-rubber interaction. In particular, the precursor functionalities induced the formation of anisotropic shaped silica particles, unlike the spherical ones derived from TEOS.

- Different precursors give rise to particle networks with different degrees of continuity, depending on physical and chemical properties of particles they originate. Spherical or slightly anisotropic particles with homogeneous size show the best self assembling behavior and form continuous networks. When particles contain surface groups able to interact with

each other (e.g. hydroxyl, amino and thiol groups), the formation of chemical bonds makes the filler-filler interaction stronger along the network.

- The network continuity within the composite is the main prerequisite to obtain strong rubber reinforcement. Not homogeneous distribution of the filler and irregular segregation of particles induce large voids in the network, lowering the dynamic-mechanical properties. However, it appears that a strong chemical interaction among particles can balance the absence of a fully continuous network, preserving high storage modulus. This is the case of the network in NR-TMSPM, where the thiol functionality assists the bonding interaction. On the contrary, the large voids observed in the network of NR-OCTEOS are not compensated by bonding interactions among particles, which are absent or very weak due to the presence of the surface alkyl groups.

- The different filler-rubber interaction due to substituents able to chemically interact with the polymer, promotes the homogeneous distribution of the filler particles even if its contribution to the reinforcement properties is less effective than that to the filler-filler interaction. Thus filler-filler interaction governs the dynamic-mechanical properties of silica rubber composites either through the shape induced physical interactions responsible for the network formation, or by the chemical interaction among particle surface groups.

- To sum up when a choice among different functionalized silica is required, the suggestion is to look for well assembled and continuous filler networks, eventually assisted by chemical interaction among particles. The second condition seems very important, in fact in the case of NXT network, the homogeneous particle distribution is not sufficient to guarantee strength; instead the dynamic-mechanic behavior of NR-NXT is enhanced after thermal treatment which allows the sulphur-rubber interaction.

- Regarding the properties of the vulcanized composites, it is evident that the preparation of the silica *in situ* improve the rigidity, the hardness, the tensile strength and reduce the dissipation of the energy, which means an improvement in rolling resistance.

The obtained results for non-aqueous *in situ* sol-gel silica-natural rubber preparation led the following conclusions:

-The non-aqueous *in situ* sol-gel synthesis is a procedure to prepare nanocomposites allowing the *in situ* growth of small particles in rubber matrix in the absence of large

amount of water. In addition, due to the slow hydrolysis and condensation reaction rate of the precursors it possible to control at molecular level the growth of the metal oxide particles and therefore the filler-filler interaction and the dispersion in rubber matrix.

- Non-aqueous *in situ* sol-gel silica-natural rubber nanocomposites were prepared by *in situ* esterification reaction between formic acid and ethylalcohol or benzylalcohol which produce controlled amount of water for the hydrolysis and condensation reaction.
Therefore inside the dried NR it is possible to growth high amount of silica particles well distributed in a network were the particles are less aggregated and show lower filler-filler interaction in comparison with the composite prepared by conventional blending route.

- Silica-natural rubber composites were obtained containing large amount of well dispersed silica (75 phr or 43% wt) without using coupling agents.

-The nature of the alcohol involved in the esterification reaction influences the shape and the size of the silica prepared in swollen natural rubber. Silica particles produced in ethanol environment are bigger than those produced in presence of benzylalcohol, and create an effective reinforcement of the rubber when their amount is higher than 60 phr (37% wt).
In spite of the different particle dimensions, silica produced from the two different routes are equally highly dispersed in the rubber matrix, due to the lower hydrophilicity of the surface, and a large amount of filler is required to form an efficient silica network able to reinforce the composite.

-This behavior, peculiar of silica particles prepared by non aqueous in situ method, confirm that even if a homogeneous distribution of the particles in the matrix is required to obtain an efficient and strong reinforcement of the rubber, highly separated particles with low filler-filler interaction hinder an efficient filler network.
On the other side the non aqueous synthesis allows to load a large amount of silica in the rubber, which could not be loaded with the traditional blending method without using a compatibilizer or disperdent agent.

Acknowledgements

This work was supported by the Pirelli Tyre funds and by the Fondazione Cariplo at the University of Milano Bicocca.

First of all, I would like to thank Prof. ***Ignazio Renato Bellobono***, who introduced me to this group almost four years ago, encouraging me to continue my studies even when I thought had had enough.

I express my sincere and deep sense of gratitude to my supervisors Prof. *Franca Morazzoni* and Prof. *Roberto Scotti* for convincing me to do the PhD at the University of Milano Bicocca, changing my mind about how to do research, laboratory experiments and how to interact with the scientists. I have received many benefits from their experience and knowledge. Moreover, they believed in me and positively encouraged my work in a new field where none of us had specific knowledge on this particular industrial topic. In addition, the success of this work is also thanks to wonderful teamwork and the organization of the group, as well as a wonderful relationship with the Pirelli people who have a thorough understanding of this area together with scientific and academic worlds.

In particular, ***Prof. Morazzoni*** was always available by email, phone and individual meetings. Her keen scientific mind has truly influenced me. She has always been ready to show me the next objective to reach and the right direction to take when the wrong road was unfortunately ready to be taken. She was also one of the few professors with whom I didn't speak only about chemistry, but also about shopping, classical music and the piano, trips, sports and dieting. She is inspiration and representation of women in science, guiding other women to do like she did.

Regarding ***Prof. Scotti*****,** I really appreciated his continuous support and guidance during these three quick years; as well as the time he spent with me daily, providing valuable explanations about the numerous technical and theoretical questions that I had. Moreover, he has always been ready to help me with precision in all the difficult situations even when he has no time or a clear view of the circumstances.
I have learned a lot from him, not only from a scientific point of view but also learning how a professor can interact with his student. Furthermore, he can talk hours and hours about scuba diving, museums, holiday destinations, cuisine and wine tasting giving you complete details.

Many thanks are extended to ***Raffaella Donetti,*** tutor from Pirelli Tyre, who helped, taught, introduced me to the industry reality, giving me suggestions and showing me the correct way to start to study a new material. In the beginning she followed me step by step, by showing me from the method to produce a new compound to how to characterize it. Besides, thanks to her organization, I always found a reply to all my emails and phone calls at any time of the day, and a quick analysis of the result for the product I prepared.
Moreover, not only from the experiment part I received her help, and thank her for her patience, but I also learned a simple and efficacious method to make beautiful slides and good presentations. In addition, during the EUROFILLER conference in Dresden, I had the

opportunity to know her better in a different work context. Also, I would like to thank her for availability, before giving birth to her child. All her actions show work and scientific passion that she has which aren't easy to find. This is what she taught me.

I am also very thankful for the support and help from the group of new raw materials of Pirelli Tyre (***Thomas Hanel, Luca Giannini, Nahmias Marco, Luca Castellani, Ratti Giuseppina, Rossiello Luigia, Parazzoli, Francesco, Lostritto Angela, Vincenzo Boffa***), the chemical group for swelling analysis and simple inorganic characterization (***Medaglia Gabriele, Matteo Caminati, Manfredi Giuseppe, Davide Turco, Marco Colombo, Marco Arimondi***), the compounding group (***Pietropaolo Santo, Ganci Elio, Massimino Paolo***), the mechanical analysis group (***Pinto Alessandro, Casarin Giancarlo and Davide Rossi, Risieri***) and for curing (***Angelo Musto, Magda, Giuseppe Fruini and Romano***); the group of TEM and SEM analysis (***Tino Readaelli and Manuela Loi***).

I would like to acknolewledge Prof. ***Markus Niederberger*** for his seven months of hospitality in the Multifunctional Materials group at the materials Department in the ETH Swiss Federal Institute of Technology of Zurich (Switzerland); for his support and useful discussion during my research and for his patience and availability for reviewing my PhD thesis.
Regarding my time spent in Zurich, I would like to thank ***Staniuk Malwina, Erdem Derya*** and **Shi Nan** for the lunches that we had together on the terrace, for the weekends in Prague, Genève and Lausanne; ***Bettina*** for her PhD defense party in Lenzburg; ***Cheng Wei*** for his support at\in TEM and SEM analysis; ***Kränzlin Nik*** for his beautiful and funny speeches in the lab; ***Heiligtag Florian*** for helping at the beginning of my stay in Zurich; ***Tervoort-Gorokhova Elena*** for her nice 20th anniversary party at ETH and for her nice suggestions on polymer composites, ***Dorota Koziej*** for her suggestions and parties at the rowing club and ***Idalia Bilecka*** for her introduction to microwave synthesis and lunches on the terrace. Furthermore, I thank for beautiful time spent together in the lab to ***Sandra Hilaire, Li Luo, Guobo Zeng, Rahel Böhlen*** and ***Felix Rechberger***. In addition to those I would like to thank secretary ***Gisela Angst*** for making all the documents and permits for my Zurich stay and found an accommodation.

Thank also for ***Nadia Santo*** from CIMA Interdepartmental Center of Advanced Microscopy, University of Milano, for nice TEM sessions.

Thank ***DelVille Marie-Hélène*** from Institut de Chimie de la Matière Condensée de Bordeaux, CNRS, Université Bordeaux for reviewing my PhD Thesis.

Also about Zurich, I will not forget the beautiful time spended with ***Andrea Penna*** (Mantova), ***Paola Orsolini*** and ***Michela Puddu*** (Roma), ***Andrea Arcifa*** (Catania), ***Giovanni dell'Olio*** (Barcellona), ***Michele Furlotti*** (Zurich) and ***Sara Crocetti*** (Firenze) and ***Davide Morselli*** (Modena). With them I visited a lot of places: Bern, Geneva, Lausanne, Lucerne, San Galen, Constance, Einsiedeln and of course Zurich, and I did a lot of travels to go to work.

Acknowledgements

Regarding my group in Italy I really would like thank to ***Massimiliano D'Arienzo***, which become for me, in the last four years of my stay, a good friend and a good colleague. He is the first one which made me fascinate in this work and research.
Thank to ***Maurizio Crippa***, whom started the PhD with me, which during the three years he never stopped making noise in the office and in the corridor with his phone, his voice and sockets.
Thank to ***Luciano Tadiello***, the new PhD student and ***Luca Bollani***, the new master student, which will continuous my work on silica and nanocomposites.
Thank also to all the students of degree and master degree that spend a part of their study in our lab: ***Monica Resnati, Davide Fumagalli, Daniele Crosta, Luca Malchiodi, Alessandro Ciappei, Davide Sala*** and ***Matteo Redaelli.***
Thank also to ***Edoardo Alquati***, a degree student, how helped me to prepare in situ sol gel silica composites. I will not forget his nice comment to the materials used and also his chocolate croissants.
Thank also for ***Stefano Marchionna, Mario Beretta, Michele Mauri, Annalisa Colombo, Alberto Bianchi, Paola Frigerio*** and ***Angeloclaudio Nale*** for nice conversations.
Thank also to ***Erika Herrera*** which lived 3 years in my same office and how shared with me all my emotions. Thank to Prof. ***Claudio Maria Mari***, Dott. ***Riccardo Ruffo*** and ***Matteo Salomone*** which allowed me to use the tools in their laboratory and for the guest conversations.
Thank to ***Prof. Gian Paolo Brivio***, dean of PhD in Material Science, for his good organization of the courses and for his many permissions to summer school and conference, thank for ***Maria Cristina Fassina*** which helped for the documentation part.
The last thank, form academic part of view, is given to ***Julia Weekes***, which encouraged me to study English and improve my level. Without her I will never be able to write a English thesis and I never get a presentation. Thank also for her English correction thesis.

I could not complete this thesis without the plentiful support and love from my family: my mum, dad and my brother.
Thank for my uncle ***Maher,*** my aunt ***Elizabeth*** and my cousins ***Amanda, Amy*** and ***Kamal*** from Dublin, ***Georges Ghabour*** from Dubai, ***Lesley*** and ***Alex*** and ***Samah*** from London, ***Bishoy Dawood*** and his family from Toronto.
Thank for the small Egyptian Coptic community in Milano: ***Giulia*** and ***Aldo***, ***Ferial***, ***Iva, Hala, Magdi, Sherin, Atef, Noha, Walaa, Nadra, Monica, Mikel, Charly, Essam, Yustina, Marianna*** e ***Mino Bimen,*** and ***Amal Attia*** and many other.
Thank for ***Anba Kirollos***, ***Abuna Bimen*** and ***Abuna Luca*** for having been close in the difficult moments of my life.
Thank for my childhood friends ***Valentina Ongaro***, ***Cristina Lualdi***, ***Ilaria Alfano, Manuela Bolumetto*** and ***Giuseppe Perfetti.***
and many other friends…

List of Papers

- L. Wahba, M. D'Arienzo, R. Donetti, T. Hanel, F. Morazzoni, R. Scotti, L. Tadiello; *In situ sol-gel obtained silica-rubber nanocomposites: influence of the filler precursors on the improvement of the mechanical properties*. **RCS Advances Accepted.**

- R. Scotti, L. Wahba, M. D'Arienzo, R. Donetti, N. Santo, F. Morazzoni; *Rubber-silica nanocomposites obtained by in-situ sol-gel method: particle shape influence on the filler-filler and filler-rubber interactions*. **Soft matter.** *2012*, 8, 2131-2143.

- A. Gervasini, L. Wahba, M. Dario, J-F. Lamonier, *Surface, structural, acidic and redox characterization of binary mixed-oxide MoO_3-SiO_2*. **Materials Sciences and Applications***, 2012,* 3, 195-212.

- M. D'Arienzo, J. Carbajo, A.Bahamonde, S. Polizzi, R. Scotti, L. Wahba, F. Morazzoni; *Photogenerated Defects in Shape-Controlled TiO_2 Anatase Nanocrystals: A Probe To Evaluate the Role of Crystal Facets in Photocatalytic Processes*; **JACS**. *2011*, 133, 17652–17661.

- M. D'Arienzo, M. Crippa, P. Gentile, C. M. Mari, S. Polizzi, R. Ruffo, R. Scotti, L. Wahba, F. Morazzoni; *Sol–gel derived mesoporous Pt and Cr-doped WO_3 thin films: the role played by mesoporosity and metal doping in enhancing the gas sensing properties*; **J Sol-Gel Sci. Technol.** *2011, DOI 10.1007/s10971-011-2568-7.*

- M. Crippa, E. Callone, M. D'Arienzo, K. Müller, S. Polizzi, L. Wahba, F. Morazzoni, R. Scotti; *TiO_2 nanocrystals grafted on macroporous silica: A novel hybrid organic–inorganic sol–gel approach for the synthesis of highly photoactive composite material*; **Applied Catalysis B: Environmental**, *2011*, 104, 282–290.

- M. D'Arienzo, A. A. Essawy, R. Scotti, L. Wahba, F. Morazzoni, P. Gentile, I. R. Bellobono, S. Polizzi; *Membrane-Assisted Charge Separation and Photocatalytic Activity in Embedded TiO_2:A Kinetic and Mechanistic Study*; **J. Phys. Chem. C** *2010*, 114, 15755–15762.

- M. D'Arienzo, L. Armelao, A. Cacciamani, C. M. Mari, S. Polizzi, R. Ruffo, R. Scotti, A. Testino, L. Wahba, F. Morazzoni; *One-Step Preparation of SnO_2 and Pt-Doped SnO_2 As Inverse Opal Thin Films for Gas Sensing*; **Chem. Mater**. *2010*, 22, 4083–4089.

- M. D'Arienzo, R. Scotti, L. Wahba, C. Battocchio, E. Bemporad, A. Nale, F. Morazzoni; *Hydrothermal N-doped TiO_2: Explaining photocatalytic properties by electronic and magnetic identification of N active sites*; **Applied Catalysis B: Environmental**, 93, *2009*, 149-155.